



January 2023

## Quantification Of Rigidity And Synthesis Of Cyclobutane Bisimide Building Blocks

Joseph Earl Mcgilligan Robertson

[How does access to this work benefit you? Let us know!](#)

Follow this and additional works at: <https://commons.und.edu/theses>

---

### Recommended Citation

Robertson, Joseph Earl Mcgilligan, "Quantification Of Rigidity And Synthesis Of Cyclobutane Bisimide Building Blocks" (2023). *Theses and Dissertations*. 5696.  
<https://commons.und.edu/theses/5696>

This Dissertation is brought to you for free and open access by the Theses, Dissertations, and Senior Projects at UND Scholarly Commons. It has been accepted for inclusion in Theses and Dissertations by an authorized administrator of UND Scholarly Commons. For more information, please contact [und.common@library.und.edu](mailto:und.common@library.und.edu).

DECEMBER 2023

QUANTIFICATION OF RIGIDITY AND  
SYNTHESIS OF CYCLOBUTANE BISIMIDE  
BUILDING BLOCKS



JOSEPH EARL MCGILLIGAN ROBERTSON

BACHELOR OF SCIENCE IN CHEMISTRY

Grand Valley State University, 2017

A dissertation  
submitted to  
The School of Graduate Studies  
of the  
University of North Dakota  
in partial fulfillment of the requirements  
for the degree of  
Doctor of Philosophy

Grand Forks, North Dakota  
December  
2023

Copyright 2023 Joseph Earl McGilligan Robertson

Cover artwork copyright 2023 Elizabeth Kathlyn DeForest



This dissertation, submitted by Joseph Earl McGilligan Robertson in partial fulfillment of the requirements for the Degree of Doctor of Philosophy from the University of North Dakota, has been read by the Faculty Advisory Committee under whom the work has been done and is hereby approved.

---

Dr. Qianli Rick Chu

---

Dr. Guodong Du

---

Dr. Evgenii Kozliak

---

Dr. Ayush Asthana

---

Dr. Beth Klemetsrud

This dissertation is being submitted by the appointed advisory committee as having met all requirements of the School of Graduate Studies at the University of North Dakota and is hereby approved.

---

Chris Nelson  
Dean of the School of Graduate Studies

---

Date



# Table of Contents

Indexes .....	x
Figures .....	x
Schemes .....	xiii
Tables.....	xiii
Appendix Figures.....	xiv
Appendix A.....	xiv
Appendix B.....	xvii
Appendix C.....	xvii
Appendix D .....	xviii
<b>No table of figures entries found. ....</b>	<b>Error! Bookmark not defined.</b>
Acknowledgments.....	xx
Abstract .....	1
Chapter 1: Quantification of Rigidity for Small Organic Molecules .....	4
Introduction.....	4
Methods .....	6
Construction of Rotamer Ensemble.....	6
Calculation of Volume.....	8
Results and Discussion .....	10

Verification of method with hydrocarbons.....	10
Correlation of $R_{gf}$ to Conformational Entropy.....	13
Applications .....	16
Composite $R_{gf}$ .....	21
Limitations .....	23
Conclusions and Future Work .....	23
Chapter 2: Synthesis and Characterization of Bisimide building blocks .....	26
Introduction.....	26
Synthetic approach .....	29
Experimental .....	31
Synthesis of N-(2-hydroxyethyl)-1,2-dimethylmaleimide (protoCBDO-2).....	31
Synthesis of N-(ethyl ethanoate)-1,2-dimethylmaleimide (protoCBDE-6).....	32
Synthesis of N-((S)-methyl 1-methylethanoate)-1,2-dimethylmaleimide (protoCBDE-7).....	33
Synthesis of N-allyl-1,2-dimethylmaleimide (protoCBDV-1) .....	34
Synthesis of N-(ethyl-2-acetate)-maleimide (protoCBDAc-1) .....	35
Synthesis of N-dihydroxy-1,2-dimethylmaleimide (protoCBDH-1).....	36
Maleimide (protoCBBI-2).....	37
Syntheses of N,N'-di(2-hydroxyethyl)-1,2,3,4-tetramethylcyclobuta[1,2-c:3,4-c']bisimide (CBDO-2) .....	38

Syntheses of N,N'-di(ethyl ethanoate)-1,2,3,4-tetramethylcyclobuta[1,2-c:3,4-c']bisimide (CBDE-6).....	39
N,N'-di((S)-methyl 1-methylethanoate)-1,2,3,4-tetramethylcyclobuta[1,2-c:3,4-c']bisimide (CBDE-7).....	40
Synthesis of N,N'-di(ethyl-2-acetate)-cyclobuta[1,2-c:3,4-c']bisimide (CBDAc-1) .....	40
Synthesis of N,N'-diallyl-1,2,3,4-tetramethylcyclobuta[1,2-c:3,4-c']bisimide (CBDV-1) .....	41
Synthesis of N,N'-dihydro-cyclobuta[1,2-c:3,4-c']bisimide (CBBI-2) .....	42
Synthesis of N,N'-dihydro-1,2,3,4-tetramethylcyclobuta[1,2-c:3,4-c']bisimide (CBBI-1).....	42
Synthesis of N,N'-dihydroxy-1,2,3,4-tetramethylcyclobuta[1,2-c:3,4-c']bisimide (CBDH-1). 43	
Synthesis of N,N'-di(2-hydroxyethyl)cyclobuta[1,2-c:3,4-c']bisimide (CBDO-3) .....	44
Synthesis of N,N'-di(n-propanoic acid)-1,2,3,4-tetramethylcyclobuta[1,2-c:3,4-c']bisimide (CBDA-6).....	44
Synthesis of N,N'-di(ethanoic acid)-1,2,3,4-tetramethylcyclobuta[1,2-c:3,4-c']bisimide (CBDA-7).....	45
Synthesis of poly(hexamethylene N,N'-di(ethanoate)-1,2,3,4-tetramethylcyclobuta[1,2-c:3,4-c']bisimide) (PCBBI-1) .....	46
Synthesis of N,N'-di(2-hydroxyethyl)-1,2,3,4-tetramethylcyclobuta[1,2-c:3,4-c']bisimide hexanoate) (PCBBI-2).....	47
Results and Discussion .....	47
Description of a model CBBI .....	47

Synthesis of model compound .....	49
Versatility of CBBi synthesis.....	50
Thermal properties of select CBBIs .....	56
Syntheses of CBBi-based polymers.....	62
Conclusions and Future work.....	64
Chapter 3: Optimization of [2+2] Photocycloaddition using Solution Phase Ethylene.....	66
Introduction.....	66
History of CBA <sub>n</sub> -1 and CBeA <sub>n</sub> -1 syntheses.....	69
Methods and Materials .....	72
Synthesis of CBA <sub>n</sub> -1 .....	72
Synthesis of CBeA <sub>n</sub> -1 and CPDA <sub>n</sub> -1.....	76
Synthesis of imide from CBA <sub>n</sub> -1 .....	76
Experimental .....	77
cis-1,2-cyclobutanedicarboxylic anhydride (CBA <sub>n</sub> -1) .....	77
cis-3,4-cyclobutanedicarboxylic anhydride (CBeA <sub>n</sub> -1) .....	77
bis-1,1'-(cyclopropane-2,3-dicarboxylic acid anhydride) (CPDA <sub>n</sub> -1).....	78
cis-(n-phenyl)cyclobutane-1,2-carboximide .....	78
Results and Discussion .....	79
Synthesis of CBA <sub>n</sub> -1 .....	79

Purification of CBA <sub>n</sub> -1 by distillation .....	80
Synthesis and Distillation of CBe <sub>n</sub> -1 and CPD <sub>n</sub> -1.....	81
Appendices.....	83
Appendix A: Selected NMR Spectra .....	83
Appendix B: Crystallographic Data .....	150
Appendix C: Selected HRMS spectra .....	161
Appendix D: Selected IR spectra .....	175
Appendix E: Rigidity Data .....	189
References.....	197

# Indexes

## Figures

Figure 1: Rotamer ensemble for hydroquinone aligned to minimize RMSD for all atoms (left) and excluding hydrogens (right).....	8
Figure 2: Comparison of Van der Waals volume calculations using Monte Carlo volume approximation in this work to published values using geometric sum of spheres calculations. <sup>16</sup> Series consists of straight chain hydrocarbons with backbone #C of 4-22. ....	11
Figure 3: The $R_{gf}$ for two series of alkanes, straight chain and cyclic, with two different $E_{win}$ compared, to the natural log of the number of carbons in the chain. ....	12
Figure 4: Conformational entropy, $S_{conf}$ , as a function of $R_{gf}$ for 110-115 structures. Complete data can be found in the appendix. ....	14
Figure 5: Global minimum rotamers for adipic acid (a) and sebacic acid (b) compared with the the highest energy rotamer in the respective ensembles when $E_{win} = 6.0$ kcal/mol..	19
Figure 6: $R_{gf}$ values for polyester repeat units showing good agreement between the calculated and composite methods. ....	22
Figure 7: Structure of a Kapton repeat unit (top) and sheets of the material which show its color <sup>22</sup> (bottom) .....	27
Figure 8: The general skeletal core of cyclobutane-containing bisimides. ....	28
Figure 9: The crystal structure of CBDA-7 where the central bisimide core is displayed using the space-fill model to emphasize its bulky skeleton. ....	29



Figure 10: Poly(cyclobutanebisimide)-1, PCBBI-1 and poly(cyclobutanebisimide)-2, PCBBI-2, synthesized as part of this work. ....	29
Figure 11: The four major portions of a CBBI. ....	30
Figure 12: Retrosynthetic analysis of a generic CBBI showing the many ways to assemble the 4 core portions and achieve the desired skeletal core. ....	31
Figure 13: A model CBBI compound, cyclobutane diol 2, or CBDO-2.....	48
Figure 14: The crystal structure of CBDO-2 which shows the angle between the imide rings (blue) and the cyclobutane ring (red) to be 110.7°.....	49
Figure 15: Crystals of CBDO-2 which exhibit no color.....	49
Figure 16: Cyclobutane diacid product, CBDA-7, obtained via oxidation of CBDO-2. ....	51
Figure 17: Three protoCBBI structures, protoCBDE-6 (top left), protoCBDE-7 (top middle), and protoCBDV-1 (top right). Below each is the corresponding CBBI monomer, CBDE-6 (bottom left), CBDE-7 (bottom middle), and CBDV-1 (bottom right).....	51
Figure 18: TGA (black line) and DSC (red line) of CBDO-2 from 25°C to 800°C with ramp rate 20°C/min. ....	56
Figure 19: Detail of Figure 18 showing concurrent melt and dehydration of CBDO-2. ....	57
Figure 20: CBDO-2 and the possible thermal dehydration product formed at 317°C.....	57
Figure 21: TGA (black line) and DSC (red line) of CBDE-6 from 25°C to 800°C with ramp rate 20°C/min. ....	58
Figure 22: Detail of 7 showing concurrent melt and degradation of CBDE-6, likely to CBDA-6. ..	59
Figure 23: General mechanism for a retro-ene reaction of the type observed in the degradation of CBDE-6. ....	59

Figure 24: CBDE-6 and the likely thermal degradation product formed at 299°C.....	60
Figure 25: TGA (black line) and DSC (red line) of CBDV-1 from 25°C to 800°C with ramp rate 20°C/min. ....	61
Figure 26: TGA (black line) and DSC (red line) of CBDO-3 from 25°C to 700°C with ramp rate 15°C/min. ....	62
Figure 27: PCBBI-2 solid showing score marks after being stabbed with a spatula (left); the same sample, crumbled due to handling, in better lighting to showcase superb colorless clarity (right).....	63
Figure 28: The 3 major oligomeric constituents of PCBBI-1 and their mono- and dipropyl substituted forms. ....	64
Figure 29: The multiple pathways to construct the cyclobutane bisimide (CBBI) monomer building block from the common starting material, maleic anhydride derivative. ....	65
Figure 30: A typical Hanovia medium-pressure mercury photochemical reactor lamp (left) and a typical photochemical reaction vessel with the quartz cooling jacket in place (right). It's placed in a stand which facilitates submersion of the vessel into a heating or cooling bath. ....	67
Figure 31: The four products of the reaction between maleic anhydride and acetylene. From left to right: cis-3,4-cyclobutenedicarboxylic anhydride (CBeAn-1), trans,trans-bis-1,1'- (cyclopropane-2,3-dicarboxylic acid anhydride), cis,trans-bis-1,1'-(cyclopropane- 2,3-dicarboxylic acid anhydride), and cis,cis-bis-1,1'-(cyclopropane-2,3- dicarboxylic acid anhydride). The isomeric cyclopropanes are collectively referred to as CPDAn-1.....	71

Figure 32: Simplified reaction apparatus for synthesis of CBAn-1 known as the Light Array for Photochemical Reactions Apparatus or LAPRA. Left: LAPRA in open position for easy access to mixture. Right: LAPRA in closed position. ....	74
Figure 33: A typical UV-B bulb used in the synthesis of CBAn-1.....	74
Figure 34: Vacuum jacketed, short path distillation head used for the purification of CBAn-1. Adapters installed to prevent overflow in the case of bumping. ....	75

## Schemes

Scheme 1: Synthesis of protoCBDO-2.....	50
Scheme 2: a) Synthesis of CBDH-1 showing that while the synthesis of protoCBDH-1 was successful, the key step of [2+2] photocycloaddition was not. b) Synthesis of CBDH-1 showing that swapping the order of the reactions results in success. ....	53
Scheme 3: Synthesis of CBDAc-1.....	54
Scheme 4: Synthesis of CBDA-6 via halo-imide coupling.....	55

## Tables

Table 1: Volume approximation measurements and error analysis for cyclopropane. ....	16
Table 2: Rgf values for several diol species commonly found in polyesters. ....	18
Table 3: Rgf values for several diacid species commonly found in polyesters.....	18
Table 4: Rgf values for repeat units of common polyesters.....	21

## Appendix Figures

### *Appendix A*

Figure A 1: $^1\text{H}$ -NMR of CBBI-1 at room temperature. ....	84
Figure A 2: $^{13}\text{C}$ -NMR of CBBI-1 at room temperature. ....	85
Figure A 3: $^1\text{H}$ -NMR of CBBI-2 at room temperature. ....	86
Figure A 4: $^{13}\text{C}$ -NMR of CBBI-2 at room temperature. ....	87
Figure A 5: $^1\text{H}$ -NMR of CBDA-6 at room temperature. ....	88
Figure A 6: $^{13}\text{C}$ -NMR of CBDA-6 at room temperature. ....	89
Figure A 7: DEPT135 of CBDA-6 at room temperature. ....	90
Figure A 8: $^1\text{H}$ -NMR of CBDA-7 at room temperature. ....	91
Figure A 9: $^{13}\text{C}$ -NMR of CBDA-7 at room temperature. ....	92
Figure A 10: HSQC of CBDA-7 at room temperature. ....	93
Figure A 11: $^1\text{H}$ -NMR of CBDAc-1 at room temperature. ....	94
Figure A 12: $^{13}\text{C}$ -NMR of CBDAc-1 at room temperature. ....	95
Figure A 13: DEPT135 of CBDAc-1 at room temperature. ....	96
Figure A 14: HSQC of CBDAc-1 at room temperature. ....	97
Figure A 15: HMBC of CBDAc-1 at room temperature. ....	98
Figure A 16: COSY of CBDAc-1 at room temperature. ....	99
Figure A 17: $^1\text{H}$ -NMR of CBDE-6 at room temperature. ....	100
Figure A 18: $^{13}\text{C}$ -NMR of CBDE-6 at room temperature. ....	101
Figure A 19: DEPT135 of CBDE-6 at room temperature. ....	102

Figure A 20: $^1\text{H}$ -NMR of CBDE-7 at room temperature.....	103
Figure A 21: $^{13}\text{C}$ -NMR of CBDE-7 at room temperature.....	104
Figure A 22: DEPT135 of CBDE-7 at room temperature. ....	105
Figure A 23: H-C correlation of CBDE-7 at room temperature. ....	106
Figure A 24: $^{13}\text{C}$ -NMR of CBDH-1 at room temperature. ....	107
Figure A 25: $^1\text{H}$ -NMR of CBDO-2 at room temperature using synthetic method 1 .....	108
Figure A 26: $^1\text{H}$ -NMR of CBDO-2 at room temperature using synthetic method 2 .....	109
Figure A 27: $^{13}\text{C}$ -NMR of CBDO-2 at room temperature using synthetic method 1 .....	110
Figure A 28: $^1\text{H}$ -NMR of CBDO-3 at room temperature .....	111
Figure A 29: $^{13}\text{C}$ -NMR of CBDO-3 at room temperature .....	112
Figure A 30: HSQC of CBDO-3 at room temperature .....	113
Figure A 31: HMBC of CBDO-3 at room temperature .....	114
Figure A 32: $^1\text{H}$ -NMR of CBDV-1 at room temperature.....	115
Figure A 33: $^{13}\text{C}$ -NMR of CBDV-1 at room temperature.....	116
Figure A 34: DEPT135 of CBDV-1 at room temperature .....	117
Figure A 35: HSQC of CBDV-1 at room temperature.....	118
Figure A 36: HMBC of CBDV-1 at room temperature.....	119
Figure A 37: COSY of CBDV-1 at room temperature .....	120
Figure A 38: $^1\text{H}$ -NMR of protoCBBI-2 (maleimide) at room temperature.....	121
Figure A 39: $^{13}\text{C}$ -NMR of protoCBBI-2 (maleimide) at room temperature.....	122
Figure A 40: $^1\text{H}$ -NMR of protoCBDAc-2 at room temperature.....	123
Figure A 41: $^{13}\text{C}$ -NMR of protoCBDAc-2 at room temperature.....	124

Figure A 42: $^1\text{H}$ -NMR of protoCBDE-6 at room temperature .....	125
Figure A 43: $^{13}\text{C}$ -NMR of protoCBDE-6 at room temperature .....	126
Figure A 44: $^1\text{H}$ -NMR of protoCBDE-7 at room temperature .....	127
Figure A 45: $^{13}\text{C}$ -NMR of protoCBDE-7 at room temperature .....	128
Figure A 46: $^1\text{H}$ -NMR of protoCBDH-1 at room temperature .....	129
Figure A 47: $^{13}\text{C}$ -NMR of protoCBDH-1 at room temperature .....	130
Figure A 48: $^1\text{H}$ -NMR of protoCBDO-2 at room temperature .....	131
Figure A 49: $^{13}\text{C}$ -NMR of protoCBDO-2 at room temperature .....	132
Figure A 50: DEPT135 of protoCBDO-2 at room temperature .....	133
Figure A 51: HSQC of protoCBDO-2 at room temperature .....	134
Figure A 52: $^1\text{H}$ -NMR of protoCBDV-1 at room temperature .....	135
Figure A 53: $^{13}\text{C}$ -NMR of protoCBDO-2 at room temperature .....	136
Figure A 54: $^1\text{H}$ -NMR of CBAAn-1 at room temperature .....	137
Figure A 55: $^1\text{H}$ -NMR of CBAAn-1 in $\text{CDCl}_3$ at room temperature .....	138
Figure A 56: $^{13}\text{C}$ -NMR of CBAAn-1 in $\text{CDCl}_3$ at room temperature .....	139
Figure A 57: $^1\text{H}$ -NMR of powder containing mixture of CPDAn-1 .....	140
Figure A 58: $^{13}\text{C}$ -NMR of powder containing mixture of CPDAn-1 .....	141
Figure A 59: DEPT135 of powder containing mixture of CPDAn-1 .....	142
Figure A 60: $^1\text{H}$ -NMR of crystal of CPDAn-1 which was coated in powder .....	143
Figure A 61: $^{13}\text{C}$ -NMR of crystal of CPDAn-1 which was coated in powder .....	144
Figure A 62: $^1\text{H}$ -NMR of CBI-1 .....	145
Figure A 63: $^{13}\text{C}$ -NMR of CBI-1 .....	146

Figure A 64: DEPT135 of CBI-1 .....	147
Figure A 65: HSQC of CBI-1 .....	148
Figure A 66: HMBC of CBI-1 .....	149

*Appendix B*

Figure B 1: Crystal data and structure for CBDA-7 .....	151
Figure B 2: Crystal data and structure for CBDE-6 .....	152
Figure B 3: Crystal data and structure for CBDE-7 .....	153
Figure B 4: Crystal data and structure for CBDH-1.....	154
Figure B 5: Crystal data and structure for CBDO-1.....	155
Figure B 6: Crystal data and structure for protoCBDAC-1 .....	156
Figure B 7: Crystal data and structure for protoCBDE-6 .....	157
Figure B 8: Crystal data and structure for protoCBDH-1.....	158
Figure B 9: Crystal data and structure for CBeAn-1 .....	159
Figure B 10: Crystal data and structure for CPDAn-1 .....	160

*Appendix C*

Figure C 1: Full high resolution mass spectrum for CBDE-6.....	162
Figure C 2: Predicted [M+Na] peaks for CBDE-6 (top) and measured (bottom).....	163
Figure C 3: Full high resolution mass spectrum for PCBBI-1.....	164
Figure C 4: Predicted [M+Na] peaks for a-b-a oligomer of PCBBI-1 (top) and measured (bottom) .....	165

Figure C 5: Predicted [M+Na] peaks for monopropyl-substituted a-b-a oligomer of PCBBI-1 (top) and measured (bottom) .....	166
Figure C 6: Predicted [M+Na] peaks for dipropyl-substituted a-b-a oligomer of PCBBI-1 (top) and measured (bottom) .....	167
Figure C 7: Predicted [M+Na] peaks for cyclic dimer of PCBBI-1 (top) and measured (bottom) .....	168
Figure C 8: Predicted [M+Na] peaks for a-b-a-b-a oligomer of PCBBI-1 (top) and measured (bottom) .....	169
Figure C 9: Predicted [M+Na] peaks for monopropyl-substituted a-b-a-b-a oligomer of PCBBI-1 (top) and measured (bottom) .....	170
Figure C 10: Predicted [M+Na] peaks for dipropyl-substituted a-b-a-b-a oligomer of PCBBI-1 (top) and measured (bottom) .....	171
Figure C 11: Predicted [M+Na] peaks for a-b-a-b-a-b-a oligomer of PCBBI-1 (top) and measured (bottom) .....	172
Figure C 12: Predicted [M+Na] peaks for monopropyl-substituted a-b-a-b-a-b-a oligomer of PCBBI-1 (top) and measured (bottom) .....	173
Figure C 13: Predicted [M+Na] peaks for monopropyl-substituted a-b-a-b-a-b-a oligomer of PCBBI-1 (top) and measured (bottom) .....	174

*Appendix D*

Figure D 1: IR spectra for CBBI-1 .....	176
Figure D 2: IR spectra for CBBI-2 .....	177
Figure D 3: IR spectra for CBDO-2 .....	178
Figure D 4: IR spectra for CBDE-6 .....	179



Figure D 5: IR spectra for CBDE-7 .....	180
Figure D 6: IR spectra for CBDV-1.....	181
Figure D 7: IR spectra for protoCBDAc-1.....	182
Figure D 8: IR spectra for protoCBDE-6.....	183
Figure D 9: IR spectra for protoCBDE-7 .....	184
Figure D 10: IR spectra for protoCBDH-1 .....	185
Figure D 11: IR spectra for protoCBDO-2 .....	186
Figure D 12: IR spectra for protoCBDV-1.....	187
Figure D 13: IR spectra for (N-phenyl)-cis-1,2-cyclobutancarboximide .....	188

*Appendix E*

Figure E 1: Data for Figure 3.....	190
Figure E 2: Data for Figure 4 when $E_{win} = 2.5$ kcal/mol .....	191
Figure E 3: Data for Figure 4 when $E_{win} = 6.0$ kcal/mol .....	194

## Acknowledgments

A couple pages of typed words is a woefully inadequate way to express the gratitude I have for all those who played a part in my development as a scientist, but it is my duty to try so that they may feel even a glimmer of that thanks.

I would like to thank Dr. Qianli Rick Chu who believed in me, even at the times which I could not believe in myself. His enthusiasm and excitement as an educator, researcher, and scientist will serve me as a model for how to truly love and enjoy the work I do in the laboratory. His encouragement for me to try new things to which I'd never been exposed was invaluable in developing my confidence as a researcher. My success would have been impossible without his guidance and support.

I would like to collectively thank my current committee members Dr. Guodong Du, Dr. Jenya Kozliak, Dr. Ayush Asthana, and Dr. Beth Klemetsrud for their support and guidance as I approached the end of my degree. I would also like to thank them individually; Dr. Du, for always knowing how to navigate the graduate school paperwork and for training me on the NMR; Dr. Kozliak, for bringing his experience as a researcher and helping me focus my efforts; Dr. Asthana, for discussing with me and helping me understand the conventions of quantum chemists; and Dr. Klemetsrud, for keeping me focused on the impact of my research.

I would also like to thank my past committee members Dr. Irina Smoliakova, Dr. Jerome Delhommelle, and Dr. Min Wu for their willingness to serve as a guiding voice. Specifically, to Dr. Smoliakova, I would like to extend my appreciation for her guidance while I served as a Teaching

Assistant for her courses. I will consider myself lucky to glean even a portion of the tenacity and earnestness with which she confronts teaching, research, and life.

I'm eternally grateful to the University of North Dakota Chemistry Department and its chair, Dr. Alena Kubatova, for allowing me the opportunity to pursue my graduate studies and providing a space wonderfully suited to do so. I would also like to recognize and thank Kim Myrum who is incredibly capable and willing to handle any problem I bring to her, even if it is not her job, which given the array of questions I've brought to her, I'm sure has been the case.

I would like to thank current and former members of Dr. Chu's research group for their examples, assistance, or being a great partner for discussion. These include former members Drs. Rahul Shahni, Dominic Nkemnong, Houssein Amjour; current graduate members Solmaz Asadi, Mostafa Manjahi, Sierra Ward, and Diane Tangmi; and current undergraduate members Erica Nguon, Tyler Yanez, and Ian Lin. Additionally, I have many thanks for other graduate students and friends who left the department before me, Muneer Shaik, Wen Sun, Audrey Lavallie, Sarah Reagan, Jess Emond, Soléne Bechelli, Ali Sepehri, and many more.

I want to express my thanks to Dr. Angel Ugrinov of NDSU for his help with X-ray crystallography and mass spectrometry, both in collecting and interpreting data and helping me refine my techniques.

I also want to give a special thanks to my mentors in the Computational Research Center at UND, Aaron Bergstrom and Dave Apostol, for their guidance and compassion during my assistantship and for helping me build my skills in coding and computation.

I want to thank those closest to me in life. First, my parents John and Rose, for always believing in me and for teaching me everything you need to know to be a human, I only wish I paid more attention. To my brother, James, for his enthusiasm and interest in my studies at every stage, I miss you every day. And to my girlfriend and partner, Liz, whose sacrifice in moving with me 900 miles from our home and supporting me throughout the best and worst moments is a gesture of love and kindness which I struggle to capture in words. I love you all so much.

Finally, I want to say that this is not an exhaustive list of those who have helped me along the way, there are simply too many kind hands to list. Please know that if you, even for a moment, think you belong here, you do.

In memory of my brother James  
who taught me  
that the mechanics of universe  
need not be mysterious

## Abstract

The quantification of a molecule's conformational rigidity was achieved via development of a new measure called the Rigidity Factor,  $Rg_f$ . This value is a unit interval wherein molecules with corresponding  $Rg_f$  values closer to 1 are rigid and values closer to 0 are more flexible. The value is determined as a ratio between the molecule's Van der Waals volume,  $V_w$ , and its Van der Waals potential volume,  $V_{Wpot}$ . The  $V_{Wpot}$  was defined as the minimum total volume occupied by a rotamer ensemble of the molecule which has been aligned according to the RMSD for all heavy atoms to achieve a minimum volume. The rotamer ensembles were constructed using CREST (a tool in the xtb suite of programs) or Gromacs. The volumes were calculated using a custom Python script written for this project which uses a Monte Carlo volume approximation method. The script was written to take advantage of parallel computing architecture when present.

The  $Rg_f$  was calculated for several series of similarly structured molecules. These series include straight-chain alkanes, cycloalkanes, diols, diacids, and polymer repeat groups. The values for each series fit the expected trend of longer backbones having a greater flexibility and thus lower  $Rg_f$ . It was observed that rotamer ensembles which represented a molecule with the capability of intramolecular hydrogen bonding, these rotamers dominate the ensemble. This gives a higher  $Rg_f$  than expected and is more similar to a cyclic isomer of similar length. In one case, the repeat unit for polybutylene succinate, PBS, the H-bond donors were replaced with methyl groups. This destroyed intramolecular H-bond potential and the  $Rg_f$  of the molecule more closely resembled the expected value.

Conformational entropy,  $S_{conf}$ , for each compound was calculated using CREST. These values were plotted against  $Rg_f$  for each compound and found to have a general correlation, i.e. structures

with lower  $Rg_f$  have higher  $S_{conf}$ . Several compounds were identified which had a higher-than-expected  $S_{conf}$  despite having a very high  $Rg_f$ . It was theorized that degenerate rotamers born from the rotation of methyl groups provide this entropy. Since these structures are spatially and volumetrically equivalent, this rotation is not reflected in  $Rg_f$  calculations.

A series of new cyclobutane-containing, difunctional monomers (CBDx) was developed for the intention of being used in polymeric materials. Two polymers were synthesized using two different CBDxs and were shown to be colorless and very lightweight. The monomers were built on a maleic anhydride skeletal core and each contain a central cyclobutane moiety created in the key [2+2] photocycloaddition step between two maleic anhydride or imide olefins. This key step was achieved using low power, fluorescent UV-A light sources. By using these sources, the syntheses were much more efficient and safer than traditional photochemical reactions which often necessitate the use of specialized glassware to mitigate the dangers of the broad-spectrum UV bulbs employed.

A poly(cyclobutanebutanebisimide), or PCBBI-1, was synthesized using a cyclobutane-containing diester (CBDE-6) and 1,7-heptandiol. The polymer was confirmed via NMR and HRMS of the soluble oligomeric components. The bulk material had a foamy texture with a very low density. The polymer was colorless.

A second polymer, PCBBI-2, was synthesized using a cyclobutane-containing diol (CBDO-2) and adipic acid. The extremely poor solubility of the material precluded NMR or HRMS analysis. Polymerization was assumed based on physical characteristics of bulk material which was extremely similar to PCBBI-1.

A classic [2+2] photocycloaddition reaction between maleic anhydride and dissolved ethylene gas was improved on the measures of safety, efficiency, and reduced complexity. This was achieved by using a UV source which targeted the absorption of the maleic anhydride starting material. In doing so, the use of high-power UV photoreaction bulbs can be avoided. This eliminates the need for specialized cooling glassware thus reducing apparatus complexity. An isolated yield of 70% was achieved via vacuum distillation after 5 days reaction time.

A similar reaction using acetylene gas was performed but did not provide the same high efficiency. However, the reaction was a success as a crystal structure of the desired product was collected for the first time. Additionally, a new polymorph of a side product of the reaction, biscyclopropanedicarboxylic anhydride, CPDAn-1, was collected.

In total, 21 compounds are presented here. Aside from maleimide and its photo dimer, all of these compounds are either not present or virtually ignored in literature for various reasons as discussed. Eleven of these compounds are novel and initial characterizations are presented herein. Further characterizations are provided for the remainder. Characterization includes 10 initial crystal structures reported for both novel and extant species.



# Chapter 1: Quantification of Rigidity for Small Organic Molecules

## Introduction

Rigidity and flexibility are terms most applicable in the field of structural engineering, however they receive wide use among chemists when discussing molecular structure.<sup>1-4</sup> The rigidity of a molecule can have a variety of impacts on its properties and researchers continue to study its effect in areas such as drug<sup>5,6</sup> or polymer<sup>7-9</sup> development. Despite the frequency with which these terms are encountered, they elude a universally accepted quantitative chemical definition. It can be trivial to define molecules as flexible or rigid when contrasted with one another, but a system that is able to broadly quantify a molecule's rigidity, absent this type of explicit comparative analysis, has not adequately been developed.

In recent decades, methods have been published which seek to measure the rigidity or flexibility of a molecule.<sup>10-12</sup> Generally, these systems limit their focus to the capability of measuring the authors' molecules of interest. More often, the output of the method is qualitative rather than quantitative, i.e. a molecule or portion thereof is rigid or nonrigid. This binary scale experiences similar limitations as comparative analysis.

Irrespective of these limitations, much of the work has focused on biological macromolecules such as proteins.<sup>12</sup> By and large, the favored method of defining the rigidity of proteins is through the qualitative identification of rigid regions. This is acceptable when the structure may be partitioned into secondary or tertiary structures, as proteins ubiquitously are, or when only portions thereof are of interest, such as active sites. However, this approach is applicable neither

to the repetitive nature of typical synthetic polymers, where the structure is expected to behave similarly along its entire length, nor to smaller organic molecules, where the structure lacks higher degrees of order and must be considered as a whole.

Here, we outline a method that describes a molecule's rigidity according to the newly defined property called rigidity factor,  $Rg_f$ . This value is defined as the ratio of the Van Der Waals volume<sup>13</sup>,  $V_W$ , to the minimum possible total volume occupied by the molecule when all rotamers below a set energy threshold are overlapped onto one another. This ensemble volume is likewise newly defined and called the Van der Waals potential volume,  $V_{Wpot}$ . A similar approximation of total volume, the hydrodynamic radius, is presently used in a variety of applications such as DOSY, however since this value is a spherical approximation of total volume, its application to small molecules is limited.

The simple relationship is shown in **Equation 1**. The volumes are calculated using a Monte Carlo (MC) volume approximation program written for this purpose. Accordingly, this method describes a molecule which may be colloquially considered rigid (e.g., Benzene) to have an  $Rg_f$  near or equal to 1. This is because the space occupied by the rotamer ensemble is very near or the same as that of its Van Der Waals volume. Likewise, a molecule which has a flexible structure will be able to potentially occupy a much larger volume, thus reducing the  $Rg_f$ .

$$Rg_f = \frac{V_W}{V_{Wpot}}$$

**Equation 1**

The first of two data sets presented here is for a series of saturated, single-chain hydrocarbons and saturated, monocyclic hydrocarbons. The second data set is the calculation of  $Rg_f$  for monomers used in polymers, primarily polyesters. The methods are general enough to be adapted to molecules or coordination complexes of any type, but these specific sets were chosen for their generality and real-world application, respectively.

## Methods

Methods for constructing rotamer ensembles vary. Because  $V_{Wpot}$  is intrinsically tied to the rotamer ensemble, specifying the method used in the construction of rotamer ensembles is crucial to the repeatability of the  $V_{Wpot}$  measurements and should be described when reporting  $Rg_f$  values. As such, much of the methodology discussed herein will focus on the methods used for rotamer ensemble construction and the determination of the Van der Waals potential volume,  $V_{Wpot}$ .

### *Construction of Rotamer Ensemble*

Although the concept of conformer ensembles is quite common in literature, the similar concept of rotamer ensembles is much less so. The conformer ensemble and rotamer ensemble are similar concepts in that they are both ensembles of rotational isomers for a compound. The difference between the two is that members of a conformer ensemble are determined purely on an energetic basis whereas members of a rotamer ensemble are determined based on spatial occupancy difference regardless of energetic degeneracy. Ideally, in either case, each member of the ensemble represents an achievable local energetic minimum for the structure. In the work presented here, a rotamer ensemble is defined as the ensemble which contains all energetic

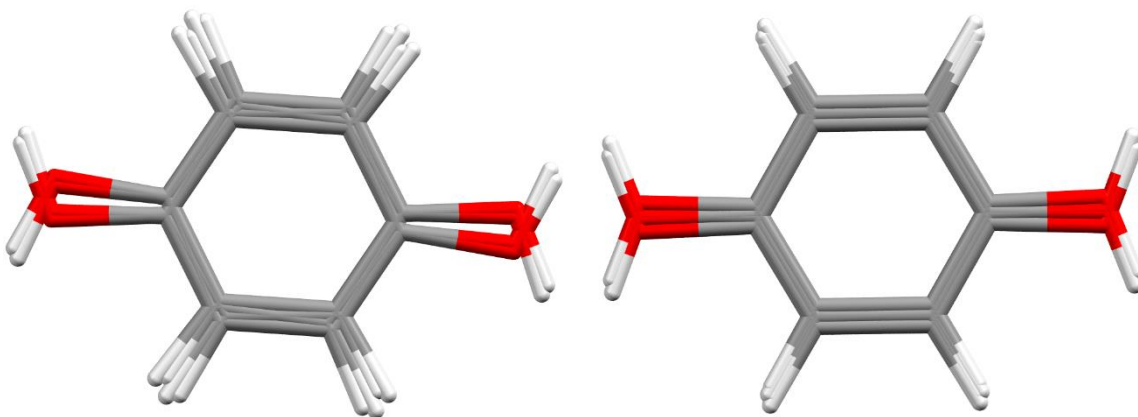
minimum rotamers beneath a specific window above the global minimum ( $E_{\text{win}}$ ) and which have an energy difference greater than a threshold ( $E_{\text{thr}}$ ). This definition closely mirrors the accepted definition of a conformer ensemble but is explicitly provided to eliminate ambiguity.

To further illustrate the differences between a conformer and a rotamer ensemble, n-butane may be considered as a model structure. The rotamer ensemble for butane contains three structures, staggered butane (the global minimum) and two enantiomeric gauche conformations achieved by rotation of the dihedral  $60^\circ$  or  $120^\circ$ . In the generation of a conformer ensemble, one of the gauche conformations will be energetically degenerate and discarded. This is often ideal for applications regarding thermodynamic properties, but in the case of  $V_{\text{Wpot}}$ , this will not accurately reflect the motion of the molecule as it rotates about the dihedrals. Therefore, the rotamer ensemble must be used.

Rotamer ensembles for a large series of molecules with differing properties were constructed using Conformer-Rotamer Ensemble Sampling Tool (CREST)<sup>14</sup> which is part of a larger package of semi-empirical methods, eXtended Tight-Binding (xtb).<sup>15</sup> The first dataset included 115 structures at 2.5 kcal/mol above the global minimum with a differentiation threshold of 0.1 kcal/mol. The second dataset included 110 structures at 6.0 kcal/mol above the global minimum with a differentiation threshold of 0.1 kcal/mol. All other properties were left at default values.

Because  $Rg_f$  is sensitive to the size and alignment of the rotamer ensemble, the methods used should always be reported. An important consideration when aligning the rotamer ensemble is whether to include hydrogens in the calculation of the RMSD. In the presented work, hydrogens were not considered so as to exclude ensemble “jittering” due to hydrogen rotation (Figure 1).

Additionally, this keeps consistency with conventional uses of RMSD such as its broad use in biochemistry when comparing proteins. However, it is recognized that their inclusion in alignment can be readily accommodated when such hydrogen rotations are of interest.



*Figure 1: Rotamer ensemble for hydroquinone aligned to minimize RMSD for all atoms (left) and excluding hydrogens (right).*

#### *Calculation of Volume*

The geometric summation of overlapping spheres method for the calculation of  $V_w$  as described by Bondi<sup>13</sup> is encompassing and well-suited for singular structures. Though methods have been published which allow the simplified approximation of the method for larger molecules,<sup>16</sup> modern computing hardware allows for direct application of Bondi's method with remarkable efficiency on even very large scales. Given the widely accepted accuracy of values determined this way, this method was chosen as the basis by which subsequent methods were compared.

Despite the robustness of Bondi's method, it becomes inordinately complicated when applied to ensembles of overlapped rotamers such as those constructed in the determination of  $V_{w_{pot}}$ . For

this reason, a 3D Monte Carlo volume approximation method was used instead as this method is well suited for the determination of volume of irregular shapes.

The software and scripts for this process were written specifically for this project in Python. The steps the script takes to calculate the volume of the ensemble follow standard Monte Carlo volume approximation methods. For completeness, the steps are presented here as follows:

1. Receive input from user detailing input file (multi-frame .xyz), output file name (.txt), and number of points ( $n$ ) to be used.
2. Load each rotamer from input file into memory as sets of atoms. Atoms are described using 3D cartesian coordinates in Å and atom element, which automatically defines Bondi radius also in Å.
3. Determine bounding box dimensions. Default is 2 Å beyond the furthest atom center in each of the six cartesian directions. This bounding box is always a cuboid.
4. A point within that box is generated then checked to see if it intersects with any atom as determined by the atom's Bondi radius. This step is terminated at first instance of intersection ( $n_i$ ) to save computation time. Repeat for  $n$  points.
5. The ratio of  $n_i$  to  $n$  is determined.
6. This ratio is multiplied by the calculated volume of the bounding box to give the approximate volume of the ensemble (**Equation 2**).
7. A file is created which contains the output in Å<sup>3</sup> as well as several computational and file creation details.

$$V = V_{box} \left( \frac{n_i}{n} \right)$$

**Equation 2**

Given the random nature of Monte Carlo methods, it is possible that the test points may be generated unequally thus giving the artificial appearance of a higher or lower volume. To be assured that the  $V_{Wpot}$  calculated was repeatable and not subject to such random variation, each volume calculation was conducted in triplicate. For the comparison of  $Rg_f$  with  $S_{conf}$ ,  $n = 500,000$  and the rotamer ensemble used for  $V_{Wpot}$  was the one generated in the first trial of  $S_{conf}$ . For all other calculations,  $n = 100,000$ , unless otherwise noted.

## Results and Discussion

### *Verification of method with hydrocarbons*

In order to verify the accuracy of the volume calculation, several of the results for  $V_W$  produced by the Monte Carlo (MC) volume approximation script were compared to published values which used the standard summation of spheres methods<sup>16</sup> and it was found to agree within statistical limits (**Figure 2**). Both MC and a summation of spheres (geometric) methods were conducted and are presented in the figure. As expected, the geometric method was identical to literature values whereas the MC method trended slightly lower as molecular weight increased, but it was still within an acceptable range. The MC method was used in calculation of both  $V_W$  and  $V_{Wpot}$  to avoid any systemic error between volume calculations. Therefore, it may be confidently said that for the purpose of calculating molecular volumes, the Monte Carlo volume approximation is adequate.

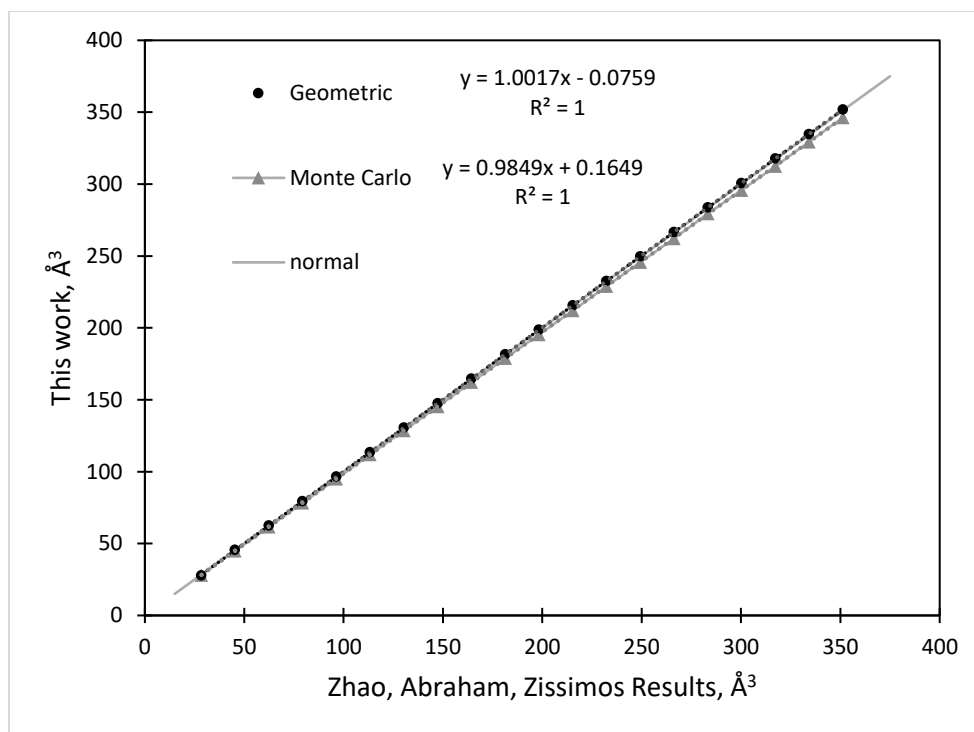


Figure 2: Comparison of Van der Waals volume calculations using Monte Carlo volume approximation in this work to published values using geometric sum of spheres calculations.<sup>16</sup>

Series consists of straight chain hydrocarbons with backbone #C of 4-22.

After confidence in the method was established, calculation of  $Rg_f$  values for series of structurally similar molecules was carried out. **Figure 3** presents data for a series of straight chain alkanes and a series of monocyclic alkanes, each with the same number of carbon atoms in the backbone. The trends observed conform to the expected behavior in that a molecule with more conformational constraints, i.e. a cycloalkane, will have an  $Rg_f$  value closer to 1 and a molecule with more unrestrained rotation, such as a straight chain alkane, will have an  $Rg_f$  value approaching 0. Also as expected, within each series,  $Rg_f$  decreases as chain length increases.  $Rg_f$  of both series exhibits a linear relationship with the natural log of the number of carbons in the chain or cycle.



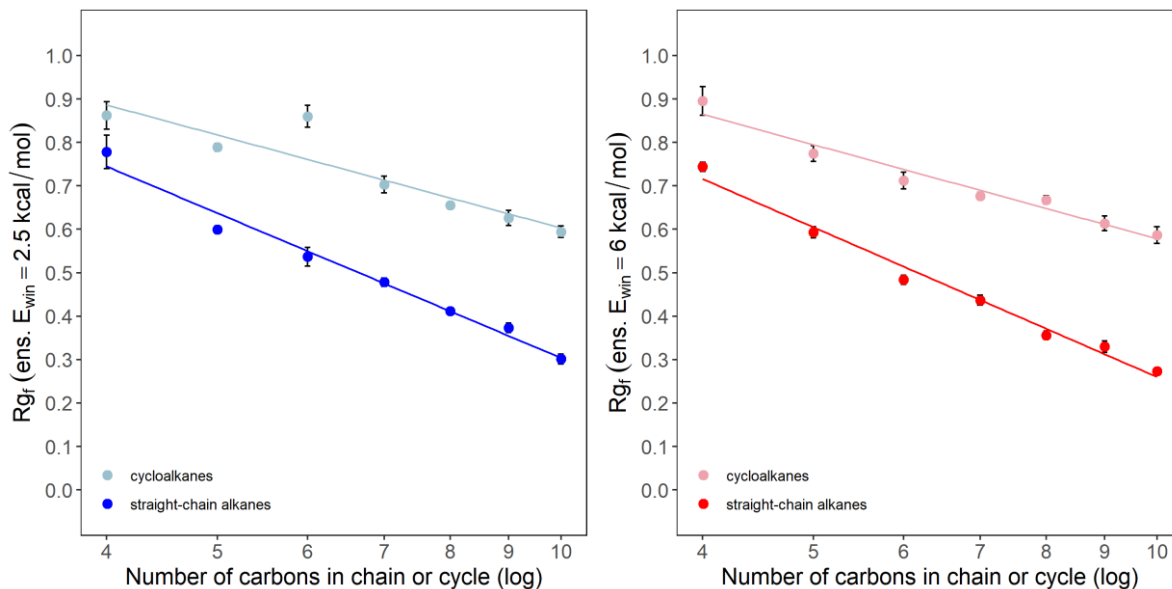


Figure 3: The  $Rg_f$  for two series of alkanes, straight chain and cyclic, with two different  $E_{win}$  compared, to the natural log of the number of carbons in the chain.

Because of this predictability, it was shown that it may be possible to predict the rigidity of a molecule when the  $Rg_f$  for others in a series or of similar structure have been calculated. However, addition or removal of atoms may have a large impact on the associated volumes. For instance, the  $Rg_f$  for butane found in the appendix is 0.744 while a structurally similar compound such as 1,2-ethanediol found in **Table 2** is 0.591. It is reasonable to postulate that the lower  $Rg_f$  of 1,2-ethanediol is the rotation of the hydroxyl groups, which may account for significant volume in the rotamer ensemble. The manner in which terminal groups, namely methyl groups, contribute is discussed in the next section.

### *Correlation of $Rg_f$ to Conformational Entropy*

To ground  $Rg_f$  in first principles chemistry, effort was made to determine correlations with fundamental properties of molecules. Given that  $Rg_f$  is a measure of conformational disorder, the obvious choice was to investigate its relationship with conformational entropy,  $S_{conf}$ .

The determination of conformational entropy is still an active area of research.<sup>17</sup> Typical energy calculations used in vibrational frequency simulations (in programs such as Gaussian09, GAMESS, etc) conform to the Born-Oppenheimer approximation in that the entropy of a molecular system may be separated into three distinct terms each representing a discrete contribution to the absolute entropy of the molecule (**Equation 3**).

$$S = S_{vib} + S_{trans} + S_{rot} \quad \text{Equation 3}$$

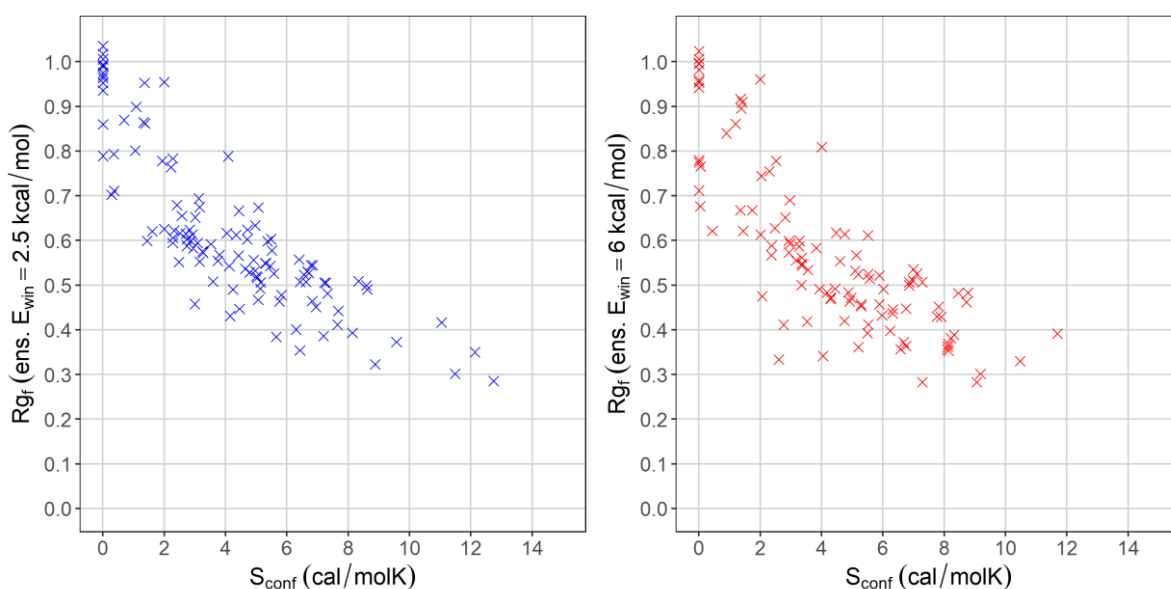
These three contributions are the vibrational, translational, and rotational entropies. Explicitly, there is a final term for the contribution from electronic motion,  $S_{elec}$ , though in most cases it is equivalent to zero due to an additional approximation that the first and higher excited states are inaccessible.

$S_{vib}$  can then be further split into terms representing the harmonic oscillator, its anharmonic correction, and conformational entropy,  $S_{conf}$ . It is by this method that CREST extrapolates conformational entropy its “entropy mode”<sup>18</sup> and is an application of an earlier method<sup>19</sup> (**Equation 4**).

$$S_{vib} = S_{HO} + S_{anharm} + S_{conf} \quad \text{Equation 4}$$

Specifics for the methods may be found in the associated references. Simply put,  $S_{\text{conf}}$  is the contribution to total entropy due to a molecules capability to assume different conformational isomers. This “entropy mode” was the method used to determine conformational entropy for all studied compounds.

In **Figure 4**, the  $S_{\text{conf}}$  is plotted as a function of  $Rg_f$  and shows the general correlation between the two values for both  $E_{\text{win}}$ . The data points in the figure represent the varied collection of molecules investigated thus far in this work including straight-chain alkanes, cycloalkanes, aliphatic diols, aliphatic diacids, aromatic diols, aromatic diacids, representations of polymer repeat groups, and some special cases such as water. The data used may be found in the appendix.



*Figure 4: Conformational entropy,  $S_{\text{conf}}$ , as a function of  $Rg_f$  for 110-115 structures. Complete data can be found in the appendix.*

A compound with  $S_{\text{conf}} = 0.0$  cal/molK may initially indicate a completely rigid structure. This was often the case with structures such as cyclopropane, water, CBDAn-1, dimethylmaleic anhydride,

which each also had an  $R_{gf} \approx 1$ . However, by definition,  $S_{conf}$  is the entropy of the conformer ensemble, which is constructed based on energetic criteria, and not the rotamer ensemble, which is constructed based on spatial criteria. It was possible for a compound to produce a conformer ensemble with a single structure but a rotamer ensemble with more than one, e.g. cyclohexane, or for the energy differences to be so small that they are excluded from the rotamer ensemble, e.g. p-phthalic acid. For the latter, it was simply a matter of rotamer ensemble construction parameters, in this case, setting  $E_{thr} = 0.1$  kcal/mol caused rotamers formed by the rotation of the carboxylic acids to be discarded. This may be “corrected” if desired. However, in the former, when a conformer ensemble was constructed for cyclohexane with  $E_{win} = 2.5$  kcal/mol, a single structure was produced, cyclohexane chair conformation. Any conformer ensemble which contains a single structure will have a  $S_{conf} = 0$ . The analogous rotamer ensemble contained two structures, the chair and its ring flip enantiomer, thus giving cyclohexane a  $R_{gf} = 0.860$ . This disparity of  $S_{conf} \approx 0$  with a  $R_{gf} < 1$  was also observed in other highly symmetric molecules such as cyclopentane, cycloheptane, and tetramethylbutane. Since these molecules are not considered rigid by any definition, it may be concluded that  $S_{conf}$  of these structures is a poor indicator of rigidity.

Some notable outliers are values with  $R_{gf} > 1$ . By definitions presented here, this is impossible and so may initially be a cause for concern. However, this anomaly is due to the random nature of the Monte Carlo volume approximation. When a rotamer ensemble has a volume very near or exactly the same as its reference structure, any small deviations from the mean can have an outsized impact on the  $R_{gf}$ . The largest error observed due to this is found in cyclopropane ( $R_{gf}$ : 1.024  $S_{conf}$ : 0.0 cal/molK). The Monte Carlo volume approximation values and associated error are presented in **Table 1**.

	MC appx 1	MC appx 2	MC appx 3	mean	sd
<i>V<sub>w</sub></i>	54.745	53.418	54.163	54.108	0.665
<i>V<sub>wpot</sub></i>	52.922	53.198	52.468	52.863	0.369
			R <sub>gf</sub>	1.024	0.014

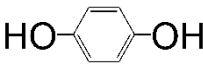
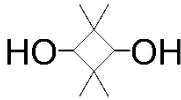
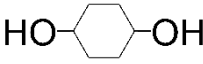
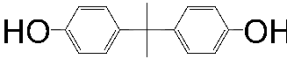
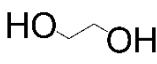
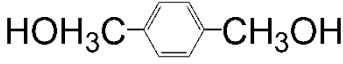
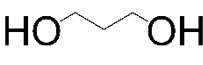
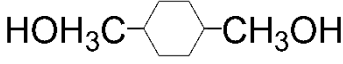
*Table 1: Volume approximation measurements and error analysis for cyclopropane.*

The relationship between the number of rotors in a molecule and its  $S_{\text{conf}}$  has been investigated in literature<sup>17</sup> and is very similar to the conformation ensemble size estimates presented above. In the reference, Chan et al. consider rotatable bonds rather than chain length. For example, in the case of butane, there are 3 rotatable bonds, including rotations about terminal carbon axes. Rotation about these bonds gives rise to 27 rotamers when all atoms are in staggered conformations. By this relationship, the number of rotamers grows exponentially according to  $3^n$  where  $n$  is the number of rotatable bonds. However, as discussed here and in the reference, as the number of rotatable bonds grows, steric effects quickly hinder the assumption of many expected conformations.

### *Applications*

The method was used to calculate the  $R_{gf}$  for a collection of common difunctional monomers primarily used in the synthesis of polyesters. The compounds examined were diols and diacids and their associated  $R_{gf}$  are found in **Table 2** and **Table 3**, respectively. When the structures were arranged in order of  $R_{gf}$ , it became clear that  $R_{gf}$  generally correlated with colloquial descriptors of rigidity, i.e. structures that would be described as rigid have a higher  $R_{gf}$  and structures that would be called flexible have a lower  $R_{gf}$ .

An exception to these trends was found in **Table 3** where sebacic acid had  $R_{gf}$  values far greater than would be expected, especially when compared to shorter diacids. When these ensembles were inspected in a 3D molecular visualization program, it became clear that the energy of the global minimum was greatly reduced due to extensive hydrogen bonding between the carboxylic acid groups. This caused the structures to behave more like cyclic structures than linear. Figure 5 contains the highest and lowest energy rotamers for each ensemble to illustrate that even at energies close to 6.0 kcal/mol above the global minimum, sebacic acid still exhibited intramolecular hydrogen bonding. This intramolecular hydrogen bonding thus induced a degree of rigidity to the structure and gave a larger than expected  $R_{gf}$ .

Name	$R_{gf}$ Ens. $E_{win} = 2.5$ kcal/mol	$R_{gf}$ Ens. $E_{win} = 6.0$ kcal/mol	Structure
<b>hydroquinone</b>	<b>0.953</b>	<b>0.917</b>	
<b>2,2,4,4-Tetramethyl-1,3-cyclobutanediol*</b>	<b>0.884</b>	<b>0.850</b>	
<b>1,4-cyclohexanediol*</b>	<b>0.740</b>	<b>0.648</b>	
<b>bisphenol A</b>	<b>0.624</b>	<b>0.652</b>	
<b>1,2-ethanediol</b>	<b>0.612</b>	<b>0.617</b>	
<b>para-xylylene glycol</b>	<b>0.603</b>	<b>0.611</b>	
<b>1,3-propanediol</b>	<b>0.602</b>	<b>0.544</b>	
<b>1,4-cyclohexanedimethanol*</b>	<b>0.616</b>	<b>0.524</b>	

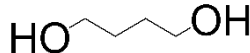
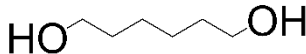
<b>1,4-butanediol</b>	<b>0.549</b>	<b>0.491</b>	
<b>1,6-hexanediol</b>	<b>0.416</b>	<b>0.391</b>	

Table 2: *R<sub>gf</sub>* values for several diol species commonly found in polyesters.

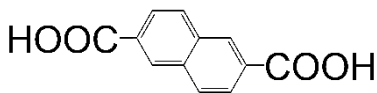
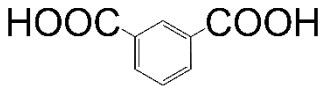

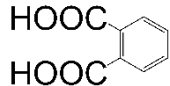
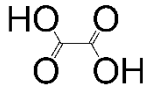

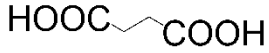

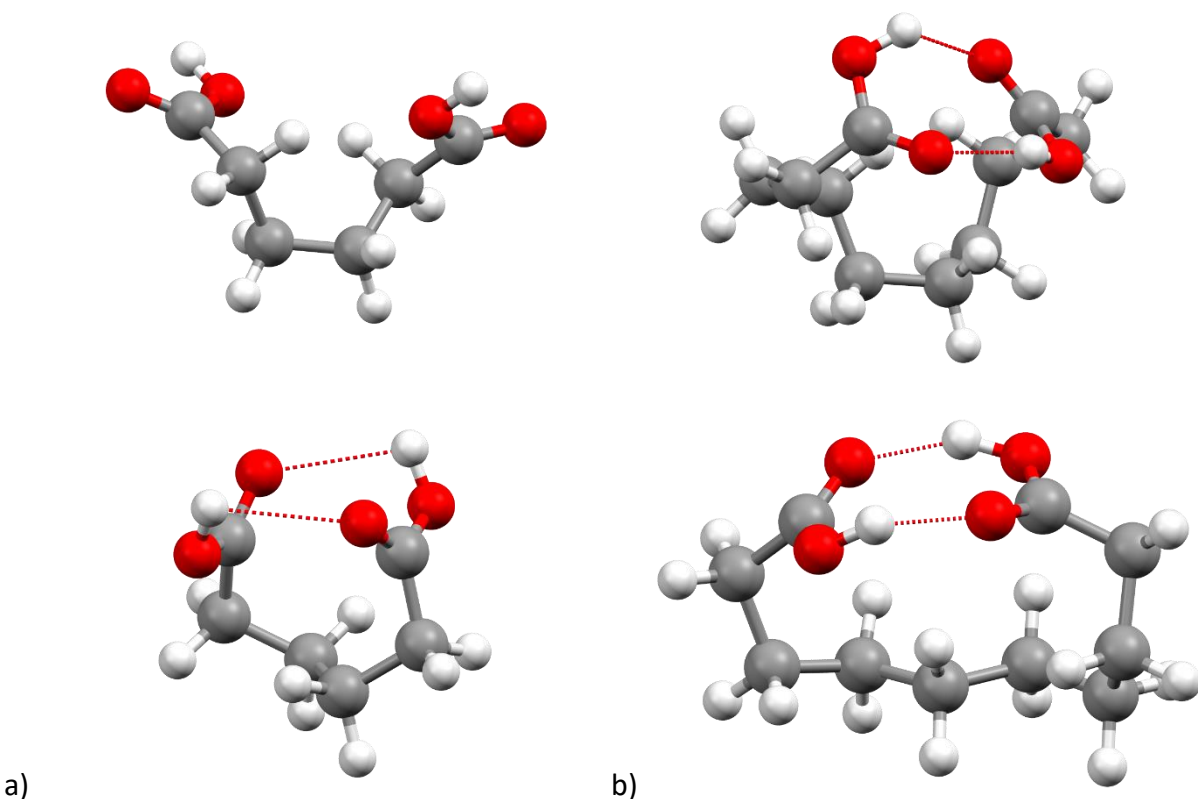
Name	<i>R<sub>gf</sub></i> Ens. <i>E<sub>win</sub></i> = 2.5 kcal/mol	<i>R<sub>gf</sub></i> Ens. <i>E<sub>win</sub></i> = 6.0 kcal/mol	Structure
<b>2,6-naphthalenedicarboxylic acid</b>	<b>0.963</b>	<b>0.954</b>	
<b>m-phthalic acid</b>	<b>0.955</b>	<b>0.961</b>	
<b>p-phthalic acid</b>	<b>0.953</b>	<b>0.955</b>	
<b>o-phthalic acid</b>	<b>0.694</b>	<b>0.690</b>	
<b>oxalic acid</b>	<b>0.652</b>	<b>0.599</b>	
<b>1,4-cyclohexanedicarboxylic acid*</b>	<b>0.596</b>	<b>0.492</b>	
<b>succinic acid</b>	<b>0.464</b>	<b>0.457</b>	
<b>p-phenylenediacetic acid</b>	<b>0.554</b>	<b>0.472</b>	
<b>sebacic acid</b>	<b>0.574</b>	<b>0.444</b>	$\text{HOOC}(\text{CH}_2)_8\text{COOH}$
<b>adipic acid</b>	<b>0.393</b>	<b>0.389</b>	$\text{HOOC}(\text{CH}_2)_4\text{COOH}$
<b>suberic acid</b>	<b>0.592</b>	<b>0.341</b>	$\text{HOOC}(\text{CH}_2)_6\text{COOH}$

Table 3: *R<sub>gf</sub>* values for several diacid species commonly found in polyesters.

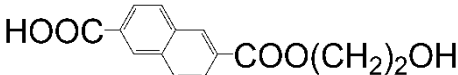
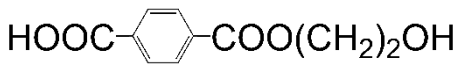
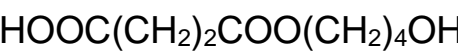
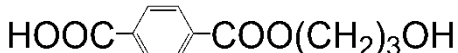


*Figure 5: Global minimum rotamers for adipic acid (a) and sebacic acid (b) compared with the the highest energy rotamer in the respective ensembles when  $E_{win} = 6.0$  kcal/mol.*

Besides this, the main contributions to larger  $Rg_f$  values appear to be a greater aromatic character and smaller molecular weight. Both these observations are in line with what is expected. First, it's widely accepted that aromatic rings impart a large degree of rigidity to a structure, so this observed trend is not surprising. Second, a smaller molecule is predicted to have a higher rigidity due to the consequence of an inherently smaller rotamer ensemble. It's tempting here to liken molecular rigidity to macroscale structural rigidity, but since the definition of  $Rg_f$  is independent of external forces and relies only on the number and variability of a structure's rotamers, such a comparison would be disingenuous. Although it should be noted that comparison to macroscale properties such as this is a convenient method for the rationalization of molecular rigidity.



Furthermore,  $R_{gf}$  values were determined for a varied series of repeat units of common, simple polymers which are composed of two monomers (**Table 4**). Again, they largely follow the same trends as monomers wherein aromatic character and longest chain length are the most important factors for their placement on the scale. As in the diacid values, a major exception is observed with the polybutylene succinate (PBS) repeat unit which has an  $R_{gf}$  of 0.674 and 0.412 with  $E_{win} = 2.5$  and 6.0 kcal/mol, respectively. In the case of the lower  $E_{win}$ , it is even the most rigid structure in the series. As it contains no aromatic structure, it was expected to have a much lower  $R_{gf}$ . The reason for this is the same as with sebacic acid in that intramolecular hydrogen bonding imparts a dominating cyclic structure to the ensemble. To verify this, the hydrogen bond donating sites on the carboxylic acid and hydroxyl group were both replaced with a methyl group and the  $R_{gf}$  of the new structure was measured. The  $R_{gf}$  with  $E_{win} = 2.5$  kcal/mol of the new structure was found to be a more expected 0.285 and was the lowest of the range. The  $V_{wpot}$  for methylated PBS with  $E_{win} = 6.0$  kcal/mol could not be measured because the rotamer ensemble constructed was far too large to analyze in a reasonable timeframe with current methods and hardware.

Name	$R_{gf}$ Ens. $E_{win} =$ 2.5 kcal/mol	$R_{gf}$ Ens. $E_{win} =$ 6.0 kcal/mol	Structure
<b>Polyethylene naphthalate (PEN)</b>	<b>0.543</b>	<b>0.492</b>	
<b>Polyethylene terephthalate (PET)</b>	<b>0.447</b>	<b>0.420</b>	
<b>Polybutylene succinate (PBS)</b>	<b>0.674</b>	<b>0.412</b>	
<b>Polytrimethylene terephthalate (PTT)</b>	<b>0.431</b>	<b>0.361</b>	


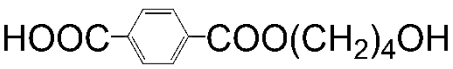
<b>Polycyclohexane-dimethylene terephthalate (PCT)</b>	<b>0.323</b>	<b>0.302</b>	
<b>Polybutylene terephthalate (PBT)</b>	<b>0.384</b>	<b>0.283</b>	
<b>Methylated polybutylene succinate</b>	<b>0.285</b>	-	$\text{H}_3\text{COOC}(\text{CH}_2)_2\text{COO}(\text{CH}_2)_4\text{OCH}_3$

Table 4:  $R_{gf}$  values for repeat units of common polyesters.

#### Composite $R_{gf}$

As the length and complexity of a polymer repeat unit increases, the size of the rotamer ensemble also increases. In addition, the amount of possible comonomer pairs is functionally infinite. Given that the calculation of so many comonomer pairs could be prohibitively computationally expensive, a method was developed to quickly produce a rough, predictive  $R_{gf}$  for polymer repeat units. This was achieved by simply calculating the product of the  $R_{gf}$  of each monomer and that of the linker structure. This relationship is illustrated in **Equation 2** where  $R_{gf1}$  and  $R_{gf2}$  are the  $R_{gf}$  for each monomer and  $R_{gfL}$  is the  $R_{gf}$  for the linker. This method allows for the fast and easy examination of general trends when looking at the rigidity of repeat units without having to construct rotamer ensembles and calculate the  $R_{gf}$  for every possible combination of monomers.

$$\text{composite } R_{gf} = R_{gf1} * R_{gf2} * R_{gfL} \quad \text{Equation 2}$$

The obtained composite  $R_{gf}$  values for repeat units of several polyesters are presented in **Figure 6** alongside calculated  $R_{gf}$  values of the entire structure. The figure shows that the piecemeal

composite  $R_{gf}$  is a good approximation of the wholesale calculated  $R_{gf}$ . A notable exception is PBS which exhibits a higher-than-expected  $R_{gf}$ . Examination of the ensemble shows that, like in previous similar cases, this is due to extensive intramolecular hydrogen bonding. In this case, a model structure in which all hydrogens participating in hydrogen bonding were replaced with methyl groups. The  $R_{gf}$  was much lower than that of the non-methylated version and was more similar to the expected value for a structure with such high aliphatic character.

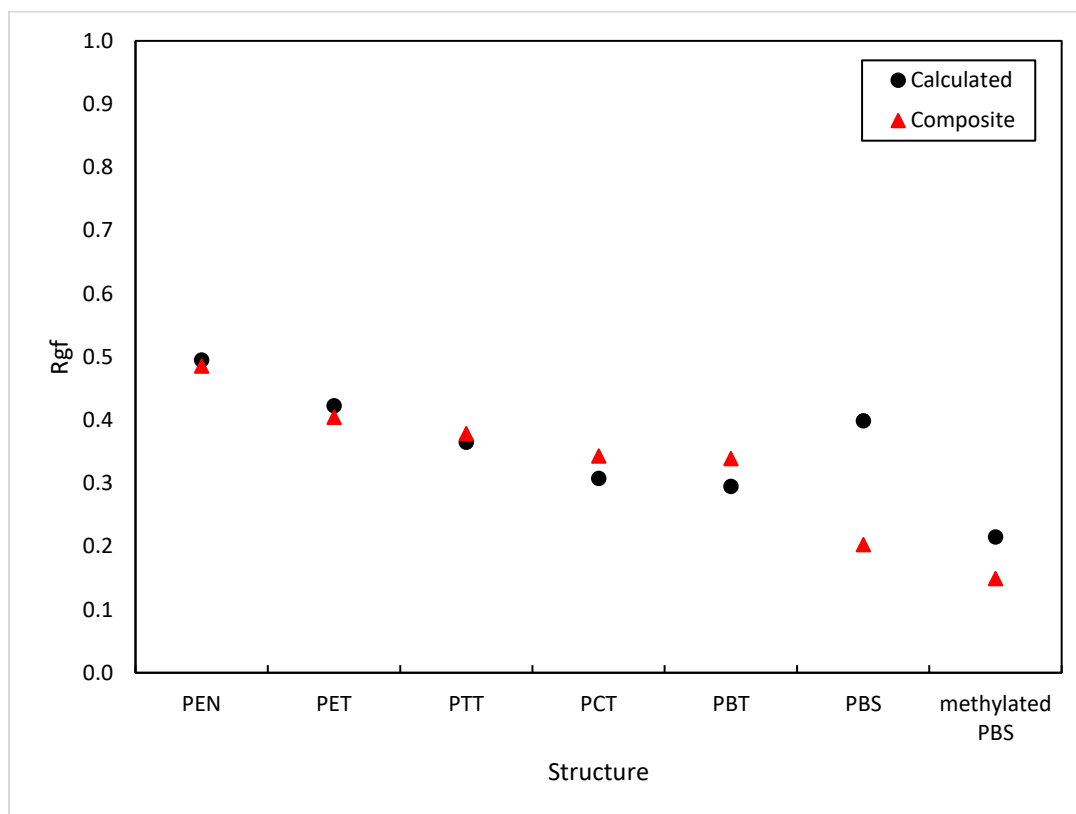


Figure 6:  $R_{gf}$  values for polyester repeat units showing good agreement between the calculated and composite methods.

### *Limitations*

A limitation of this method was encountered when it was used to describe very large molecules which may be more appropriately described as random coils. Since such molecules statistically exist almost entirely as a coil, the inclusion of non-coiled conformers gave a final  $Rg_f$  that does not appropriately describe the molecule. In such a case, the hydrodynamic radius of a structure may be used as a similar, spherical approximation of total volume. It was also recognized that it may be possible to statistically weight structures in the calculation of  $V_{Wpot}$  according to the probability of their existence.

As discussed, the method with which the rotamer ensemble was aligned has a large impact on the resulting  $V_{Wpot}$  and consequently the  $Rg_f$ . The most significant consideration was whether to consider hydrogens in the calculation of the RMSD. In the work presented here, hydrogens were not considered.

### Conclusions and Future Work

In summary, a method of quantifying the rigidity of small molecules was developed. To do so, two new properties were defined, the Van der Waals potential volume,  $V_{Wpot}$ , and rigidity factor,  $Rg_f$ .  $V_{Wpot}$  is the minimum total volume occupied by the overlapped local minimum energy conformers of a compound.  $Rg_f$  is the ratio of the Van der Waals volume,  $V_W$ , to the  $V_{Wpot}$  ensuring that the rigidity of a molecule is described on a unit scale.

To carry out this work and calculate the newly defined  $V_{Wpot}$ , a purpose-built Python script was used. This script calculated the volume of single molecules and ensembles using Monte Carlo volume approximation methods and was written to take advantage of parallel computing

architecture when available. The accuracy of volumes calculated by the Python script was verified by comparing the outputs for single molecules to accepted values from literature.

$Rg_f$  values for all compounds presented here were compared to the conformational entropy,  $S_{conf}$ , of the same compound.  $S_{conf}$  was calculated using the CREGEN stand-alone module included in xtbCREST. The ensemble for the calculation was the rotamer ensemble provided as output from the initial CREST simulation and is the same ensemble used for the calculation of  $V_{Wpot}$ . The  $Rg_f$  and  $S_{conf}$  were generally correlated. Some notable exceptions were likely due to freely rotatable, terminal methyl groups which contribute to the  $S_{conf}$  but are overlapped in the  $V_{Wpot}$ . This general correlation may suggest that  $Rg_f$  is an inherent reflection of conformational disorder in a molecule.

Using this method, it was shown that the  $Rg_f$  of small organic molecules correlates with the colloquial designation on the rigid-to-flexible scale. Several series of similarly structured molecules were analyzed, and their trends allow for predictive analysis of molecules not directly studied.

It should be stressed that  $Rg_f$  is not meant as a predictor of macroscale properties. Instead, this work seeks to give a more framed definition to the concept of rigidity, one that is lacking in current literature. In doing so, chemists, materials scientists, and all others who take molecular rigidity into consideration may have a better working language with which to describe these properties quantitatively. It is our hope that the definition of rigidity in this manner may be used as a descriptive tool when examining molecules for specific applications such as use in polymer development.



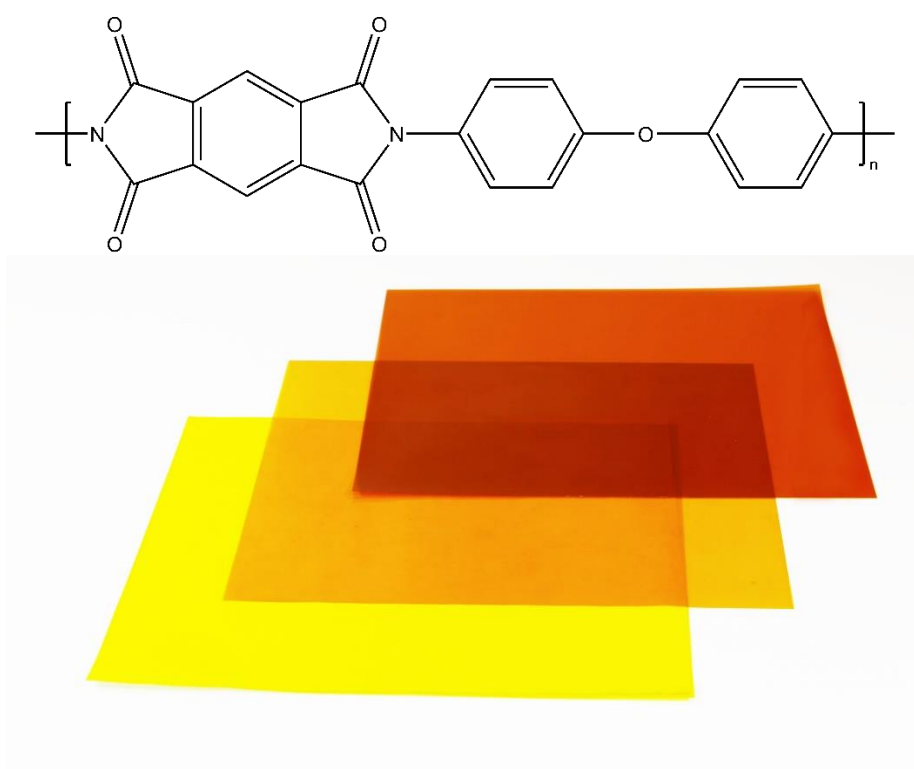
## Chapter 2: Synthesis and Characterization of Bisimide building blocks

### Introduction

A necessary component of condensation polymers (i.e. polyesters, polyamides, polyimides, etc) is the backbone consisting of difunctional monomers. The properties of the discrete monomers have a great impact on the properties of the macroscale materials. A classic example of this can be found when comparing two polyamides, Nylon 66 and Kevlar. Although the amide linkages between monomers and repeat units are identical and ostensibly allow for the same degree of hydrogen bonding between chains, the properties of the materials vary greatly. For instance, Nylon 66 is a strong, highly stretchable material which is often spun into fiber for use in textiles. Conversely, Kevlar is an extremely strong, highly resilient material which does not stretch. It's most often used in applications which require high impact resistance and low weight such as high-performance tire reinforcement and personal body armor. One major explanation for these differences in the materials is the differences in the properties of the monomers. Nylon 66 is composed of flexible, saturated carbon chains between linkages whereas Kevlar is composed of rigid, aromatic rings. In this case, it is the rigidity of the Kevlar which leads to the high strength and low flexibility of the material. Thus, the modification of these monomers is of great interest due, in large part, to giving researchers the capability of affecting properties of the material from the molecular scale.

Color is an extremely important aspect of polymer development. Colorless polymers are ideal not only because they can be used in applications where visual acuity through the material is essential, but impurities or imperfections are easier to identify. Additionally, in cases where color

is desired, they can be more easily colored during processing. Polyimides, such as Kapton® (**Figure 7**), are a class of high performance polymers, but often there is extensive conjugation about the imide linkage which gives the bulk material a color that ranges from bright yellow to deep brown. Thus, colorless bisimide monomers have been of interest in literature.<sup>21</sup> These colorless bisimides monomers break the conjugation around the imide by substituting the aromatic core with aliphatic moieties.

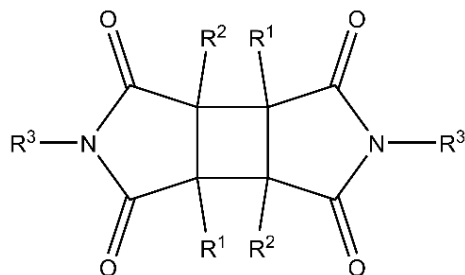


*Figure 7: Structure of a Kapton repeat unit (top) and sheets of the material which show its color<sup>22</sup> (bottom)*

Here, we addressed this desire for colorless polyimides and have presented a novel class of cyclobutane-containing bisimide (CBI) building blocks for use in polymer synthesis. The general structure of these CBIs (**Figure 8**) consisted of the nominal cyclobutane rings with symmetric imide groups. The cyclobutane moiety has been demonstrated in the past as an interesting

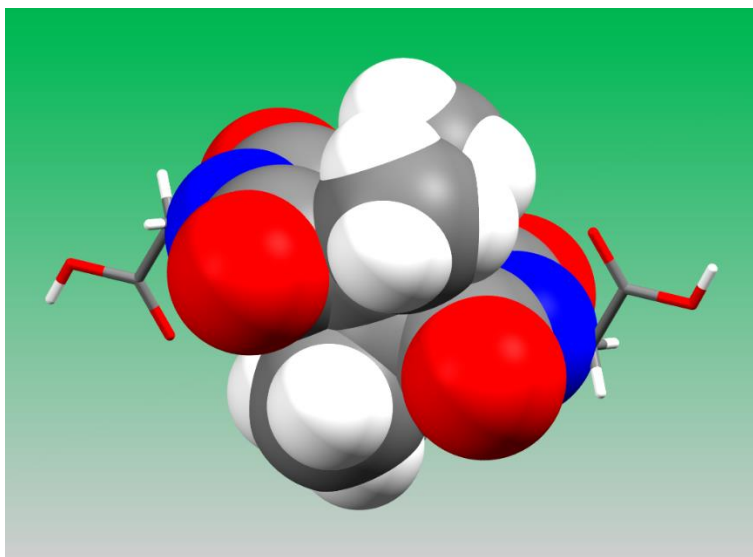


component of semi-rigid monomer building blocks.<sup>20,23</sup> In the structures developed thus far, the imide groups were exclusively trans.

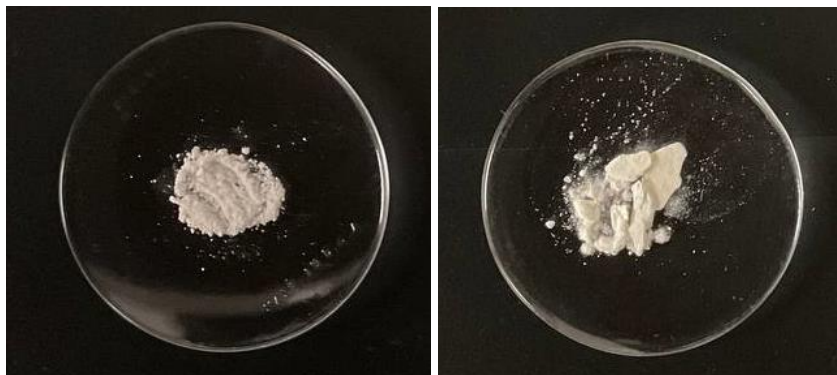


*Figure 8: The general skeletal core of cyclobutane-containing bisimides.*

The CBBI monomers presented here could be of interest to researchers and in industry for several key reasons. First, the unique, aliphatic “knot” that exists between the imide units (**Figure 9**) breaks the conjugation through the imide groups. Consequently, polymers synthesized thus far with CBBIs have been colorless (**Figure 10**). Groups  $R^1$  and  $R^2$  may help further stabilize the imide group by sterically hindering nucleophilic attack, a facet not true with aromatic bisimides. Additionally, the versatility of  $R^3$  allows for incorporation into many kinds of step-growth polymers. In the case that  $R^3$  contains a vinyl group, the CBBI may potentially be used as a cross linker in addition polymers. Present work also shows that side chains on  $R^3$  may impact solubility and state of matter for the monomer.



*Figure 9: The crystal structure of CBDA-7 where the central bisimide core is displayed using the space-fill model to emphasize its bulky skeleton.*



*Figure 10: Poly(cyclobutanebisimide)-1, PCBBI-1 and poly(cyclobutanebisimide)-2, PCBBI-2, synthesized as part of this work.*

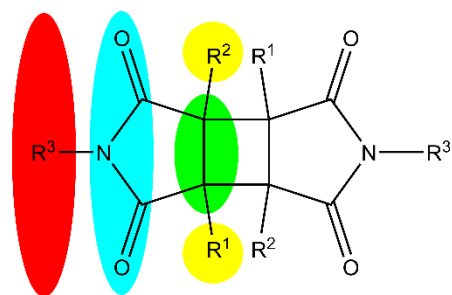
#### *Synthetic approach*

Previous work within our group focused on the synthesis of dianhydrides.<sup>24</sup> These dianhydrides were then hydrolyzed to the analogous tetracarboxylic acids. Some of the dianhydride compounds were used in the synthesis of polyimides via the classic polyamic acid imidization

route. However, the structure cyclobutanedianhydride-5 (CBDAn-5), exhibited little to no tetracarboxylic acid product, even when subjected to harsh conditions.

On the outset of this work, it was hypothesized that hydrolysis was indeed taking place, but the methyl groups on the cyclobutane ring forced the carboxylic groups close together and that the energy of the molecule would be reduced by the recondensation of the ring. This would explain why the product could not be isolated. If this were true, then CBDAn-5 would be able to form a bisimide via a standard condensation reaction. Ultimately, this was indeed proven to be correct by the synthesis of CBDH-1.

The modular nature of the symmetric bisimide core exhibits four discrete portions (**Figure 11**). First, the functional site,  $R^3$  (red). Second, the conjugated 5 atom network which makes up the imide (blue). Third, the aliphatic cyclobutane core (green). Fourth and final are the  $R^1$  and  $R^2$  groups which sit as pendants to the direction of the polymer backbone (yellow).



*Figure 11: The four major portions of a CBI.*

Because of this, the synthesis of CBIs was analyzed from a retrosynthetic standpoint (**Figure 12**). Direct imidization is shown on the left. The second path, through the middle, was the synthesis of an imide from the maleic anhydride derivative. The third path, on the right, begins with a

maleimide derivative onto which the desired R<sup>3</sup> group is installed via *N*-alkylation. All synthetic pathways here may begin with a maleic anhydride derivative.

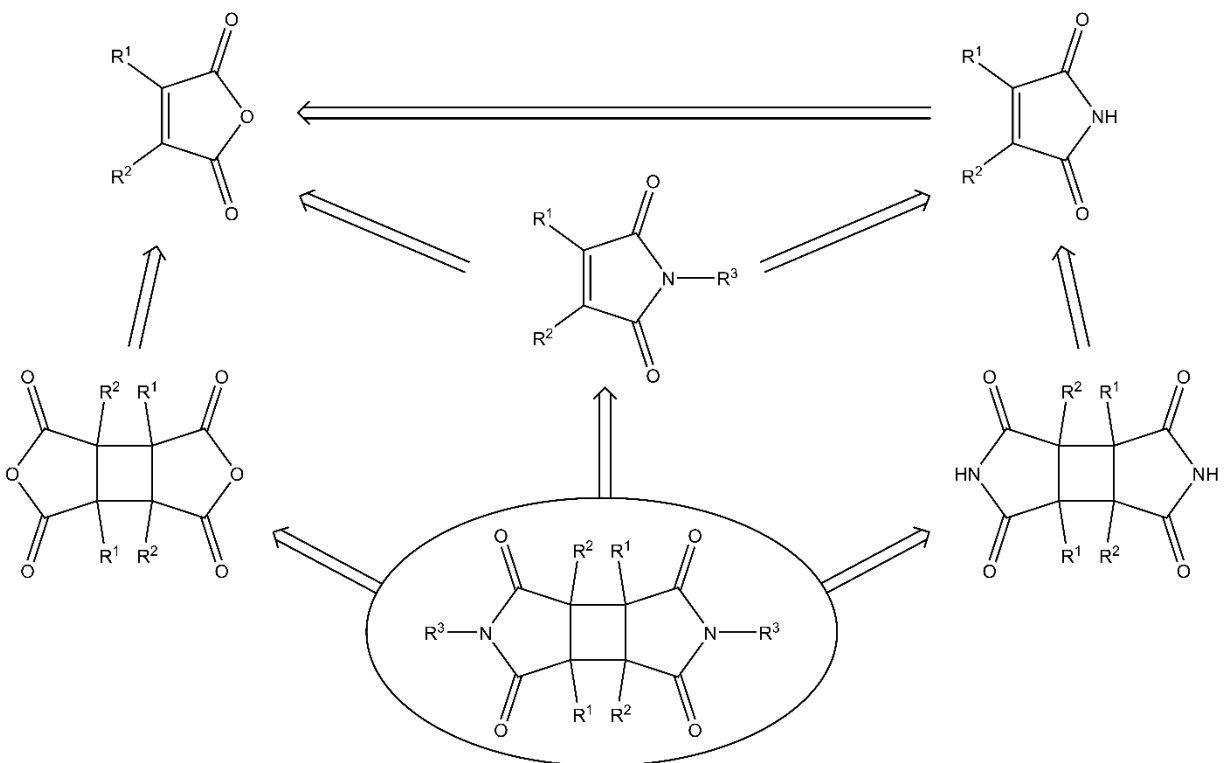


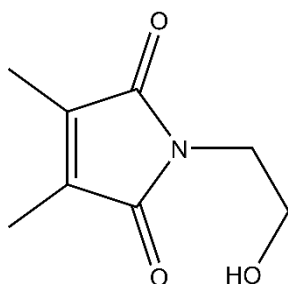
Figure 12: Retrosynthetic analysis of a generic CBBI showing the many ways to assemble the 4 core portions and achieve the desired skeletal core.

## Experimental

### Synthesis of *N*-(2-hydroxyethyl)-1,2-dimethylmaleimide (protoCBDO-2)

12.0702g of dimethyl maleic anhydride (DMMA) and 13.0063g (2.2eq) of 1-aminoethanol were placed in a 500mL round bottom flask with 300mL of toluene and a stir bar. The flask was fitted with a Dean-Stark trap and a Vigreux column. The mixture was set to reflux while stirring for 6 hours at which time the flask was removed from heat and covered in foil to protect from exposure to light. No liquid was observed in the Dean-Stark trap. The mixture was extracted with 1x 100mL

1M HCl, 1x 50 mL NaHCO<sub>3</sub>, and 2x 50mL NaCl. The organic layer had little to no product so the aqueous layer was extracted with EtOAc which also resulted in little to no product in the organic layer. The aqueous layer was evaporated to dryness. 20mL of DI H<sub>2</sub>O was placed in the flask to dissolve the solids and the solution was extracted with 3x 50mL EtOAc. The organic layer was evaporated and left on high vac overnight. 7.9163g (49% yield) of yellow, oily product were collected in a vial. Upon sitting in the storage vial for a few hours, the oil solidified to a hard, yellowish solid.

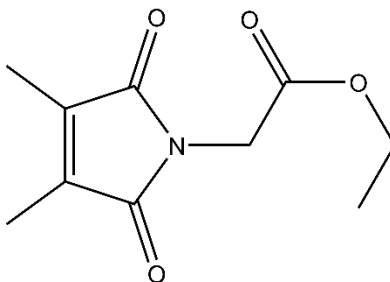


<sup>1</sup>H-NMR (400 Hz, DMSO-d<sub>6</sub>) δ 4.75 (s, 1H), 3.45 (m, 4H), 1.90 (s, 6H); <sup>13</sup>C-NMR (100 Hz, DMSO-d<sub>6</sub>) δ 172.26, 137.05, 58.49, 40.53, 8.87. FT-IR (ν<sub>max</sub>, cm<sup>-1</sup>): 3503 (m, OH stretching), 2888-2981 (w, CH stretches), 1689 (s, C=O stretching), 1675 (w, C=C stretching), 1436 (CH bending), 1403 (OH bending), 1362 (m, CH bending), 1336 (m, CH bending), 1242 (w, CN stretching), 1024 (m, CN stretching), 730 (s, C=C bending).

*Synthesis of N-(ethyl ethanoate)-1,2-dimethylmaleimide (protoCBDE-6)*

2.0260g of DMMA<sub>n</sub> and 2.8781g (1.25eq) of glycine ethyl ester hydrochloride were added to a 100mL round bottom flask with 50 mL toluene and a stir bar. 1.2175g of Na<sub>2</sub>CO<sub>3</sub> was added to the solution. The flask was fitted with a Vigreux column and left to reflux for 18 hours. The organic layer was washed with 1x 20 mL 1M HCl, 1x 10mL 1M HCl, and 2x 10mL brine. The organic layer

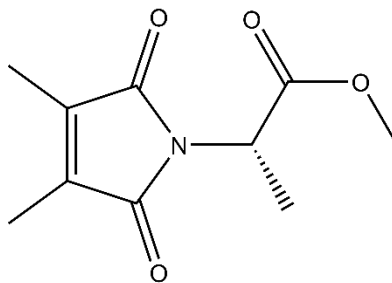
was evaporated under reduced pressure and left in an oil bath at 40°C under a high vac overnight. 2.8691g of white solid product was obtained. Structure was determined unambiguously via SCXRD.



$^1\text{H-NMR}$  (400 Hz, DMSO- $d_6$ )  $\delta$  4.22 (s, 2H), 4.13 (q,  $J = 7.07$  Hz, 2H), 1.94 (s, 6H), 1.19 (t,  $J = 7.08$ , 3H);  $^{13}\text{C-NMR}$  (100 Hz, DMSO- $d_6$ )  $\delta$  171.45, 168.24, 137.87, 61.73, 39.16, 14.43, 8.96. FT-IR ( $\nu_{\text{max}}$ ,  $\text{cm}^{-1}$ ): 2981 (w, CH stretching), 1733 (s, C=O stretching from ester), 1699 (s, C=O stretching from imide), 1669 (m, C=C stretching), 1429 (CH bending), 1390 (m, CH bending), 1374 (m, CH bending), 1215 (CN stretching), 1099 (m, CO stretching), 1019 (m, CO stretching), 974 (s, CH bending), 741 (C=C bending).

*Synthesis of N-((S)-methyl 1-methylethanoate)-1,2-dimethylmaleimide (protoCBDE-7)*

0.9998g DMMAAn, 1.2957g (1.2eq) L-alanine methyl ester hydrochloride, and 1.4g (1.3eq) were placed in a 100mL round bottom flask with 50mL toluene. The flask was fitted with a water-cooled Liebig condenser and refluxed in an oil bath for 18 hours. The reaction was washed with 2x 20mL 1M HCl, and 2x 20mL brine. The organic layer was dried over  $\text{CaCl}_2$  and set in an oil bath at 50°C under high vac overnight. 0.4492g (27% yield) of pure product was obtained and verified via  $^1\text{H-NMR}$ . Pure compound was liquid at room temperature.

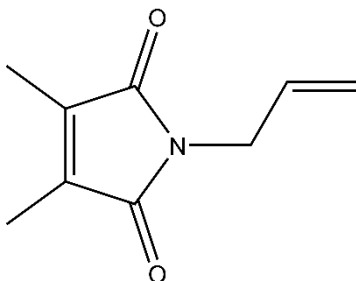


$^1\text{H-NMR}$  (400 Hz, DMSO- $d_6$ )  $\delta$  4.78 (q,  $J = 7.10$  Hz, 1H), 3.63 (s, 3H), 1.92 (s, 6H), 1.46 (d,  $J = 7.16$ , 3H);  $^{13}\text{C-NMR}$  (100 Hz, DMSO- $d_6$ )  $\delta$  171.27, 170.67, 137.64, 52.94, 47.11, 15.44, 8.92. FT-IR ( $\nu_{\text{max}}$ ,  $\text{cm}^{-1}$ ): 2954 (w, CH stretching), 1746 (s, C=O stretching from ester), 1702 (s, C=O stretching from imide), 1436 (w, CH bending), 1399 (m, CH bending), 1229 (br, CN stretching), 1078 (m, CO stretching), 1030 (m, CO stretching), 733 (C=C bending).

*Synthesis of N-allyl-1,2-dimethylmaleimide (protoCBDV-1)*

6.4857g of DMMA and 8mL (2eq) of allylamine added to 250mL round bottom flask with 200mL toluene and stir bar. The solution became cloudy immediately upon combination of the starting materials and a large amount of white precipitate could be seen in the bottom of the flask. The flask was fitted with a Vigreux column and set in an oil bath with a temperature of 110°C. After 15 minutes, the solids redissolved but the solution remained cloudy. By 2.75 hours, the solution was no longer cloudy and droplets of insoluble material were visible suspended in solution. After 3.5 hours, the reaction was removed from heat, stoppered, and covered in foil to protect it from light. The reaction was washed with 1x 10mL H<sub>2</sub>O and 2x 10mL brine. The reaction was then placed under reduced pressure in a water bath around 40-50°C by use of a rotary evaporator to remove solvent. This was unsuccessful because the product evaporated with the toluene. Yield could not be determined due to loss of product and lack of isolated product. Structure

determined via  $^1\text{H-NMR}$  analysis with comparison to subsequent [2+2]photocycloaddition dimerization.



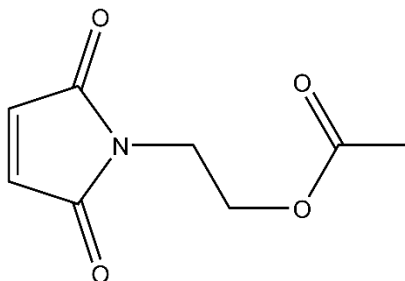
$^1\text{H-NMR}$  (400 Hz, DMSO- $d_6$ )  $\delta$  5.78 (td,  $J = 16.88, 5.23$  Hz, 1H), 5.08 (d,  $J = 11.65$  Hz, 1H), 5.04 (d,  $J = 18.87$  Hz, 1H), 4.00 (d,  $J = 3.80$  Hz, 2H), 1.91 (s, 6H);  $^{13}\text{C-NMR}$  (100 Hz, DMSO- $d_6$ )  $\delta$  171.78, 137.24, 133.20, 116.47, 39.78, 8.89. FT-IR ( $\nu_{\text{max}}$ ,  $\text{cm}^{-1}$ ): 2922 (w, CH stretching), 1699 (s, C=O), 1432 (w, CH bending), 1399 (m, CH bending), 926 (br, C=C from allyl), 733 (s, C=C bending from ring).

*Synthesis of N-(ethyl-2-acetate)-maleimide (protoCBDAc-1)*

2.4441g ethanolamine was placed in 50mL round bottom flask with 30mL glacial acetic acid. 4.3678 maleic anhydride (MAN) was added in small batches to the solution with a stir bar. The reaction was stirred at room temperature for 10 minutes, then 5mL of concentrated  $\text{H}_2\text{SO}_4$  was added. The flask was then fitted with a Vigreux column and lowered into an oil bath at  $65^\circ\text{C}$  for 1 hour while stirring. Afterwards, the reaction was then neutralized using a saturated solution of  $\text{NaHCO}_3$  then extracted using EtOAc. The organic layer was washed with saturated  $\text{NaHCO}_3$  and  $\text{H}_2\text{O}$ . Evaporation of the solvent afforded white solids which showed likely product with AcOH contamination. The flask was placed in an oil bath at  $50^\circ\text{C}$  under high vac over night to afford 0.1484g (3% yield\*) of product as confirmed by  $^1\text{H-NMR}$ . Structure was determined unambiguously via SCXRD.



\*The extremely low yield was due to having spilled a large portion of the reaction mixture during initial neutralization and is not indicative of reaction efficiency.

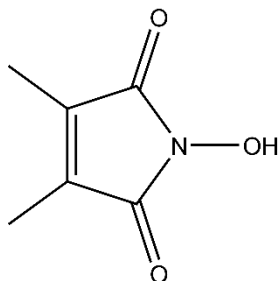


$^1\text{H-NMR}$  (400 Hz, DMSO- $d_6$ )  $\delta$  7.05 (s, 2H), 4.13 (t,  $J = 5.03$  Hz, 2H), 3.65 (t,  $J = 5.02$ , 2H), 1.94 (s, 3H);  $^{13}\text{C-NMR}$  (100 Hz, DMSO- $d_6$ )  $\delta$  171.31, 170.71, 135.11, 61.48, 36.89, 20.99. FT-IR ( $\nu_{\text{max}}$ ,  $\text{cm}^{-1}$ ): 3096 (m, CH stretching from alkene), 2981-2958 (w, CH stretches), 1772 (w, C=O stretching from ester), 1699 (s, C=O stretching from imide), 1432 (w, CH bending), 1399 (m, CH bending), 1338 (w, CN stretching), 1102 (m, CO stretching), 1068 (m, CO stretching), 968-926 (br, CH bending from alkene), 735 (C=C bending).

*Synthesis of N-dihydroxy-1,2-dimethylmaleimide (protoCBDH-1)*

3.1525g of DMMAAn, 8.4541g (4.8eq) of hydroxylamine hydrochloride, and 9.9820g (4.8eq) of sodium acetate were placed in a 200mL round bottom flask with 100mL of 1:1  $\text{H}_2\text{O}$ /ethanol solution with a stir bar. The flask was fitted with a water-cooled Liebig condenser. The reaction was refluxed in an oil bath for ~20 mins then removed from heat. The mixture was extracted using 3x 50mL EtOAc. The organic layers were combined and washed with 1x 50mL  $\text{H}_2\text{O}$  and 1x 50mL brine. The organic layer was concentrated under reduced pressure to afford a yellow liquid. Trituration with hexanes was attempted but was not successful.  $^1\text{H-NMR}$  analysis of the product showed the product was contaminated with EtOAc, EtOH, AcOH, and hexanes. The product was

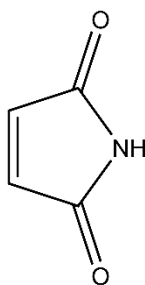
left under high vac overnight to afford 2.2583g (64% yield) of white solid.  $^1\text{H-NMR}$  and  $^{13}\text{C-NMR}$  analysis showed this was pure product. Structure was determined unambiguously via SCXRD.



$^1\text{H-NMR}$  (400 Hz, DMSO- $d_6$ )  $\delta$  10.24 (s, 1H), 1.89 (s, 6H);  $^{13}\text{C-NMR}$  (100 Hz, DMSO- $d_6$ )  $\delta$  168.82, 134.91, 9.08. FT-IR ( $\nu_{\text{max}}$ ,  $\text{cm}^{-1}$ ): 3223 (s br, OH stretching), 2981 (w, CH stretching), 1708 (s, C=O stretching), 1663 (m, C=C stretching), 1457 (m, NO stretching), 1383 (m, CH bending), 1334 (w, CN stretching), 1137 (m, CO stretching), 1091 (m, NO bending), 1021 (br, CH bending) 708 (C=C bending).

*Maleimide (protoCBI-2)*

Maleimide was used as purchased and is presented here for the sake of completeness.



$^1\text{H-NMR}$  (400 Hz, DMSO- $d_6$ )  $\delta$  10.88 (s, 1H), 6.89 (s, 2H);  $^{13}\text{C-NMR}$  (100 Hz, DMSO- $d_6$ )  $\delta$  173.21, 135.73.

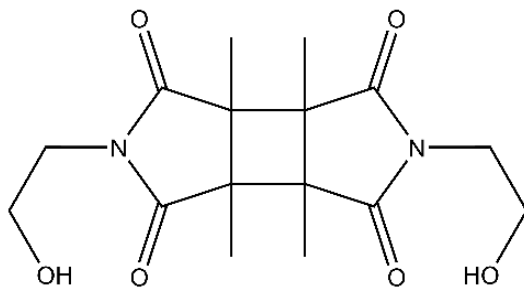
*Syntheses of N,N'-di(2-hydroxyethyl)-1,2,3,4-tetramethylcyclobuta[1,2-c:3,4-c']bisimide (CBDO-2)*

Synthetic Route 1:

1.1917g of protoCBDO-2 was placed in a 25mL round bottom flask with 30mL EtOAc. The solution was slightly cloudy. The flask was placed in between 4 UV-A bulbs. After 3 days of reaction time, crystals formed on the inner walls of the flask and the solution was clear and colorless. The crystals were knocked loose and collected via vacuum filtration to afford 0.9853g (83% yield) of pure CBDO-2. This was confirmed via  $^1\text{H-NMR}$  and  $^{13}\text{C-NMR}$  analysis. Structure was determined unambiguously via SCXRD. The supernatant was placed back into the lights to afford a second crop of product.

Synthetic Route 2:

0.0185g of protoCBDO-2 was crushed with a spatula and spread on the inner walls of a 4mL vial (Alternatively, the starting material was crushed between two glass plates). The vial was capped and placed in between 2 UV-A lights. After 3 days of reaction time,  $^1\text{H-NMR}$  analysis showed complete conversion to CBDO-2.



$^1\text{H-NMR}$  (400 Hz, DMSO- $d_6$ )  $\delta$  4.91 (t,  $J$  = 4.88 Hz, 2H), 3.59 (d,  $J$  = 4.44 Hz, 4H), 3.55 (d,  $J$  = 4.66 Hz, 4H), 1.10 (s, 12H);  $^{13}\text{C-NMR}$  (100 Hz, DMSO- $d_6$ )  $\delta$  178.23, 57.36, 49.18, 41.64, 12.65. FT-IR ( $\nu_{\text{max}}$ ,  $\text{cm}^{-1}$ ): 3488 (m, OH stretching), 2984-2949 (w, CH stretches), 1689 (s, C=O stretching), 1413

(m, CH bending), 1413 (m, OH bending), 1335 (s, CH bending), 1336 (m, CH bending), 1048 (m, CN stretching).

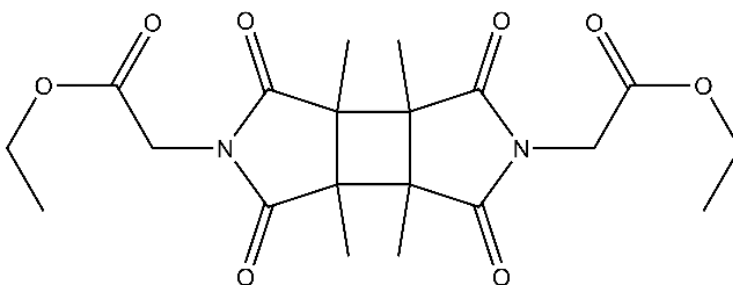
*Syntheses of N,N'-di(ethyl ethanoate)-1,2,3,4-tetramethylcyclobuta[1,2-c:3,4-c']bisimide (CBDE-6)*

Synthetic Route 1:

Same procedures as *CBDO-2: Synthetic Route 1*.  $^1\text{H-NMR}$  analysis showed ~50% conversion of protoCBDE-6 to CBDE-6 after 3 days reaction time. Structure was determined unambiguously via SCXRD.

Synthetic Route 2:

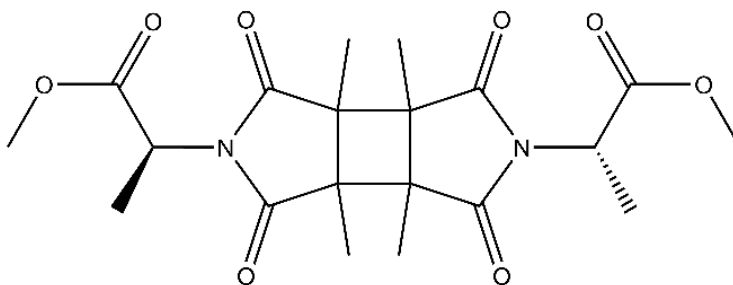
Same procedures as *CBDO-2: Synthetic Route 2* to produce CBDE-6 from protoCBDE-6 in quantitative yield.



$^1\text{H-NMR}$  (400 Hz, DMSO- $d_6$ )  $\delta$  4.30 (s, 4H), 4.19 (q,  $J = 7.11$  Hz, 4H), 1.23 (t,  $J = 7.11$ , 6H), 1.18 (s, 12H);  $^{13}\text{C-NMR}$  (100 Hz, DMSO- $d_6$ )  $\delta$  177.30, 167.48, 62.17, 49.78, 14.41, 12.56. FT-IR ( $\nu_{\text{max}}$ ,  $\text{cm}^{-1}$ ): 2981 (w, CH stretching), 1744 (s, C=O stretching from ester), 1705 (s, C=O stretching from imide), 1412 (CH bending), 1383 (m, CH bending), 1333 (m, CH bending), 1220 (s, CN stretching), 1151 (m, CO stretching), 1008 (m, CO stretching), 796 (s, CH bending).

*N,N'*-di((*S*)-methyl 1-methylethanoate)-1,2,3,4-tetramethylcyclobuta[1,2-*c*:3,4-*c'*]bisimide (CBDE-7)

0.1252g of protoCBDE-7 was placed in a 4mL vial with 4mL EtOAc. The vial was capped and placed between 2 UV-A bulbs. After 3 days reaction time, no precipitates had formed but <sup>1</sup>H-NMR analysis showed 100% conversion to product. Evaporation of solvent afforded 0.1106 (88% yield) of white solid. Structure was determined unambiguously via SCXRD using crystals recrystallized in EtOH.

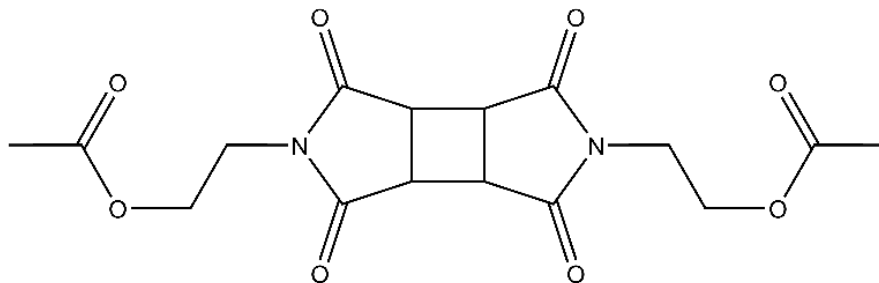


<sup>1</sup>H-NMR (400 Hz, DMSO-d<sub>6</sub>) δ 4.93 (q, J = 7.07 Hz, 2H), 3.69 (s, 6H), 1.49 (s, 3H), 1.47 (s, 3H), 1.17 (s, 6H), 1.13 (s, 6H); <sup>13</sup>C-NMR (100 Hz, DMSO-d<sub>6</sub>) δ 177.35, 176.71, 169.94, 53.06, 50.00, 49.20, 48.20, 14.29, 12.58, 12.44. FT-IR (ν<sub>max</sub>, cm<sup>-1</sup>): 2981-2953 (w, CH stretches), 1745 (s, C=O stretching from ester), 1704 (s, C=O stretching from imide), 1456 (w, CH bending), 1380 (m, CH bending), 1224 (br, CN stretching), 1168 (m, CO stretching), 1077 (m, CO stretching), 841 (m, CH bending).

*Synthesis of N,N'*-di(ethyl-2-acetate)-cyclobuta[1,2-*c*:3,4-*c'*]bisimide (CBDAC-1)

0.0586g of protoCBDAC-1 was placed in a 4mL vial with 4mL EtOAc. The solids were sparingly soluble and required sonication to fully dissolve. The vial was placed between 4 UV-A lights. After 3 hours of reaction time, crystalline precipitate was observed in the bottom of the vial. The solids

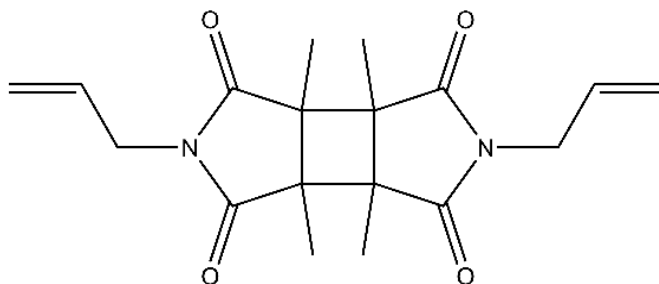
were collected via vacuum filtration to afford 0.0471g (80% yield) of pure product as determined via  $^1\text{H-NMR}$  analysis.



$^1\text{H-NMR}$  (400 Hz, DMSO- $d_6$ )  $\delta$  4.20 (t,  $J = 5.2$  Hz, 4H), 3.70 (t,  $J = 5.2$  Hz, 4H), 3.32 (s, 4H), 1.98 (s, 6H);  $^{13}\text{C-NMR}$  (100 Hz, DMSO- $d_6$ )  $\delta$  176.28, 171.07, 60.73, 41.73, 38.58, 21.02.

*Synthesis of N,N'-diallyl-1,2,3,4-tetramethylcyclobuta[1,2-c:3,4-c']bisimide (CBDV-1)*

20mL of the remaining reaction mixture from synthesis of protoCBDV-1 was placed in a 20mL glass vial. The vial was placed between 4 UV-A bulbs. After 1 day of reaction time, solid precipitate was observed at the bottom of the vial. Upon cooling, more solids precipitated. All solids were collected via vacuum filtration and washed with  $\text{Et}_2\text{O}$  to afford 0.1827g of pure product. Structure determined via  $^1\text{H-NMR}$ ,  $^{13}\text{C-NMR}$ , DEPT135, HSQC, HMBC, and COSY.

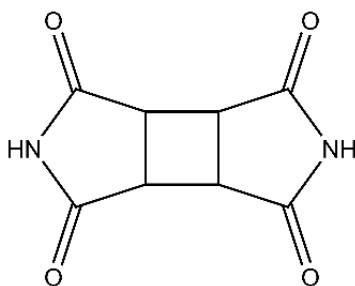


$^1\text{H-NMR}$  (400 Hz, DMSO- $d_6$ )  $\delta$  5.82 (m, 2H), 5.25 (d,  $J = 19.45$  Hz, 2H), 5.21 (d,  $J = 10.85$ , 2H), 4.07 (d,  $J = 5.67$ , 4H), 1.06 (s, 12H);  $^{13}\text{C-NMR}$  (100 Hz, DMSO- $d_6$ )  $\delta$  177.41, 131.74, 119.10, 49.41, 41.31,

12.82. FT-IR ( $\nu_{\max}$ ,  $\text{cm}^{-1}$ ): 2980 (w, CH stretching), 1699 (s, C=O stretching), 1625 (w, C=C stretching), 1424 (w, CH bending), 1387 (m, CH bending), 926 (w, C=C bending).

*Synthesis of N,N'-dihydro-cyclobuta[1,2-c:3,4-c']bisimide (CBBI-2)*

Procedure adapted from literature.<sup>25,26</sup> 0.1560g of maleimide was placed in a 200mL round bottom flask with 150mL ACN with a stir bar. The solution was degassed for several minutes with  $\text{N}_2$ . A cold finger was placed in the flask and cold tap water was allowed to flow through. The reaction was placed between 4 UV-A bulbs while stirring. After 18 hours reaction time, the suspended solids were collected via vacuum filtration to afford 0.1217g (78% yield) of slightly yellow, off-white pure product as determined by  $^1\text{H-NMR}$  and  $^{13}\text{C-NMR}$ .

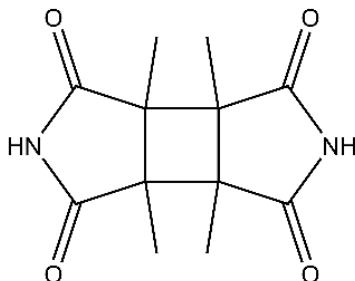


$^1\text{H-NMR}$  (400 Hz,  $\text{DMSO-d}_6$ )  $\delta$  11.63 (s, 2H), 3.30 (s, 4H);  $^{13}\text{C-NMR}$  (100 Hz,  $\text{DMSO-d}_6$ )  $\delta$  178.13, 42.97. FT-IR ( $\nu_{\max}$ ,  $\text{cm}^{-1}$ ): 3150-3072 (br, NH stretches), 3002-2981 (w, CH stretches), 1690 (s, C=O stretching), 1350 (w, CH bending), 1201 (m, CN bending), 828 (s, CH bending).

*Synthesis of N,N'-dihydro-1,2,3,4-tetramethylcyclobuta[1,2-c:3,4-c']bisimide (CBBI-1)*

0.2988g CBDAn-5 was placed in a 50mL round bottom flask. 4mL DI  $\text{H}_2\text{O}$  and 20mL of  $\text{NH}_4\text{OH}$  (23%  $\text{NH}_3$ ) was added to the flask along with a stir bar. The starting material was not immediately soluble. Reaction refluxed for 2 hours and removed from heat. Flask was stoppered and left to

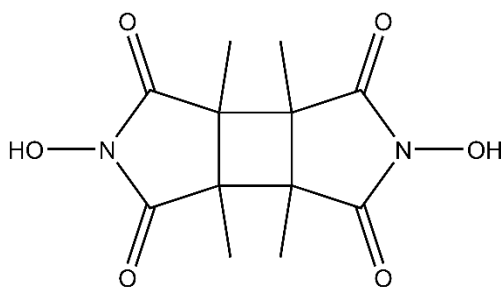
cool overnight. The resulting crystalline solids were collected via vacuum filtration to afford 0.1865g (63% yield) of pure product as determined via  $^1\text{H-NMR}$ .



$^1\text{H-NMR}$  (400 Hz, DMSO- $d_6$ )  $\delta$  11.67 (s, 2H), 1.07 (s, 12H);  $^{13}\text{C-NMR}$  (100 Hz, DMSO- $d_6$ )  $\delta$  179.49, 50.26, 12.87. FT-IR ( $\nu_{\text{max}}$ ,  $\text{cm}^{-1}$ ): 3206 (br, NH stretches), 2982 (w, CH stretches), 1689 (s, C=O stretching), 1374 (w, CH bending), 1316 (m, CN bending), 802 (s, CH bending).

*Synthesis of N,N'-dihydroxy-1,2,3,4-tetramethylcyclobuta[1,2-c:3,4-c']bisimide (CBDH-1)*

0.1340g of CBDAn-5, 0.4886g hydroxylamine hydrochloride, and 0.6425g NaOAc were placed in a 10mL round bottom flask with 6.5mL 1:1  $\text{H}_2\text{O}$ :ethanol and stir bar. The flask was fitted with a water cooled Liebig condenser and refluxed for 30 minutes. After cooling, product was extracted with EtOAc. Bulk isolated product not obtained but success determined via  $^{13}\text{C-NMR}$ . Structure was determined unambiguously via SCXRD from crystals recrystallized in ethanol.

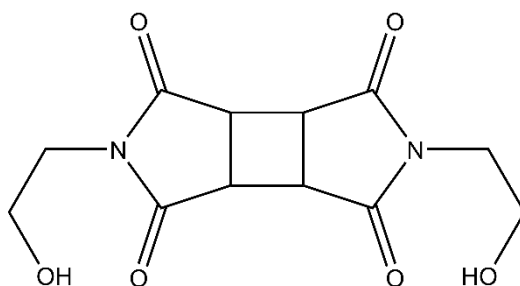


$^{13}\text{C-NMR}$  (100 Hz, DMSO- $d_6$ )  $\delta$  173.34, 47.11, 12.61.



*Synthesis of N,N'-di(2-hydroxyethyl)cyclobuta[1,2-c:3,4-c']bisimide (CBDO-3)*

0.8538 CBDAn-1 placed in a 25mL round bottom flask with 15mL ethanol. It did not dissolve. 0.7633 (~2eq) was transferred to the flask using 5mL ethanol. The flask was fitted with an air condenser and lowered into an oil bath at 100°C. After refluxing for 2.5 hours, most solids had dissolved and the solution was a translucent brown color. After an additional 2.5 hours of reflux (total 5 hours), the solution was milky and opaque. Solution was left to reflux overnight and 0.4307g (35% yield) of pure product precipitate was collected. The structure was determined via <sup>1</sup>H-NMR, <sup>13</sup>C-NMR, HSQC, and HMBC.

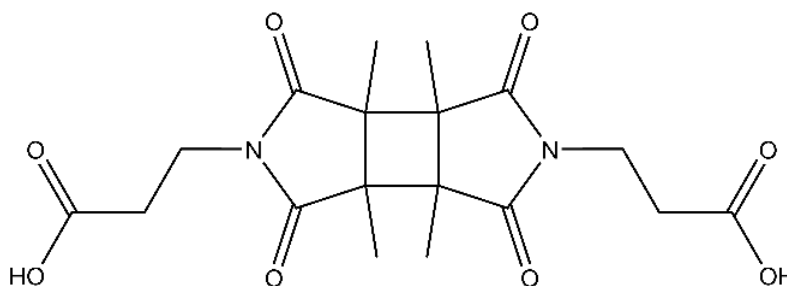


<sup>1</sup>H-NMR (400 Hz, DMSO-d<sub>6</sub>) δ 4.81 (s br, 2H), 3.52 (s, 8H), 3.32 (s, 4H); <sup>13</sup>C-NMR (100 Hz, DMSO-d<sub>6</sub>) δ 176.54, 57.59, 41.92, 41.44.

*Synthesis of N,N'-di(n-propanoic acid)-1,2,3,4-tetramethylcyclobuta[1,2-c:3,4-c']bisimide (CBDA-6)*

0.1006g CBBI-1, 0.1466g of 3-bromopropionic acid, and 0.2194g K<sub>2</sub>CO<sub>3</sub> were placed in a 25mL round bottom flask with 20mL DMF along with a stir bar. Solids did not completely dissolved even under vigorous stirring. Flask placed in oil bath at 160°C and left to reflux for 24 hours. The reaction was removed from heat and placed in the fridge for 2 days after which it was diluted with 250mL H<sub>2</sub>O and acidified with 1M HCl. It was then extracted with ~100mL EtOAc. The initial organic layer was washed with 4x 50mL H<sub>2</sub>O. The initial aqueous layer was washed with 2x 25mL

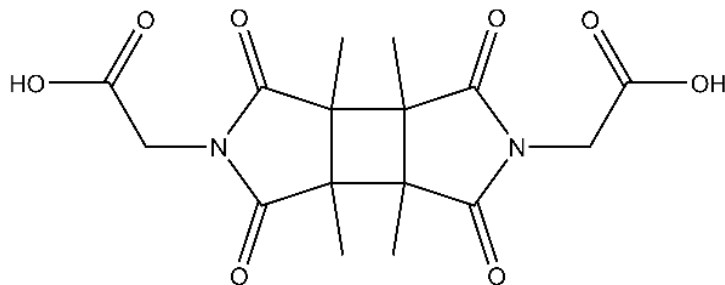
EtOAc. The organic layers were combined and the solvent evaporated to afford an off-white solid.  $^1\text{H-NMR}$  analysis determined it was mostly desired product contaminated with DMF and small amounts of starting material. After several more similar washes to remove DMF, pure product was obtained as determined by  $^1\text{H-NMR}$  and  $^{13}\text{C-NMR}$  analysis. Yield was not determined due to significant product loss during extraction.



$^1\text{H-NMR}$  (400 Hz, DMSO- $d_6$ )  $\delta$  12.49 (s, 2H), 3.67 (t,  $J = 6.75$  Hz, 4H), 2.61 (t,  $J = 6.72$  Hz, 4H), 1.05 (s, 12H);  $^{13}\text{C-NMR}$  (100 Hz, DMSO- $d_6$ )  $\delta$  177.86, 172.68, 49.22, 35.50, 31.85, 12.69.

*Synthesis of N,N'-di(ethanoic acid)-1,2,3,4-tetramethylcyclobuta[1,2-c:3,4-c']bisimide (CBDA-7)*

0.0033g CBDO-2 placed in 4mL vial with 1mL ACN and 1mL pyridine. The vial was shaken and sonicated to dissolve the starting material. 0.0492g  $\text{KMnO}_4$  was added which did not entirely dissolve. A stir bar was added and the solution was set to stir for 20 hours. 30%  $\text{H}_2\text{O}_2$  was added to the solution to remove excess  $\text{KMnO}_4$  until no more reaction was observed. Concentrated HCl was then added until the solution was colorless. The reaction was then extracted with 2x 40mL EtOAc. The organic layer was washed with brine then evaporated under reduced pressure to afford a very small amount of solids. These solids were dried under high vac for 2 days. Product determined via  $^1\text{H-NMR}$  and HSQC though  $^{13}\text{C-NMR}$  is inconsistent with expected spectra. Nonetheless, structure was determined unambiguously via SCXRD as a monohydrate.



$^1\text{H-NMR}$  (400 Hz, DMSO- $d_6$ )  $\delta$  13.37 (s, 2H), 4.18 (s, 4H), 1.17 (s, 12H);  $^{13}\text{C-NMR}$  (100 Hz, DMSO- $d_6$ )  $\delta$  177.48, 49.72, 31.17, 12.54.

*Synthesis of poly(hexamethylene N,N'-di(ethanoate)-1,2,3,4-tetramethylcyclobuta[1,2-c:3,4-c']bisimide) (PCBBI-1)*

Polymerization procedure adapted from literature<sup>27</sup> and previous work by the Chu Research Group.<sup>23</sup> 0.1059g of CBDE-6 was placed in a 10mL round bottom flask. 40 $\mu\text{L}$  of 1,7-heptandiol placed in vial with 2 mL toluene and 2 drops  $\text{Ti}(\text{OiPr})_4$ . This mixture was placed in the flask containing the CBDE-6. The vial used to weigh the diol was rinsed with 3mL and added to the reaction flask. An amount of the  $\text{Ti}(\text{OiPr})_4$  appeared to react with residual water present as evidenced by the appearance of bright white precipitate presumed to be  $\text{TiO}_2$ . The flask was fitted with a Liebig condenser and the top of the condenser was fitted with a balloon filled with nitrogen gas. The flask was placed in an oil bath at 120 $^\circ\text{C}$  and left to reflux for 18 hours. 5mL of DMF was added to the reaction and it was allowed to reflux ( $\sim 135^\circ\text{C}$ ) for 3.5 hours. After cooling, the reaction was washed with  $\text{H}_2\text{O}$  which caused precipitation of a slightly off-white solid. 0.0660g of this solid was collected via vacuum filtration.  $^1\text{H-NMR}$  analysis provided confirmation of CBBI-terminated monomeric repeat unit. HRMS analysis provided confirmation of mono-, di-, cycloid- and trimeric repeat units.

*Synthesis of N,N'-di(2-hydroxyethyl)-1,2,3,4-tetramethylcyclobuta[1,2-c:3,4-c']bisimide hexanoate)*  
(PCBBI-2)

Polymerization procedure adapted from literature<sup>27</sup> and previous work by the Chu Research Group.<sup>23</sup> 0.2585g adipic acid and 0.5045g CBDO-2 placed in 25mL round bottom flask with 16mL DMF. 10 drops of Ti(iOPr)<sub>4</sub> placed in solution, a portion of which formed a bright white precipitate presumed to be TiO<sub>2</sub>. The flask was fitted with a Vigreux condenser and placed in an oil bath at 110°C while stirring for 18 hours. The oil was turned up and the reaction was refluxed for several hours. Upon cooling, H<sub>2</sub>O was added to the solution and the resulting precipitate was collected via vacuum filtration to afford 0.4677 of very light, off-white polymer. Structure is not yet confirmed except for physical comparison to PCBBI-1.

## Results and Discussion

### *Description of a model CBBI*

The model CBBI structure, CBDO-2 (**Figure 13**), consists of the described core with R<sup>1</sup> and R<sup>2</sup> being methyl groups and R<sup>3</sup> being 2-hydroxyethyl functional groups. The nomenclature for this compound and all others follow the format established in previous work published by the Chu Research Group. In this format, multifunctional cyclobutane containing monomers are named with the format of CBx-n; where x is a one to three letter code signifying functional multiplicity (when greater than one) and the functional group identity, and n is the its sequence based on publication chronology.<sup>20,23,28</sup>

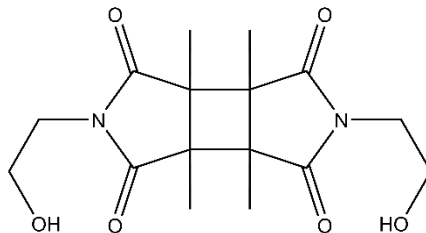


Figure 13: A model CBBI compound, cyclobutane diol 2, or CBDO-2.

According to the crystal structure (**Figure 14**), each ring within the CBBI skeleton, the two 5-member imide rings and the cyclobutane core, is planar. Previous studies have shown that the cyclobutane core of some CBs exists as a “puckered” ring which may assume more than one ring-flip conformation.<sup>23</sup> However, these planar rings themselves exist at  $110.7^\circ$  from one another. This creates a 3-dimensional, aliphatic “knot” within the polymer backbone. This is unique in that generally, bisimides exist as part of aromatic planes. As such, the imides are conjugated within these systems. The aliphatic cyclobutane core, in concert with aliphatic  $R^3$  groups, has the effect of breaking these electronic networks, isolating the conjugation to just the imide proper. Of particular note, this has the consequence of effecting no color in the compound (**Figure 15**), a property often sought in polymer chemistry. Since the bisimide skeleton is not altered in the prospective polymerizations, the resulting polymeric materials are likewise colorless. This is discussed in more detail later.

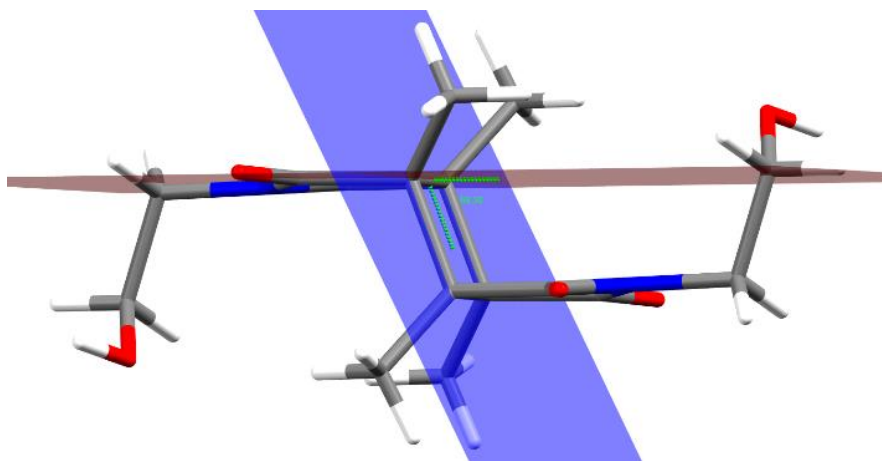


Figure 14: The crystal structure of CBDO-2 which shows the angle between the imide rings (blue) and the cyclobutane ring (red) to be  $110.7^\circ$ .

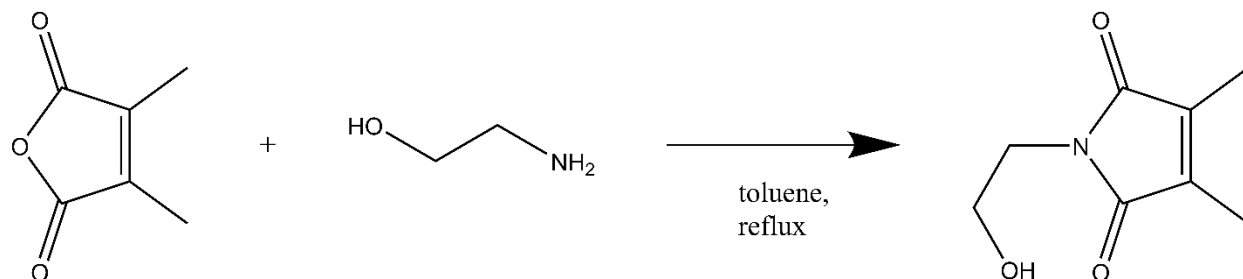


Figure 15: Crystals of CBDO-2 which exhibit no color.

#### *Synthesis of model compound*

*N*-(2-hydroxyethyl)-2,3-dimethylmaleimide (protoCBDO-2) was synthesized using a literature procedure.<sup>29</sup> This procedure is analogous to the first step of the central path in **Figure 12**. 1,2-

dimethylmaleic anhydride (DMMAAn) was stirred with ethanolamine in toluene at reflux (**Scheme 1**). Purification was achieved via column chromatography as per the reference.



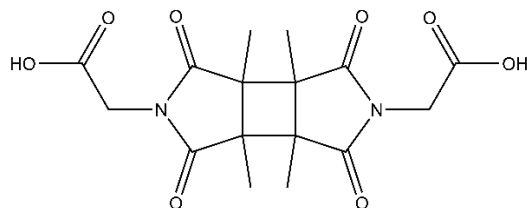
*Scheme 1: Synthesis of protoCBDO-2*

Solutions of protoCBDO-2 were prepared in ethyl acetate, acetonitrile, and acetone at approximately 40 mM. A sample of solid protoCBDO-2 was crushed and smeared on the inside walls of a vial identical to those used for the solutions. The three solutions and the solid-state reaction were all placed between 2 UV-A bulbs (15W). After 3 days, colorless crystalline precipitate was observed in ethyl acetate and acetone. The precipitate was confirmed to be CBDO-2 via <sup>1</sup>H-NMR and <sup>13</sup>C-NMR and SCXRD. The solid-state proceeded to product in 100% yield as confirmed via <sup>1</sup>H-NMR. It was also observed that residual solids of protoCBDO-2 had dimerized to CBDO-2 in the ambient light of the lab over the course of about 1 week. It should be noted that the bench where this flask was located is very near a window that gets ample sun exposure.

#### *Versatility of CBBI synthesis*

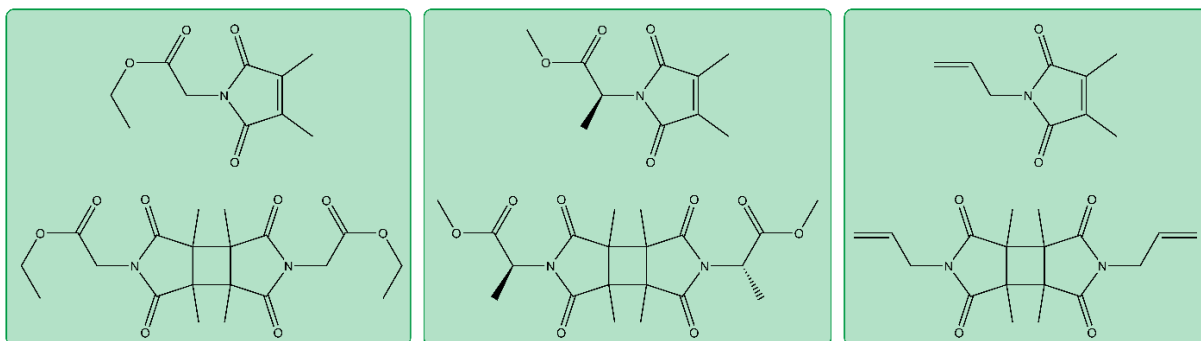
CBDO-2 was then stirred in a solution of ACN saturated with KMnO<sub>4</sub> for 18 hours. Hydrogen peroxide was added to the solution until no more gas evolved upon addition. This was followed by addition of 1 M HCl until the solution was colorless. Finally, the product was isolated via a

solvent extraction. After evaporation of solvent, product was allowed to sit under high vac for 48 hours. The resulting crystals were the oxidated product, CBDA-7 (**Figure 16**).



*Figure 16: Cyclobutane diacid product, CBDA-7, obtained via oxidation of CBDO-2.*

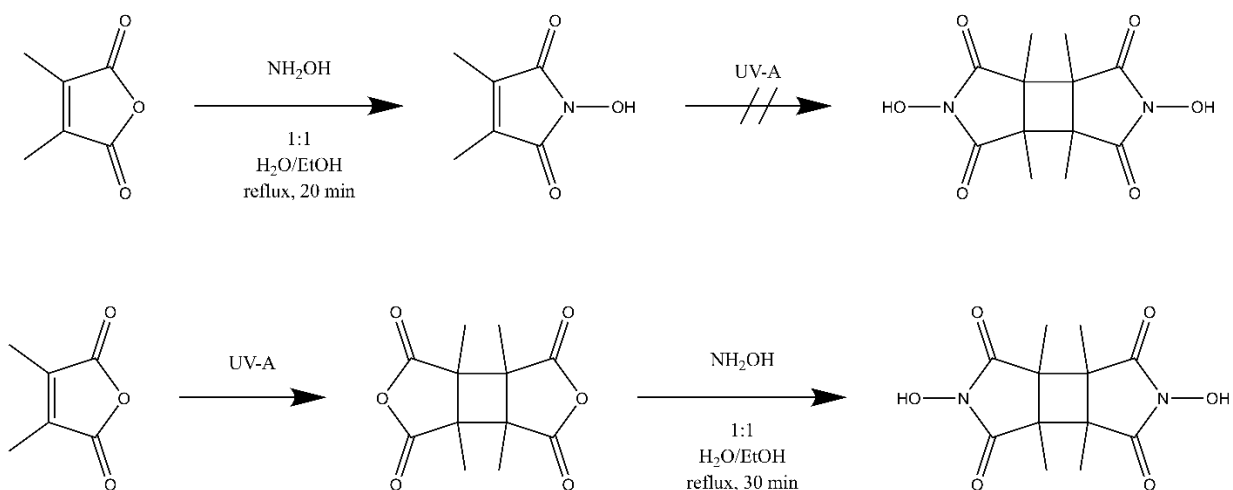
The efficiency of the [2+2] photocycloaddition step in the synthesis of CBDO-2 was surprising. Due to this, the generality of the process was explored and produced an additional 3 CBBI building blocks (**Figure 17**) using very a similar procedure. Two cyclobutane diesters, CBDE-6 and CBDE-7, were synthesized from glycine ether ester HCl and L-alanine methyl ester HCl, respectively. Although CBDE-7 was a solid at room temperature, protoCBDE-7 was a liquid and remained liquid even when placed in a refrigerator. Both CBDE-6 and protoCBDE-6 were solids at room temperature. This suggests that sidechains on R<sup>3</sup> interrupt packing of the molecules which may increase solubility, an important aspect of polymer processibility.



*Figure 17: Three protoCBBI structures, protoCBDE-6 (top left), protoCBDE-7 (top middle), and protoCBDV-1 (top right). Below each is the corresponding CBBI monomer, CBDE-6 (bottom left), CBDE-7 (bottom middle), and CBDV-1 (bottom right).*



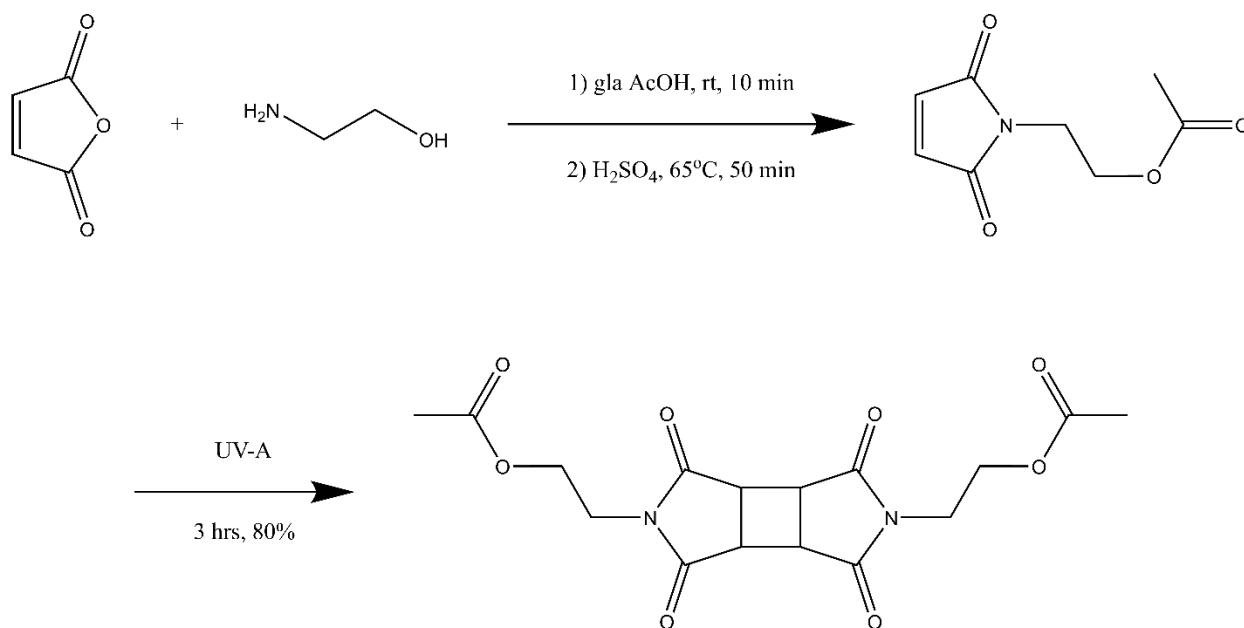
*N*-hydroxy-2,3-dimethylmaleimide (protoCBDH-1) was synthesized from DMMA and hydroxylamine. These were stirred together for 20 min in a 1:1 solution of water/ethanol at reflux (**Scheme 2a**).<sup>30</sup> The product was isolated via solvent extraction and characterized via <sup>1</sup>H-NMR, <sup>13</sup>C-NMR, and SCXRD. Samples of solid protoCBDH-1 were placed between 4 UV-A bulbs (15W), but even after several days, no product was observed. Initial inspection of the crystal structure showed that the molecule assumes a helical structure networked by hydrogen bonds. This packing does conform to the Schmidt principles<sup>31</sup> and thus the fact that protoBDH-1 does not undergo dimerization is surprisingly. To circumvent the possibility of other solid-state limitations, solution phase dimerization was attempted. Solutions of protoCBDH-1 were made in EtOAc, acetone, and ACN. After sitting between 4 UV-A bulbs (15W) for 2 days, no reaction was observed as monitored by <sup>1</sup>H-NMR. Because of this, protoCBDH-1 was unique in the series of protoCBs in that it was completely photo-inert. It was also unique in the series in that it was the only CBBI with an N-O bond. Investigations are currently underway to understand if and how this moiety inhibits the [2+2] photocycloaddition.



*Scheme 2: a) Synthesis of CBDH-1 showing that while the synthesis of protoCBDH-1 was successful, the key step of [2+2] photocycloaddition was not. b) Synthesis of CBDH-1 showing that swapping the order of the reactions results in success.*

Initial attempts to recreate the success of the previous with maleic anhydride (MAN) were unsuccessful. This is likely the case because maleic acid and fumaric acid, the products to which MAN readily hydrolyzes, are much less reactive to amines to produce the amic acid precursor necessary for imidization. For a similar reason, when an amic acid does form, the cyclization to the imide is not favored.

Considering this, an alternative route was adapted from literature.<sup>32</sup> MAN was gently heated in a solution of glacial acetic acid with ethanolamine. After about 30 minutes, concentrated sulfuric acid was added and the temperature increased. Purification was performed via solvent extraction after neutralization. While the imidization did take place, the <sup>1</sup>H-NMR showed that the hydroxyl group was unintentionally acetylated. This product, protoCBDAc-1, readily dimerized to CBDAc-1 in 3 hours at 80% yield (**Scheme 3**).



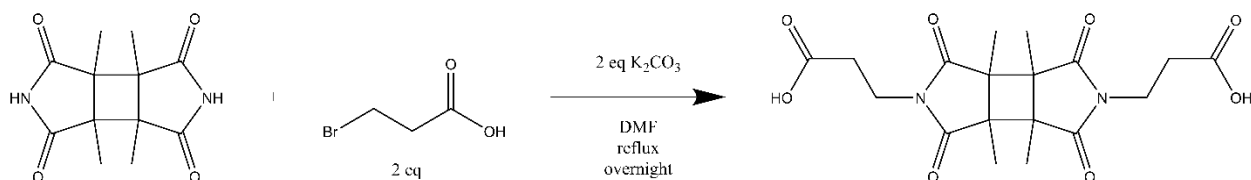
*Scheme 3: Synthesis of CBDAc-1*

To avoid the deactivation of the key photochemical step and explore the synthesis of CBBIs via dianhydrides, *trans*-cyclobutane-1,2,3,4-tetracarboxylic dianhydride (CBDAn-1) was synthesized as a starting material. This was done using a procedure developed by our group which directly irradiates MAN in ethyl acetate using 4 UV-A bulbs (15W). *Trans*-cyclobutane-1,2,3,4-tetramethyl-1,2,3,4-tetracarboxylic dianhydride (CBDAn-5) was similarly synthesized by direct irradiation of DMMA in ethyl acetate using 4 UV-A bulbs (15W). In both cases, a small amount of crystalline product precipitated after a couple hours; but the reaction was allowed to proceed over 3 days for CBDAn-1 to afford 70% yield and 4 days for CBDAn-5 to afford a 95% yield. The lower comparative yield in the former was likely due to the aforementioned labile hydrolysis of the starting material into maleic acid and fumaric acid, neither of which is photoactive in solution.

CBDH-1 was successfully synthesized using similar conditions to the synthesis of protoCBDH-1, except using CBDAn-5 in place of DMMA (**Scheme 2b**). Similarly, CBDO-3 was synthesized by

stirring CBDAn-1 with ethanolamine in ethanol at reflux. By using an alternate synthetic pathway, it was possible to achieve a desired product that was difficult or impossible to synthesize via the previous method.

Finally, in preparation for the final synthetic route, the halo-imide coupling (**Scheme 4**), two unsubstituted bisimides were synthesized. First, *trans*-1,2,3,4-tetramethylcyclobutanebisimide (CBBI-1) was synthesized by stirring CBDAn-5 in an aqueous solution of ammonium hydroxide (19% NH<sub>3</sub>) at reflux for 2 hours. Upon cooling, CBBI-1 precipitates out in about 60% yield. More product may be recovered by concentrating the reaction and washing the solids to remove any residual amic acid intermediates. *Trans*-cyclobutanebisimide (CBBI-2) was synthesized by direct photodimerization of maleimide in ACN in accordance with literature procedures<sup>25,33</sup> with the exception of using 6 UV-A bulbs (15W) in lieu of a photoreactor lamp. The solution was prepared at about 0.01 M concentration of maleimide. The flask was fitted with a cold finger through which cold tap water was circulated. It was found that higher concentrations and omission of the cold finger, thereby allowing the solution to heat to ~40°C, caused a significant formation of maleimide homopolymer. This was identified by the presence of strong, broad peaks in the <sup>1</sup>H-NMR which overlapped those for the desired product. By following these criteria, CBBI-2 precipitates as a slightly off-white solid which may be easily collected via filtration and the ACN may be recycled for subsequent reactions.



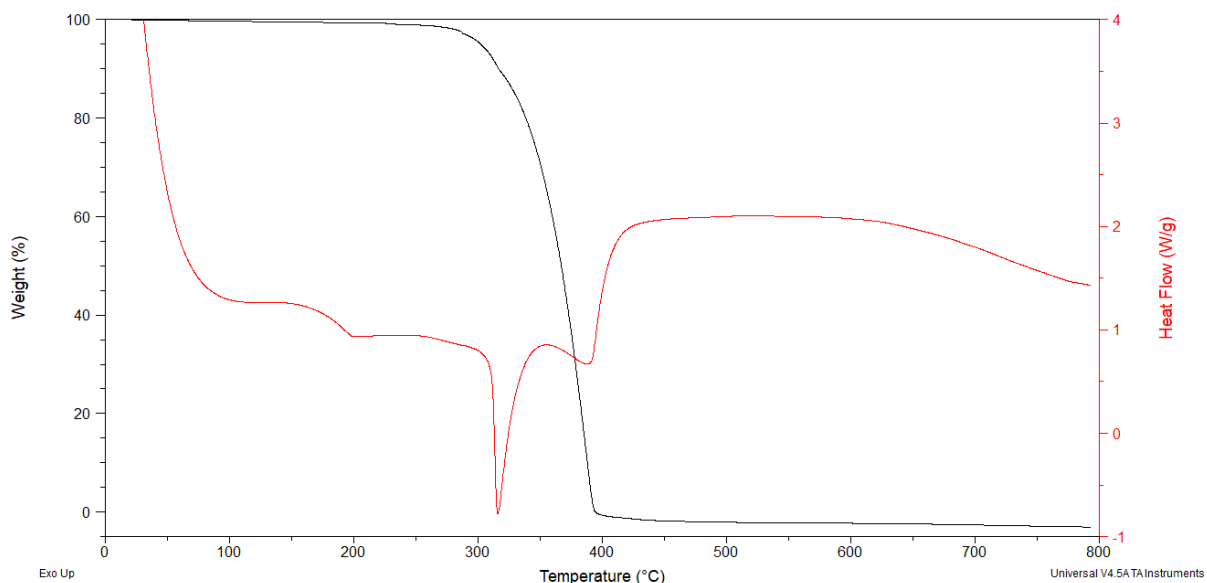
*Scheme 4: Synthesis of CBDA-6 via halo-imide coupling.*

CBBI-1 was stirred with 3-bromopropionic acid and potassium carbonate in a solution of DMF at reflux overnight. After allowing the solution to cool, precipitate was collected.  $^1\text{H-NMR}$  showed product with DMF impurity. After several washes to remove DMF, pure CBDA-6 was obtained.

#### *Thermal properties of select CBBIs*

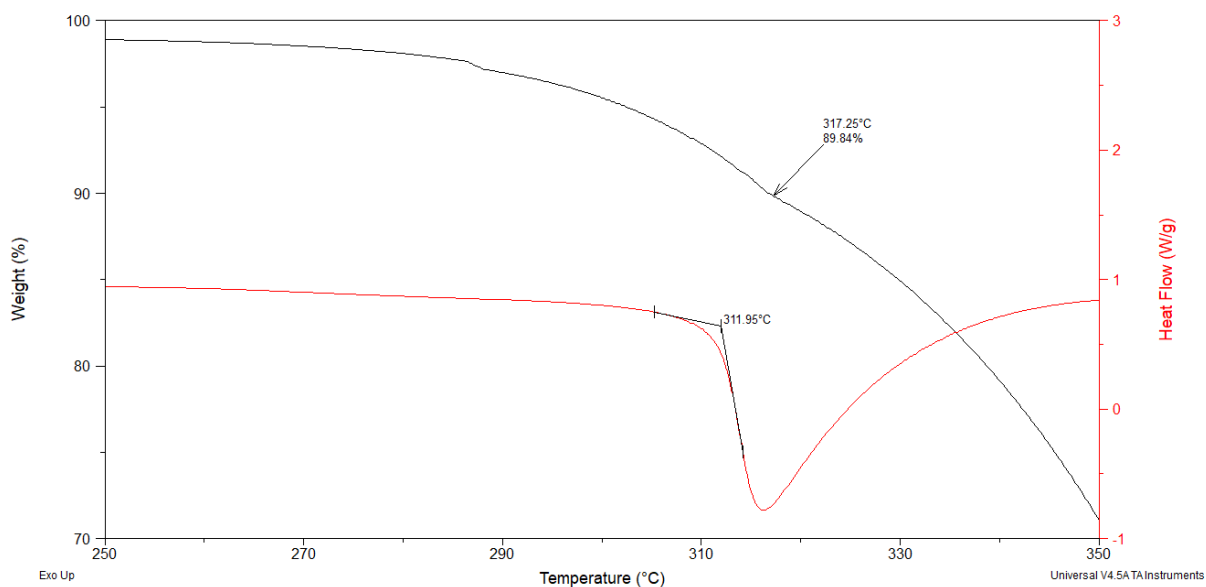
Initial melting point measurement of several CBBIs were inconclusive due to having melting points higher than the maximum of the melting point apparatus ( $260^\circ\text{C}$ ). Melting points for select CBBIs were determined via TGA/DSC measurements as part of routine thermochemical property analysis.

The full TGA/DSC data for CBDO-2 is found in **Figure 18**. Typically, the shape of the step around  $175^\circ\text{C}$  indicates a glass transition temperature in polymeric materials. Here, it is likely a shift in the crystal packing to a polymorph more stable at elevated temperatures.

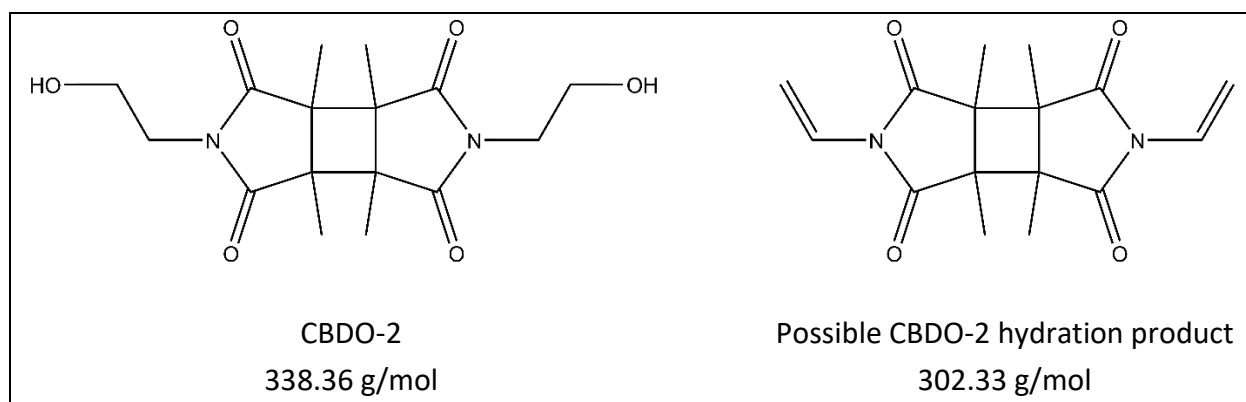


*Figure 18: TGA (black line) and DSC (red line) of CBDO-2 from  $25^\circ\text{C}$  to  $800^\circ\text{C}$  with ramp rate  $20^\circ\text{C}/\text{min}$ .*

Close inspection of the graph (**Figure 19**), shows that melting of the material at 312°C is concurrent with dehydration of the hydroxy functional groups on either side of the CBBI core. The inflection point at ~11.1% mass loss is consistent with 2 eq of water loss (36 g/mol) to produce a cyclobutane divinyl (**Figure 20**). No attempts at isolating this product were attempted.

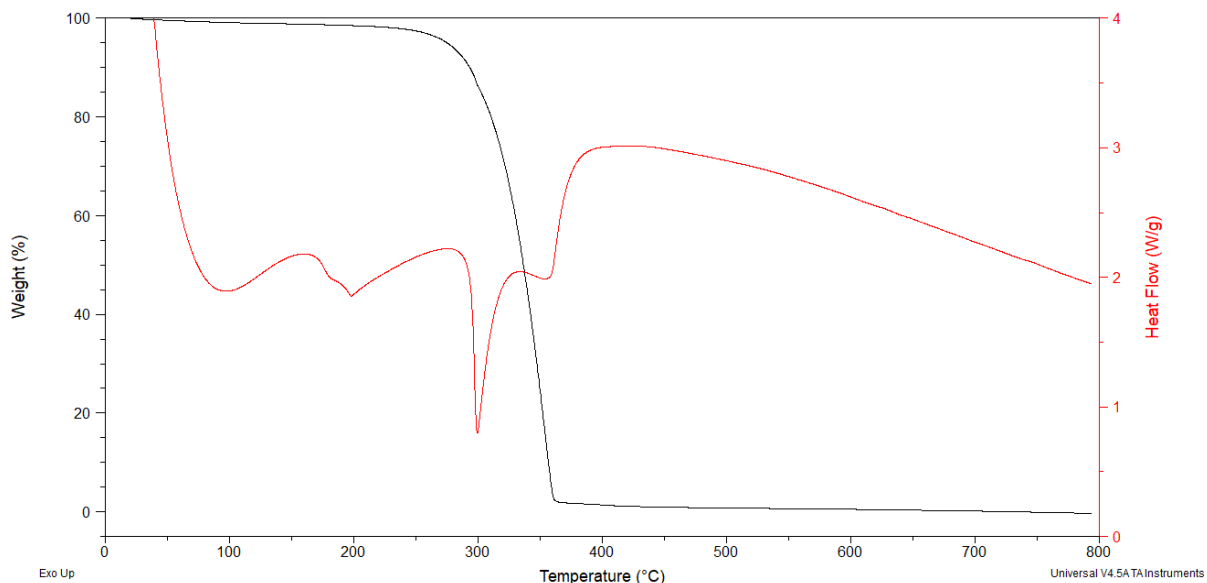


*Figure 19: Detail of Figure 18 showing concurrent melt and dehydration of CBDO-2.*



*Figure 20: CBDO-2 and the possible thermal dehydration product formed at 317°C.*

TGA/DSC of **CBDE-6** show very similar thermal events (**Figure 21**). The presence of a similar endothermic step at  $\sim 175^\circ\text{C}$  suggests that this polymorphic shift may be related to the common CBBI core of each compound. However, **CBDE-6**, shows a multistep shift absent in **CBDO-2**.



*Figure 21: TGA (black line) and DSC (red line) of CBDE-6 from  $25^\circ\text{C}$  to  $800^\circ\text{C}$  with ramp rate  $20^\circ\text{C}/\text{min}$ .*

As in the previous example, the TGA for **CBDE-6** has an inflection point at  $299^\circ\text{C}$  which coincides with the melting point of the material at  $295^\circ\text{C}$  (**Figure 22**). However, this is not a dehydration of the CBBI unit, but degradation of the ethyl ester moieties.

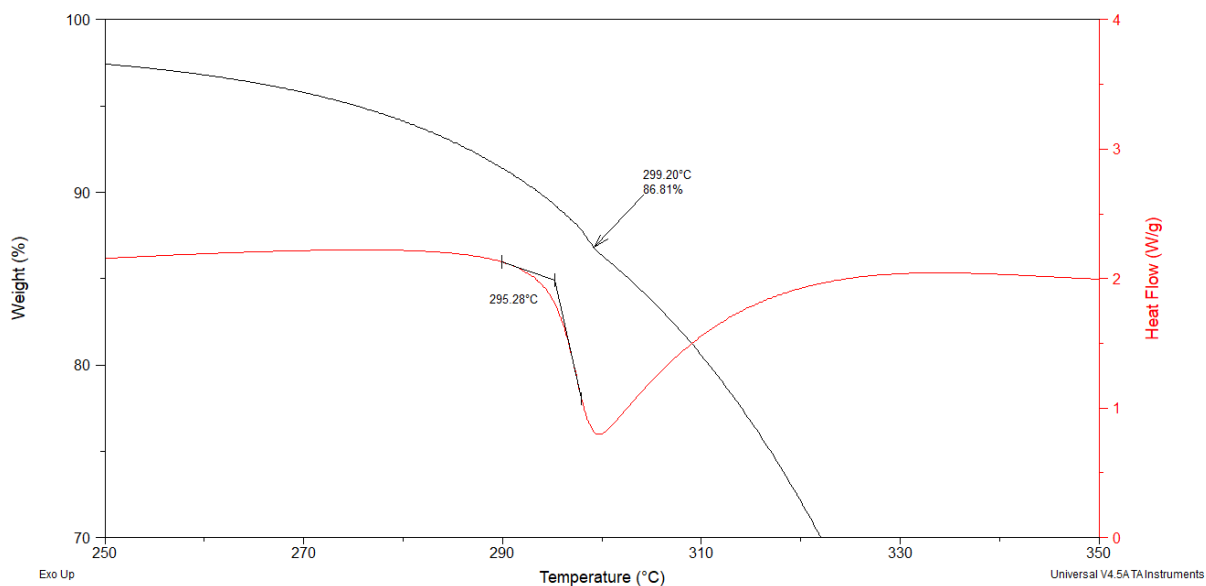


Figure 22: Detail of 7 showing concurrent melt and degradation of CBDE-6, likely to CBDA-6.

At such elevated temperatures, esters with  $\beta$ -hydrogens can undergo a retro-ene reaction giving an alkene and carboxylic acid as products (**Figure 23**). The mechanism proceeds through a six-member transition state in which the carbonyl abstracts the  $\beta$ -hydrogen from the alkyl ester. This allows the pericyclic cascade resulting in the net formation of 1  $\pi$ -bond and loss of a  $\sigma$ -bond. In the case of **CBDE-6**, these products are ethylene and, curiously, another novel product presented here, **CBDA-7**.

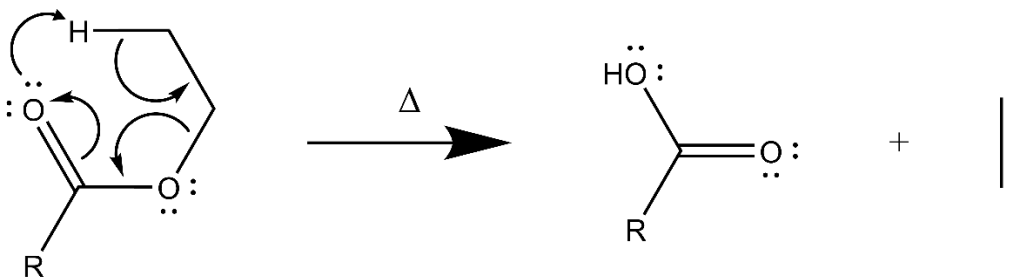


Figure 23: General mechanism for a retro-ene reaction of the type observed in the degradation of CBDE-6.



The inflection point at 13.2% mass loss is consistent with the loss of 2 eq of ethylene (56.11 g/mol) to produce **CBDA-7** ().

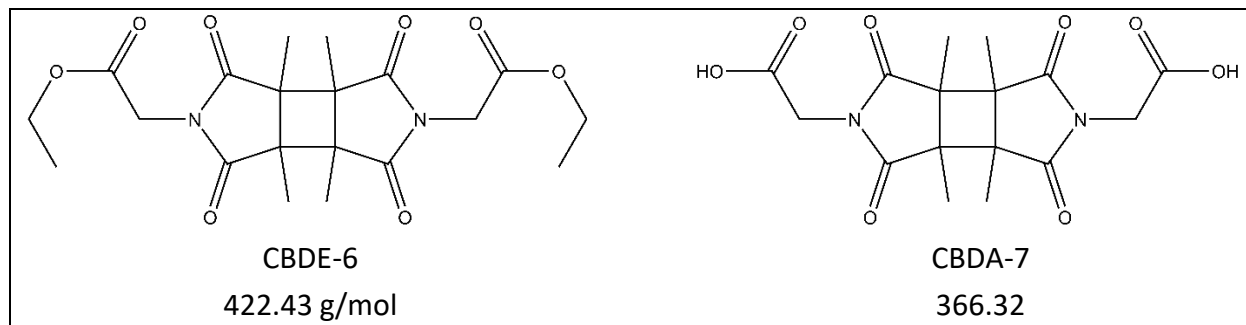


Figure 24: **CBDE-6** and the likely thermal degradation product formed at 299°C.

To investigate the hypothesis that the mass loss observed in **CBDO-2** was water, the thermal properties of **CBDV-1** were studied. This compound was chosen due to its similarities to the theorized dehydration product of **CBDO-2**. No mass loss with an inflection point should be observed because there are no moieties which are susceptible to dehydration. As shown in **Figure 25**, this is what was observed. Additionally, **CBDV-1** showed a much lower melting point which is likely due to the absence of hydrogen bond donors. Despite this, the compound is still remarkably stable. It was hypothesized that the material may polymerize at high temperatures, but there were no obvious indications of this. The melting peak shows a two-step process. It is possible that a step at ~175°C, similar to previous CBBIs, is present here, but is obfuscated by the melting point. This may explain the comparatively complex onset.

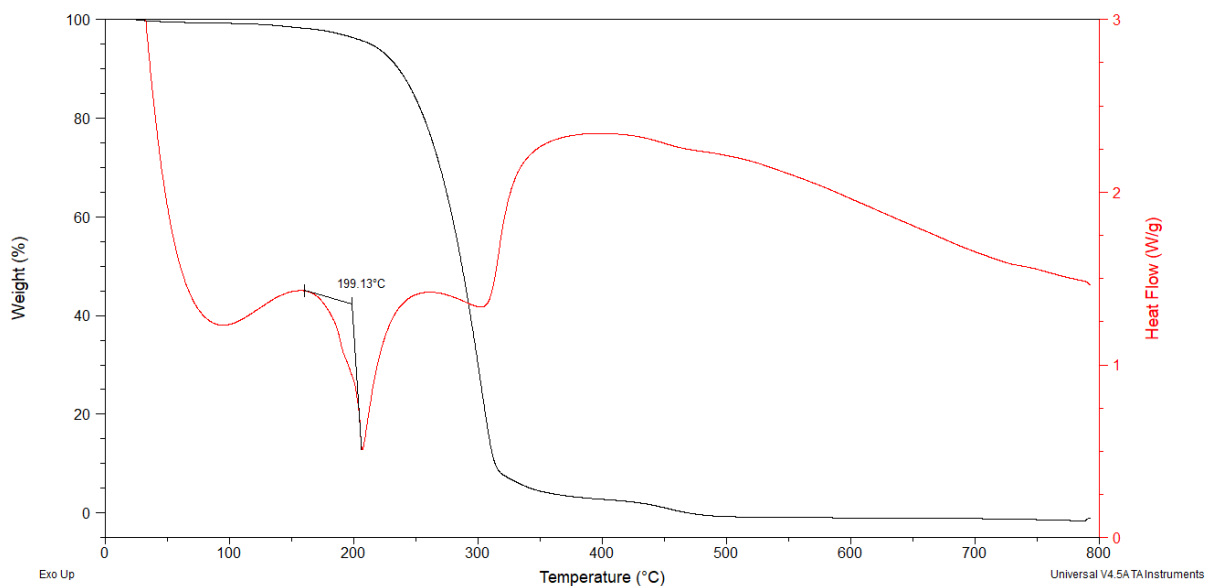


Figure 25: TGA (black line) and DSC (red line) of CBDV-1 from 25°C to 800°C with ramp rate 20°C/min.

Finally, the thermal properties of **CBDO-3** were investigated to study the thermal effect of substituents on the CB core (**Figure 26**). Like all previous CBs, there is a step around 175°C. This would suggest that if it is indicative of a polymorphic rearrangement, then it is not unique to the tetramethylated CBBI core. The melting point of 277°C is also only slightly lower than that of **CBDO-2**, which may be explained simply by the reduction in molar mass. Last, it is of note that this is the only CBBI studied in which the mass did not degrade to 0%. Whether this is a phenomenon of the material or an artifact of the different method used is not currently known.

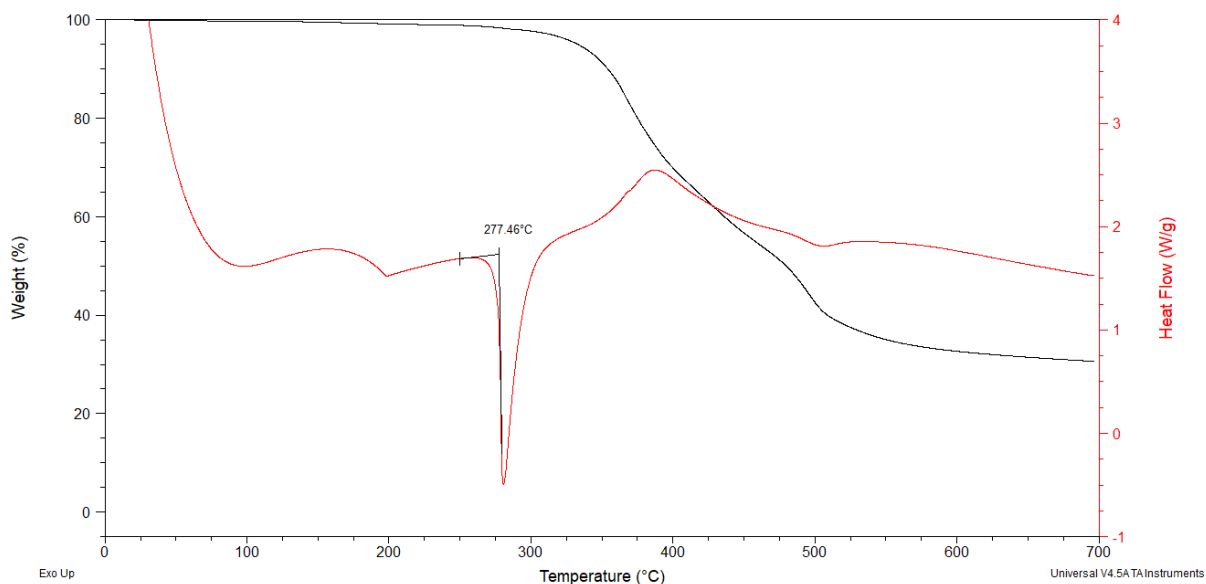


Figure 26: TGA (black line) and DSC (red line) of CBDO-3 from 25°C to 700°C with ramp rate 15°C/min.

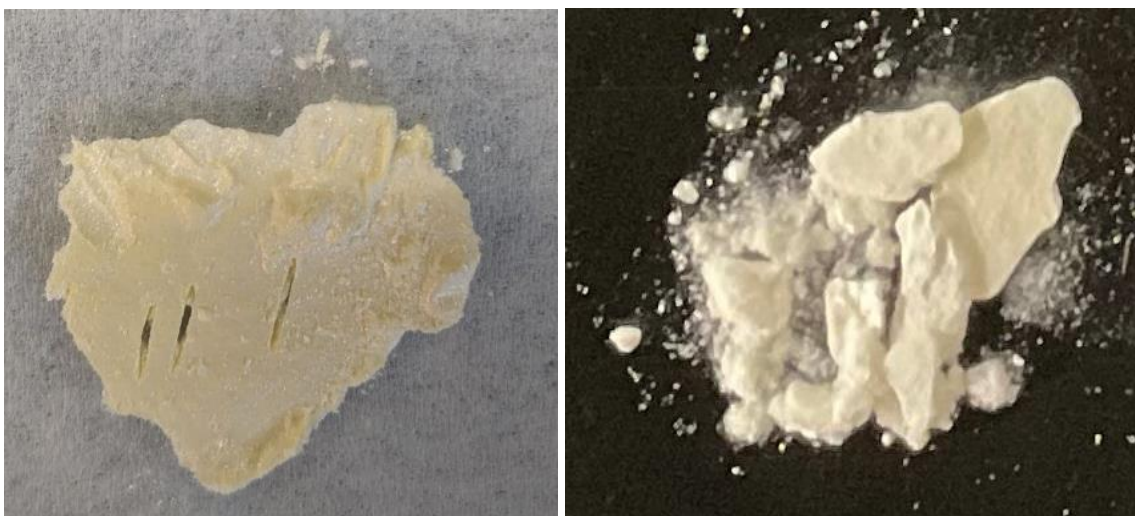
#### Syntheses of CBBI-based polymers

Two polyesters were synthesized using novel CBBI s produced as part of this work. The first, PCBBI-1, was synthesized using CBDE-6 and 1,7-heptandiol according to procedures in the experimental section. The second, PCBBI-2, was synthesized in the same manner using CBDO-2 and adipic acid. Several methods were attempted, with the reported  $\text{Ti}(\text{iOPr})_4$  determined to be the most effective. Alternative methods each faced insurmountable technical hurdles.

The first difficulty faced in the polymerization of these compounds was the high melting point for each CBBI component. TGA/DSC analysis of CBDO-2 (**Figure 19**) shows the degradation of the compounds coincides with its melting point at 311°C. This precludes all melt polymerization techniques, not only because the compound degrades as it melts, but because most comonomers would likewise evaporate or degrade prior to reaching the melting point of CBDO-2 or CBDE-6.

Secondly, the compounds are insoluble or sparingly soluble in most solvents except for DMSO and DMF. This limits the choice of solvents for solution phase polymerizations. Though to the benefit of the methods, the chosen solvent DMF can reach temperatures appropriate for the removal of polymerization byproduct, in these cases, water or ethanol. This helps drive the reaction forward according to Le Chatelier's principle.

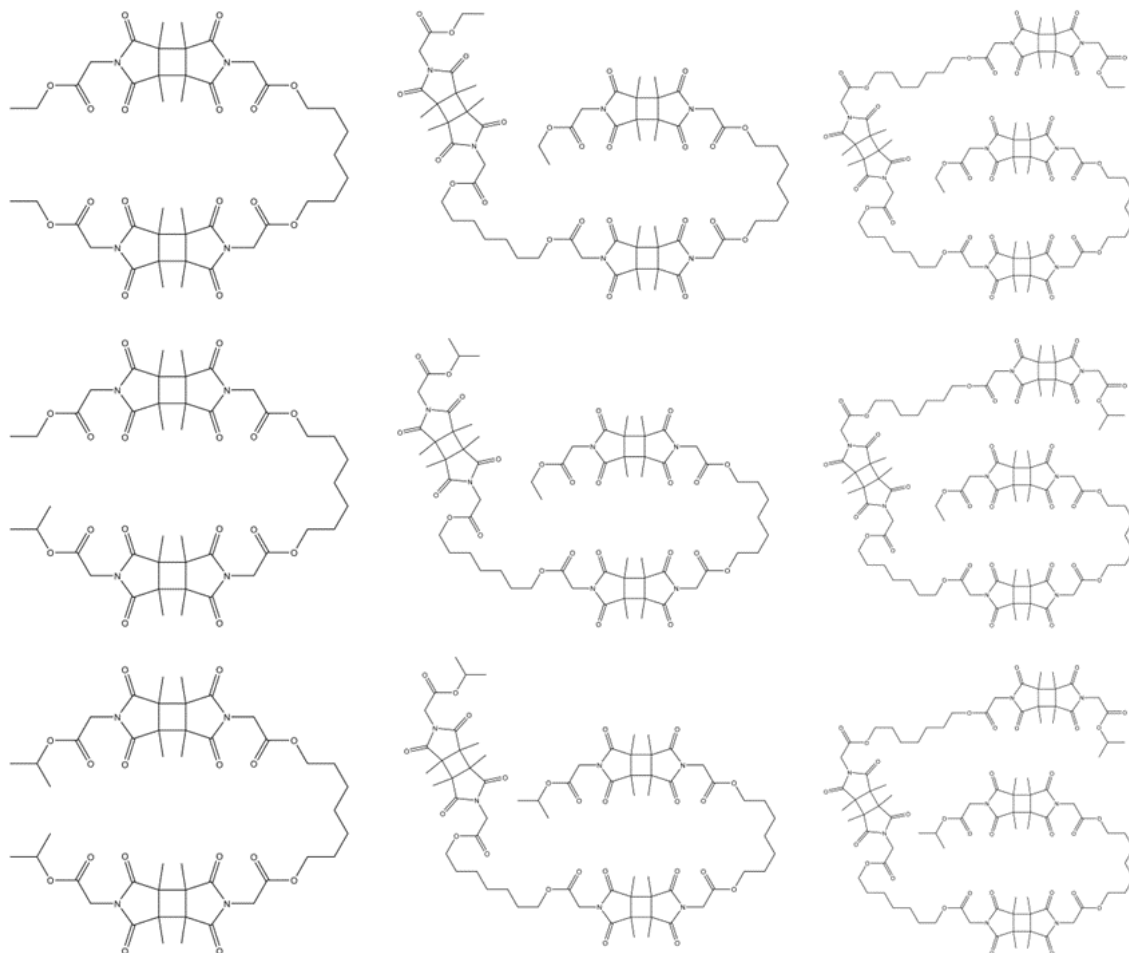
Both polymers were extremely lightweight, off-white foamy solids. After drying on vacuum filtration, they formed airy pucks (**Figure 27**). The pucks were very brittle and stabbing them with a spatula produced a crunch sound. As the polymer was handled and placed into the storage vial, powder broke off and floated around.



*Figure 27: PCBBI-2 solid showing score marks after being stabbed with a spatula (left); the same sample, crumbled due to handling, in better lighting to showcase superb colorless clarity (right).*

HRMS of PCBBI-1 showed peaks which corresponded to three oligomers of CBDE-6 and 1,7-heptandiol. These were the CB terminated mono- (a-b-a), di- (a-b-a-b-a), and trimeric (a-b-a-b-a-b-a) structures as well as the cyclodimer. The complex peak pattern is in part due to the exchange

of the terminal ethyl group with the propyl groups from the catalyst. This results in three peaks for each of the oligomeric structures observed (**Figure 28**).



*Figure 28: The 3 major oligomeric constituents of PCBB1-1 and their mono- and dipropyl substituted forms.*

### Conclusions and Future work

In the course of this work, 10 novel CBBI compounds were synthesized. In addition, six protoCBBI compounds were synthesized. Altogether, eight novel crystal structures were collected. By identifying multiple synthetic pathways to the desired product through careful retrosynthetic

analysis, it was shown that difficulties in one method may be circumvented by use of another (Figure 29).

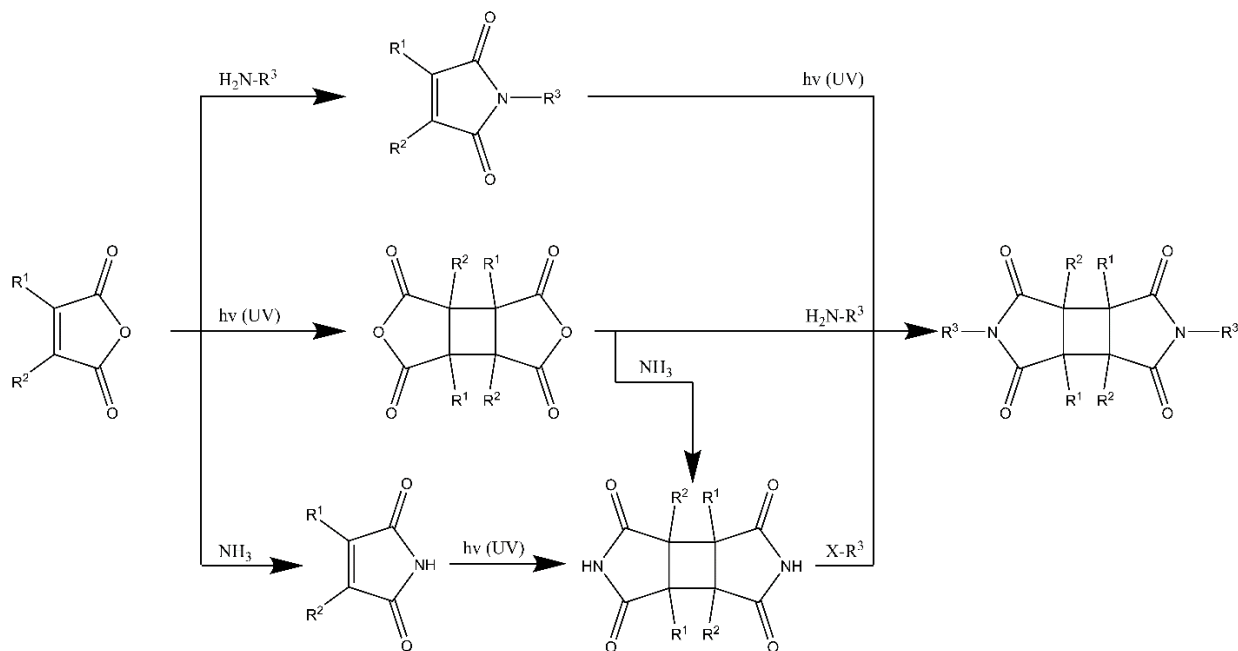


Figure 29: The multiple pathways to construct the cyclobutane bisimide (CBI) monomer building block from the common starting material, maleic anhydride derivative.

Two polyesters, PCBBI-1 and PCBBI-2, were synthesized using CBIs as one of two comonomers. The former was synthesized using CBDE-6 and 1,7-heptandiol to afford an extremely lightweight, foamy solid polymer. The presence of polymer was confirmed using <sup>1</sup>H-NMR and HRMS. The latter was synthesized using CBDO-2 and adipic acid. The structure of PCBBI-2 is not yet elucidated, in part due to the difficulty in its solubilization. The method of polymerization used a titanium catalyst which is reported in the literature to produce high molecular weights, a fact which has not yet been confirmed for these polymers. Notably, these polymers were colorless.

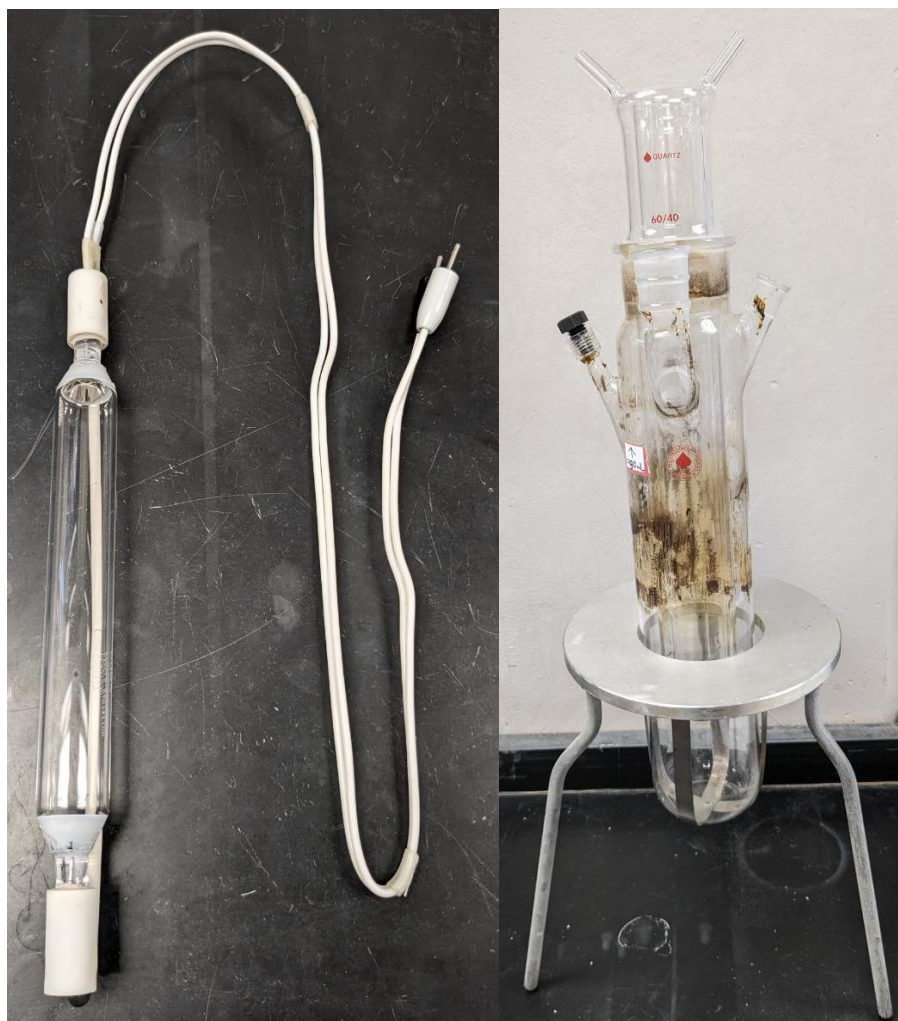
# Chapter 3: Optimization of [2+2] Photocycloaddition using Solution Phase Ethylene.

## Introduction

*Cis*-cyclobutane-1,2-dicarboxylic anhydride (CBAn-1) is an important platform molecule to consider when studying other, substituted cyclobutane anhydrides and diacids. Presented here is an optimization of that synthesis first reported in 1971.<sup>34</sup> The optimizations focus on reducing apparatus complexity and minimizing risk to the researcher from exposure to dangerous UV radiation or high temperature reaction conditions.

Processes by which a chemical change is brought to a substance by the absorption of light have been known since antiquity, using the sun as the light source. However, it wasn't until the 18<sup>th</sup> century that photochemical experimentation as we know it today began. Even then, it was around 100 years later that [2+2] photocycloaddition reactions, the mechanism by which CBAn-1 is synthesized, were described and their products were properly elucidated.<sup>35</sup>

As our understanding of chemistry and photochemistry grew through these stages, and in the time since, so has the desire to miniaturize the light source. Currently, much of the UV-absorption photochemical work in literature uses traditional, specialized photoreactor lamps. These lamps are generally a medium pressure mercury lamp which emit in a very broad-spectrum including UV and visible light. They may be found in a variety of power outputs, from 100-1000W. Common lamps in literature are usually somewhere in the middle, around 450W (**Figure 30 left**). Despite the growing prevalence of light emitting diode (LED) array light sources, these lamps remain a favorite among researchers due to their broad-spectrum emission and familiarity.



*Figure 30: A typical Hanovia medium-pressure mercury photochemical reactor lamp (left) and a typical photochemical reaction vessel with the quartz cooling jacket in place (right). It's placed in a stand which facilitates submersion of the vessel into a heating or cooling bath.*

Because of the high-power output, the bulbs are extremely bright and can get extremely hot. Thus, precautions must be made to protect the researcher, the reaction, and the equipment. This is achieved by housing the bulb in a double-walled quartz jacket through which water is cycled. The primary purpose of water cooling is to prevent the bulb from self-destructing (though modern bulbs are manufactured with a fuse that will trip prior to destruction of the bulb itself) or igniting its surroundings. Additionally, this has the effect of maintaining reactions at reasonable



temperatures.<sup>36</sup> Here, quartz is employed to allow the full UV spectrum to transmit through the glass cooling jacket. Use of standard borosilicate glass in this role is uncommon since it strongly absorbs UV radiation < 320nm.<sup>37</sup> Quartz is much more expensive than borosilicate glass and so it is not typically found in labs. Needing to purchase specialized glassware can greatly increase the cost for a reaction. These cooling jackets are often fitted for use in specific photochemical reaction vessels (**Figure 30 right**). The immutability of reaction volume severely limits the ability of the researcher to scale a reaction up or down.

Additionally, reactions must be kept behind opaque shielding to protect the researcher from exposure to the bulb's emissions. Even in a case where the reaction vessel itself is not UV transparent, the intensely bright visible light can pose a threat to the eyesight of anyone who looks at them.

Finally, most of the energy output from traditional photoreactor lamps is wasted as either heat or emitted as wavelengths which are not absorbed by the molecule of interest. A common method to circumvent this issue is by use of photosensitizers such as acetophenone. Work by previous members of the Chu Research Group has shown that use of these broad emission spectrum lamps or photosensitizers is not necessary when the molecule of interest absorbs strongly in a region that overlaps with the peak emission of the UV source.<sup>24,28,38-40</sup> This has allowed for the use of lower power bulbs which do not emit such intensely bright light and may not emit the more dangerous UV-B (280-315nm) and UV-C (100-280nm). This benefits the researcher by being much safer and easier to handle than traditional photoreactor bulbs at the cost of reaction time.

### *History of CBAAn-1 and CBeAn-1 syntheses*

The initial procedure reported by Owsley and colleagues for the synthesis of CBAAn-1 in 1971 made use of extremely low temperatures,  $-65^{\circ}\text{C}$ , a 450W medium-pressure mercury arc lamp, and 5% w/w acetophenone as a photosensitizer under an inert atmosphere of nitrogen. They note reaction times at low temperatures are on the order of 1-2 days whereas room temperature reactions are closer to 7 days. Additionally, they report ethyl acetate as the ideal solvent since other solvents (acetone, acetonitrile, and ether) produce a greater number and amount of side-products. Concentrations of starting material varied from 35-75 g/L. At 35 g/L in EtOAc, they report a yield of 71%, however, this number is based on unrecovered maleic anhydride. The overall yield based on initial starting material is 57%. Isolation was achieved via fractional distillation of product with a variable take-off head.

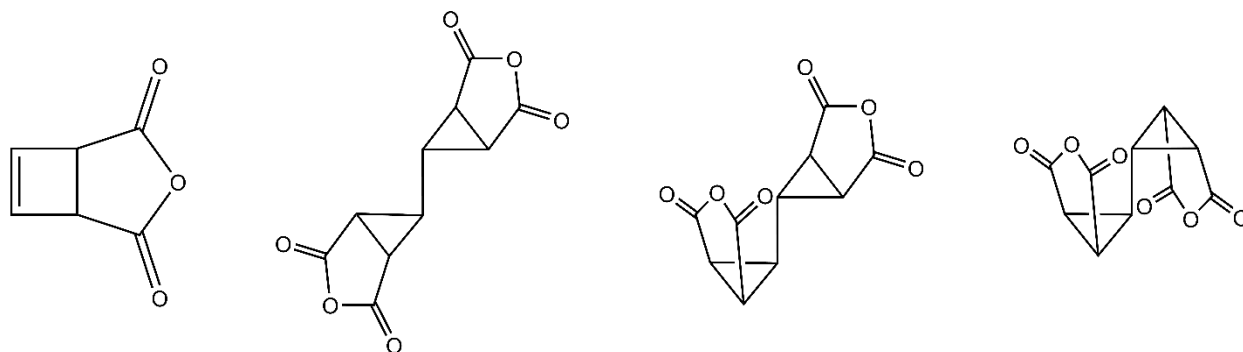
In the decades since, some improvements have been made. In 2006,<sup>41</sup> Faure and colleagues achieved much faster reaction times (5 hours) by greatly reducing the initial concentration of maleic anhydride in ACN to 2g/L. They report 75% yield, but again, this is not based on theoretical yield of CBAAn-1. Actual yield is 60%, which is comparable to Owsley. This work also made use of acetophenone and a 400W medium-pressure mercury lamp fitted with a Pyrex filter. The specificity of including a Pyrex (borosilicate) filter suggests that they intentionally excluded deeper UV wavelengths, however that is not discussed in the publication. Isolation achieved via recrystallization of crude product from cyclohexane/ether.

In 2016,<sup>36</sup> the synthesis conducted by Mercer and colleagues was very similar to the original Owsley synthesis in terms of concentration, solvent (ACN), and UV source (450W mercury lamp).

The notable difference is that they do not cool the reaction down to such low temperatures. Their reaction time was 7 days, which is in line with the observations of Owsley. Work up was removal of maleic anhydride via sublimation under strong vacuum for 2 days for a total reaction time of 9 days. The yield after this process was 73% crude product and was used without further purification.

More recent literature<sup>42-44</sup> has used this classic [2+2] photocycloaddition as a model for the development of flow chemistry apparatuses with gaseous reactants. UV sources vary from 1000W medium pressure mercury lamps to 365 nm LED arrays of varied wattage. These reactions were all performed at elevated pressures (6-12 bar). Given the nature of flow reactor set-ups, yield is difficult to compare but ranged from 0.1-22 g per hour of reactor run time.

An early synthesis for cis-3,4-cyclobutenedicarboxylic anhydride (CBeAn-1) and bis-1,1'-(cyclopropane-2,3-dicarboxylic acid anhydride) (CPDAn-1) was published in 1969<sup>45</sup> by Willy Hartmann. In his work, Hartmann determined that the photosensitized [2+2] photocycloaddition between maleic anhydride and acetylene will result in CBeAn-1 and three isomers of CPDAn-1 (**Figure 31**) in 36% and 48% yield, respectively. However, he discusses the disparity of molar ratio of yields in his work with that from an earlier synthesis,<sup>46</sup> with the conclusion that the yield ratio is likely temperature dependent. As in the work by Faure et al., Hartmann specifies using a Pyrex cooling jacket, again suggesting the purposeful exclusion of deeper UV radiation.



*Figure 31: The four products of the reaction between maleic anhydride and acetylene. From left to right: cis-3,4-cyclobutenedicarboxylic anhydride (CBeAn-1), trans,trans-bis-1,1'-(cyclopropane-2,3-dicarboxylic acid anhydride), cis,trans-bis-1,1'-(cyclopropane-2,3-dicarboxylic acid anhydride), and cis,cis-bis-1,1'-(cyclopropane-2,3-dicarboxylic acid anhydride). The isomeric cyclopropanes are collectively referred to as CPDAn-1.*

In 1976,<sup>47</sup> Bloomfield and Owsley published the first version of this synthesis optimized to obtain CBeAn-1. In doing so, they built a custom photochemical reactor that appears to be a prototype of those commercially available today. Their work made use of extremely low temperature cooling baths to keep the reaction at  $-60^{\circ}\text{C}$  and a very powerful, 1000W photoreactor bulb. They also specify that their immersion cooling jacket was made from Pyrex.

In 1999,<sup>48</sup> Gauvry and colleagues published an alternative, two step synthesis of CBeAn-1 as an alternative to the work by Owsley and Hartmann. A major motivator was the acute danger posed by the previous syntheses which all involved bubbling acetylene, an extremely flammable gas, through a solution of flammable solvent in very close contact with an intense heat source (the UV photoreactor lamp). This is a very real concern considering that even in their paper, Gauvry reports having ignited their reaction twice while synthesizing CBeAn-1 with classic methods. To avoid this, they elevate previous work<sup>49</sup> in which a solution of maleic anhydride and 1,2-

dichloroethene in EtOAc was irradiated to afford 1,2-dichlorocyclobutane-3,4-dicarboxylic anhydride as a mixture of isomers. Gauvry found that the yield is actually *improved* by the elimination of photosensitizers. The second step is a reductive chlorine elimination in the presence of activated zinc to afford CBeAn-1 in 68% overall yield.

Here, the optimizations to photochemical reactions developed by previous members of the Chu Research Group, in concert with various optimizations gleaned from the literature, were applied to the synthesis of CBAAn-1 to achieve isolated yields of 70% at ~1 week of reaction time. The major contribution is the significant reduction in apparatus complexity and in the risk imposed by it to the researcher. It is hoped that by making the synthesis safer and simpler, this important molecule may receive more interest. Attempts at using the same optimizations to afford CBeAn-1 did not yield isolated product but were successful as determined by NMR. Unambiguous confirmation of CBeAn-1 synthesis was achieved by SCXRD, a first for this product. Additionally, a new polymorph of the side product, CPDAn-1, was obtained.

## Methods and Materials

### *Synthesis of CBAAn-1*

A solution of maleic anhydride in ACN with a concentration of 75 g/L was made in a 50 or 250mL quartz round bottom flask. No additional photosensitizer was added at any point in the reaction. A hypodermic needle was extended through the entire length of a rubber septum or stopper which fit the opening of the flask. A small diameter hosing suitable for use in acetonitrile was then likewise extended through the entire length of the septum or stopper. The end of the hose was affixed with a Bubblemac Aeration Products gas dispersion stone model #11111. The septum

or stopper was then fitted on the flask and the hosing was adjusted so the stone was fully submerged in the solution. Ethylene was delivered to the reaction through this stone with the needle acting as the outlet. Ethylene was delivered vigorously for 5-10 minutes to degas the solution and saturate it with dissolved ethylene. After this saturation period, the ethylene is turned down to a very gentle flow. The reaction mixture was then placed in the custom light array for photochemical reactions apparatus (LAPRA) and irradiated using eight (8) 14.7W Ushio G15T8E UV-B fluorescent bulbs (**Figure 33**) which were each powered by Intertek SLE15-BL fixtures.

Reaction progress was monitored by  $^1\text{H-NMR}$ . Samples were collected with a syringe by poking a long needle through the septum. In cases where more solvent had to be added, it was added in the same way.



*Figure 32: Simplified reaction apparatus for synthesis of CBAn-1 known as the Light Array for Photochemical Reactions Apparatus or LAPRA. Left: LAPRA in open position for easy access to mixture. Right: LAPRA in closed position.*



*Figure 33: A typical UV-B bulb used in the synthesis of CBAn-1.*

Upon completion of the reaction, the mixture was transferred to a Pyrex round bottom flask and solvent was gently distilled using a standard distillation apparatus with a fractional column. The

solvent was collected and stored for reuse in subsequent reactions. Distillation proceeded until no more solvent was observed condensing in the column. At this time, while the reaction mixture was still liquid, it was transferred to a smaller Pyrex round bottom flask for subsequent purifying distillation. A stir bar was added to help smooth the boil.

The flask was fitted with a vacuum jacketed, short-path distillation head to which a series of adapters had been affixed (**Figure 34**). The adapters were used primarily to prevent overflow in the case of bumping or sudden boil, but also served as a makeshift extension of the fractional column.



*Figure 34: Vacuum jacketed, short path distillation head used for the purification of CBA<sub>n</sub>-1. Adapters installed to prevent overflow in the case of bumping.*



The distillation head was fitted with an analogue thermometer. No coolant was used in the condensation column. The mixture was then distilled under a vacuum at ~3 mm Hg maintained using a Welsh Chemstar 1400N vacuum pump.

The collected product was placed in a vial fitted with a septum and the atmosphere inside the vial was purged with nitrogen to prevent hydrolysis during storage. In this manner, minimal hydrolysis was observed after 5 weeks. Hydrolysis may be further inhibited by storage of the solid in pellets or chunks rather than as a powder.

#### *Synthesis of CBeAn-1 and CPDAn-1*

The methods used in the synthesis of CBeAn-1 were the same general methods as those used for CBAAn-1 except ethyl acetate was used as solvent and acetophenone was added as a photosensitizer. In cases where a large amount of CPDAn-1 polymer was formed, this was separated by centrifuge. The supernatant was then decanted and collected for work up.

Isolation was attempted using vacuum distillation prior to obtaining vacuum jacketed apparatus and was only marginally successful. Positive confirmation of product identity was obtained via SCXRD of crystals grown from concentrated reaction mixtures. NMR data in the following section are obtained from crude spectra where all other peaks can be accounted for and by comparison to published spectra when possible.<sup>48</sup>

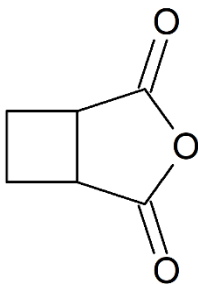
#### *Synthesis of imide from CBAAn-1*

An imide, *cis*-(*N*-phenyl)-1,2-cyclobutanecarboximide (CBI-1), was synthesized from CBAAn-1 as a proof of concept for the functionalization of CBAAn-1. The reaction was successful and the desired product was obtained in 82% yield. This shows that CBAAn-1 is thermally stable enough for efficient

imidization of the anhydride. Subsequent reactions will focus on the installation of R groups with existing functionalization. For example, if similar reactions are likewise achievable, reacting CBAAn-1 with dimethyl aspartate will afford a cyclobutanecarboximide product with a diester on the R group. This diester can be incorporated into a polymer chain and the resulting structure will have a pendant CBI group.

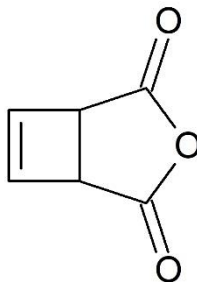
## Experimental

*cis-1,2-cyclobutanedicarboxylic anhydride (CBAAn-1)*



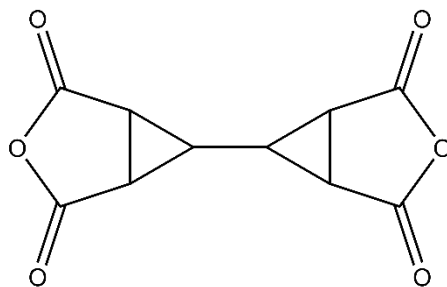
$^1\text{H-NMR}$  (400 Hz,  $\text{CDCl}_3$ )  $\delta$  3.53 (br t,  $J=4.02$  Hz, 2H), 2.78 (br m, 2H), 2.41 (br m, 2H);  $^1\text{H-NMR}$  (400 Hz,  $\text{DMSO-D}_6$ )  $\delta$  3.52 (br t,  $J=4.32$  Hz, 2H), 2.61 (br m, 2H), 2.22 (br m, 2H);  $^{13}\text{C-NMR}$  (100 Hz,  $\text{CDCl}_3$ )  $\delta$  173.4, 38.73, 23.13.

*cis-3,4-cyclobutenedicarboxylic anhydride (CBeAn-1)*



$^1\text{H-NMR}$  (400 Hz,  $\text{DMSO-D}_6$ )  $\delta$  6.59 (s, 2H), 4.08 (s, 2H)

*bis-1,1'-(cyclopropane-2,3-dicarboxylic acid anhydride) (CPDAn-1)*

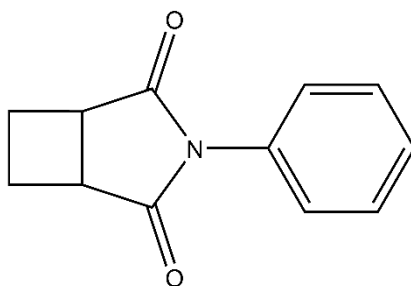


\*Mixture of 3 isomers

$^1\text{H-NMR}$  (400 Hz, DMSO- $\text{D}_6$ )  $\delta$  3.24-3.17 (s/m, 4H), 2.20-1.93 (s/m, 2H)

*cis-(n-phenyl)cyclobutane-1,2-carboximide*

0.7696 g of CBAAn-1 and 0.6327 (1.1 eq) was added to a 50mL round bottom flask with 40mL toluene and stir bar. Upon refluxing overnight, partial conversion to product was observed by  $^1\text{H-NMR}$ . The reaction was placed in a 100mL round bottom flask and 0.5 mL concentrated sulfuric acid was added. The reaction was placed back in the oil bath to reflux. Initially the reaction appeared cloudy but quickly became clear one more and a brown, oily precipitate formed. The reaction was allowed to reflux overnight again. The reaction was washed with 1x 50mL DI water, 1x 40ml  $\text{NaHCO}_3$ , and 1x 20ml brine. The organic layer was dried with  $\text{Na}_2\text{SO}_4$  and solvent was removed in vacuo to afford 1.0129g of tan solid (82% yield).



$^1\text{H-NMR}$  (400 Hz, DMSO- $\text{D}_6$ )  $\delta$  7.53 (t,  $J=7.58$  Hz, 2H), 7.44 (t,  $J=7.26$  Hz, 1H), 7.35 (d,  $J=7.92$  Hz, 2H), 3.40 (br t,  $J=3.99$  Hz, 2H), 2.63 (br m,  $J=6.08$  Hz, 2H), 2.19 (br q,  $J=7.42$  Hz, 2H);  $^{13}\text{C-NMR}$  (100 Hz,  $\text{CDCl}_3$ )  $\delta$  179.45, 133.24, 129.29, 128.73, 127.67, 38.70, 22.68. FT-IR ( $\nu_{\text{max}}$ ,  $\text{cm}^{-1}$ ): 2959 (w, CH stretching), 1691 (s, C=O stretching), 1378 (m, CN from aromatic), 1171 (s, CO stretching).

## Results and Discussion

### *Synthesis of CBAn-1*

On average, reactions proceeded to ~80% conversion at 5 days and 92-95% conversion at 10 days as estimated by peak integration of  $^1\text{H-NMR}$  spectra of crude reaction mixture. The increase in yield from days 6 to 10 is only 2-10% and so the products were usually harvested at 5-6 days of reaction time. Two major side products are identified in the  $^1\text{H-NMR}$ . First is the [2+2]photocycloaddition dimer of maleic anhydride (CBDAn-1<sup>24</sup>) and its singly and doubly hydrolyzed analogues. The second is fumaric acid, which is the more stable, trans geometric isomer of maleic acid. Maleic acid itself is formed from the hydrolysis of maleic anhydride starting material. CBDAn-1 has moderate solubility in ACN but a small amount of crystalline precipitate was still observed to form in the bottom of the flask and in the gas sparger stone. Because of this, the percentage conversion estimates above are not indicative of true conversion to product. However, since maleic anhydride is the limiting reactive species and since it is also consumed in all side-products, reduction in the integration of its peak is still an effective way to gauge when to stop the reaction.

The flow of ethylene was kept as low as possible, gauged by the formation of small bubbles about once every second. This low rate was chosen because it still kept a sufficient amount of ethylene

dissolved in solution and did not severely increase the rate of solvent evaporation. Initial trials used higher flows which greatly increased the amount of solvent lost to evaporation. Some instances were so severe that upon returning to the lab after leaving it overnight, the level was reduced to levels below the gas dispersion stone. The solution to this problem was found by decreasing the outlet size using a hypodermic needle and lowering the flow of gas. These two modifications reduced the amount of solvent loss (and thus replacement) for a 200 mL reaction to only 20mL over the course of 1 week.

#### *Purification of CBA<sub>n</sub>-1 by distillation*

Maleic anhydride was observed to have deposited on the inner walls of the column and distillation head beginning at ~90°C. In cases where there is a large amount of unreacted maleic anhydride, it may be collected in the first fraction and saved for subsequent reactions. However, in most cases, the maleic anhydride did not travel to the collection flask and the small amount in the distillation head made it extremely difficult to collect. In these scenarios, the distillation head was removed and rinsed with acetone to remove all the maleic anhydride residue. The distillation head was then replaced, and the distillation continued. The desired product, CBA<sub>n</sub>-1, was observed to boil at ~120°C at 3 mm Hg. Because of the high boiling and melting points of the product at atmospheric pressure, it is possible that it may solidify elsewhere in the system, such as in the condensation column or receiving channel. When this happens, the channel can become blocked, quickly destroying the vacuum in the distillation flask and causing the boil to cease. A heat gun may be used to clear the blockage by melting it, but it can be difficult to deliver the heat effectively when the blockage is at the tip of the receiving channel (thus is it shielded by the vacuum formed in the receiving adapter). Additionally, as observed in initial trials, when this

blockage is eventually cleared, the distillation flask immediately begins to boil vigorously, and overflow is almost certain to happen. This can be prevented by using a distillation head with a short receiving channel and by keeping all parts of the distillation head hot during the distillation.

#### *Synthesis and Distillation of CBeAn-1 and CPDAn-1*

Due to the success of the synthesis of CBAAn-1 with the modified procedure, it was decided to adapt it for the synthesis of a more synthetically useful material, *cis*-3,4-cyclobutenedicarboxylic anhydride (CBeAn-1). CBeAn-1, similar to CBAAn-1, is a known reaction, but has not received much attention, likely due to its complicated and dangerous synthesis. It is also of interesting note that CBeAn-1 was synthesized before CBAAn-1, a surprising fact given the relative difficulties between the two reactions.

Initial attempts using ACN as solvent resulted in a large formation of a poorly soluble, tan solid with a silt-like consistency and CBeAn-1 as the minor product. Given the poor solubility of the tan solid, it was assumed to be polymeric CPDAn-1 as reported by Owsley.<sup>47</sup> This was supported by SCXRD analysis of crystals from these reactions which provided the *trans,trans* isomer CPDAn-1. Additionally, this polymorph was different than the one previously reported.<sup>50</sup> The crystals were difficult to separate from the bulk powder which contained all three isomers multiple isomers, and thus the collected <sup>1</sup>H-NMR spectra were messy and inconclusive.

Subsequent attempts used EtOAc which provided a significantly reduced polymer yield. Isolation of the product via distillation was difficult because of the stepwise hydrolytic then thermal degradation of CBeAn-1. First, CBeAn-1 undergoes hydrolysis, to which it is highly sensitive. Second, the hydrolyzed product, *cis*-3,4-cyclobutenedicarboxylic acid, readily undergoes thermal

conrotatory ring-opening to afford *cis,trans*-muconic acid. This was also observed when attempting to extract CBeAn-1 with hexane. After concentration, the resulting solid is almost entirely *cis,trans*-muconic acid. Although disappointing to lose the cyclobutene product, the presence of *cis,trans*-muconic acid could only be explained if it were present, furthering the proof of the success of the synthesis.

Because of the difficulties with isolation, yields for CBeAn-1 could not be determined because pure samples were not obtained. Additionally, since it was not a desired product, yields for CPDAn-1 were not calculated.

## **Appendices**

### Appendix A: Selected NMR Spectra



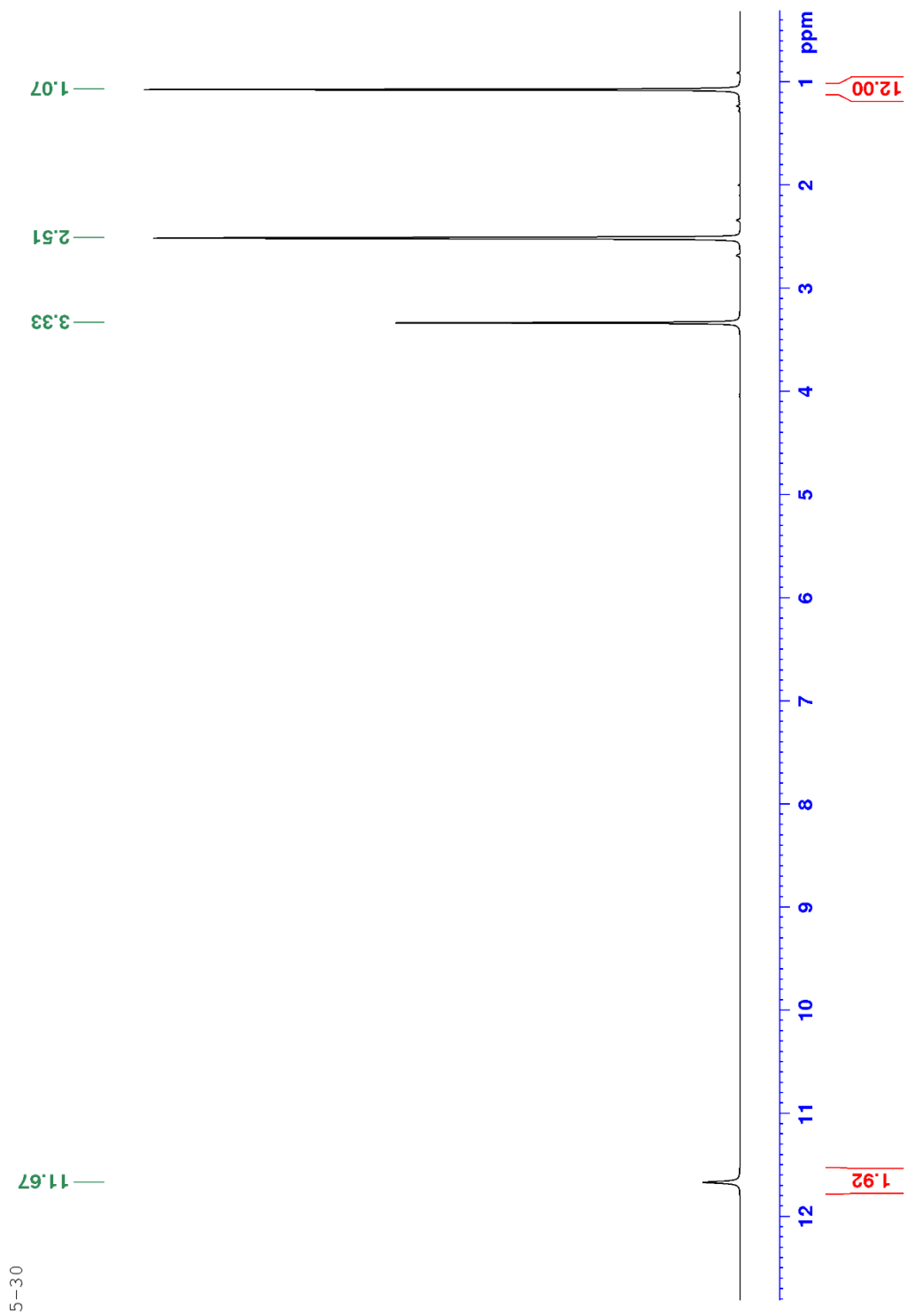


Figure A 1:  $^1\text{H-NMR}$  of CBBI-1 at room temperature.

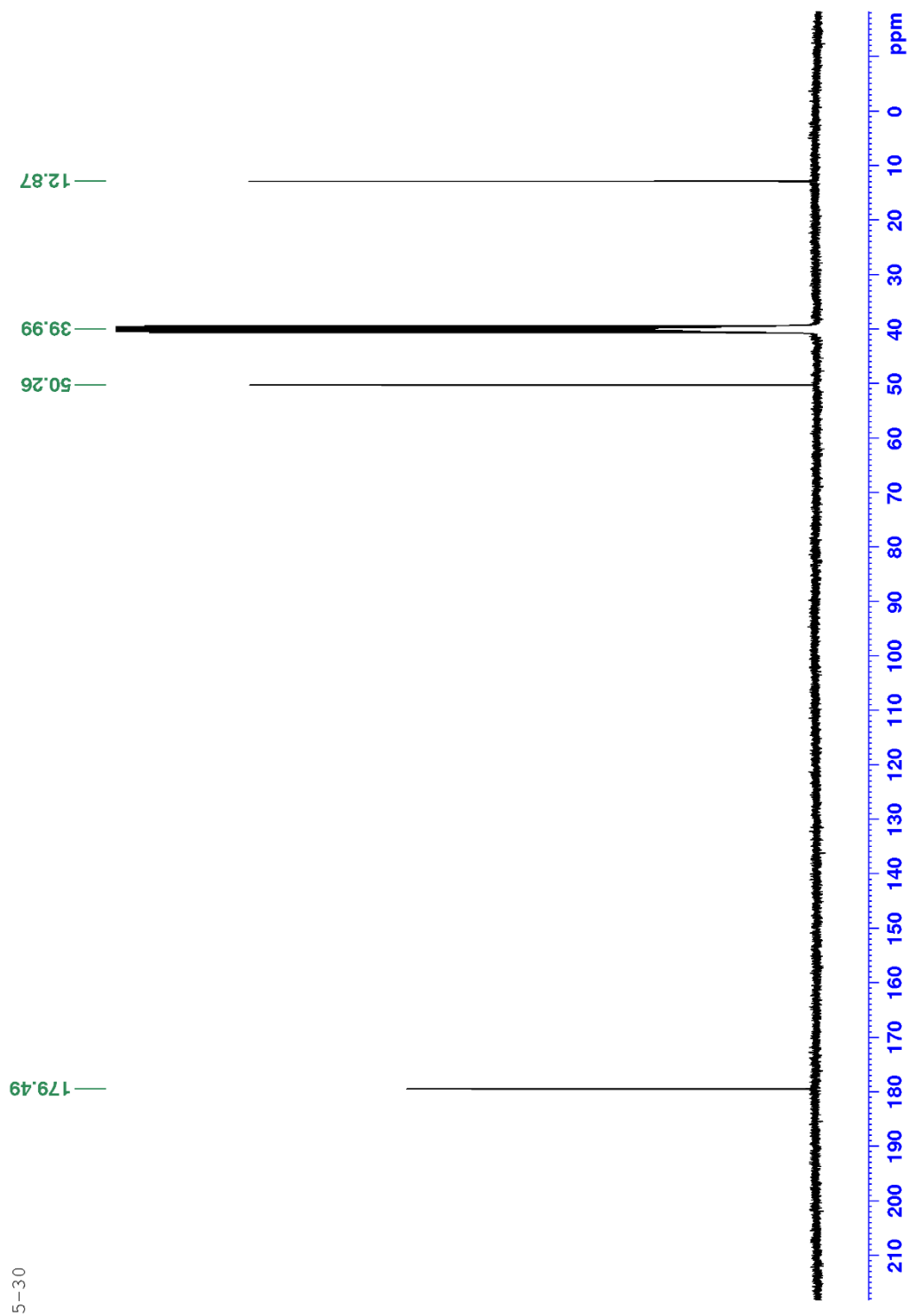


Figure A 2:  $^{13}\text{C}$ -NMR of CBBI-1 at room temperature.

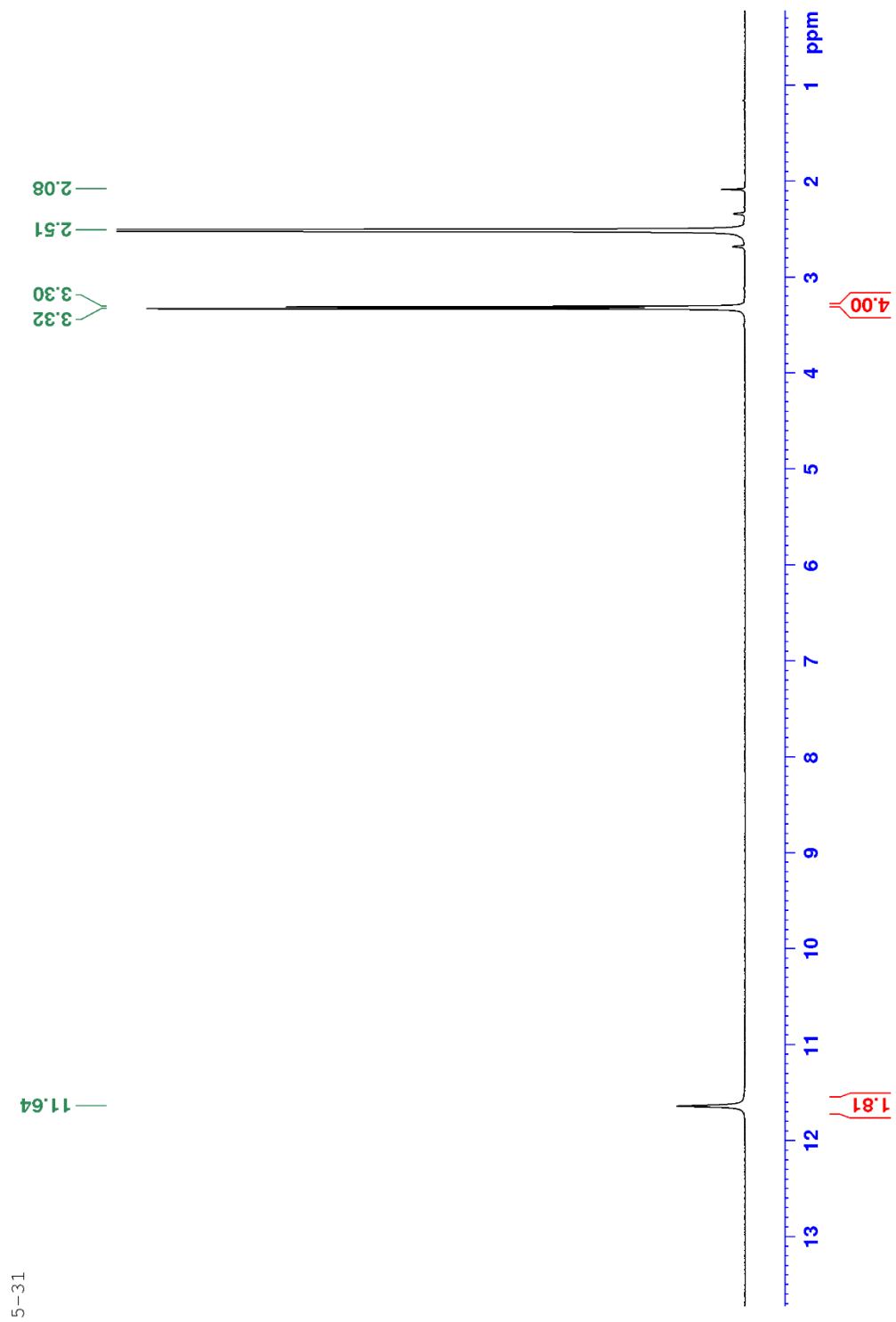


Figure A 3:  $^1\text{H-NMR}$  of CBBI-2 at room temperature.

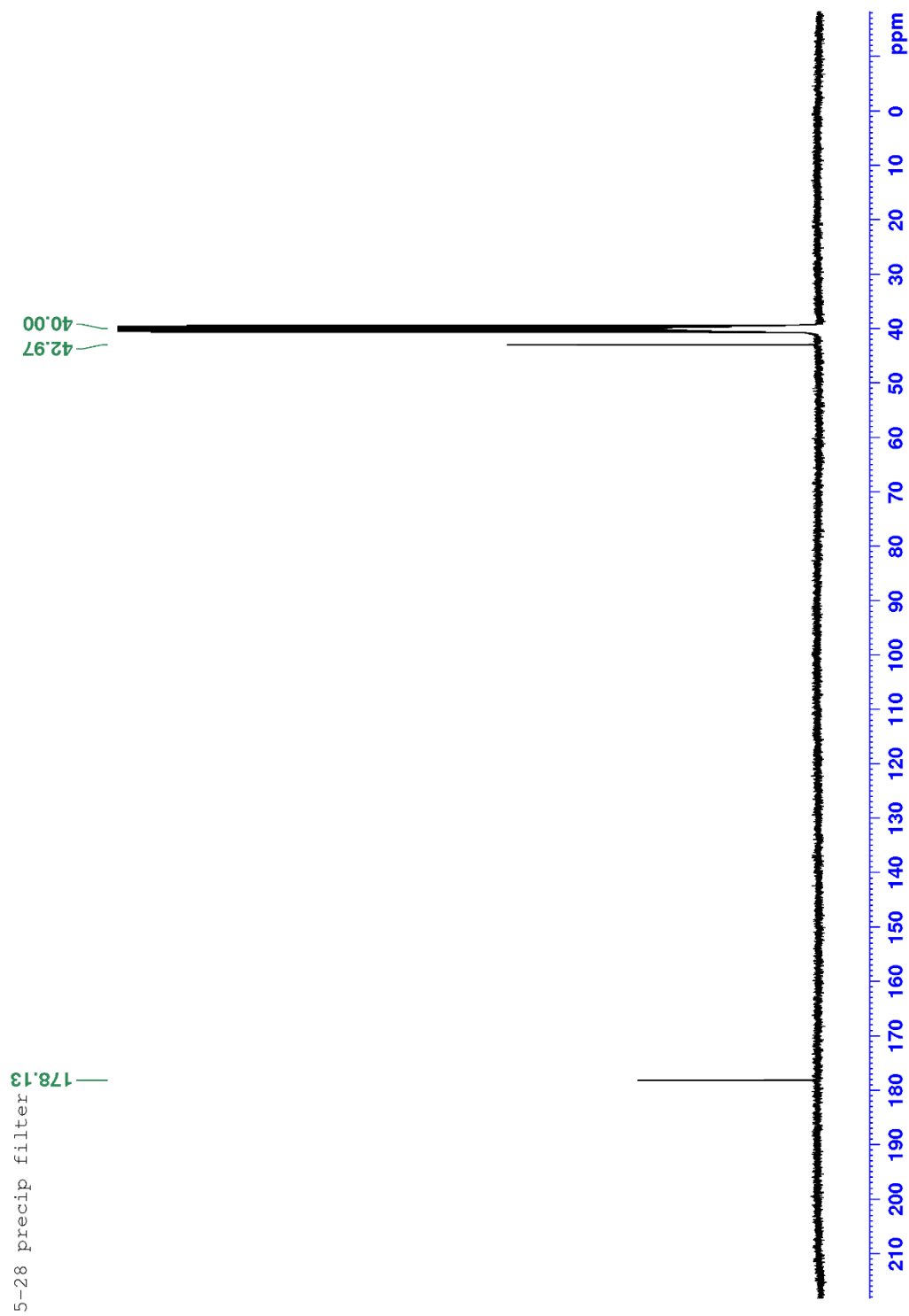
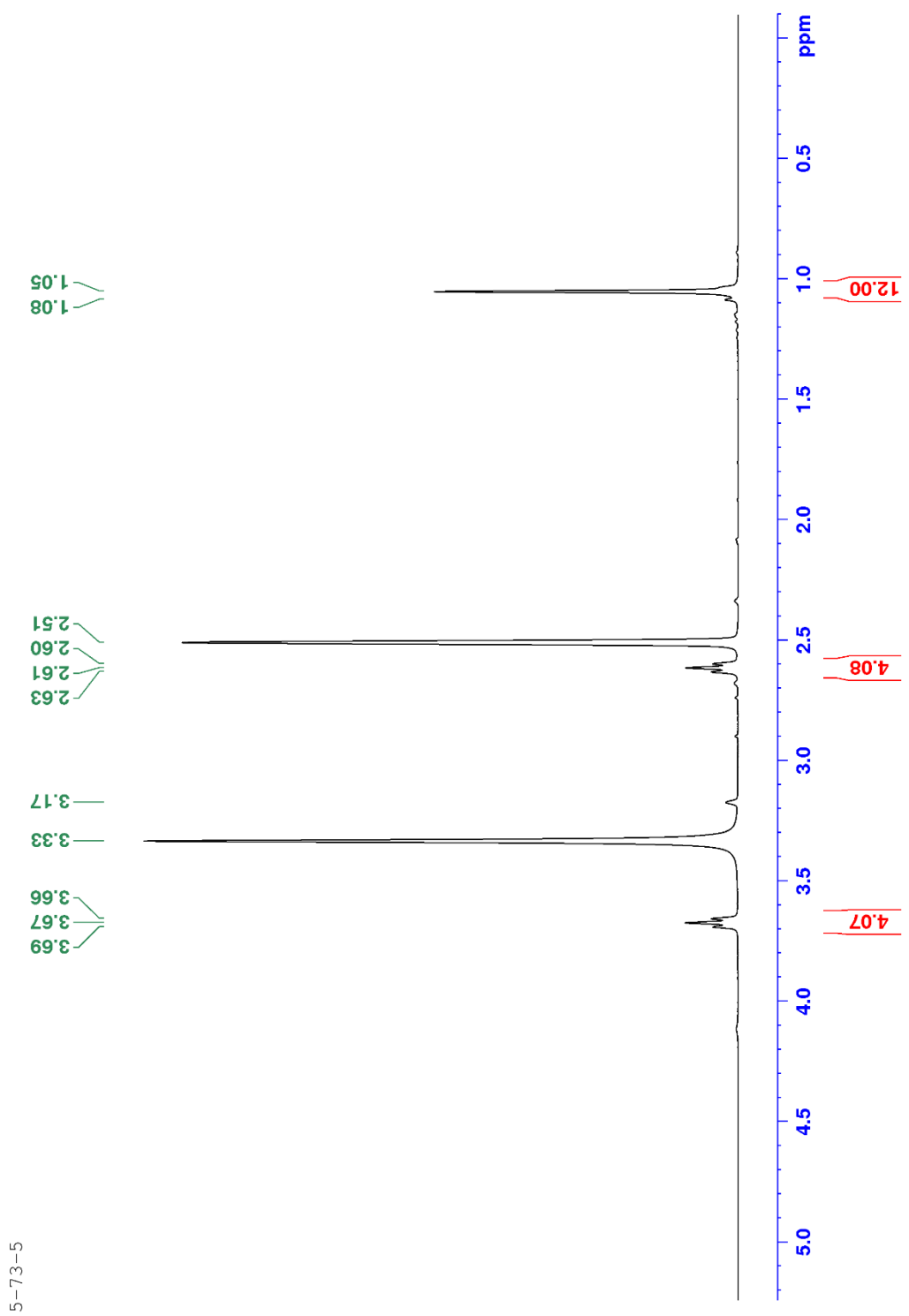


Figure A 4:  $^{13}\text{C}$ -NMR of CBBI-2 at room temperature.



5-73-5

Figure A 5:  $^1\text{H-NMR}$  of CBDA-6 at room temperature.

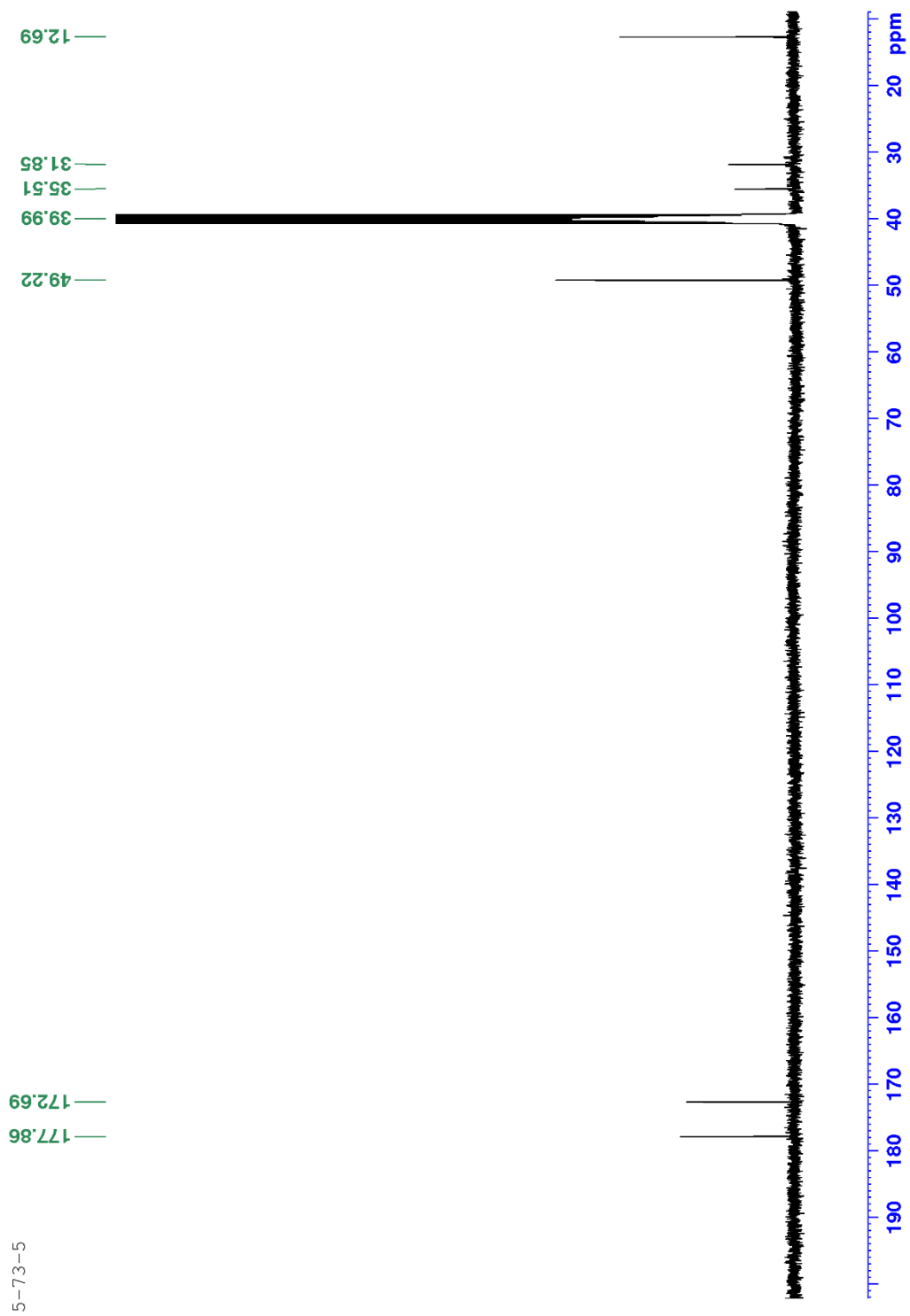
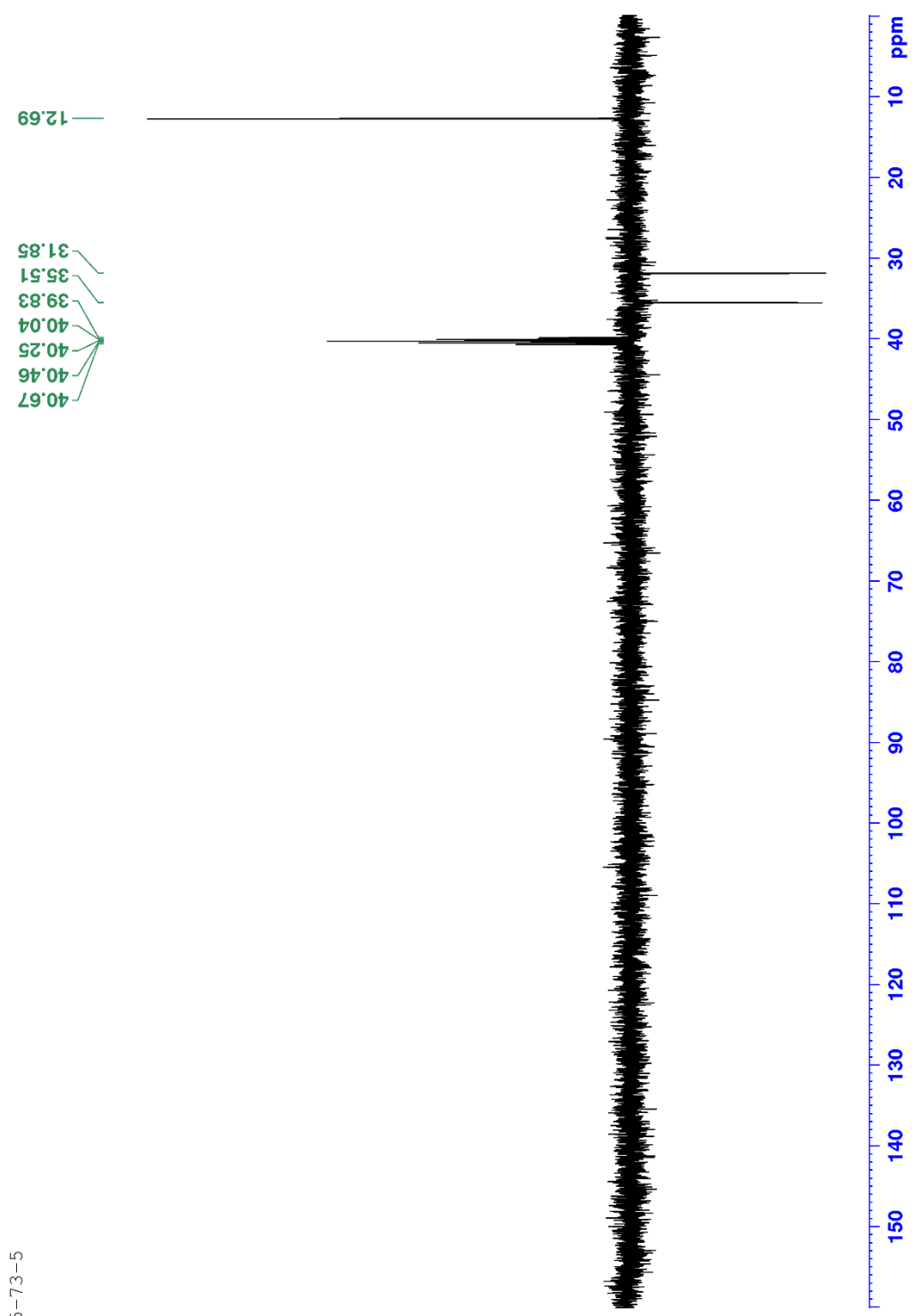


Figure A 6:  $^{13}\text{C}$ -NMR of CBDA-6 at room temperature.



5-73-5

Figure A 7: DEPT135 of CBDA-6 at room temperature.

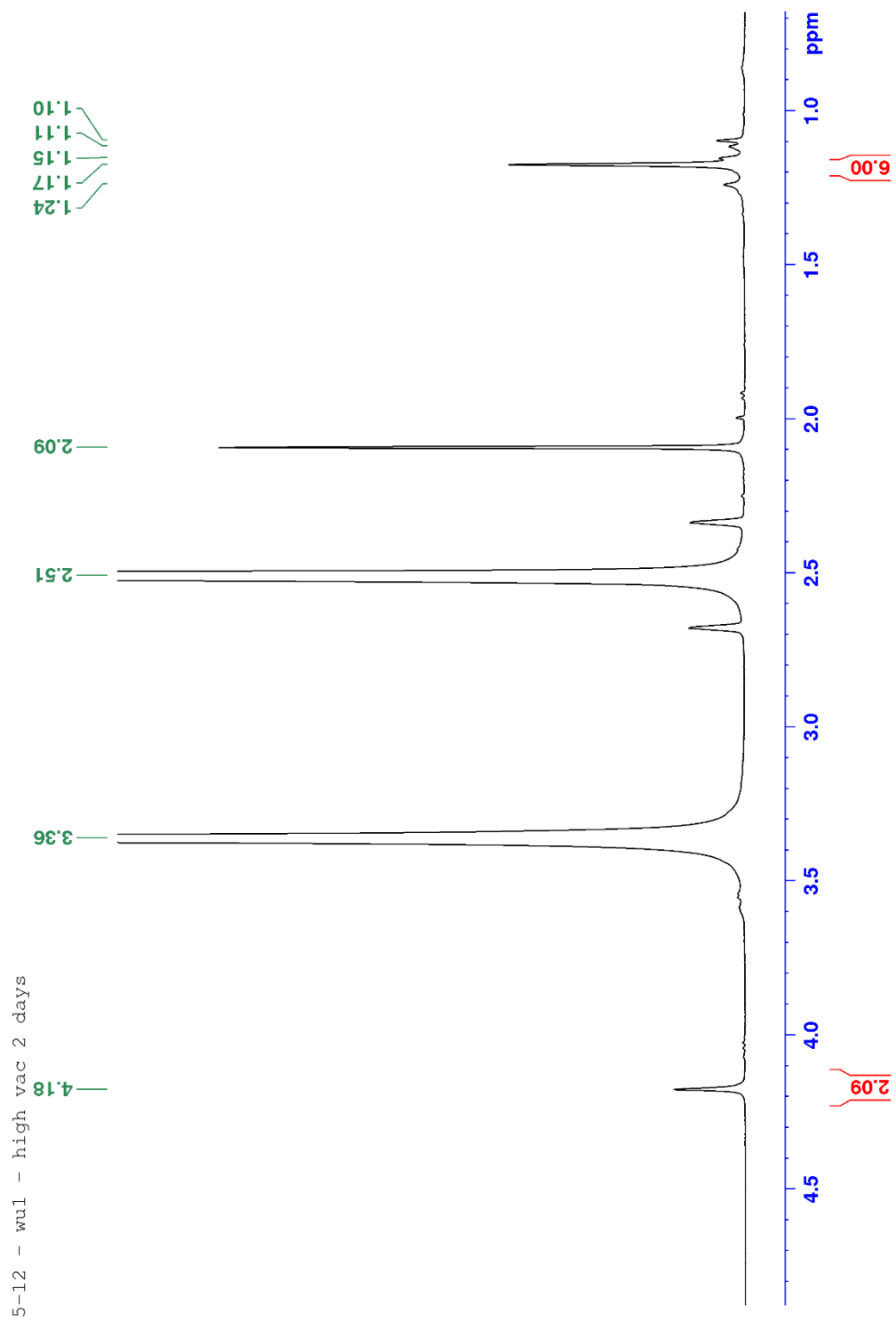


Figure A 8:  $^1\text{H}$ -NMR of CBDA-7 at room temperature.



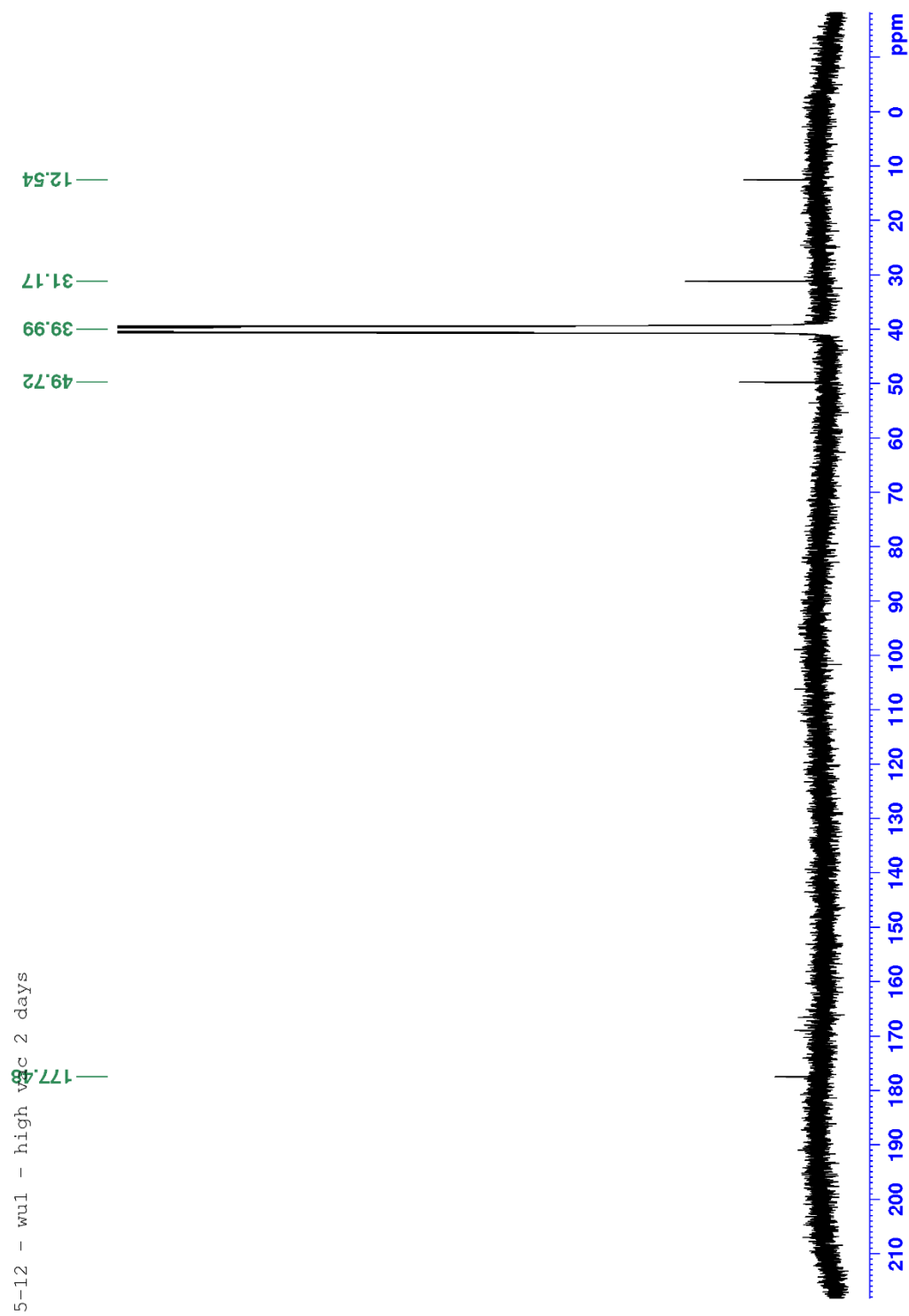


Figure A 9: <sup>13</sup>C-NMR of CBDA-7 at room temperature.

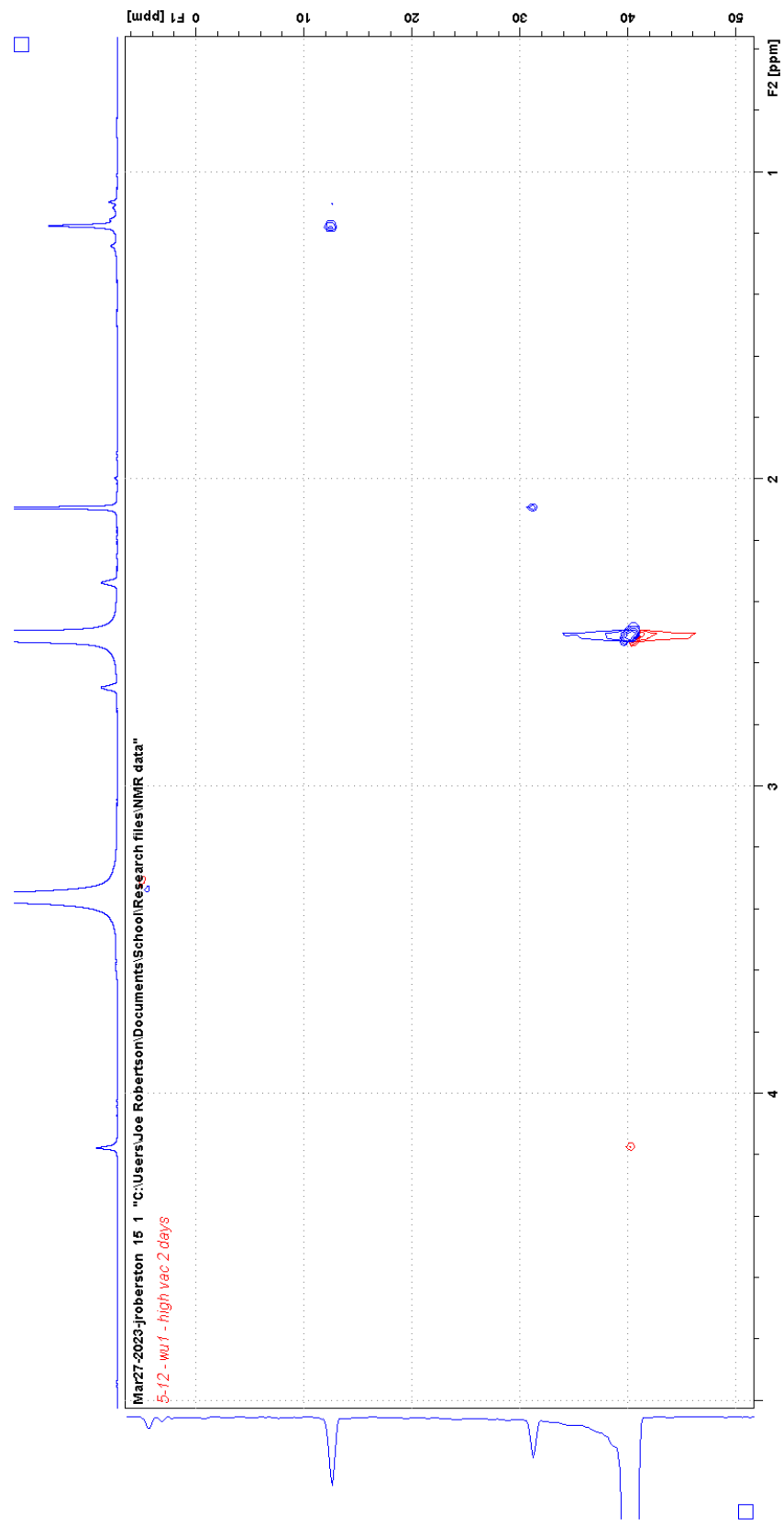


Figure A 10: HSQC of CBDA-7 at room temperature.

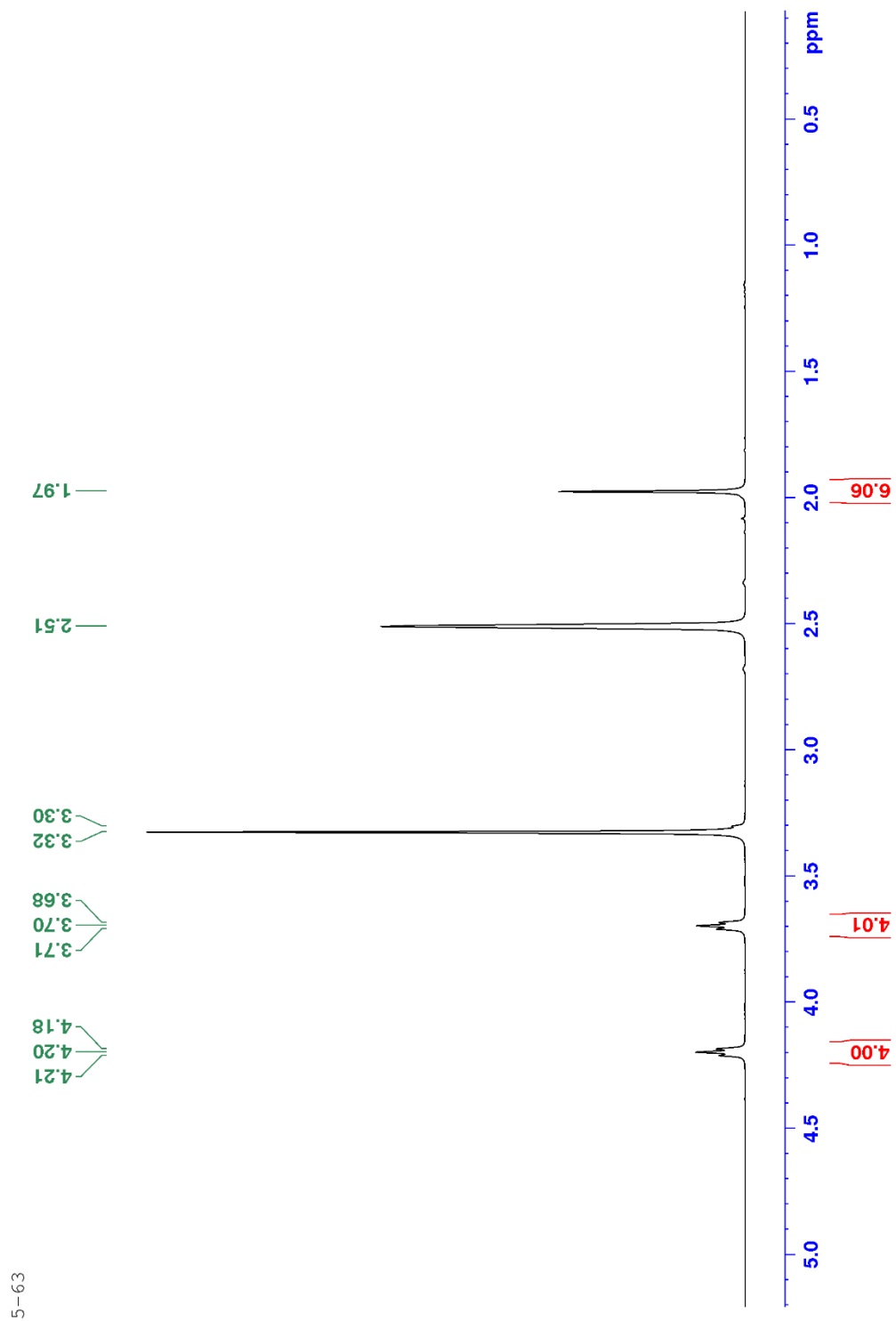
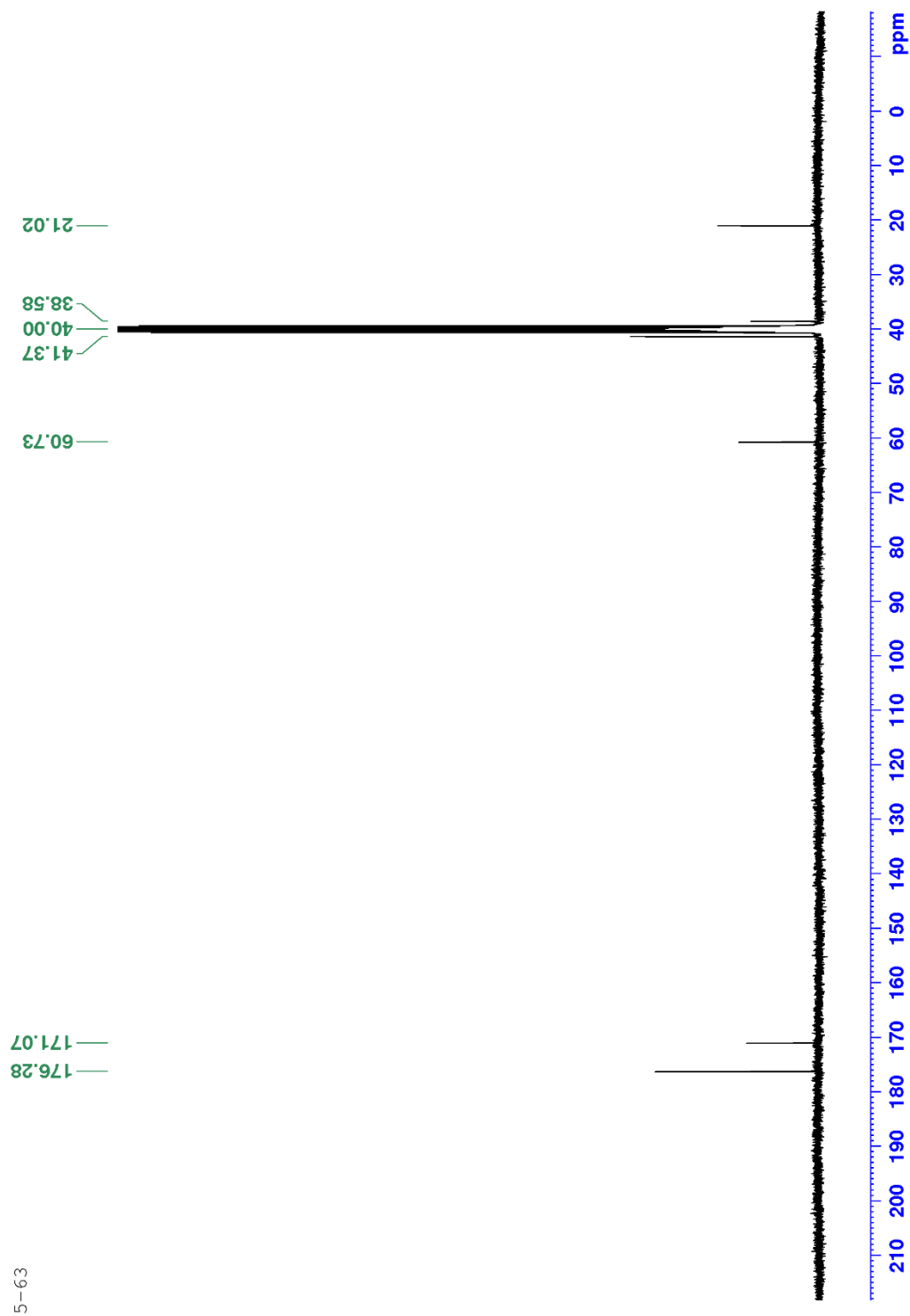
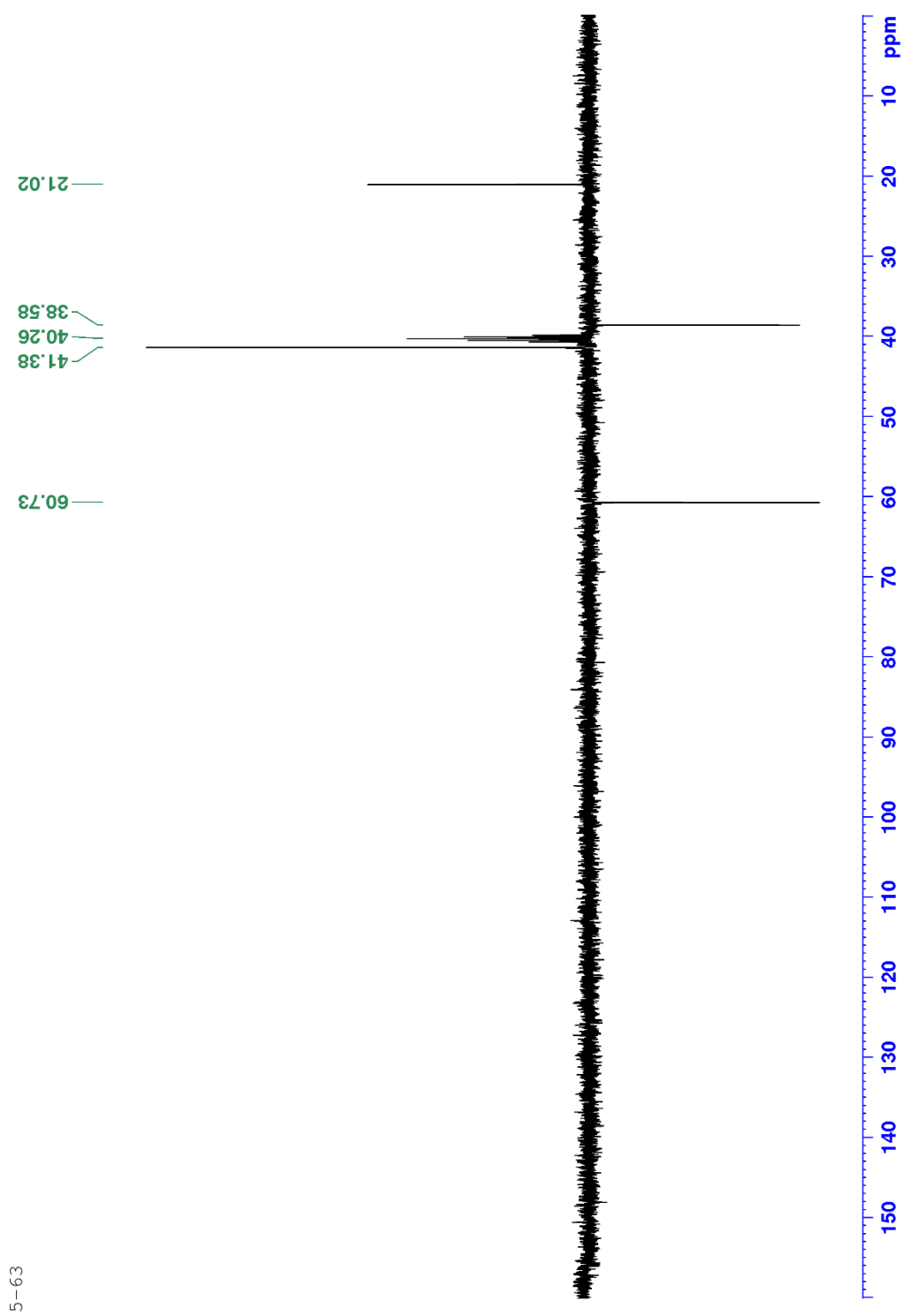


Figure A 11:  $^1\text{H-NMR}$  of CBDAc-1 at room temperature.



5-63

Figure A 12:  $^{13}\text{C}$ -NMR of CBDAc-1 at room temperature.



5-63

Figure A 13: DEPT135 of CBDAc-1 at room temperature.

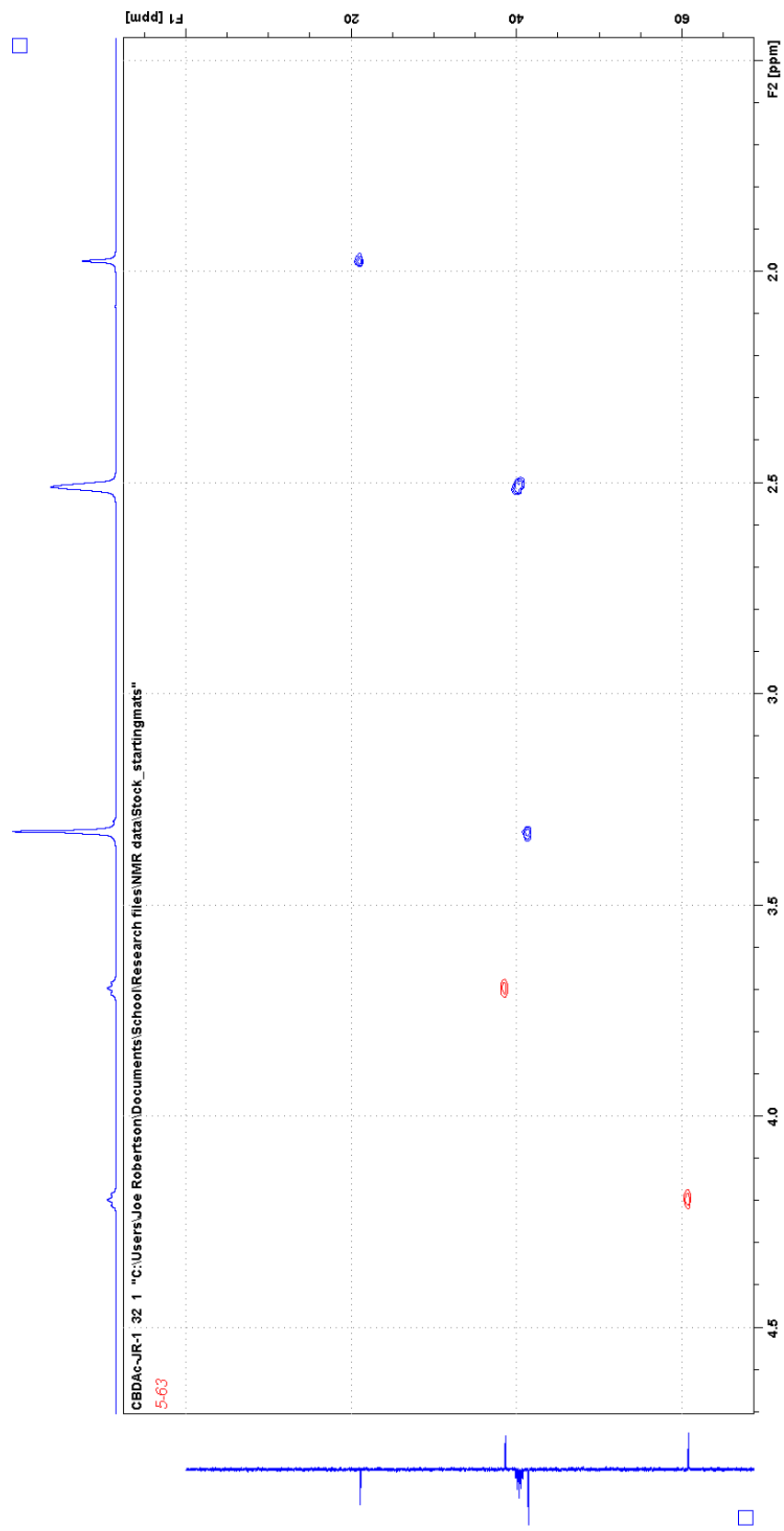


Figure A 14: HSQC of CBDAc-1 at room temperature.

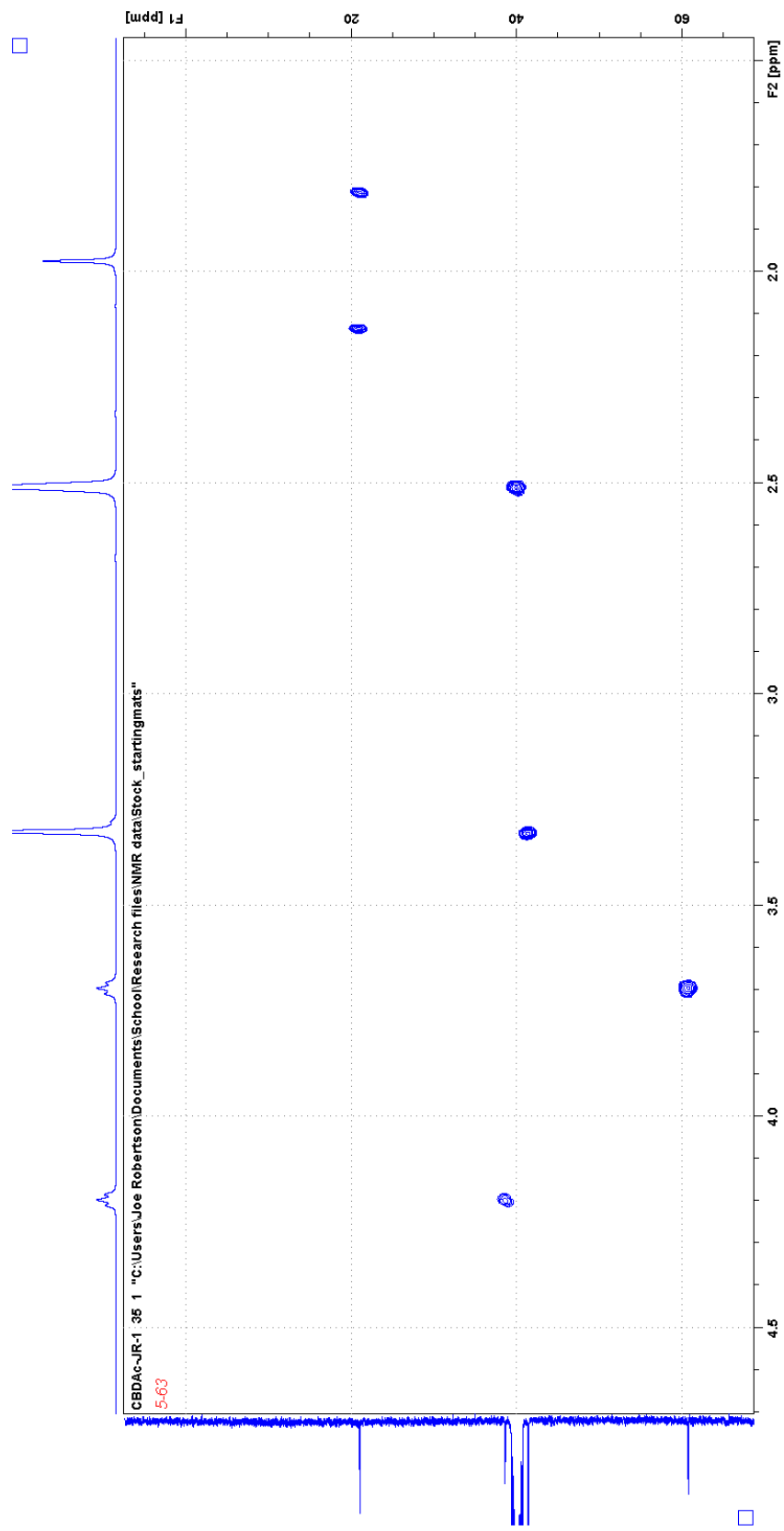


Figure A 15: HMBC of CBDAc-1 at room temperature.

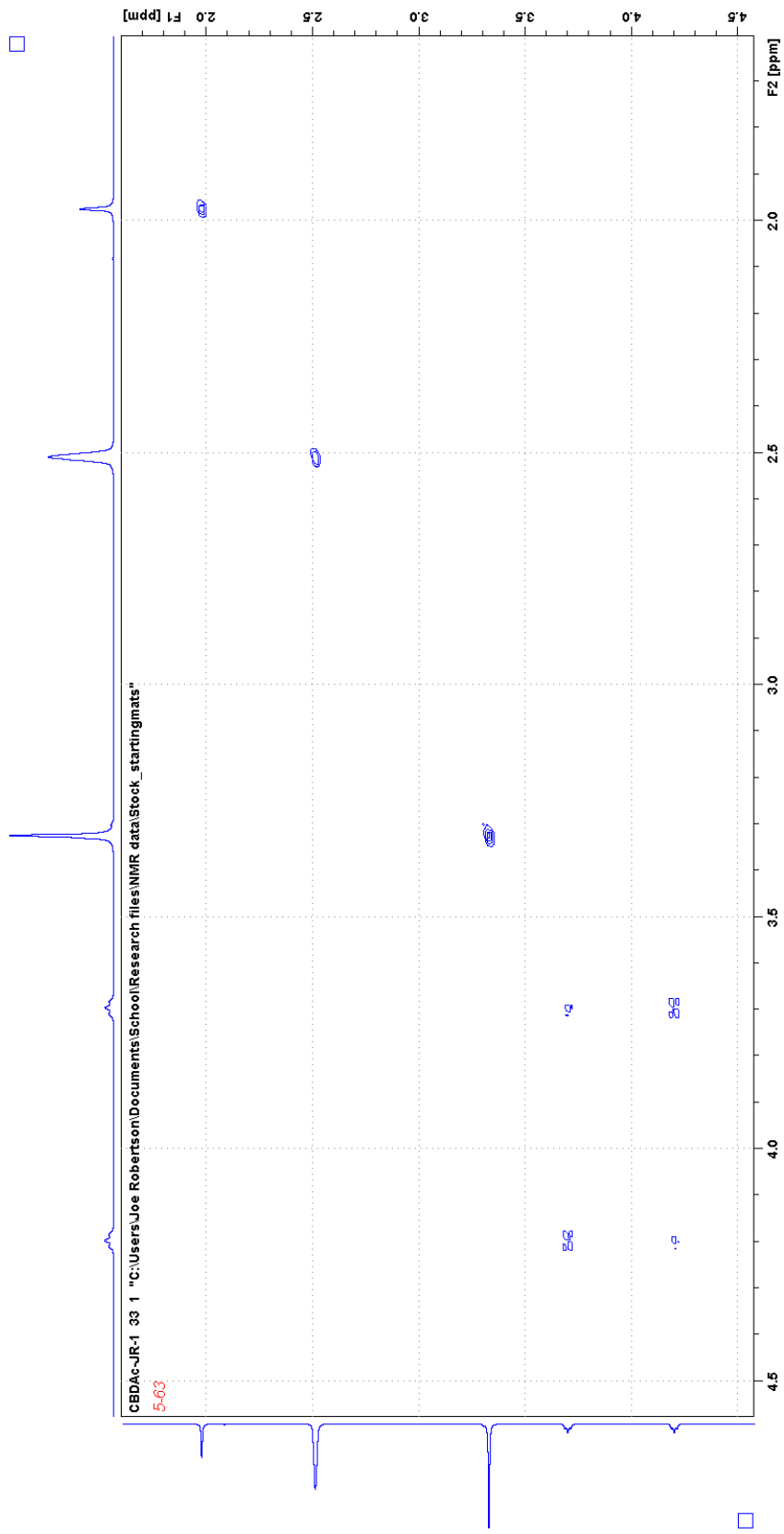


Figure A 16: COSY of CBDAc-1 at room temperature.



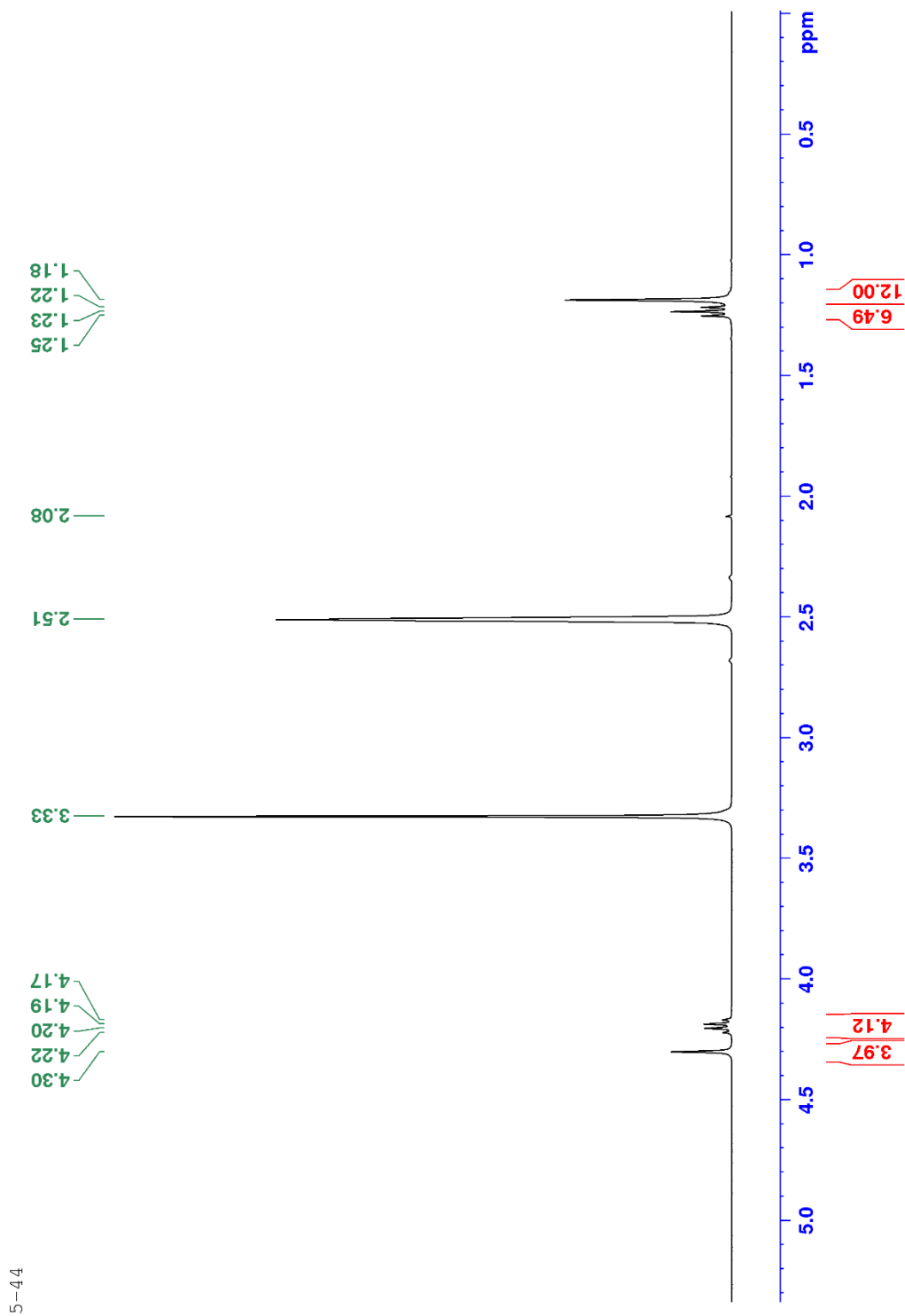
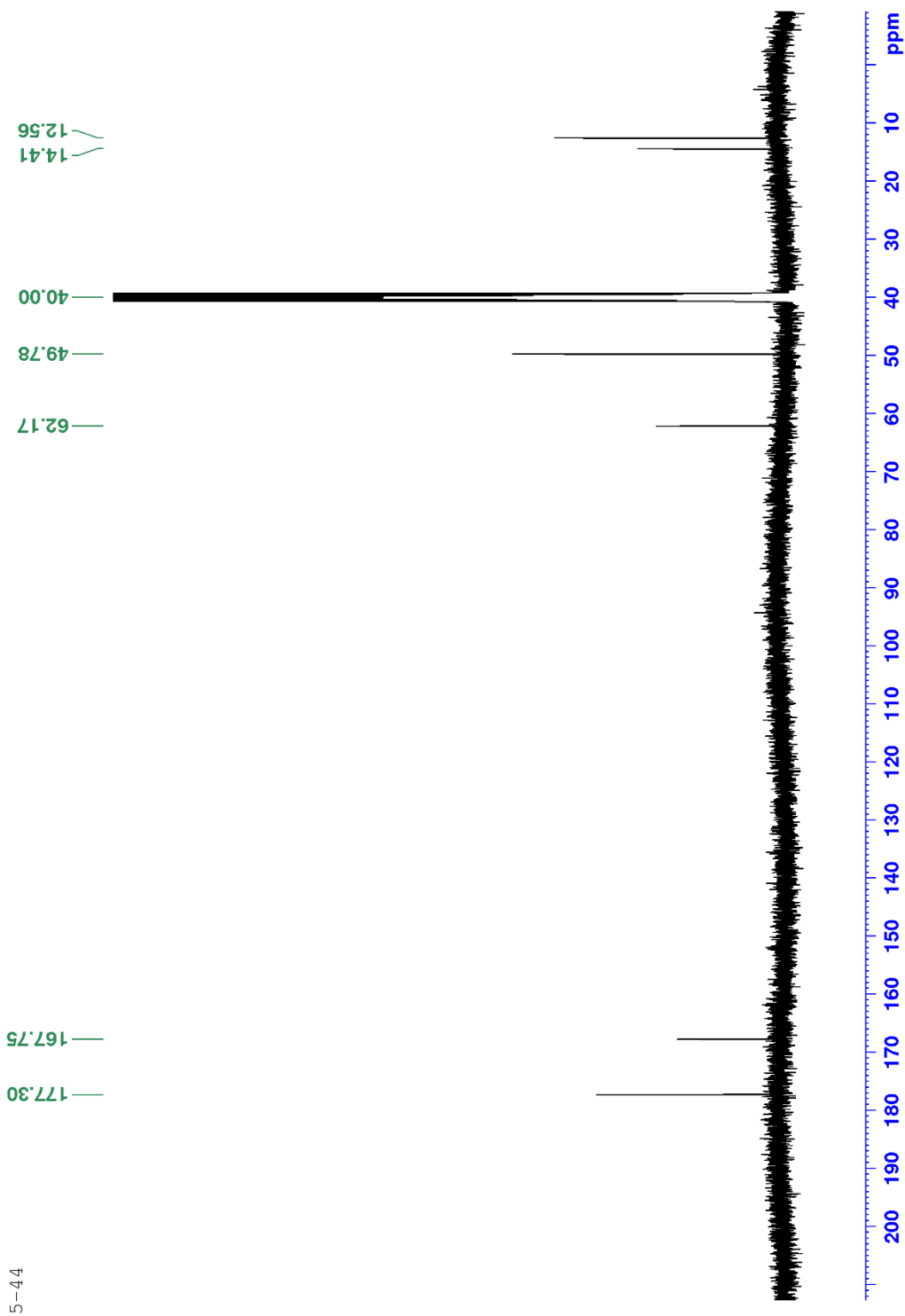


Figure A 17:  $^1\text{H-NMR}$  of CBDE-6 at room temperature.



5-44

Figure A 18:  $^{13}\text{C}$ -NMR of CBDE-6 at room temperature.

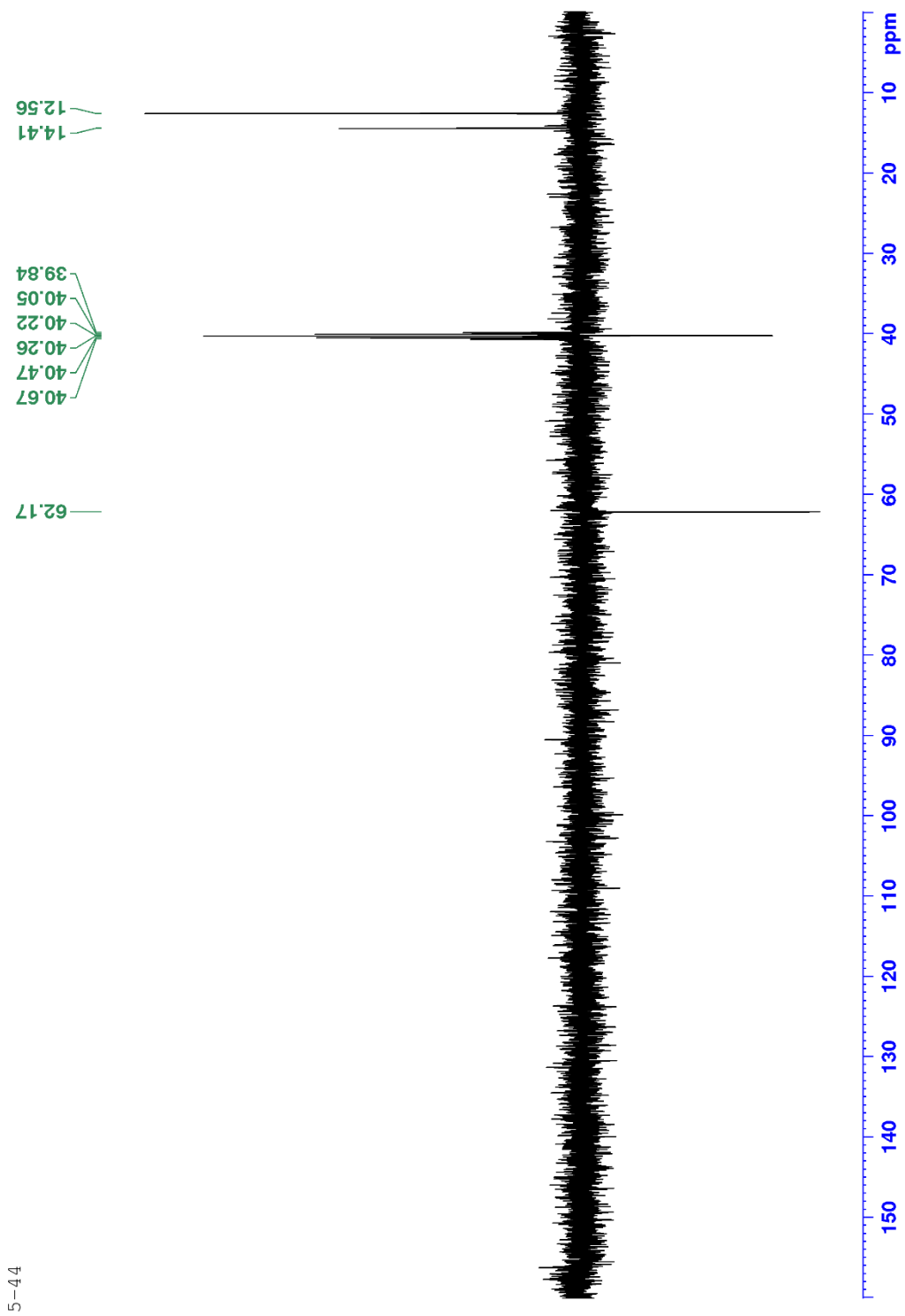


Figure A 19: DEPT135 of CBDE-6 at room temperature.

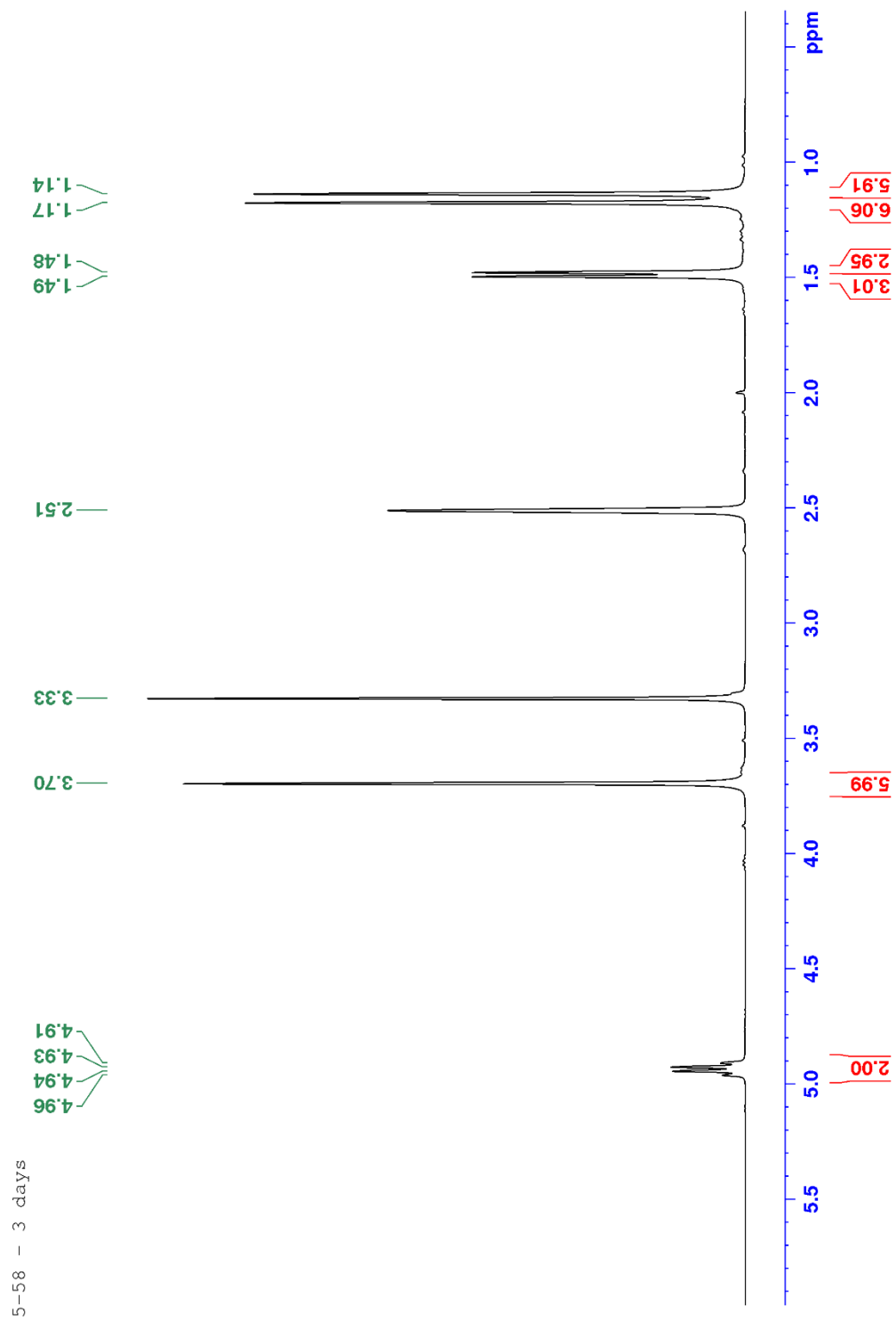


Figure A 20:  $^1\text{H}$ -NMR of CBDE-7 at room temperature.

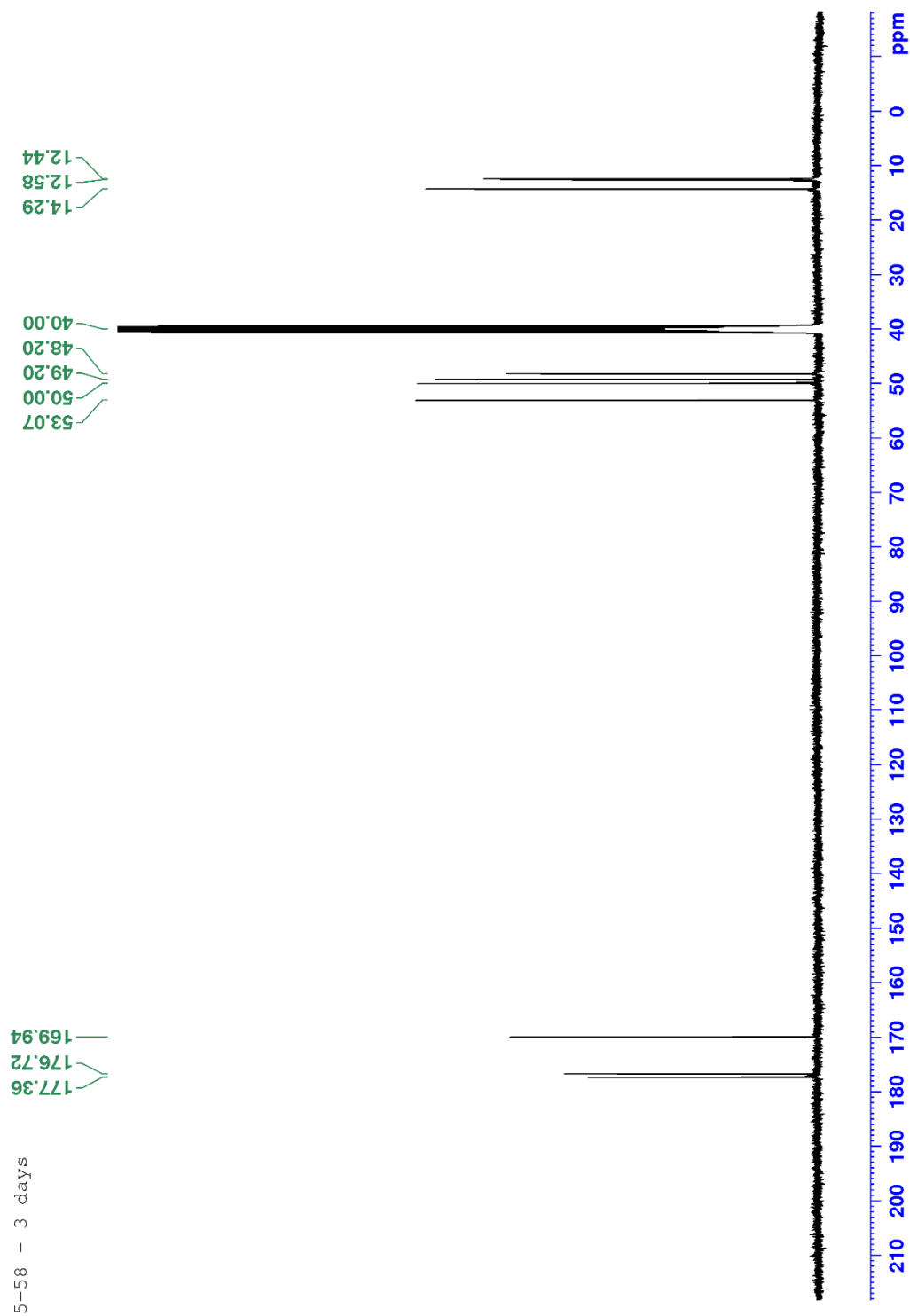


Figure A 21:  $^{13}\text{C}$ -NMR of CBDE-7 at room temperature.

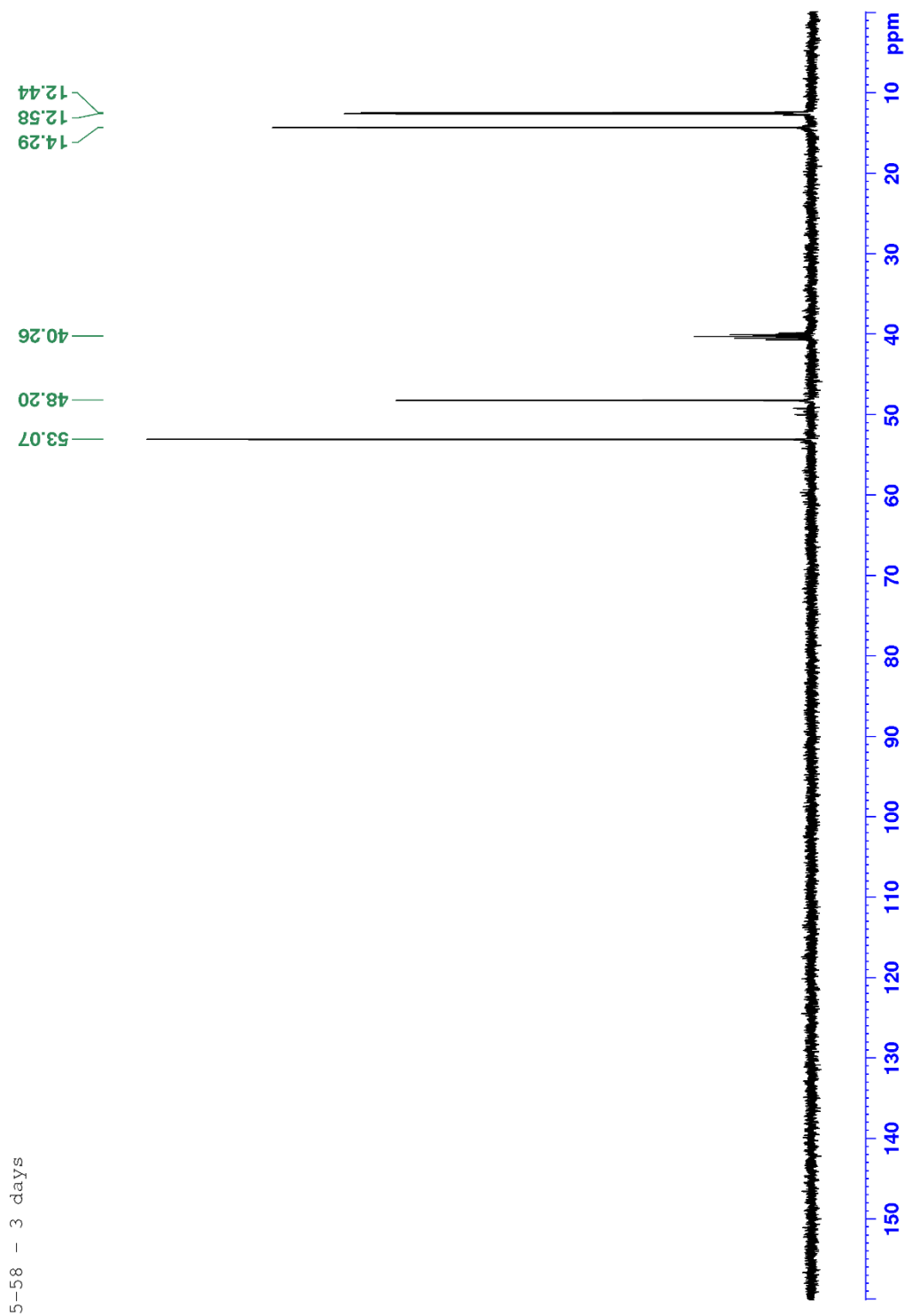


Figure A 22: DEPT135 of CBDE-7 at room temperature.

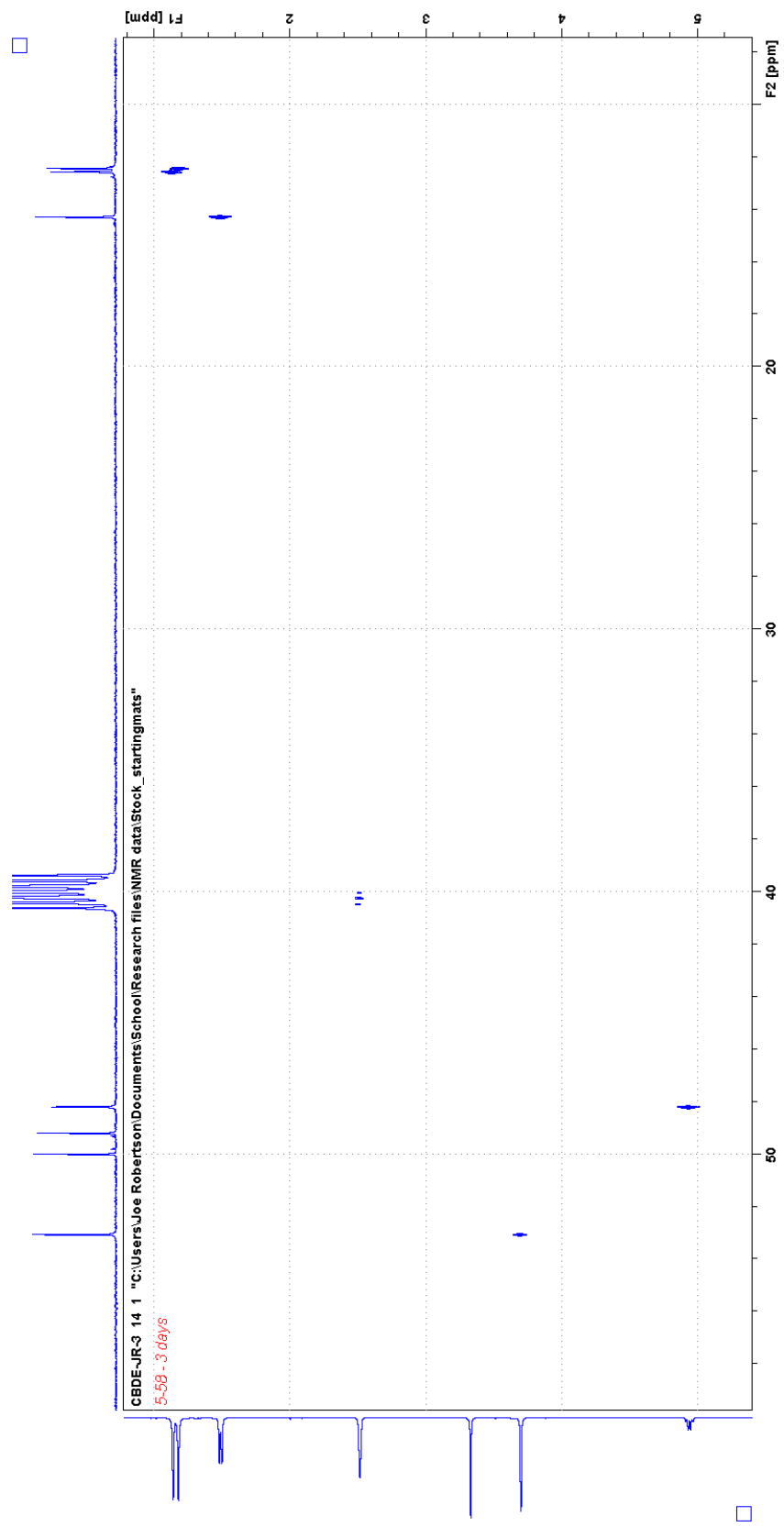


Figure A 23: H-C correlation of CBDE-7 at room temperature.

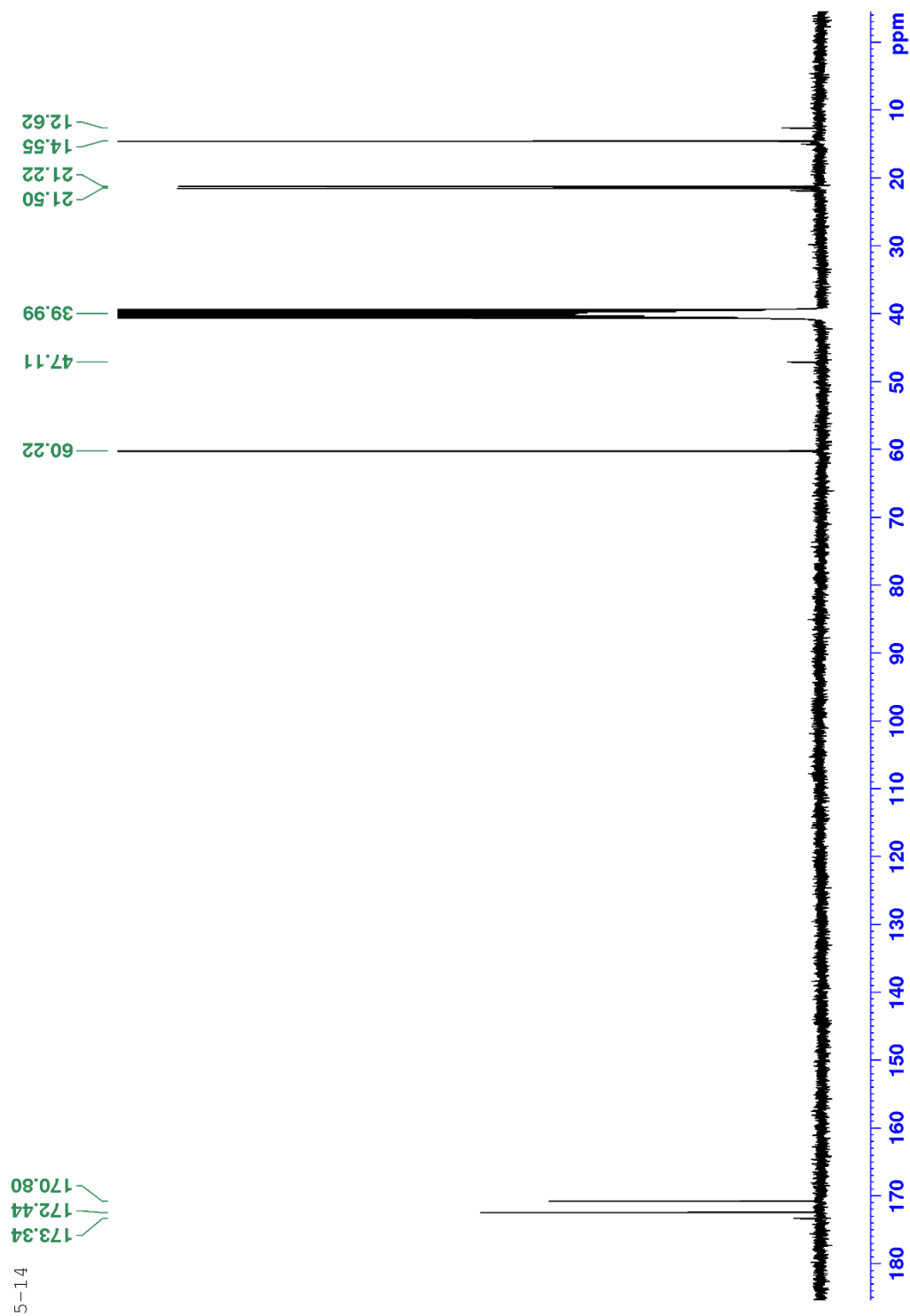


Figure A 24:  $^{13}\text{C}$ -NMR of CBDH-1 at room temperature.



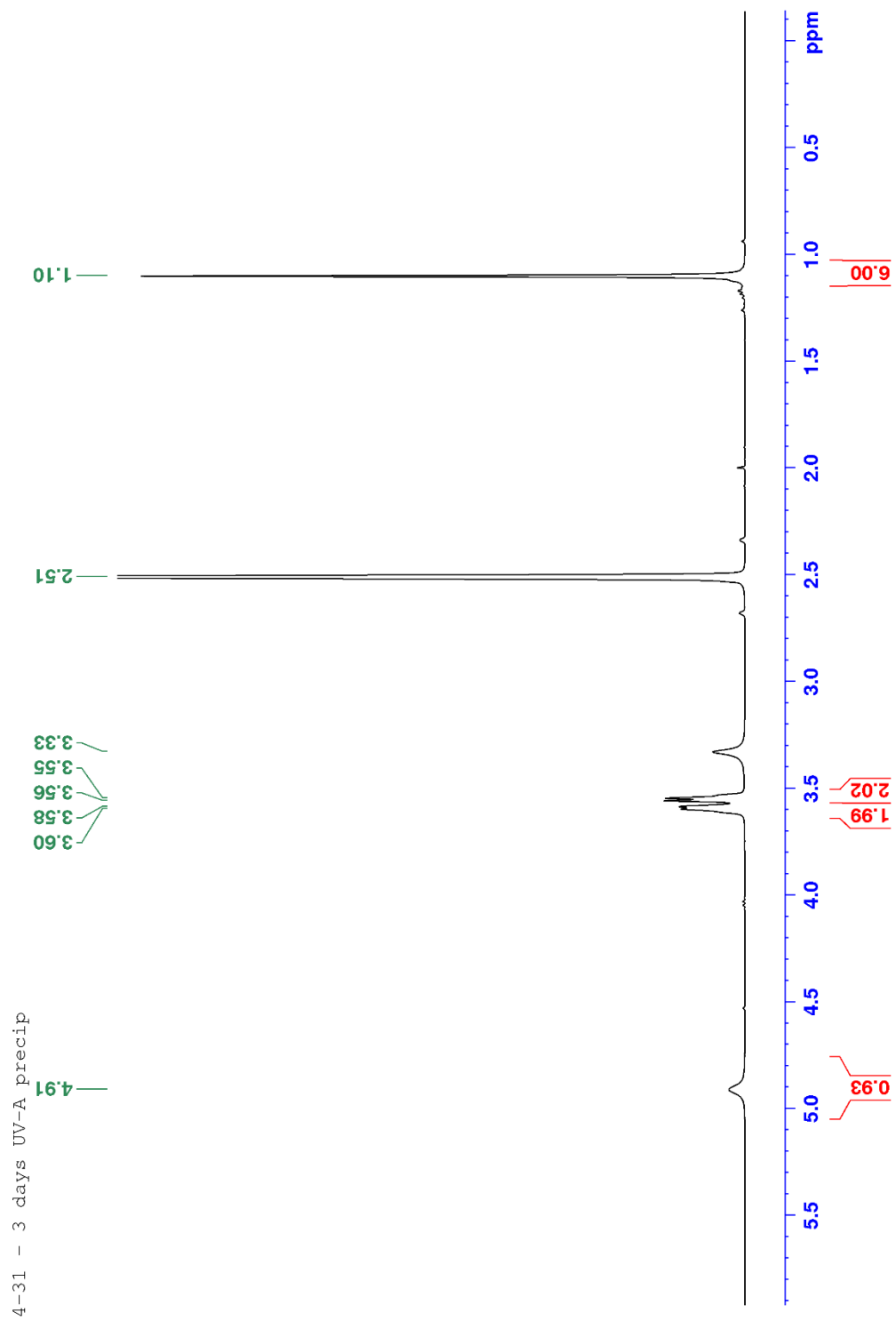


Figure A 25:  $^1\text{H-NMR}$  of CBDO-2 at room temperature using synthetic method 1

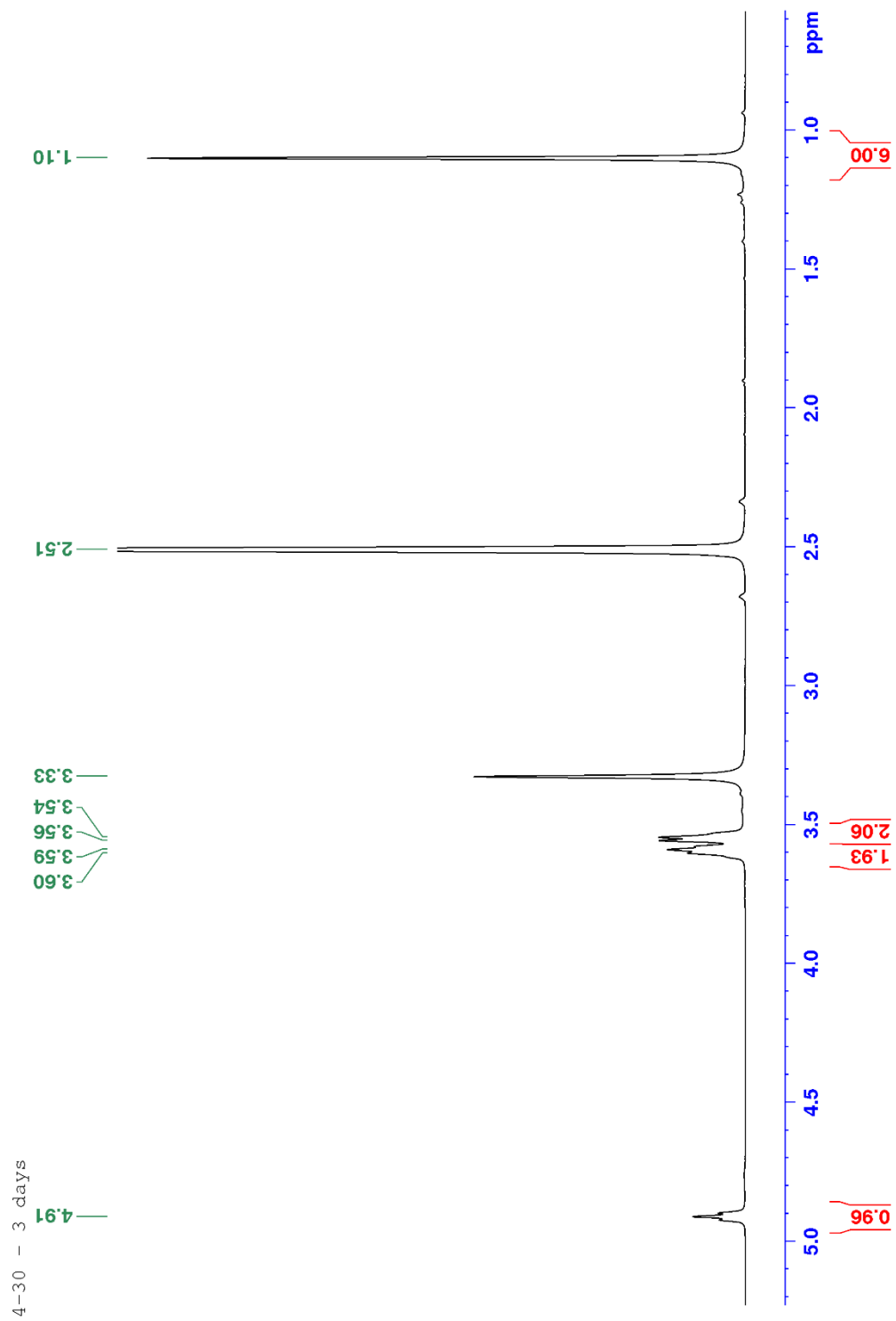


Figure A 26:  $^1\text{H}$ -NMR of CBDO-2 at room temperature using synthetic method 2

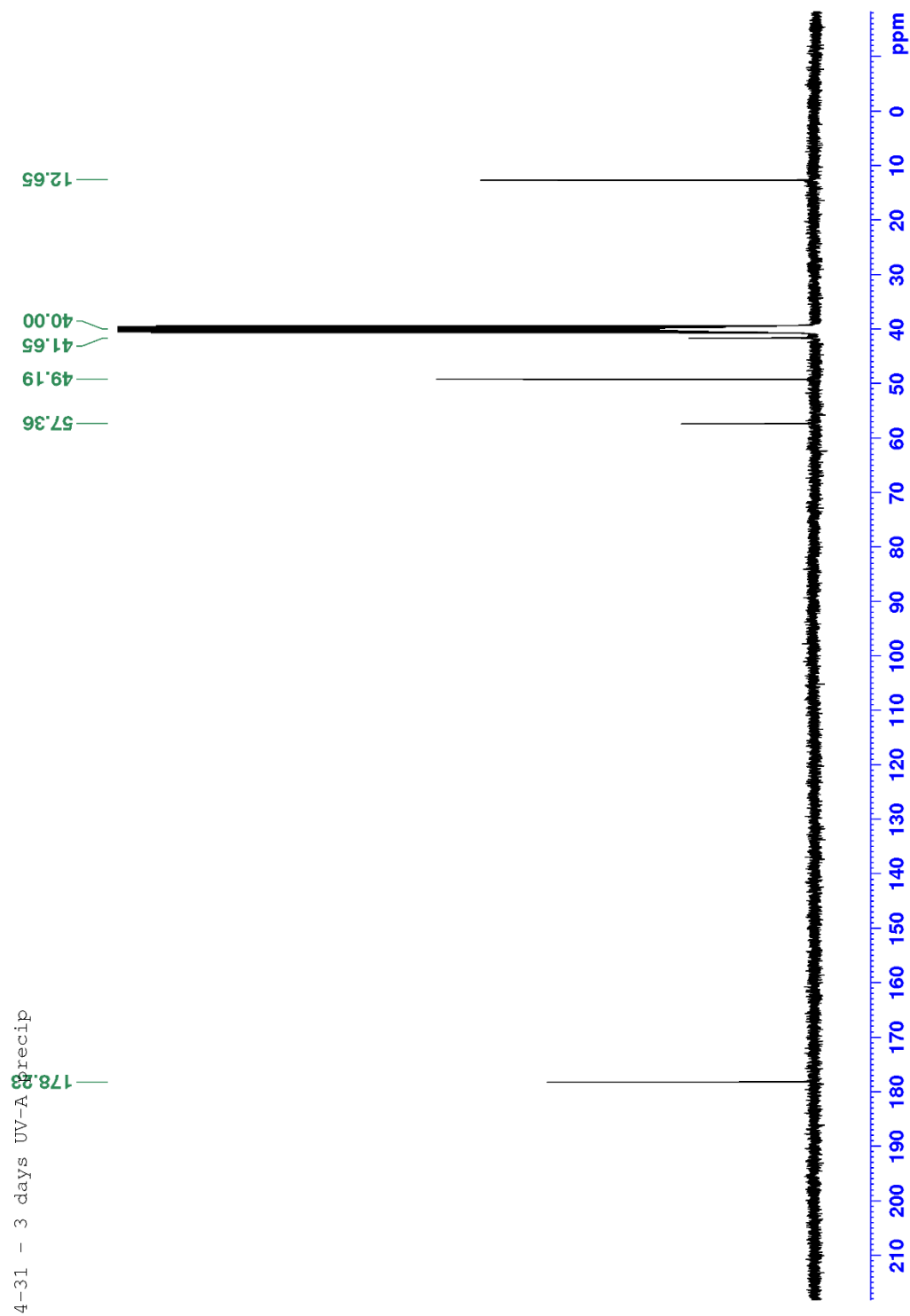


Figure A 27:  $^{13}\text{C}$ -NMR of CBDO-2 at room temperature using synthetic method 1

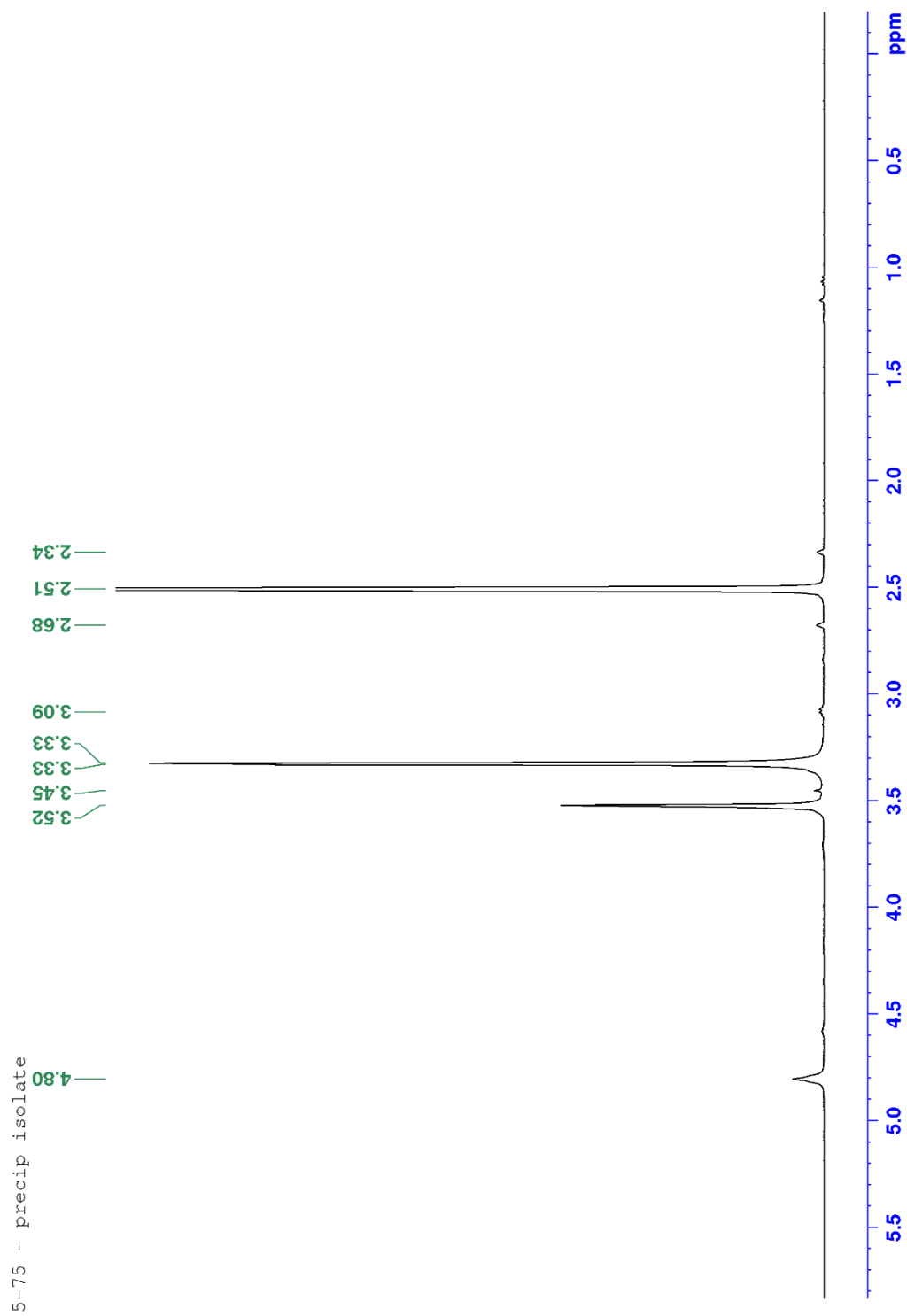


Figure A 28:  $^1\text{H}$ -NMR of CBDO-3 at room temperature

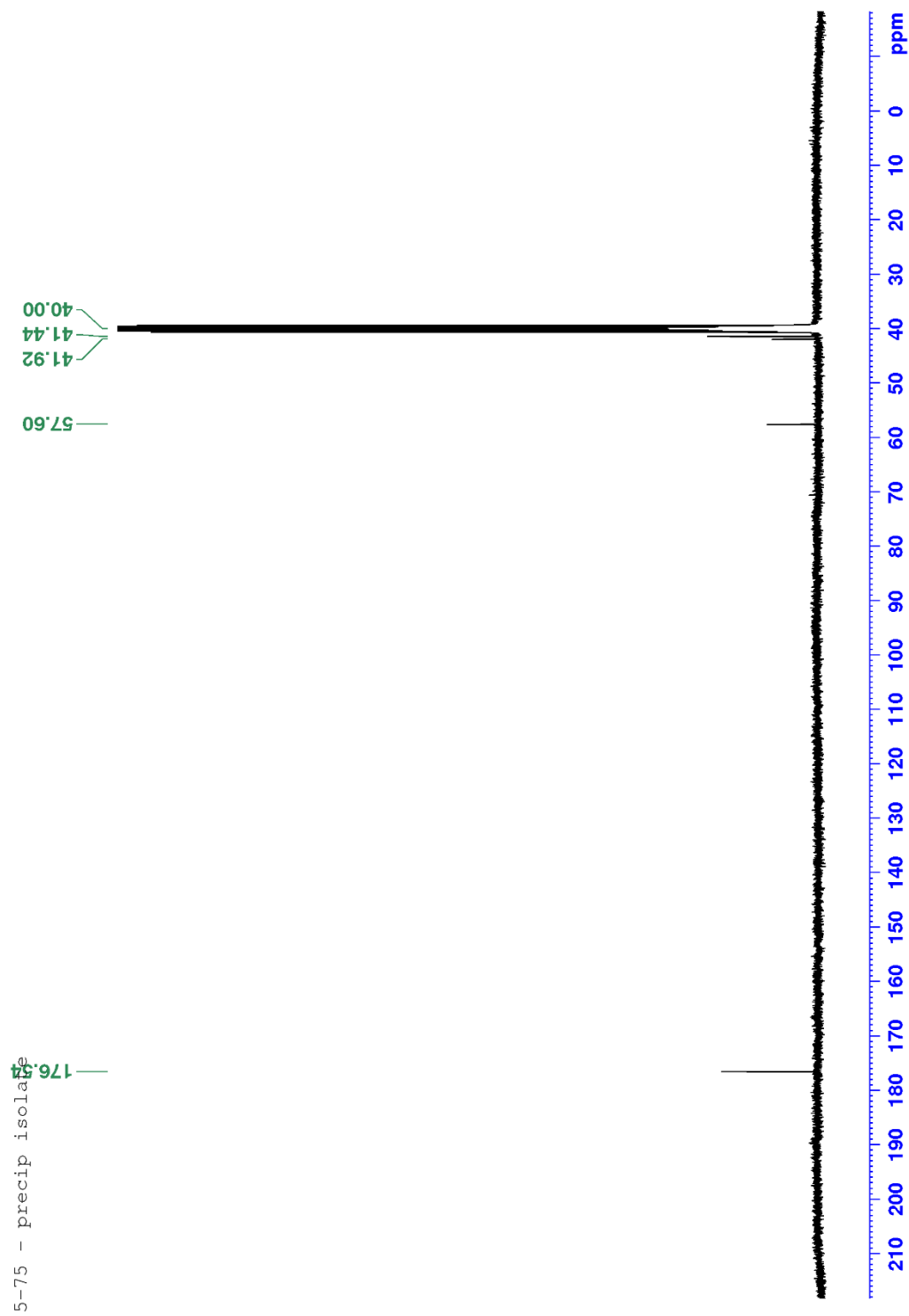


Figure A 29:  $^{13}\text{C}$ -NMR of CBDO-3 at room temperature

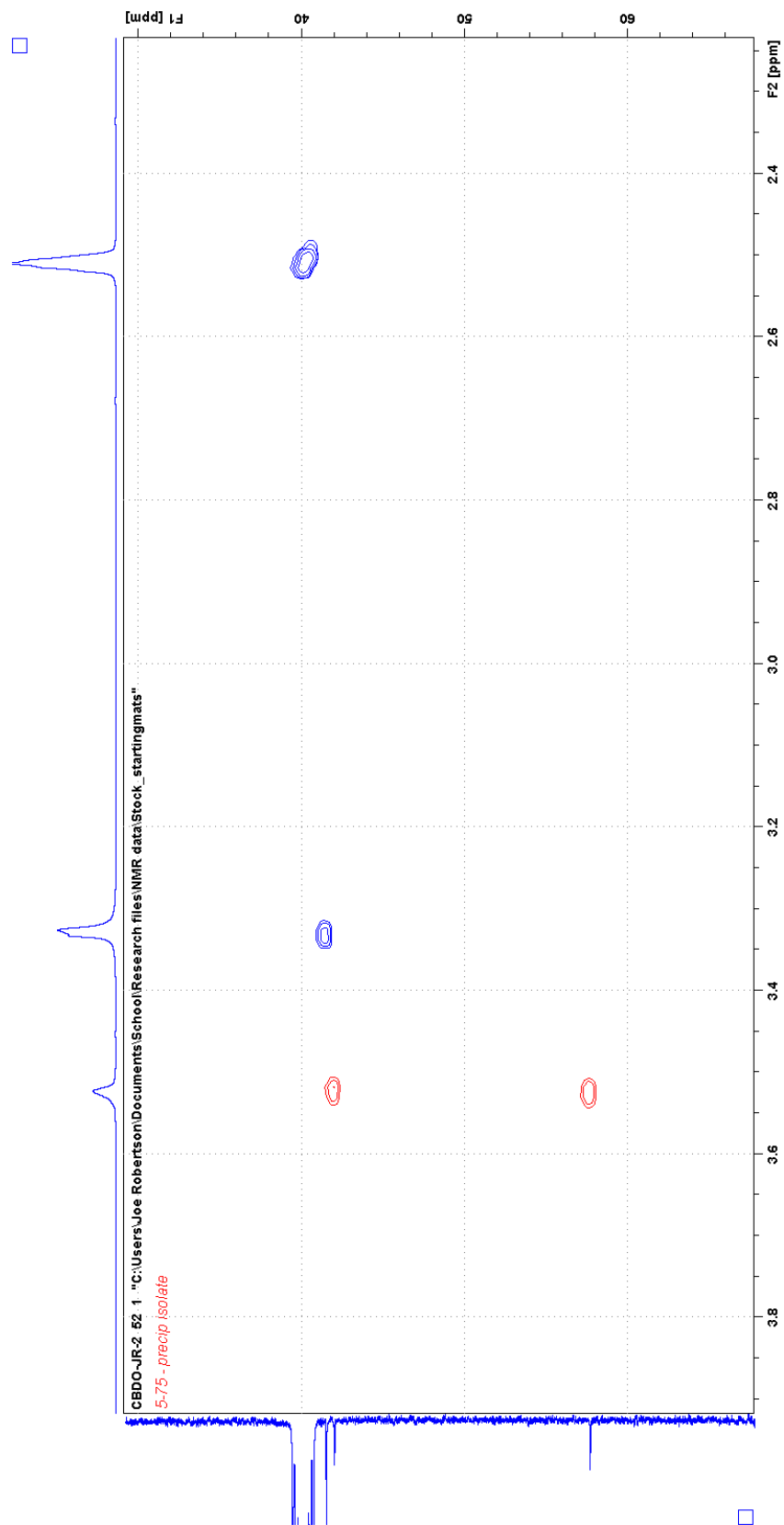


Figure A 30: HSQC of CBDO-3 at room temperature

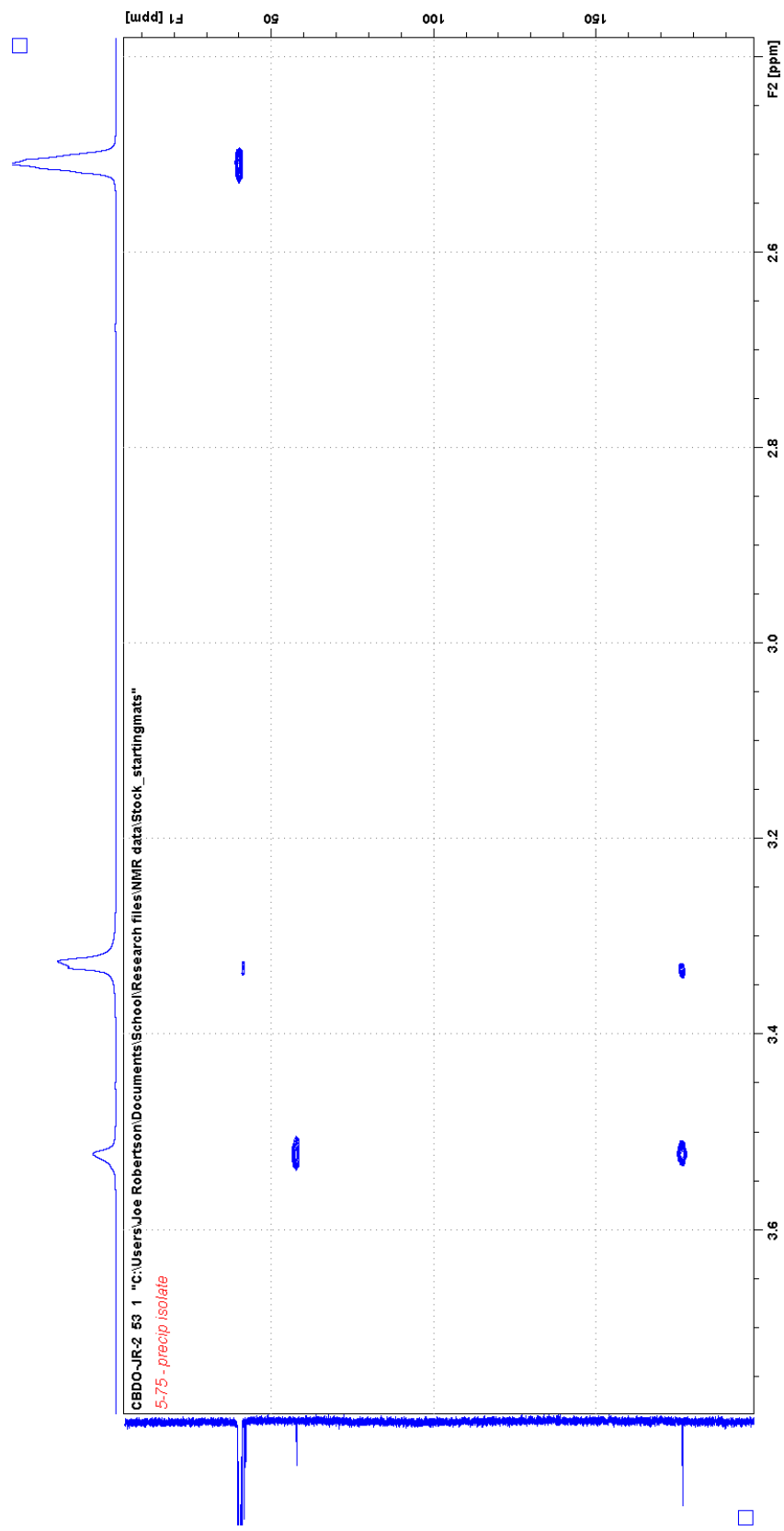


Figure A 31: HMBC of CBDO-3 at room temperature

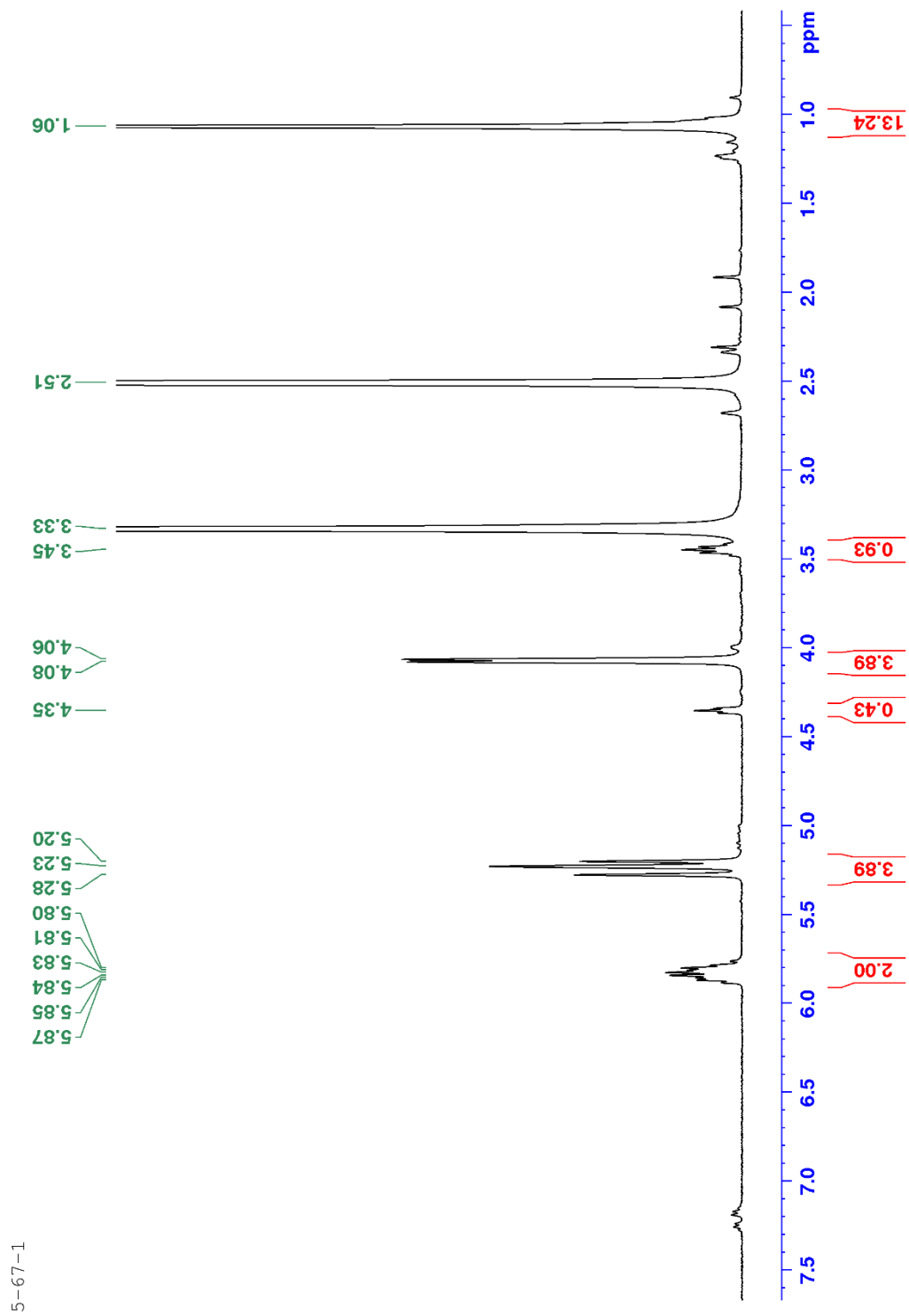


Figure A 32:  $^1\text{H-NMR}$  of CBDV-1 at room temperature



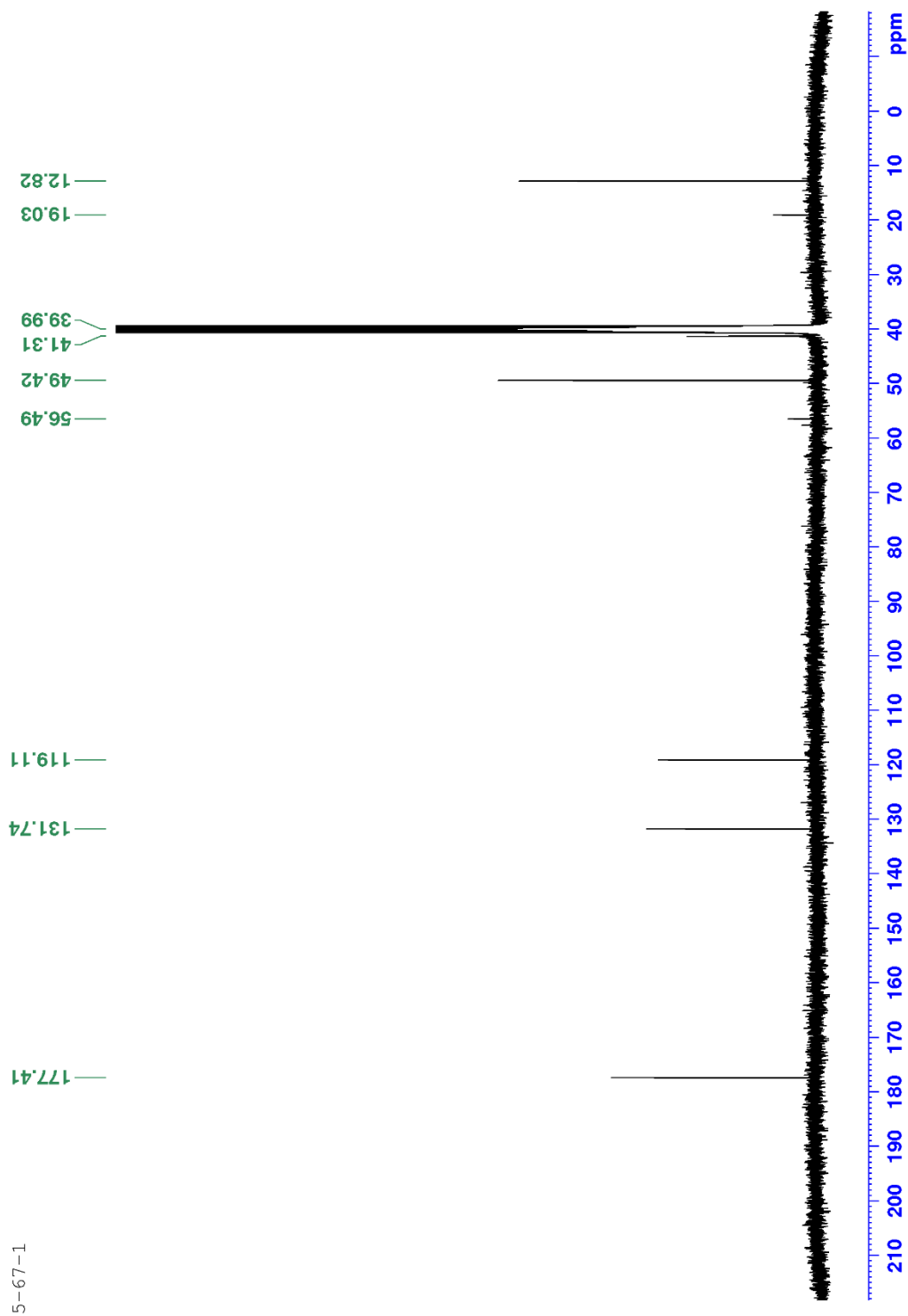


Figure A 33:  $^{13}\text{C}$ -NMR of CBDV-1 at room temperature

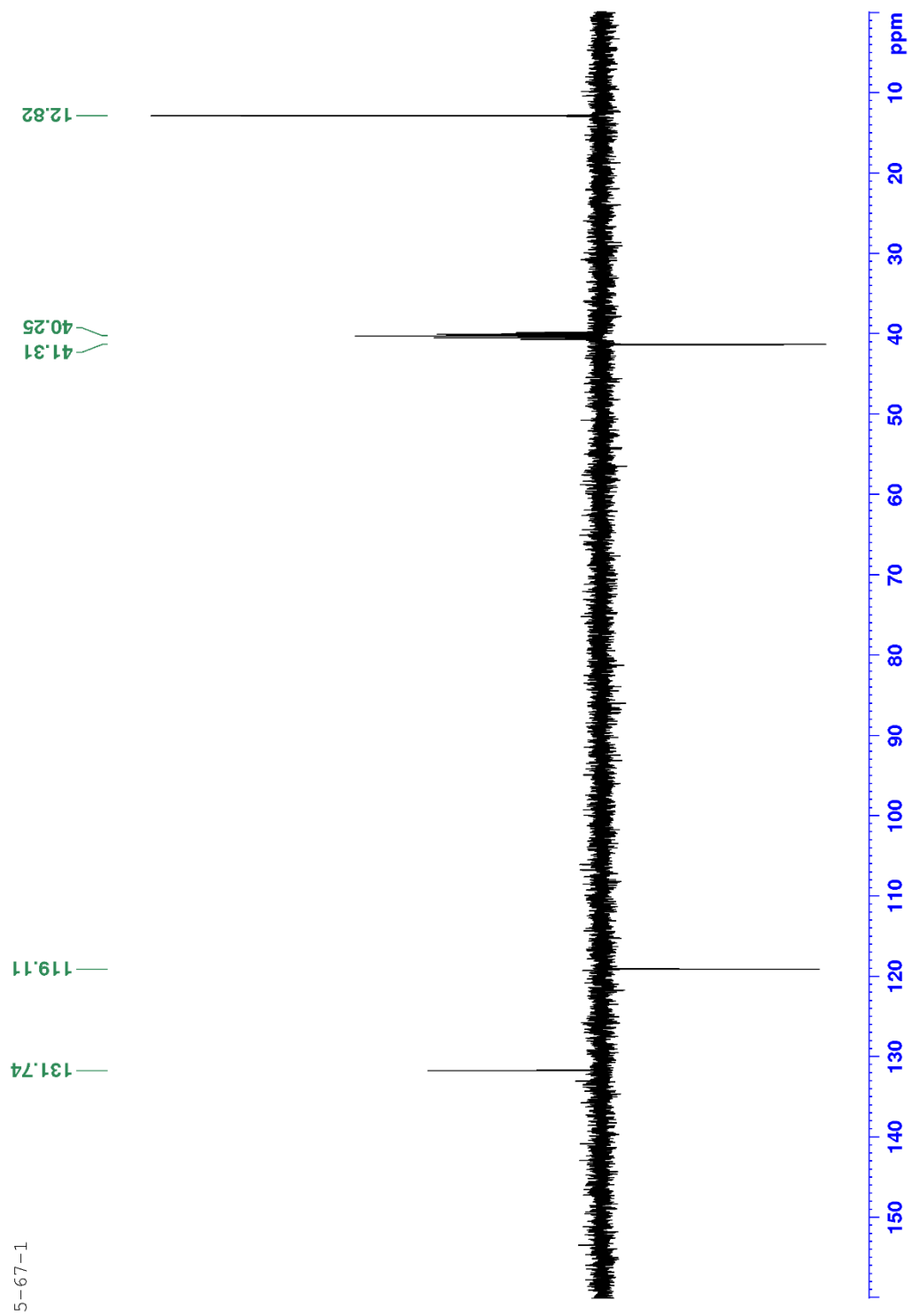


Figure A 34: DEPT135 of CBDV-1 at room temperature

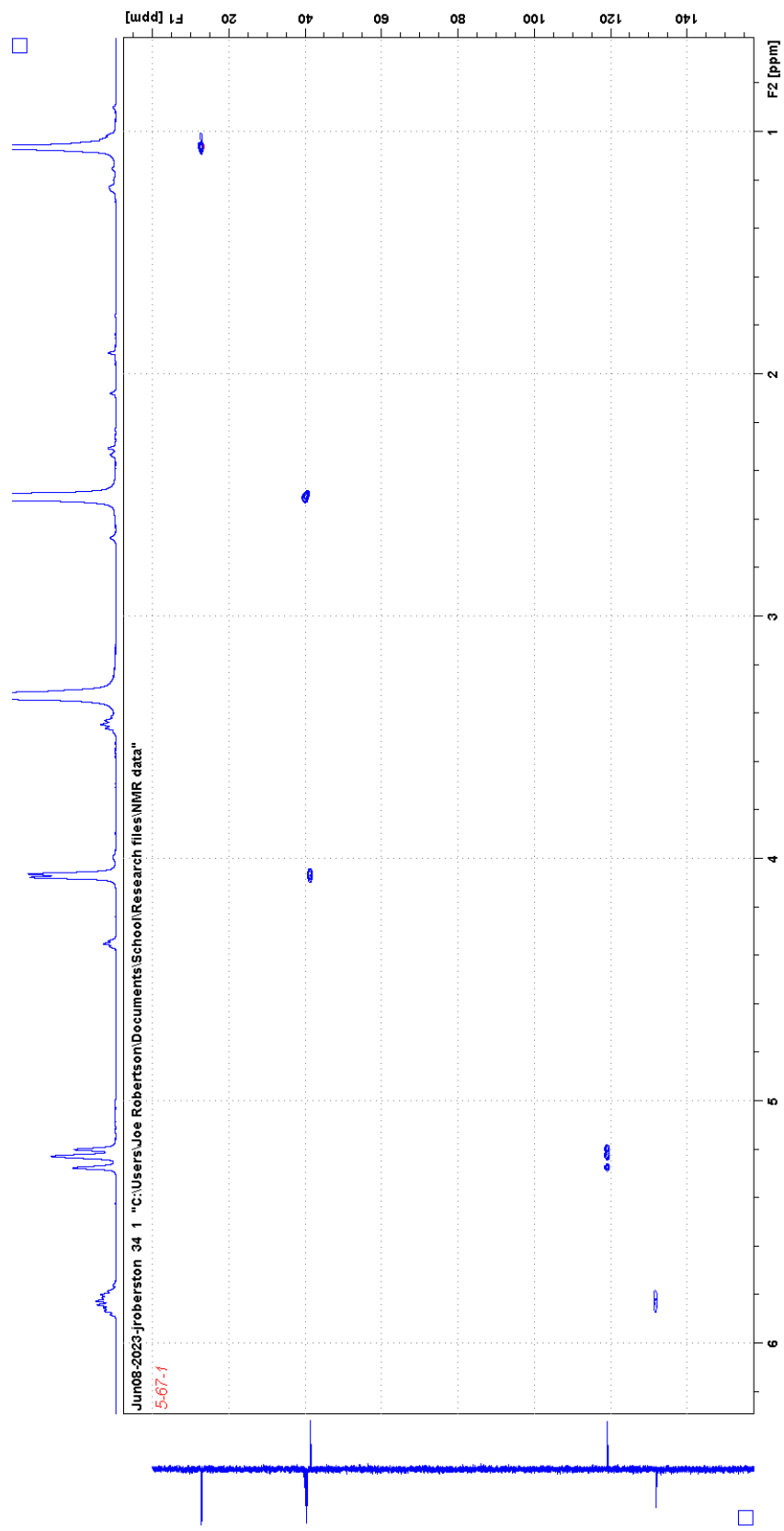


Figure A 35: HSQC of CBDV-1 at room temperature

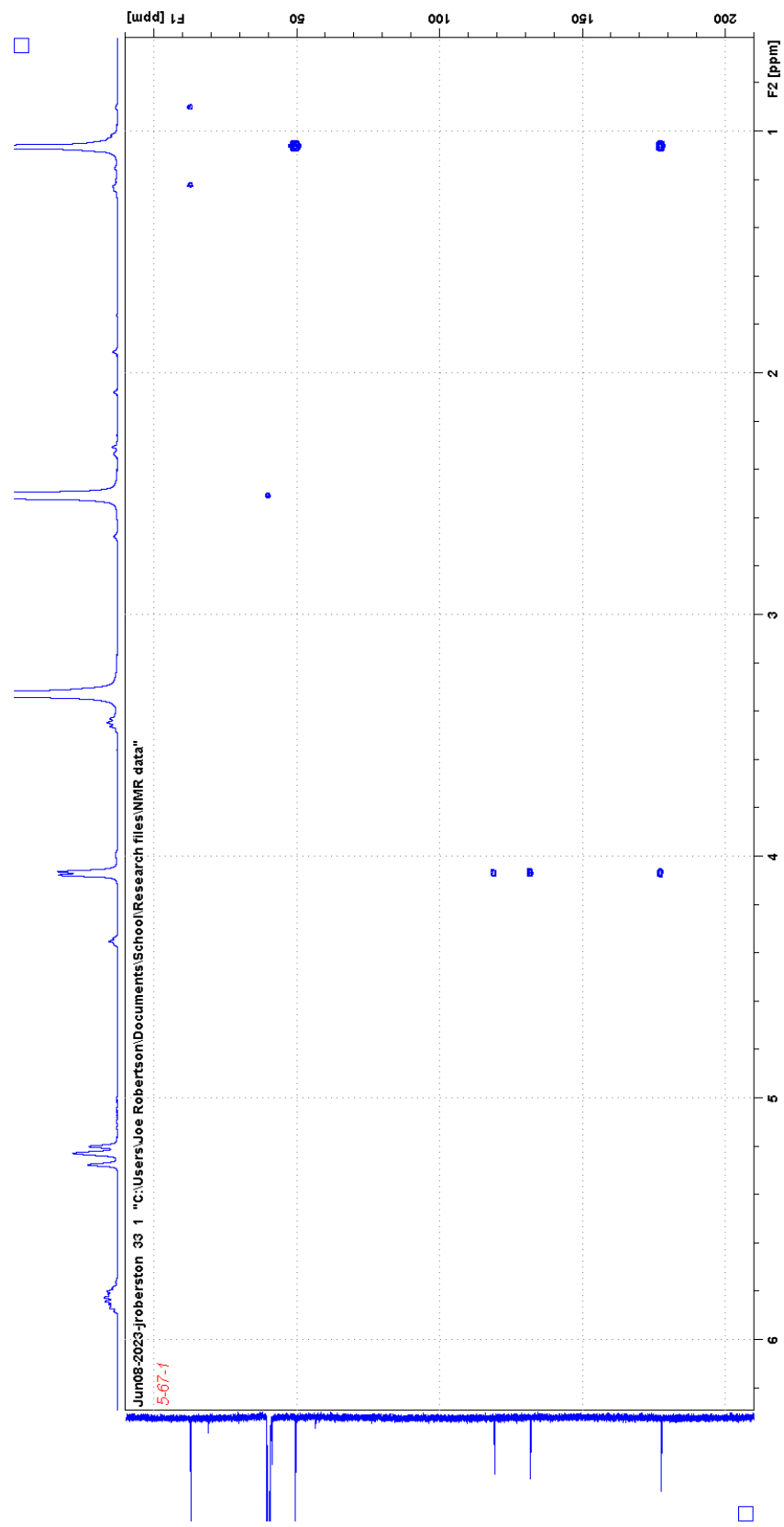


Figure A 36: HMBC of CBDV-1 at room temperature

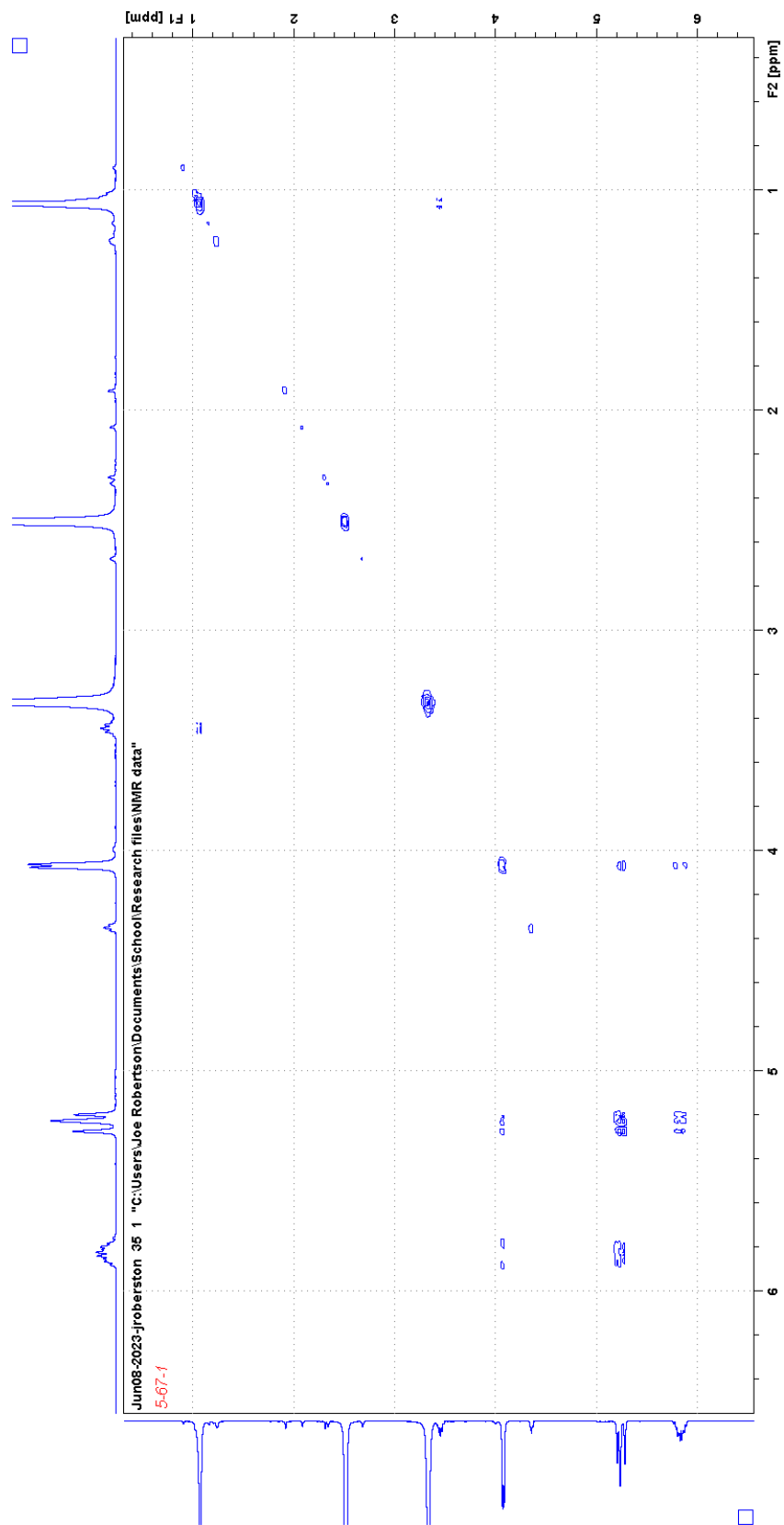


Figure A 37: COSY of CBDV-1 at room temperature

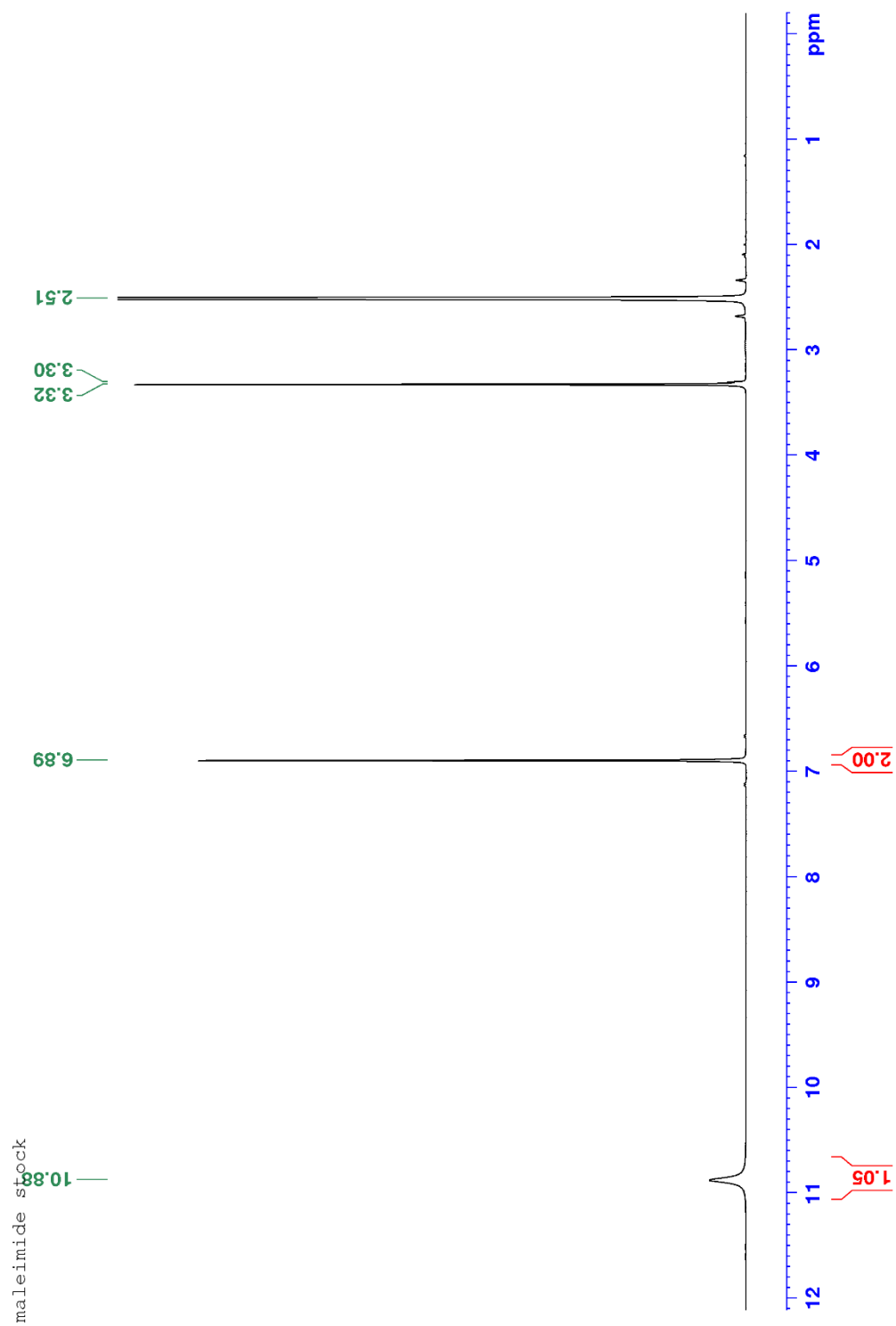


Figure A 38:  $^1\text{H-NMR}$  of protoCBB1-2 (maleimide) at room temperature

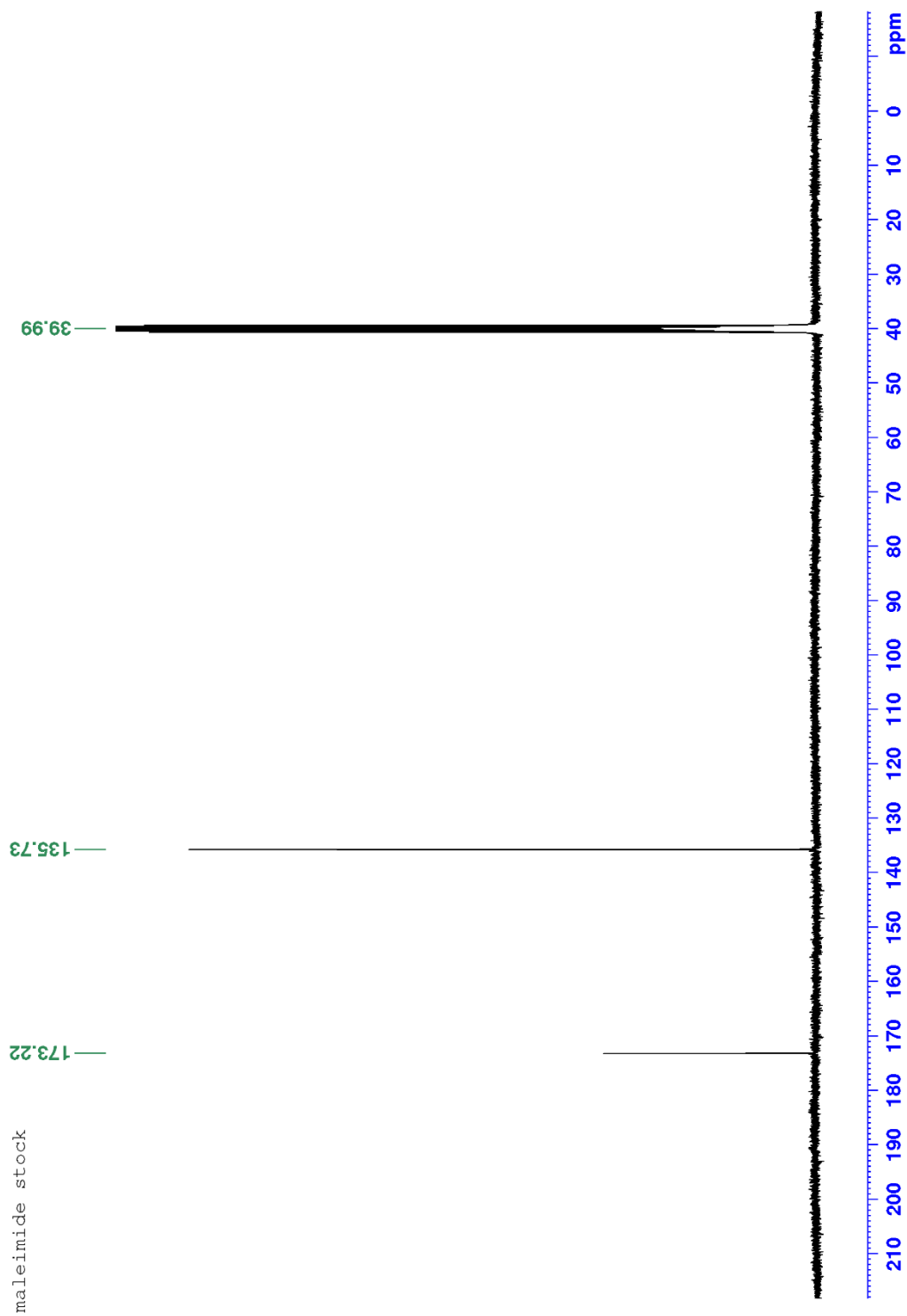


Figure A 39:  $^{13}\text{C}$ -NMR of protoCBB1-2 (maleimide) at room temperature

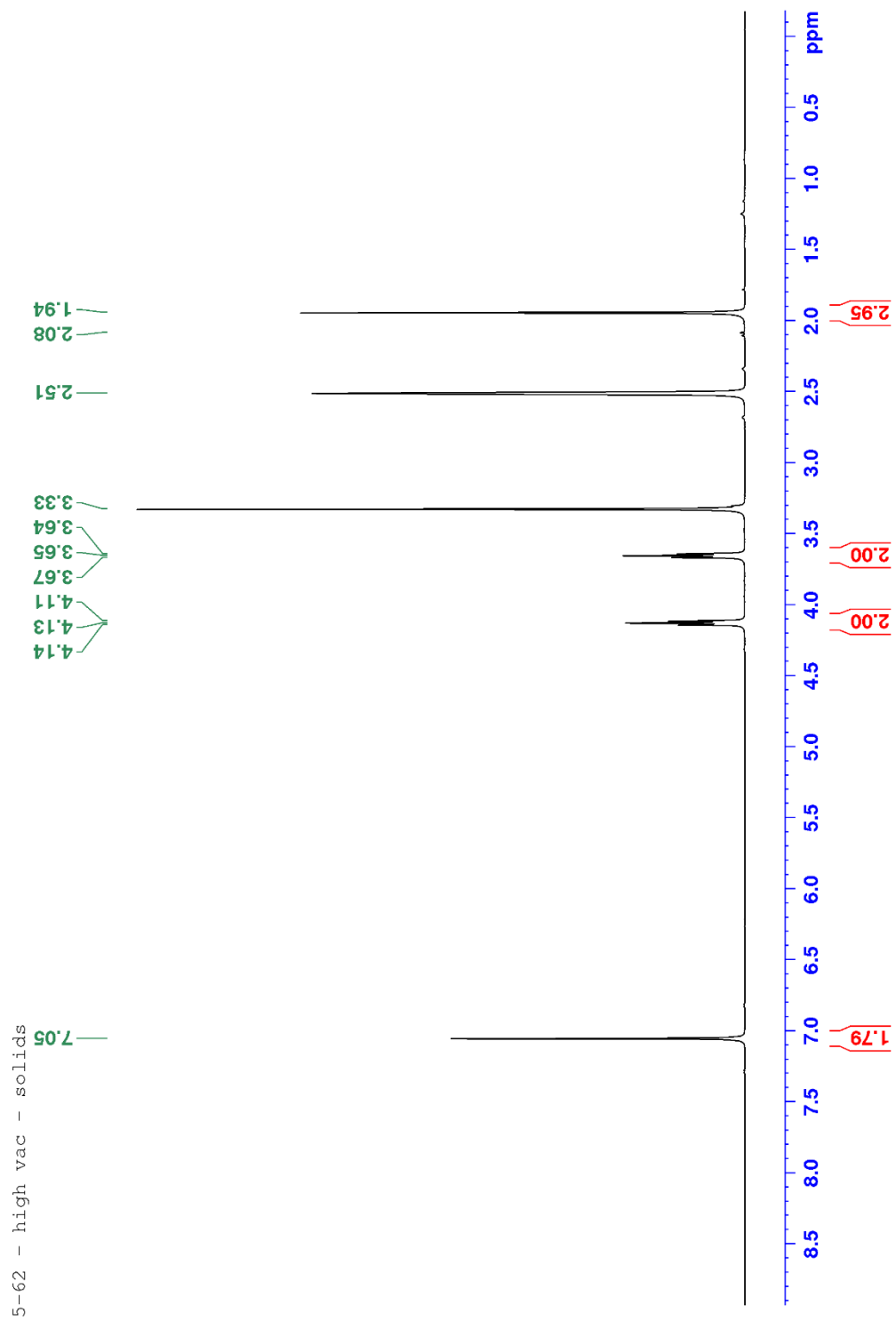


Figure A 40:  $^1\text{H-NMR}$  of protoCBDAc-2 at room temperature



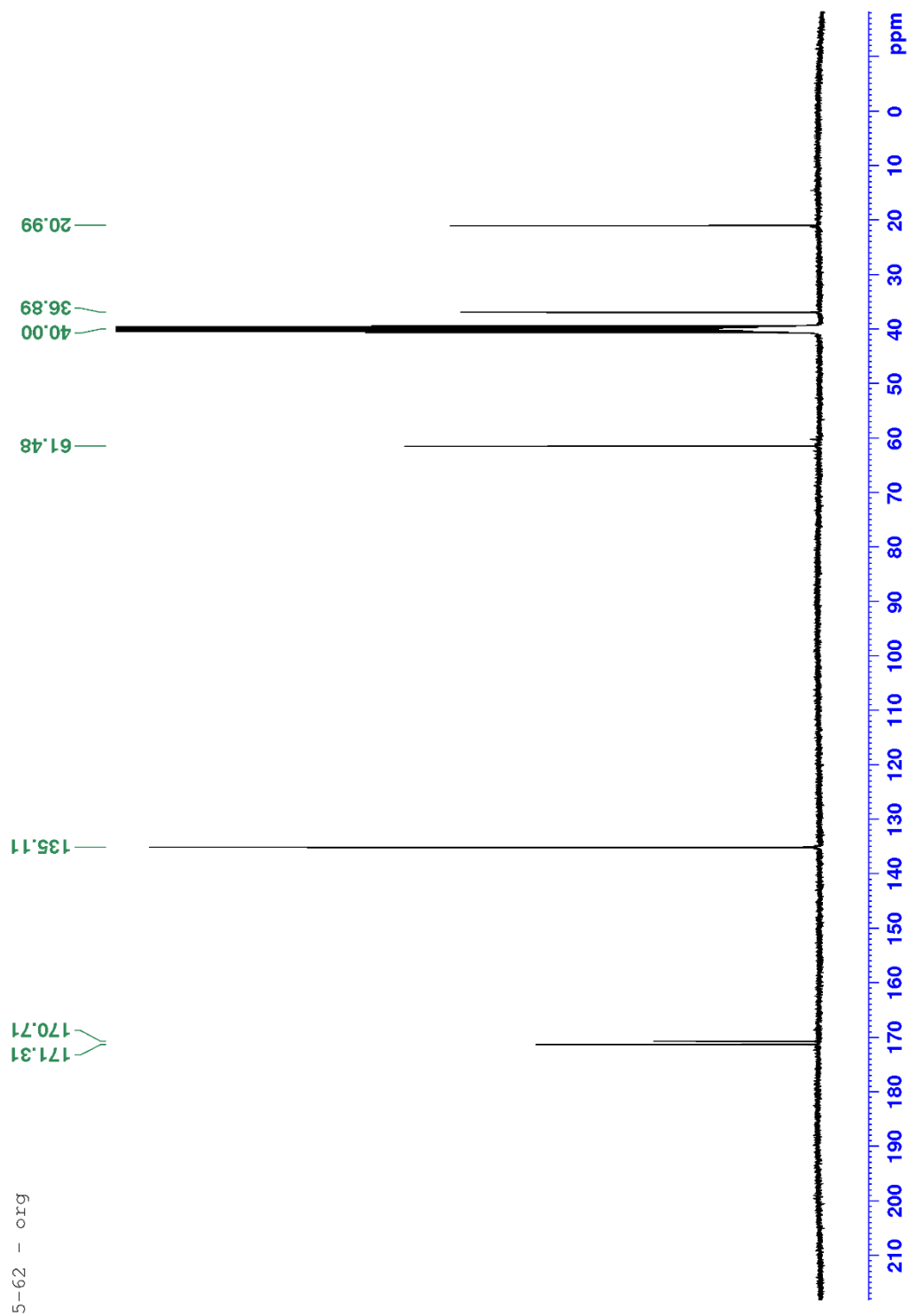


Figure A 41:  $^{13}\text{C}$ -NMR of protoCBDac-2 at room temperature

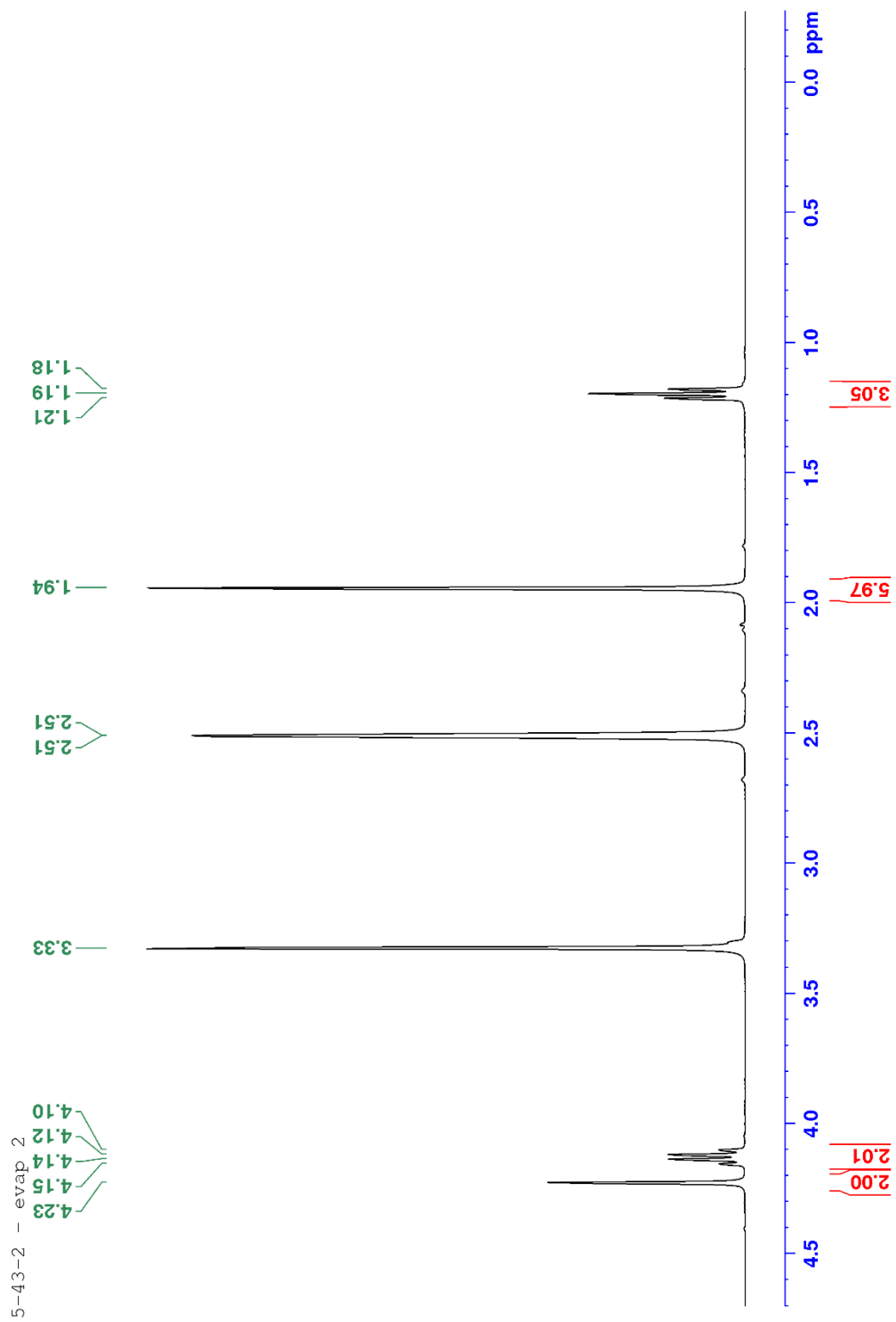


Figure A 42:  $^1\text{H-NMR}$  of protoCBDE-6 at room temperature

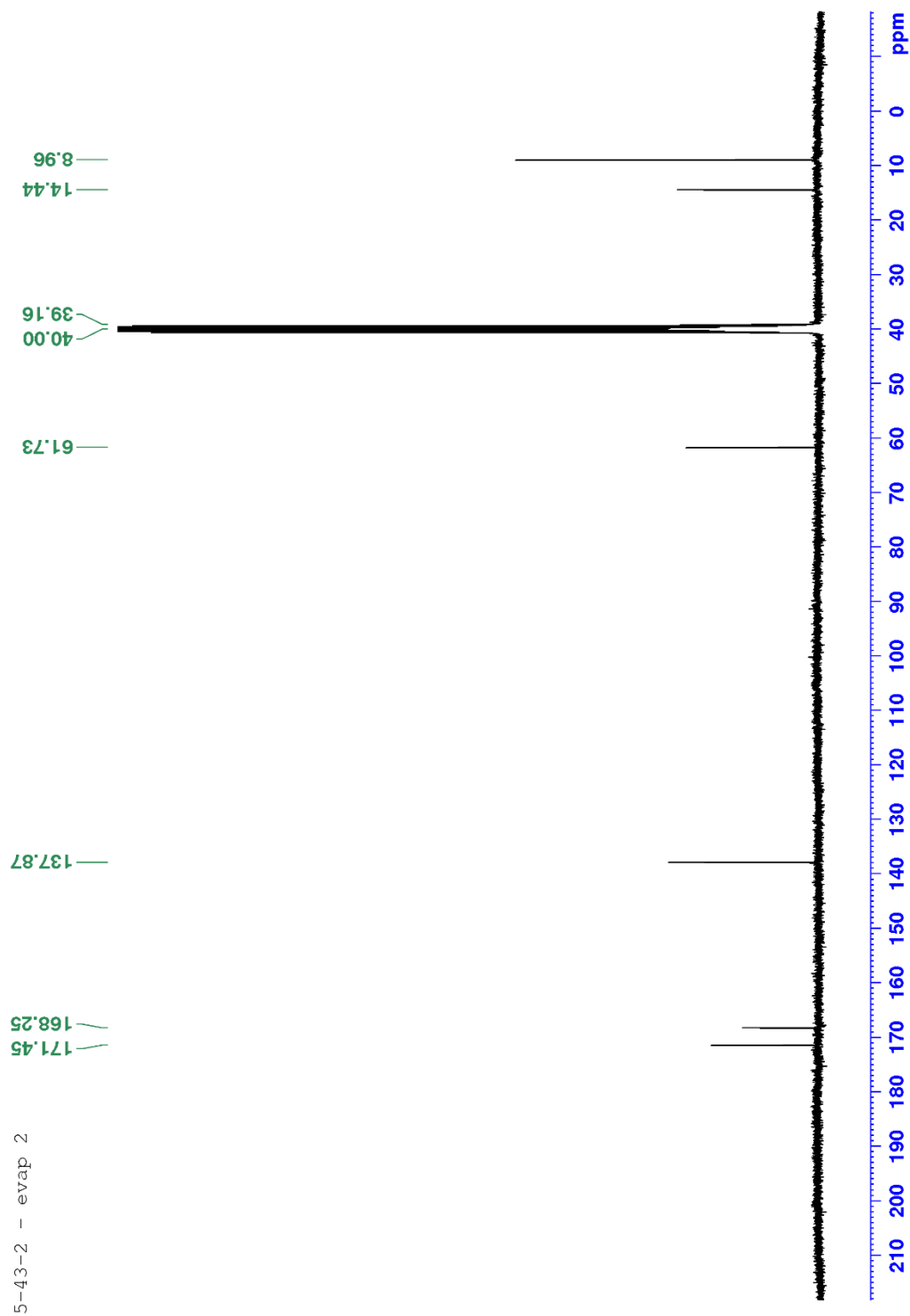


Figure A 43:  $^{13}\text{C}$ -NMR of protoCBDE-6 at room temperature

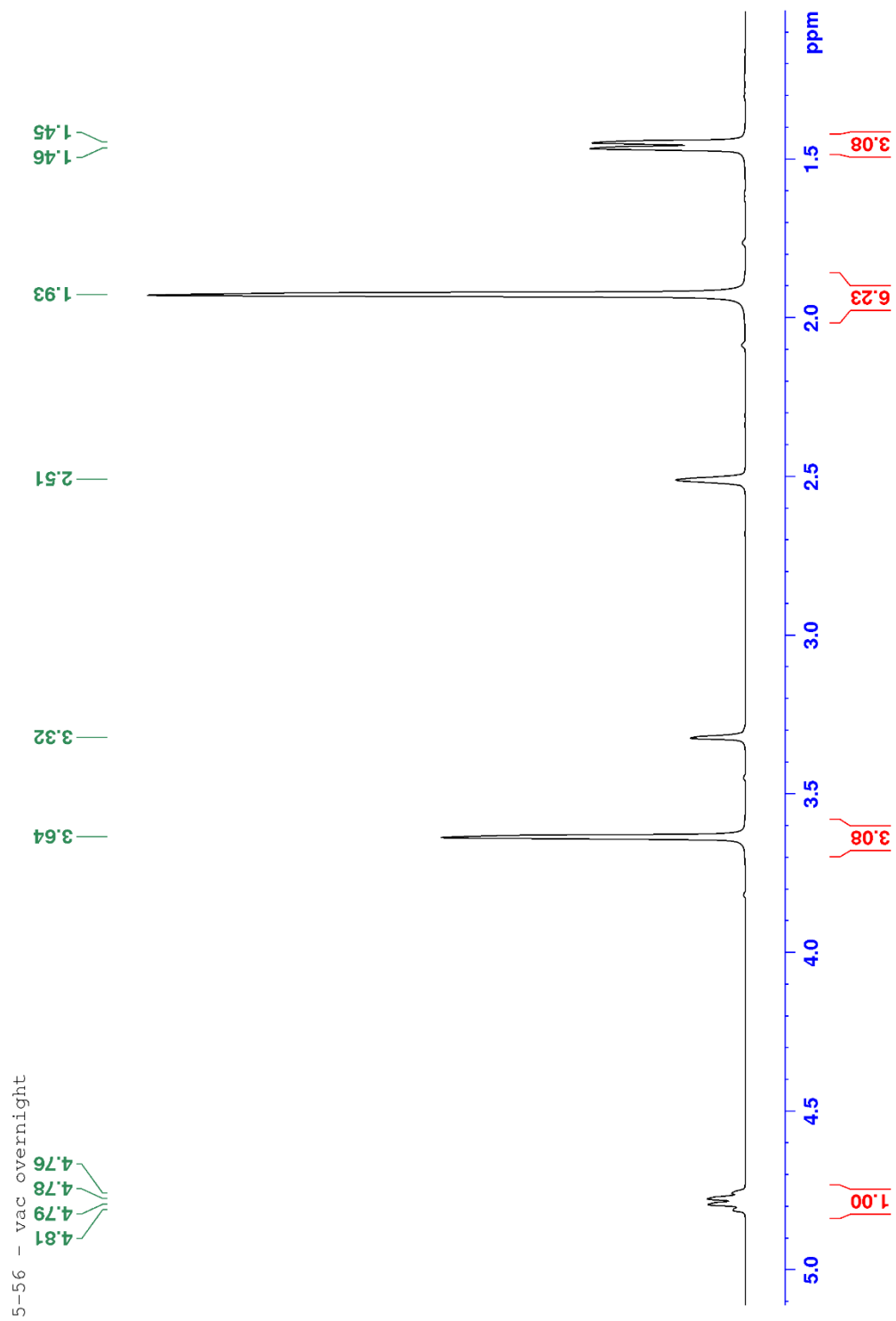


Figure A 44:  $^1\text{H-NMR}$  of protoCBDE-7 at room temperature

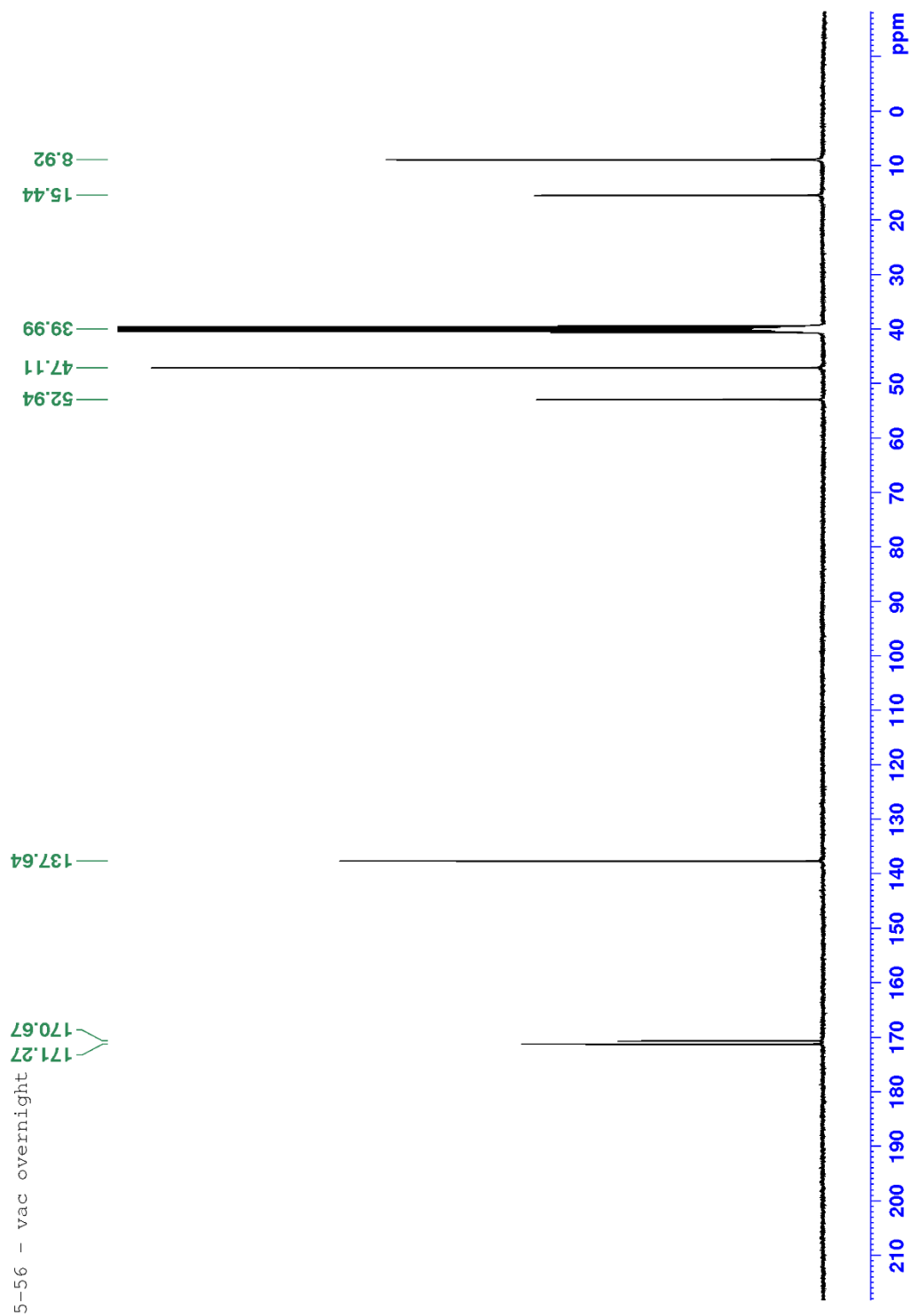


Figure A 45:  $^{13}\text{C}$ -NMR of protoCBDE-7 at room temperature

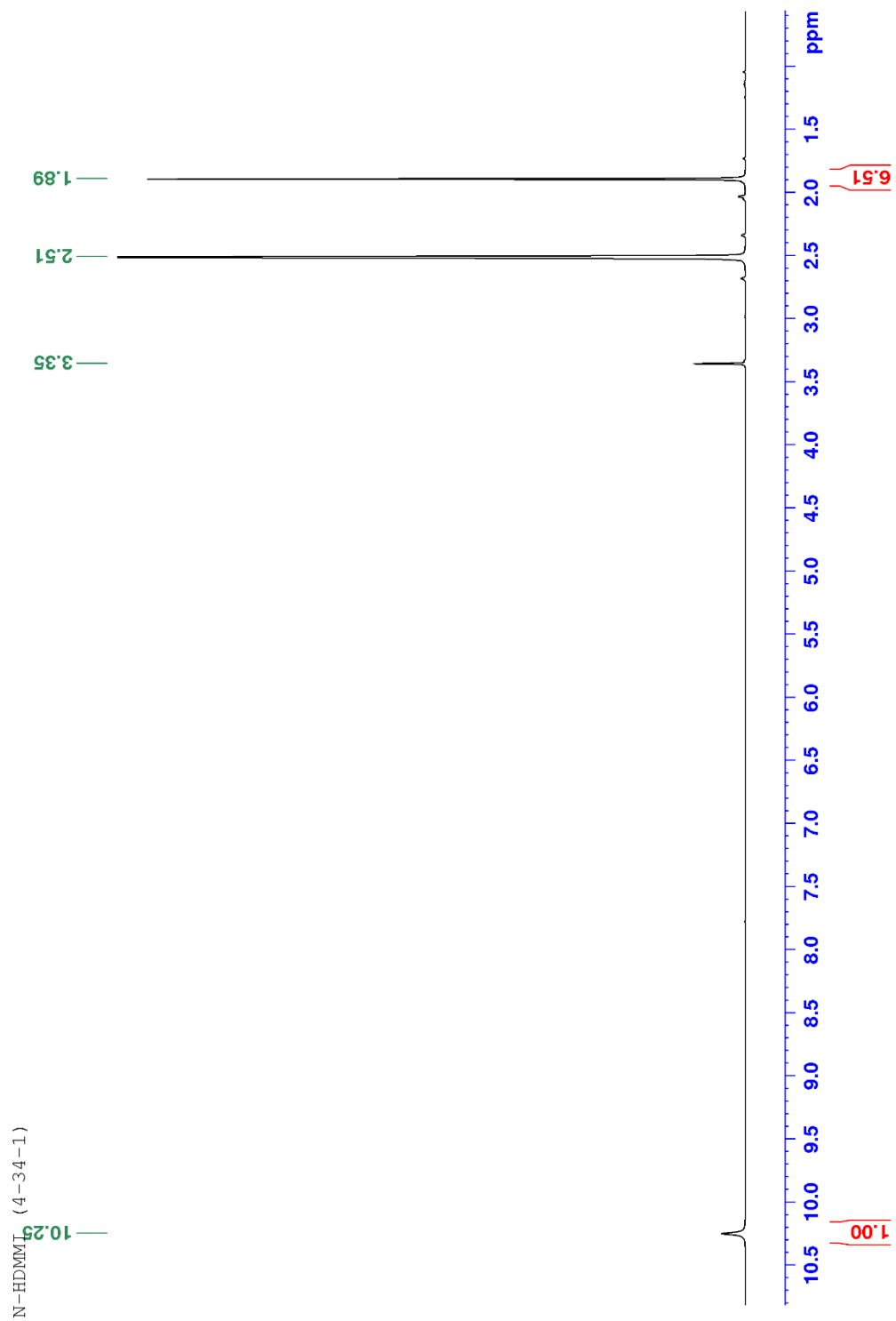


Figure A 46:  $^1\text{H-NMR}$  of protoCBDH-1 at room temperature

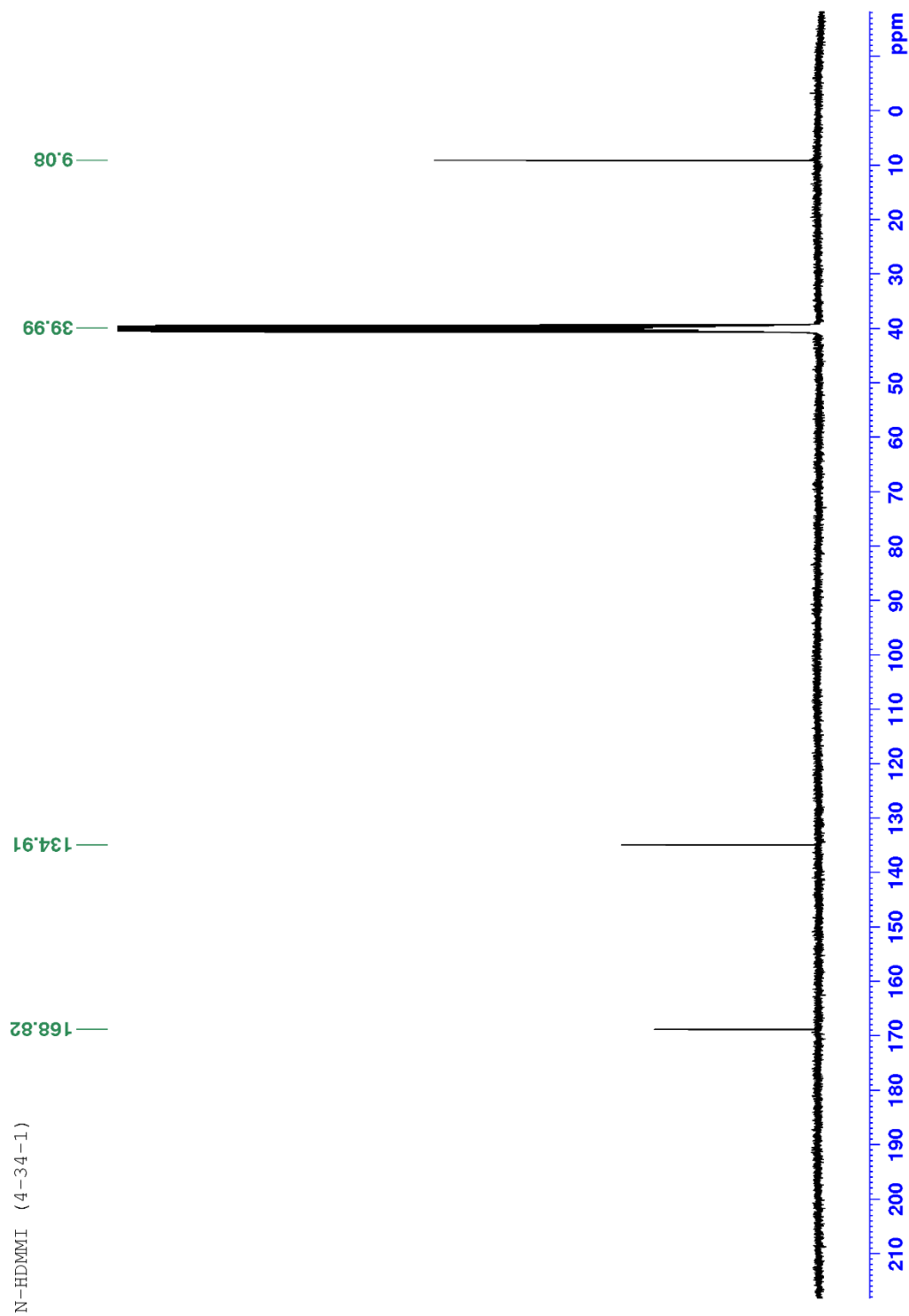


Figure A 47:  $^{13}\text{C}$ -NMR of protoCBDH-1 at room temperature

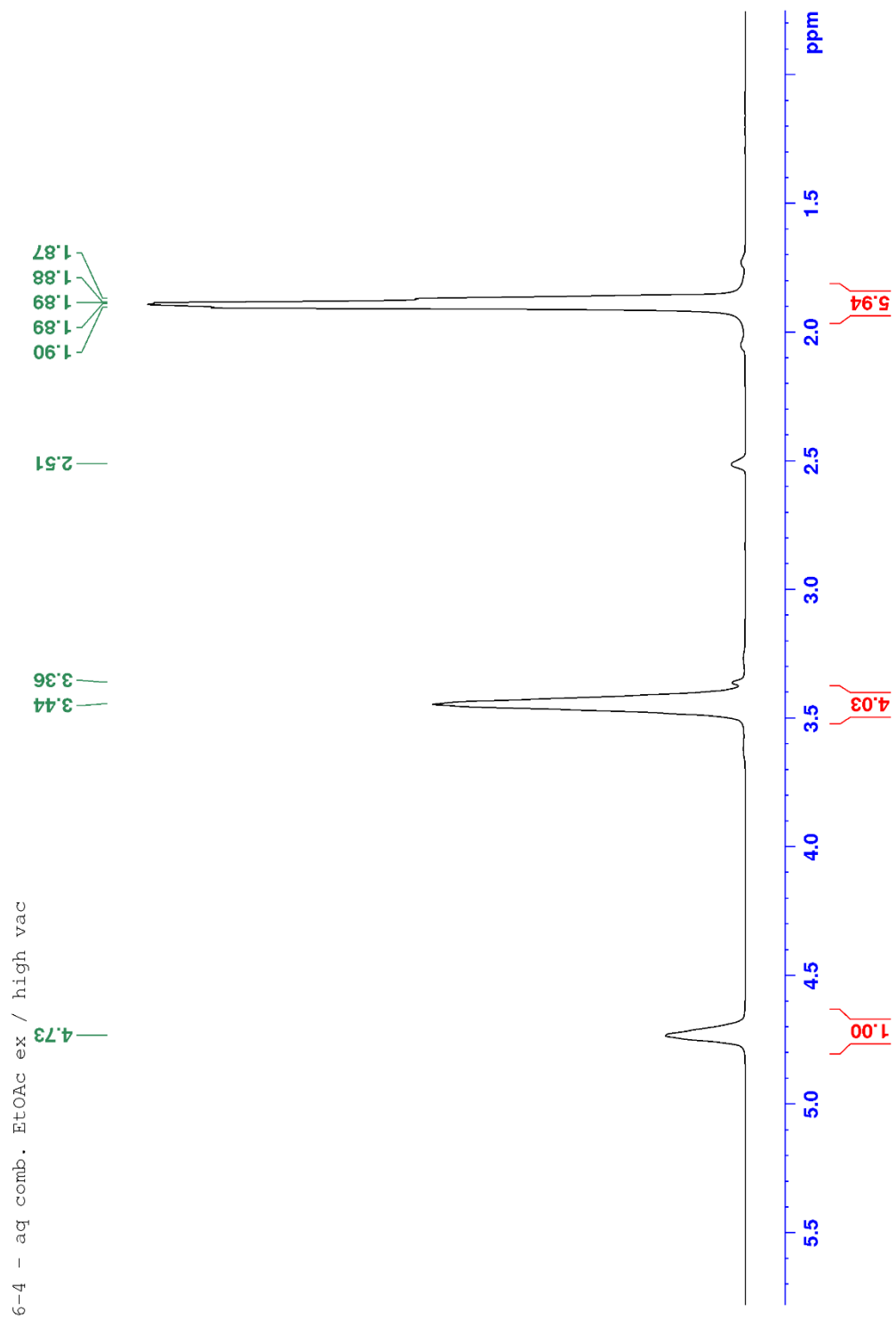


Figure A 48:  $^1\text{H}$ -NMR of protoCBDO-2 at room temperature



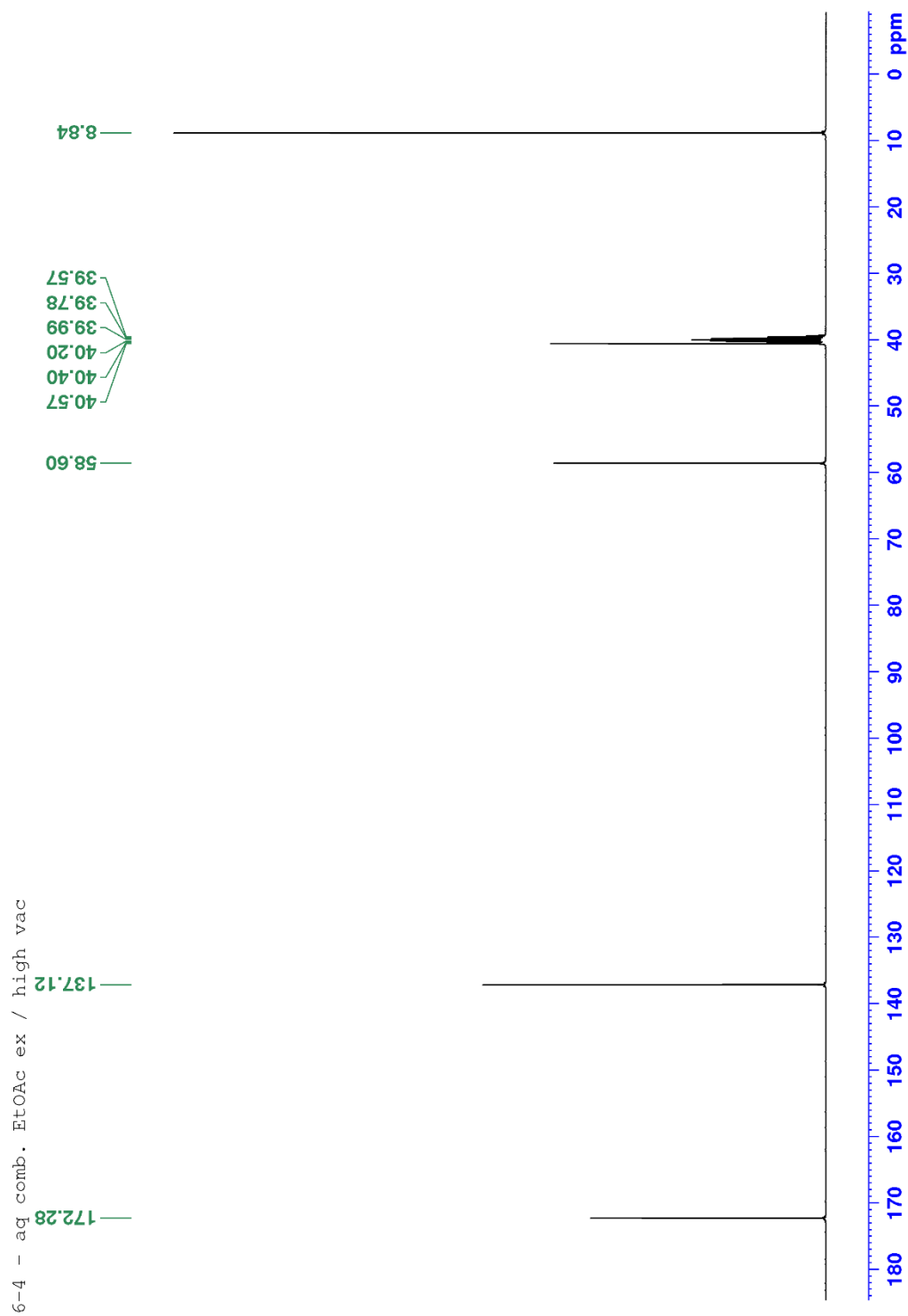


Figure A 49:  $^{13}\text{C}$ -NMR of protoCBDO-2 at room temperature

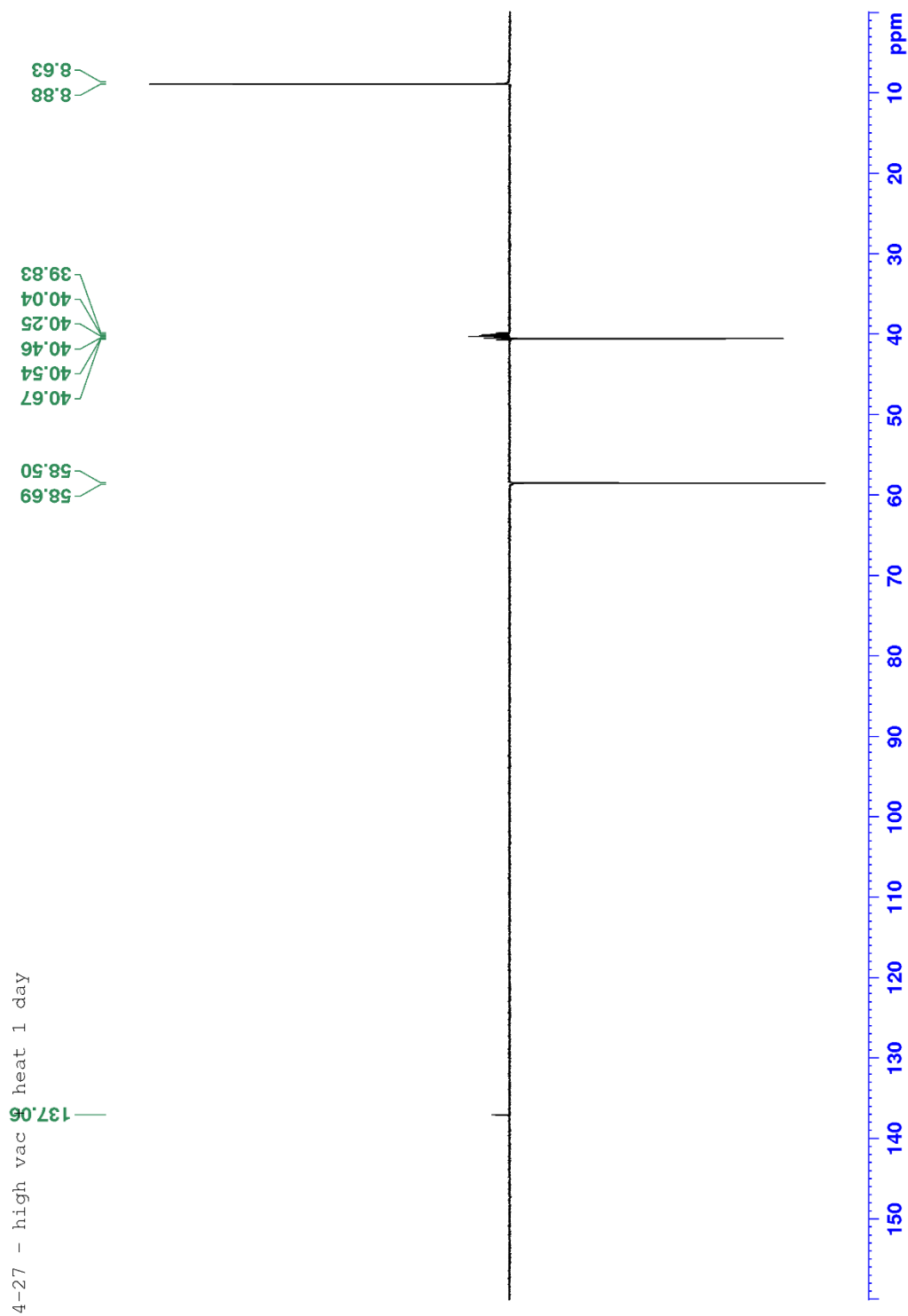


Figure A 50: DEPT135 of protoCBDO-2 at room temperature

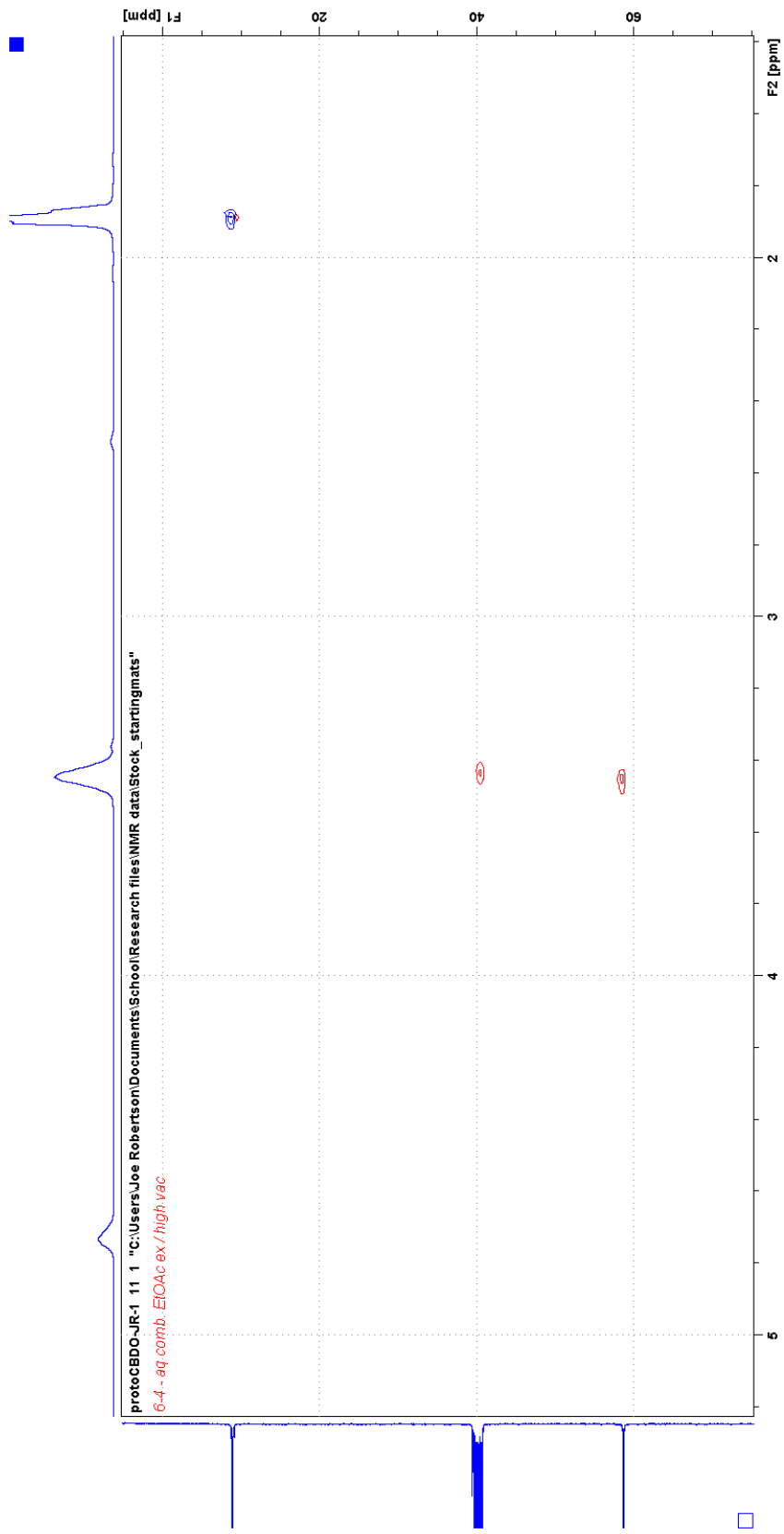


Figure A 51: HSQC of protoCBDO-2 at room temperature

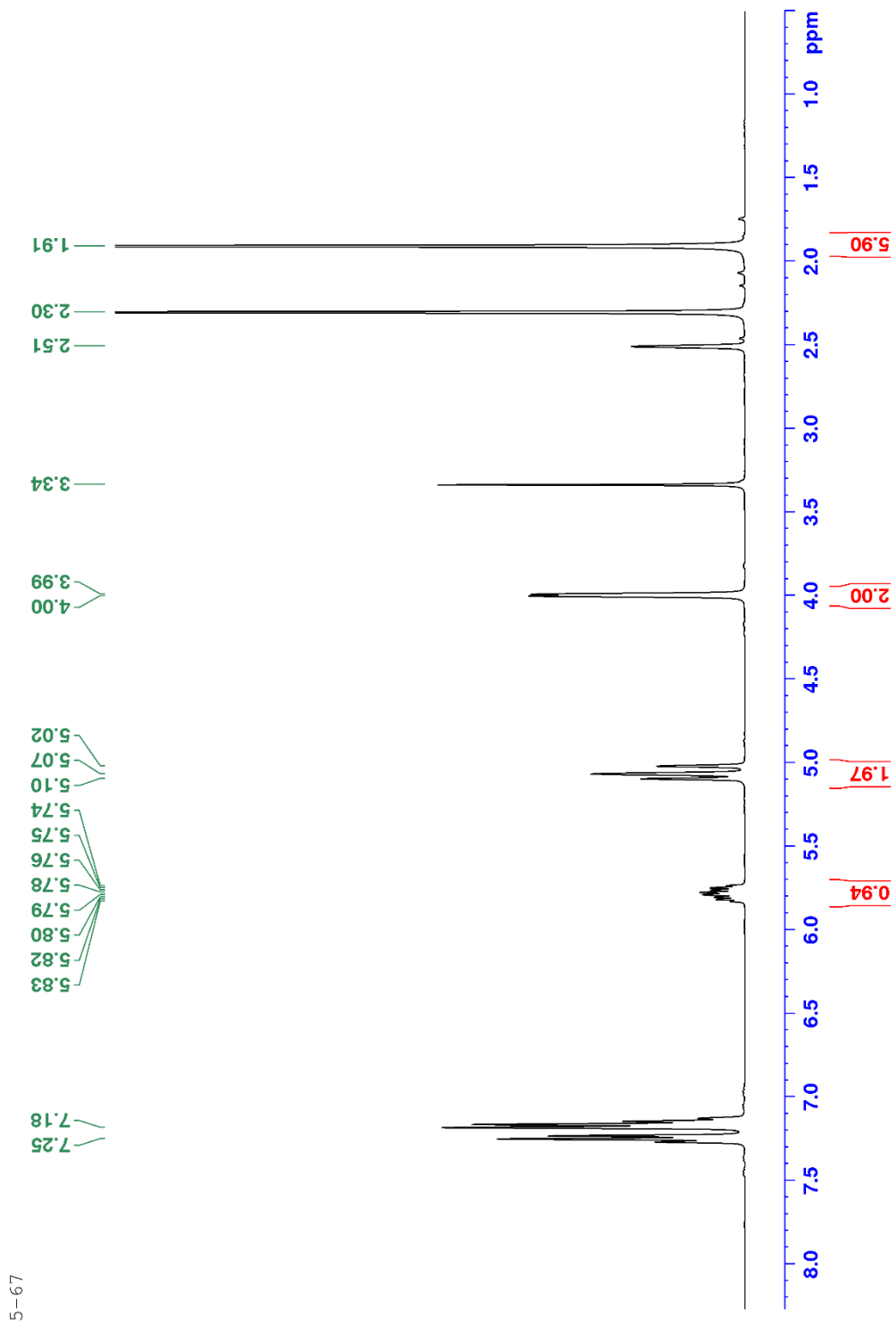


Figure A 52:  $^1\text{H-NMR}$  of protoCBDV-1 at room temperature

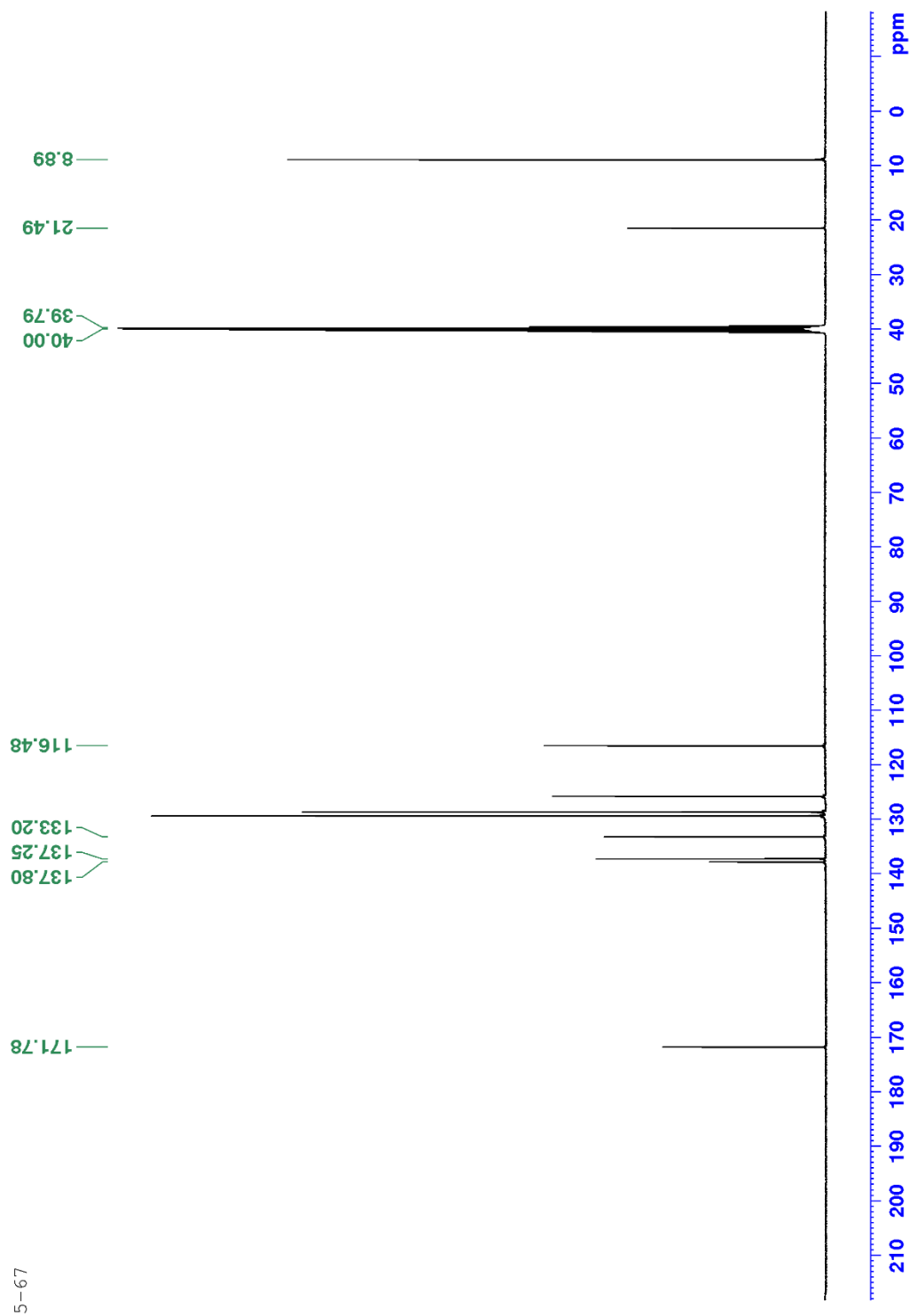


Figure A 53:  $^{13}\text{C}$ -NMR of protoCBDO-2 at room temperature

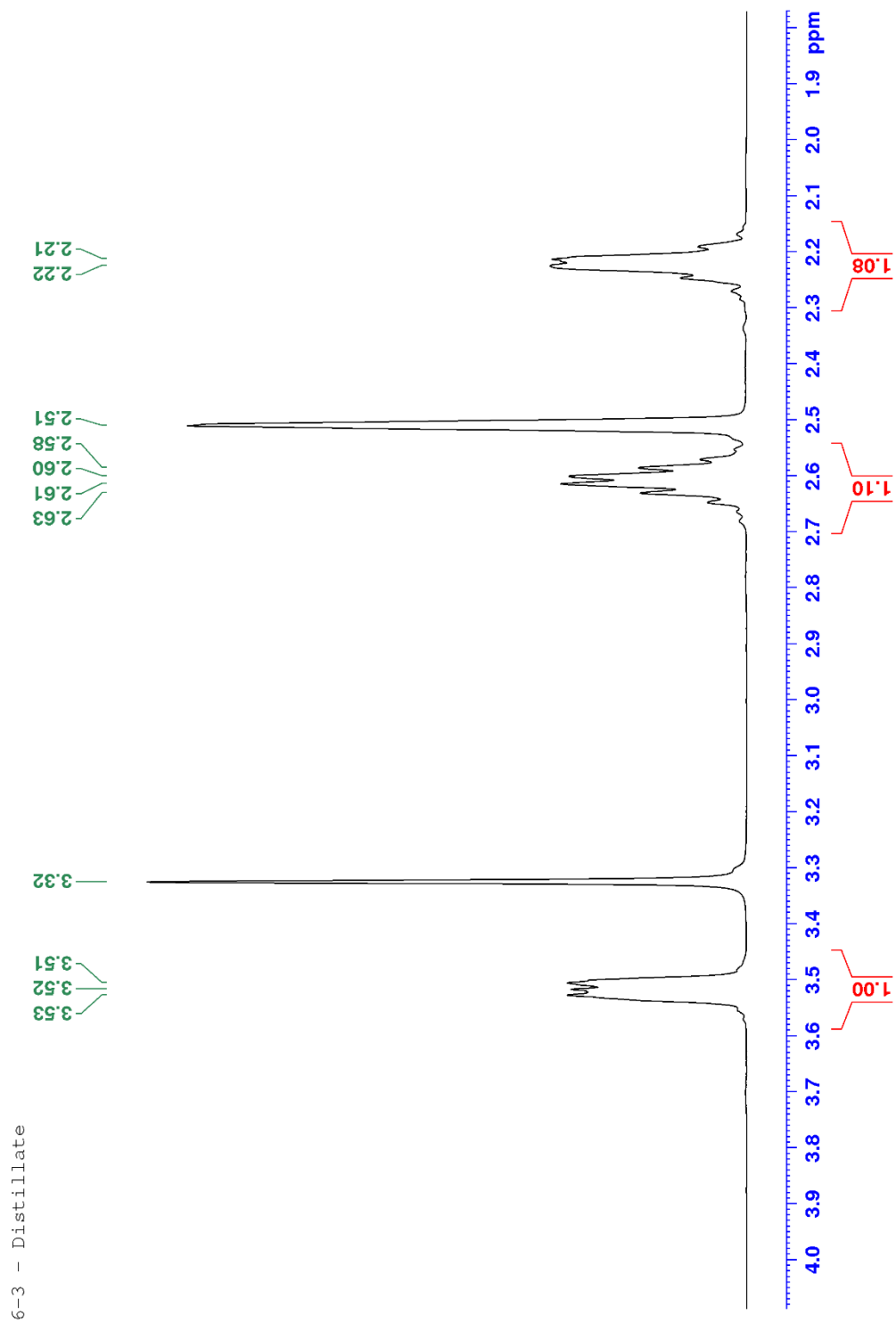


Figure A 54:  $^1\text{H}$ -NMR of CBA-1 at room temperature

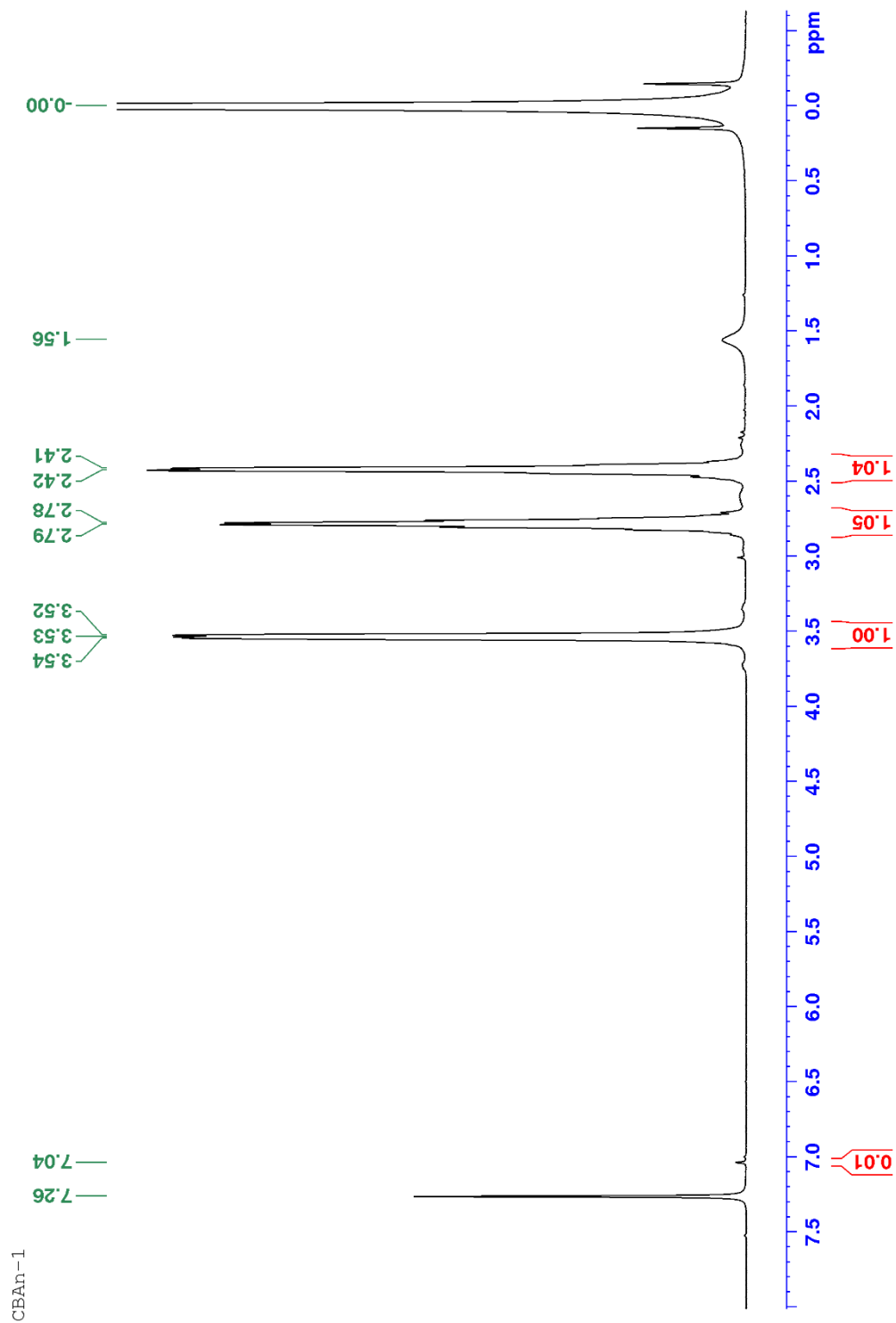


Figure A 55:  $^1\text{H-NMR}$  of CBAh-1 in  $\text{CDCl}_3$  at room temperature

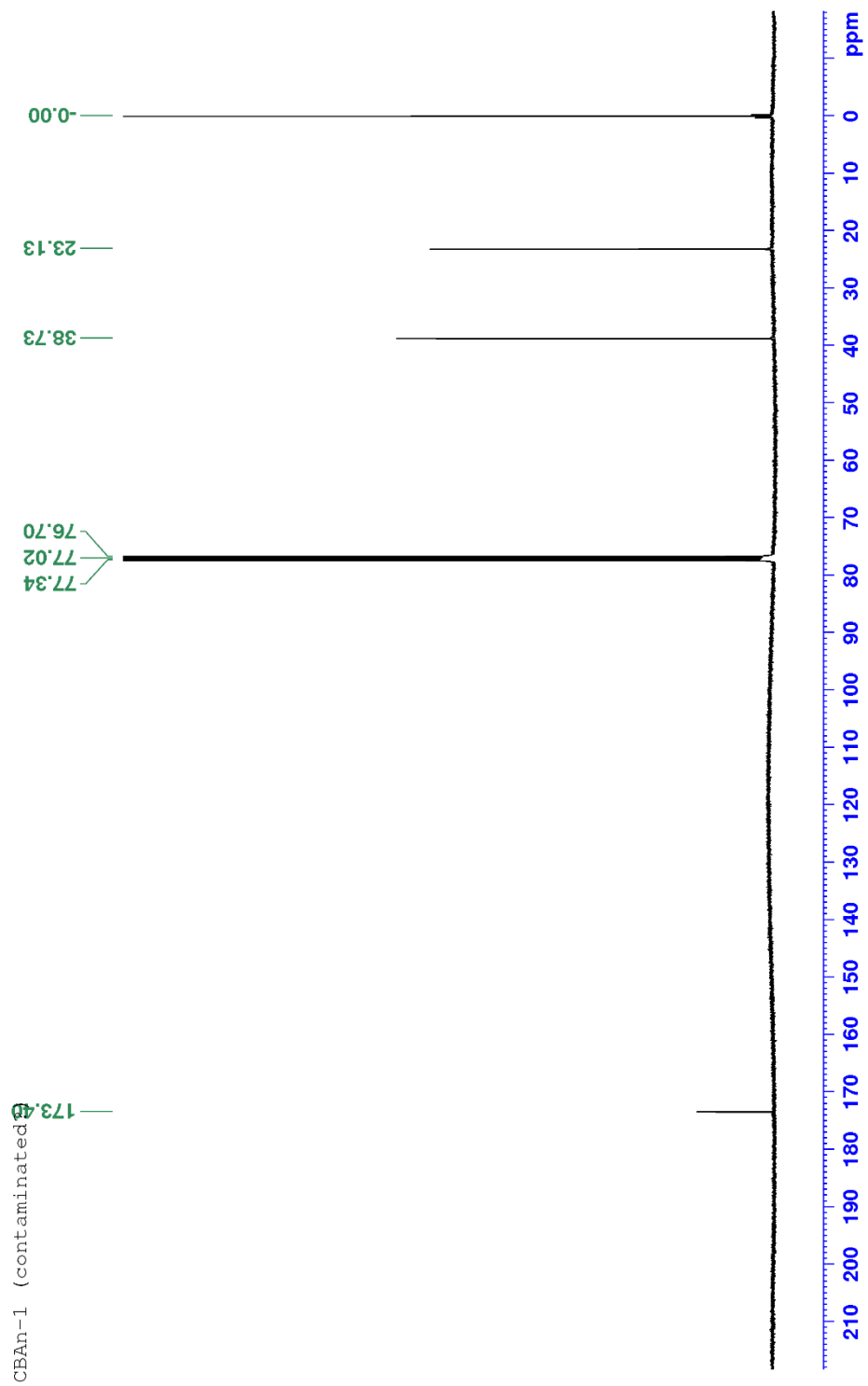


Figure A 56:  $^{13}\text{C}$ -NMR of CBAh-1 in  $\text{CDCl}_3$  at room temperature



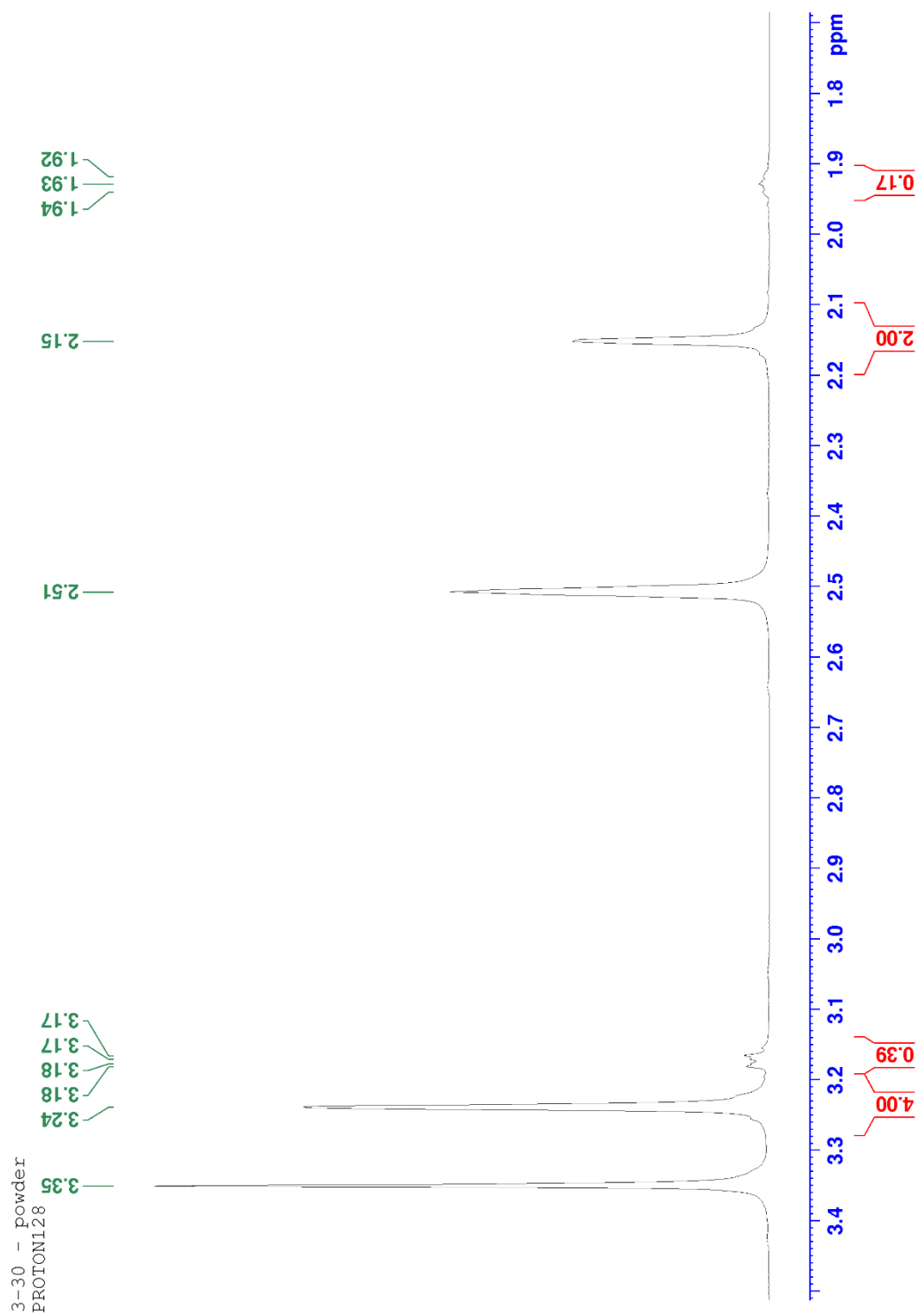


Figure A 57:  $^1\text{H-NMR}$  of powder containing mixture of CPDAn-1

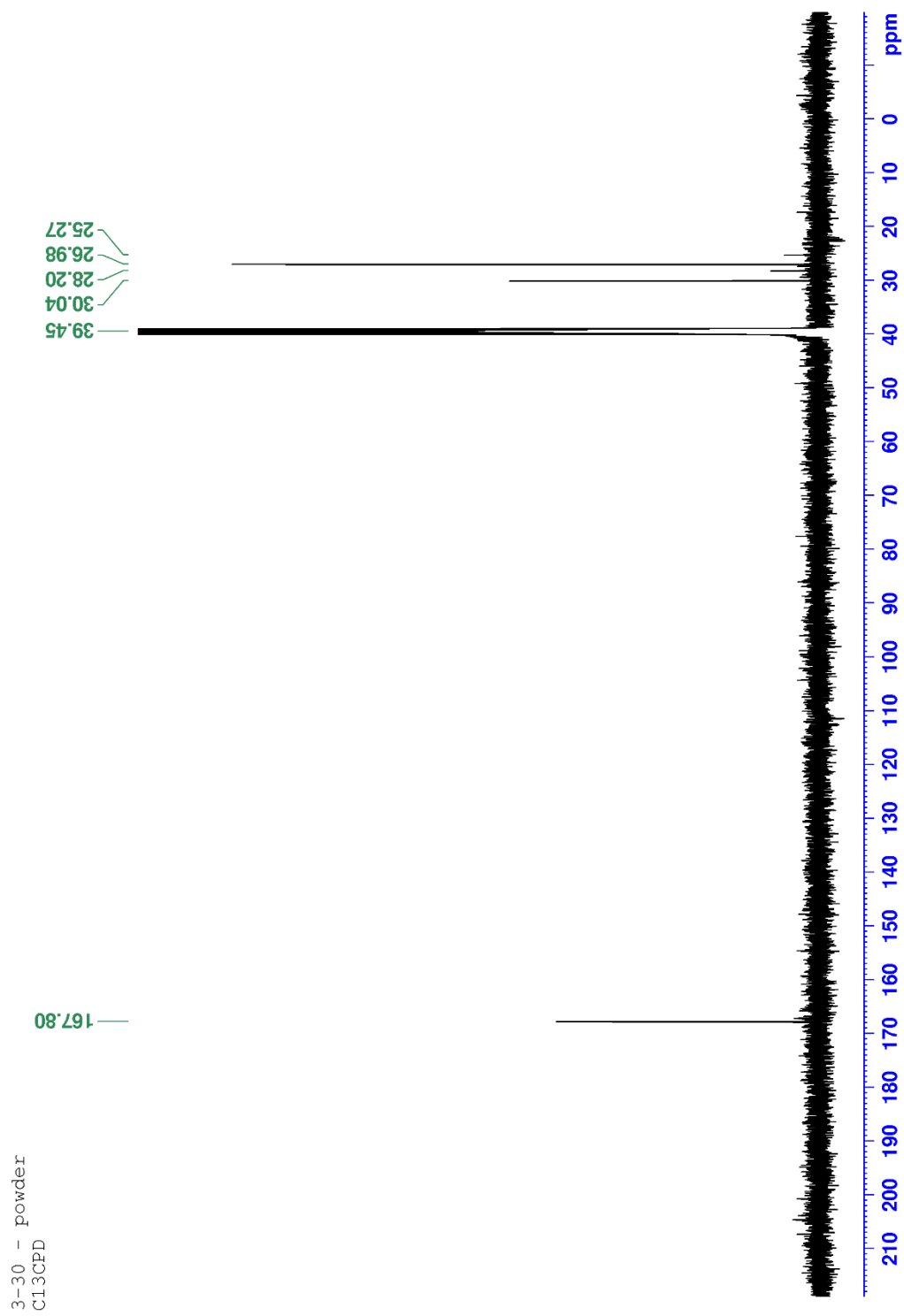


Figure A 58:  $^{13}\text{C}$ -NMR of powder containing mixture of CPDAn-1

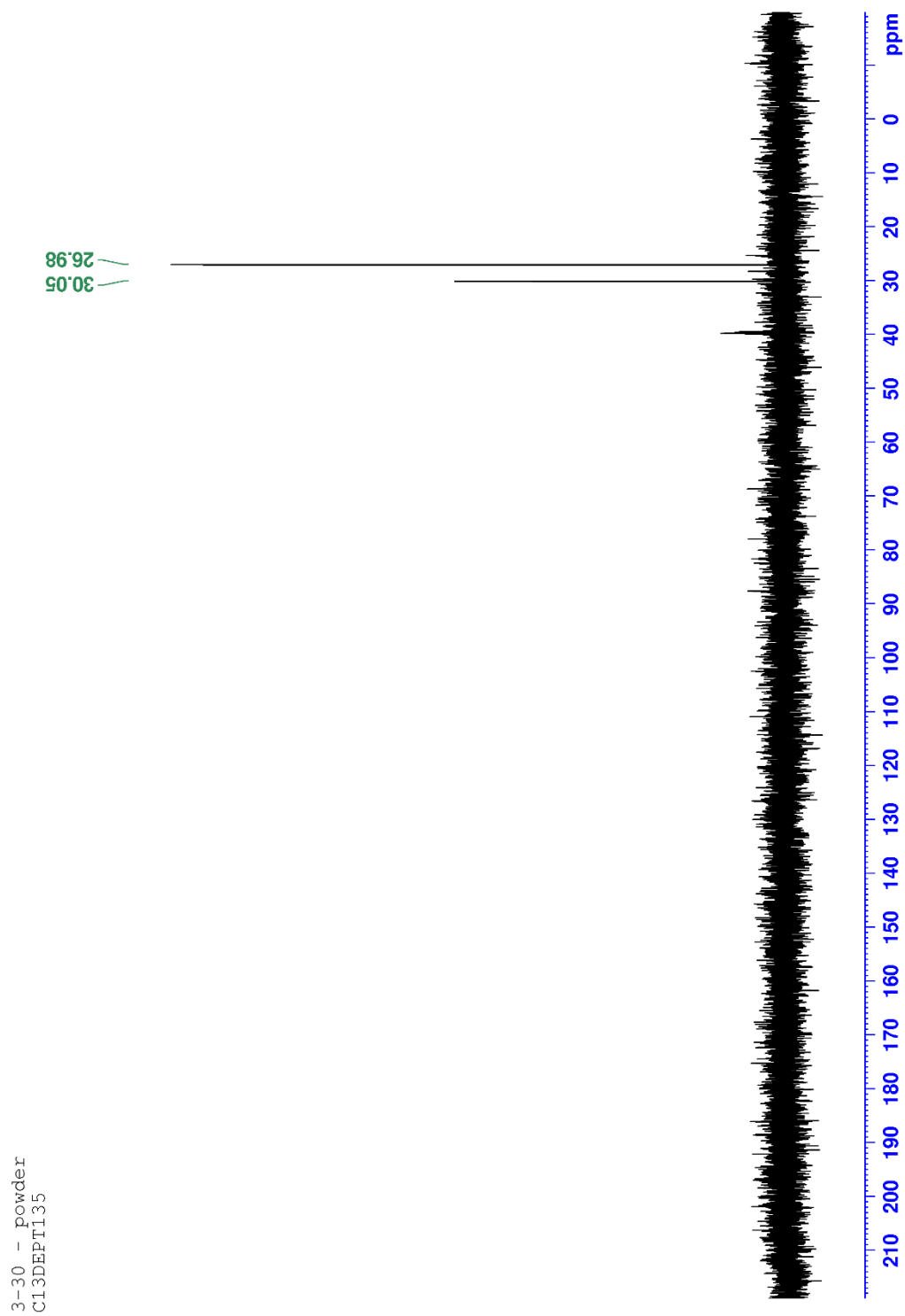


Figure A 59: DEPT135 of powder containing mixture of CPDAn-1

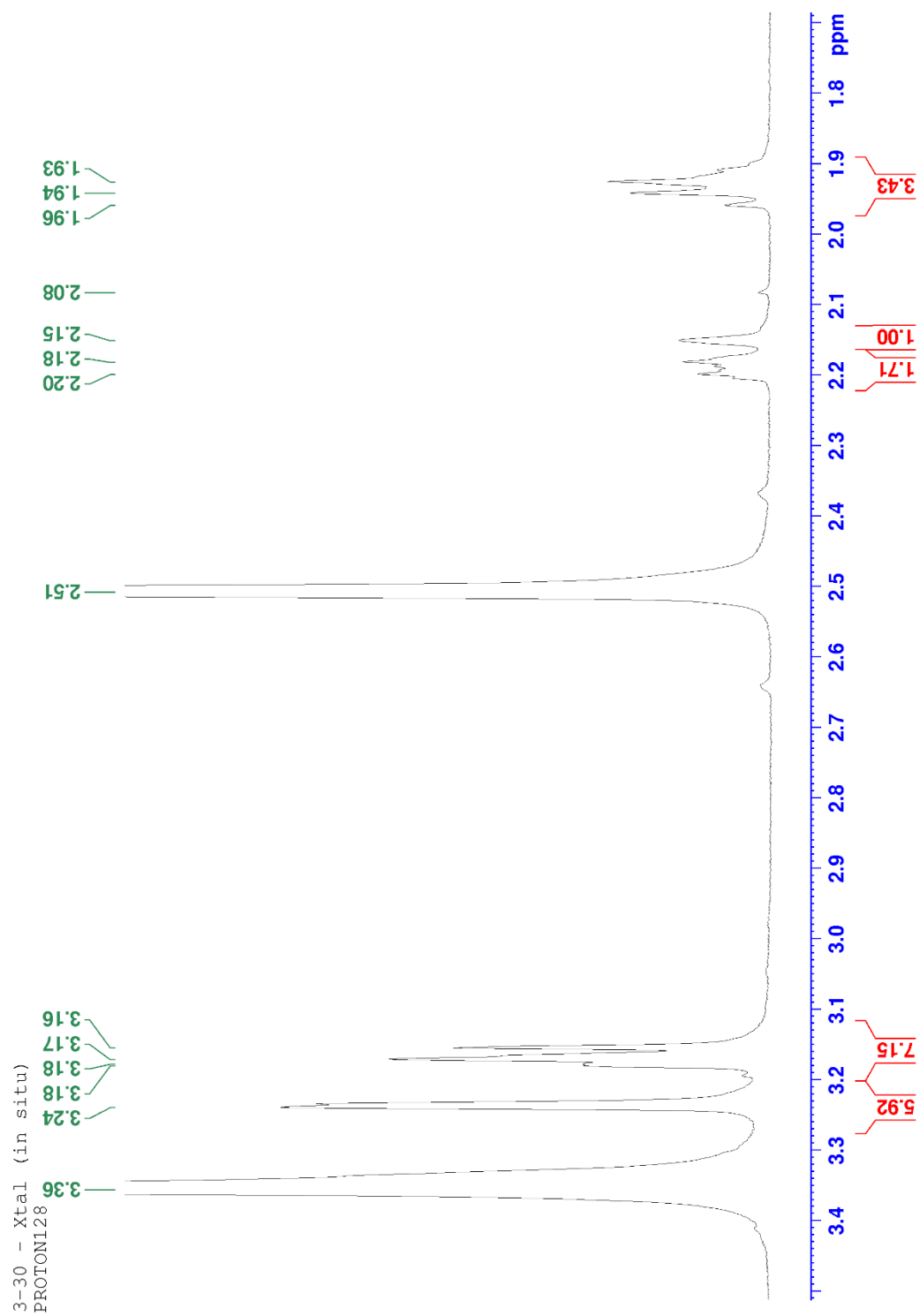


Figure A 60:  $^1\text{H-NMR}$  of crystal of CPDAn-1 which was coated in powder

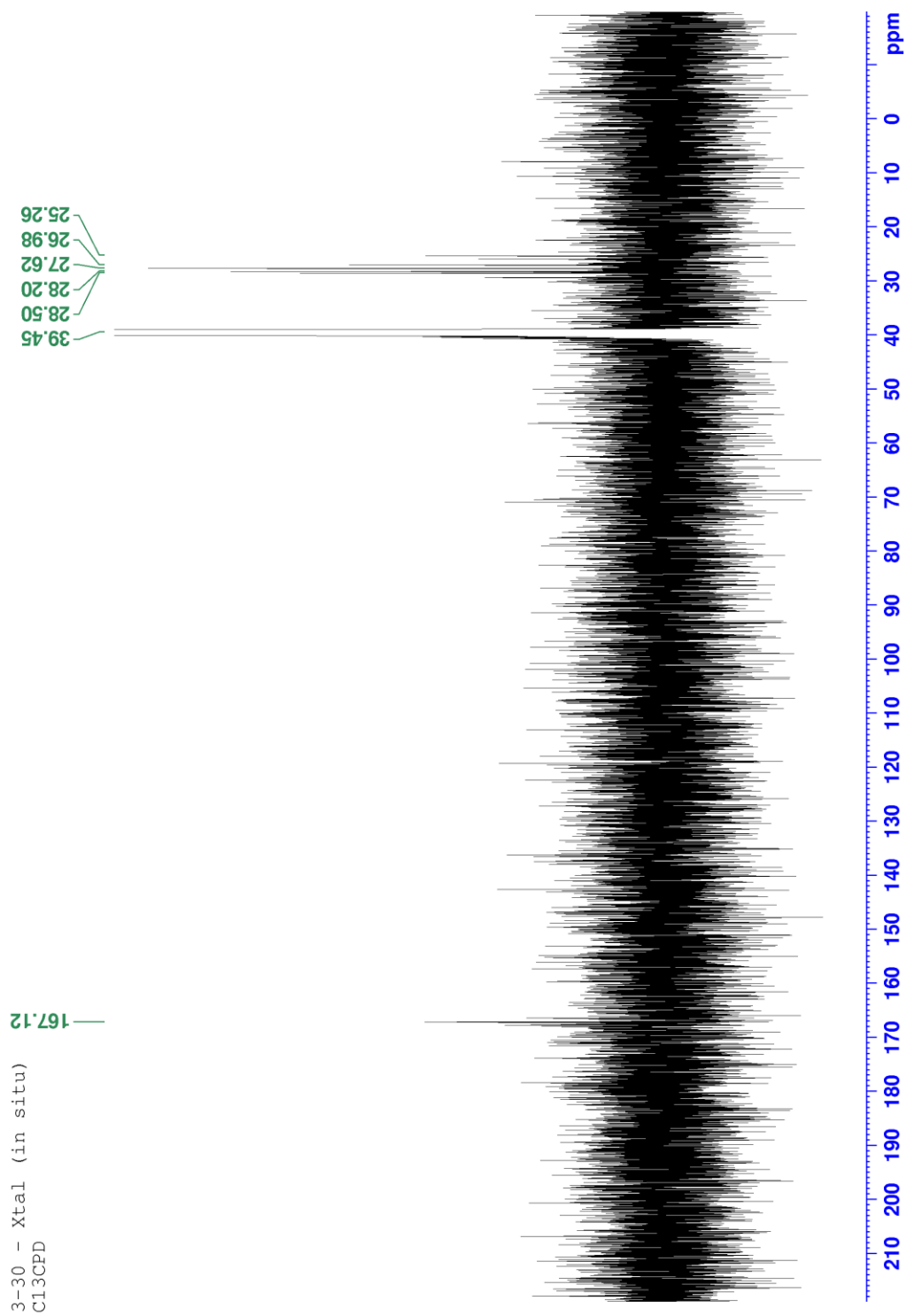


Figure A 61: <sup>13</sup>C-NMR of crystal of CPDAn-1 which was coated in powder

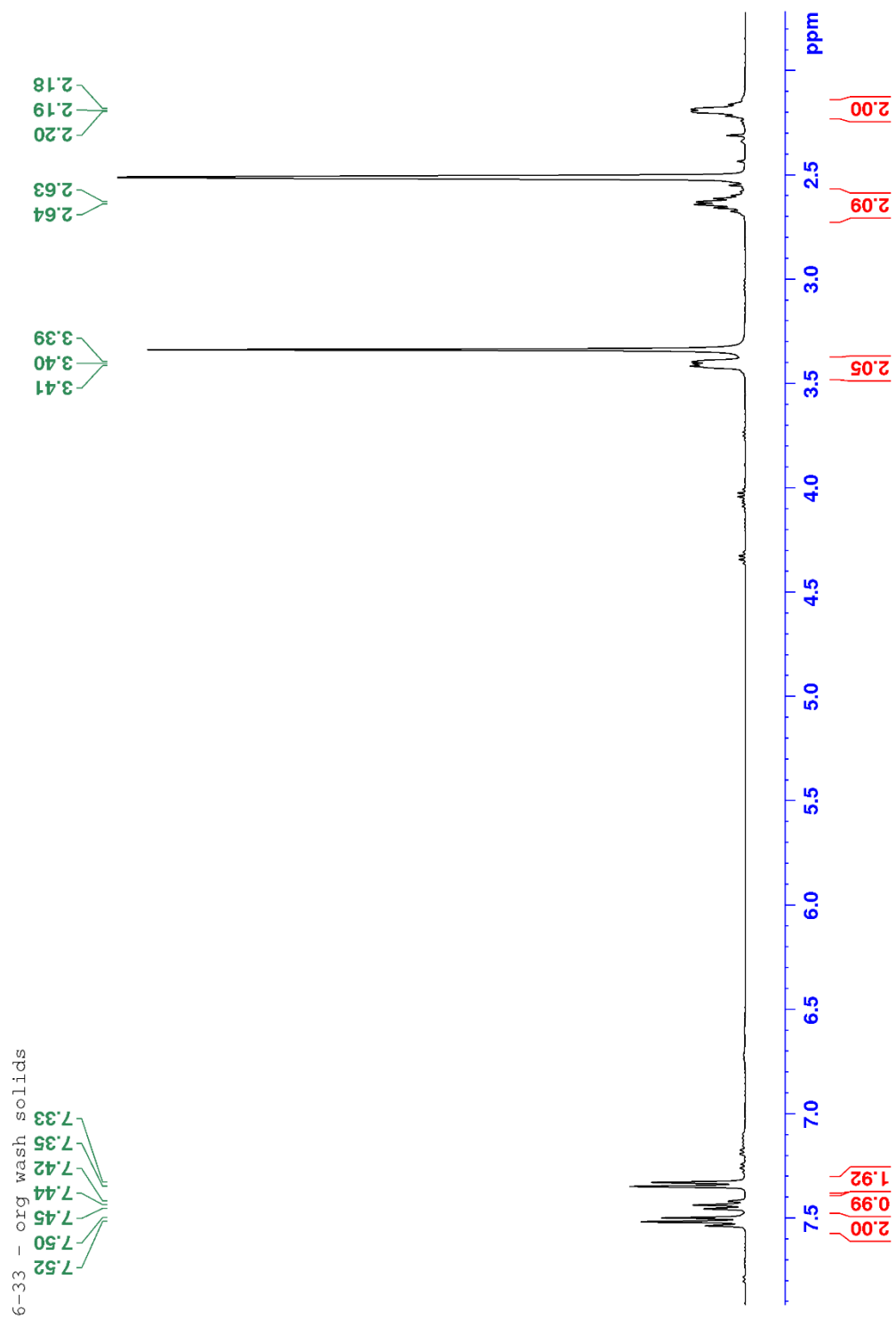


Figure A 62:  $^1\text{H-NMR}$  of CBI-1

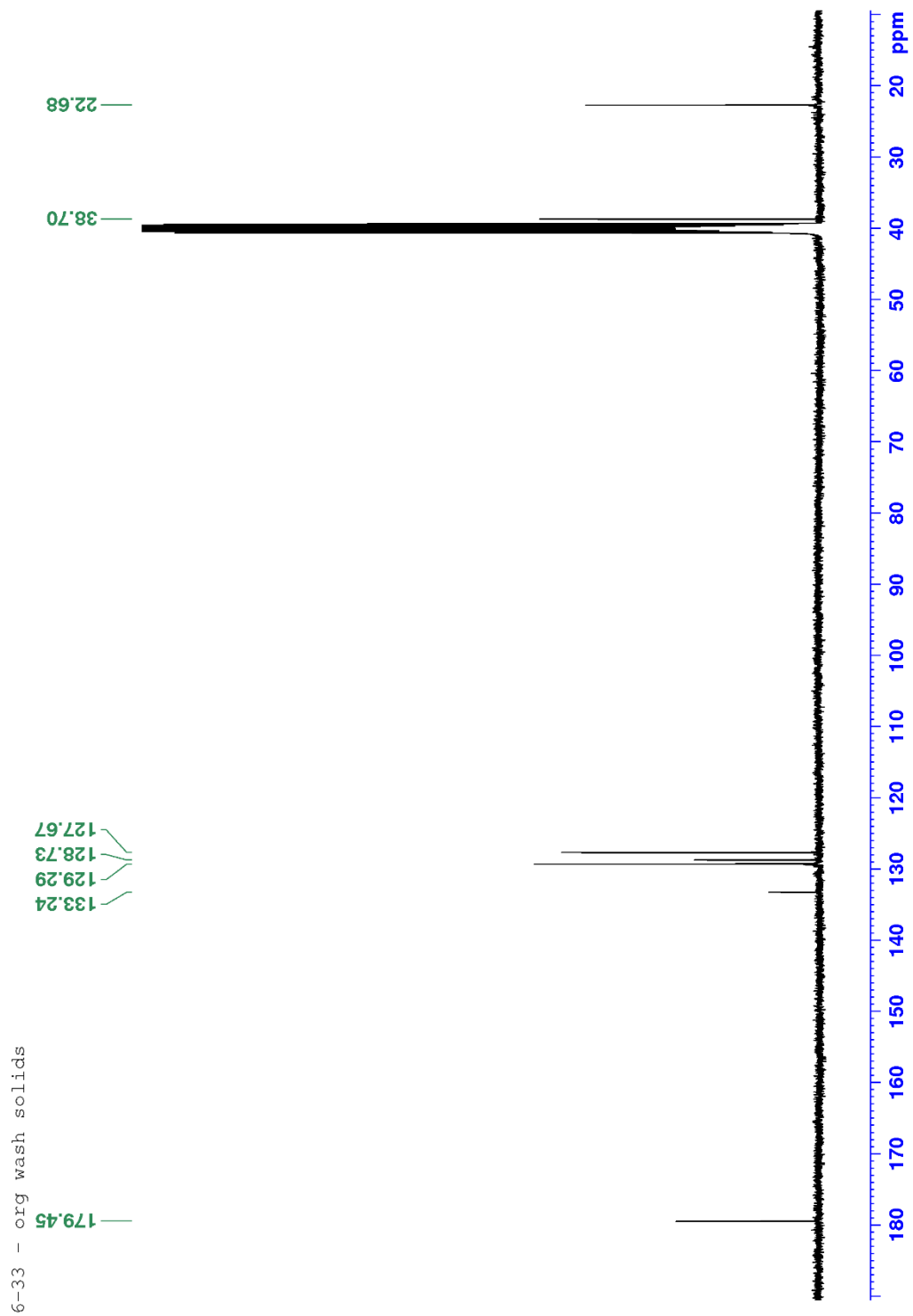


Figure A 63: <sup>13</sup>C-NMR of CBI-1

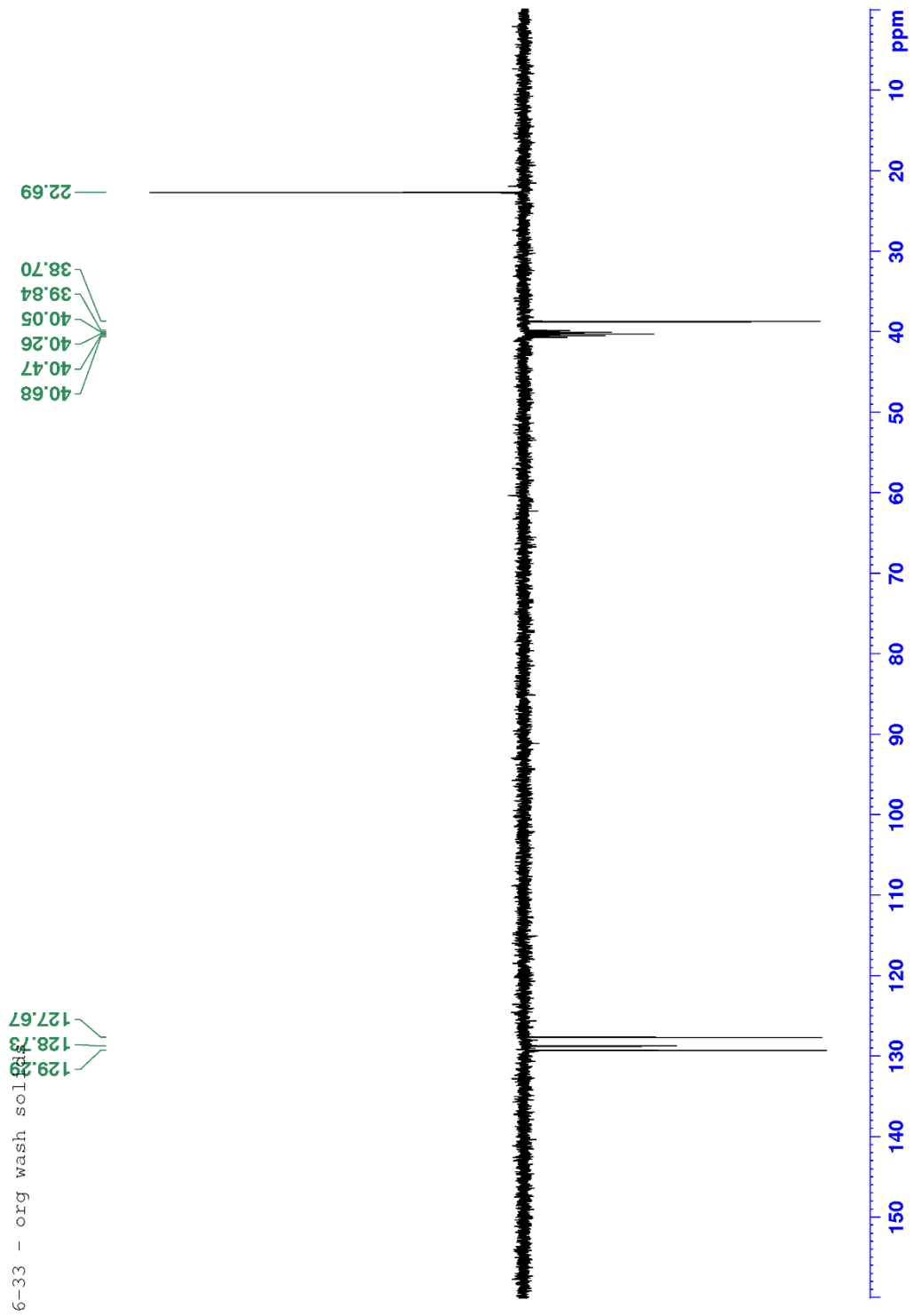


Figure A 64: DEPT135 of CBI-1



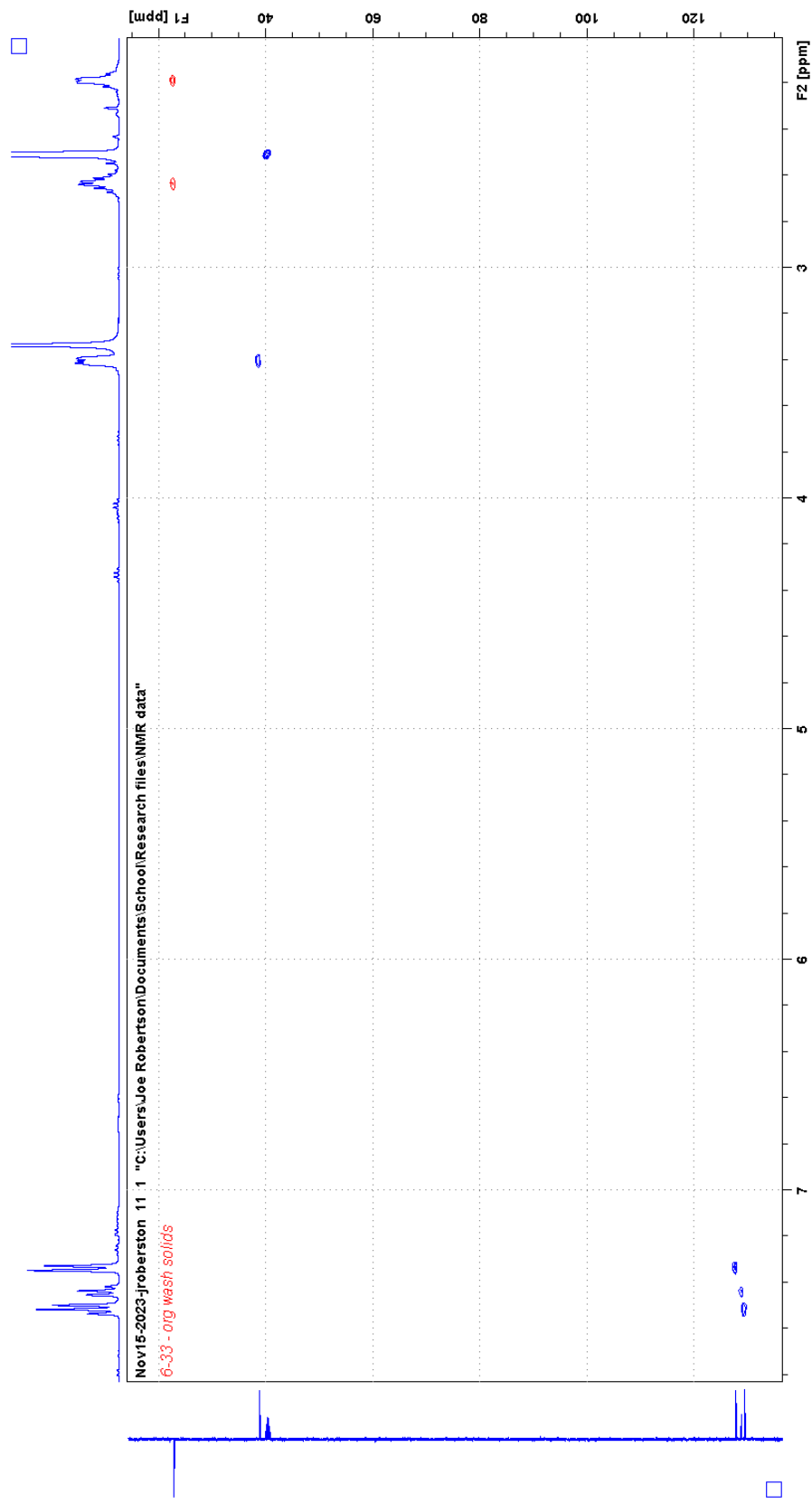


Figure A 65: HSQC of CBI-1

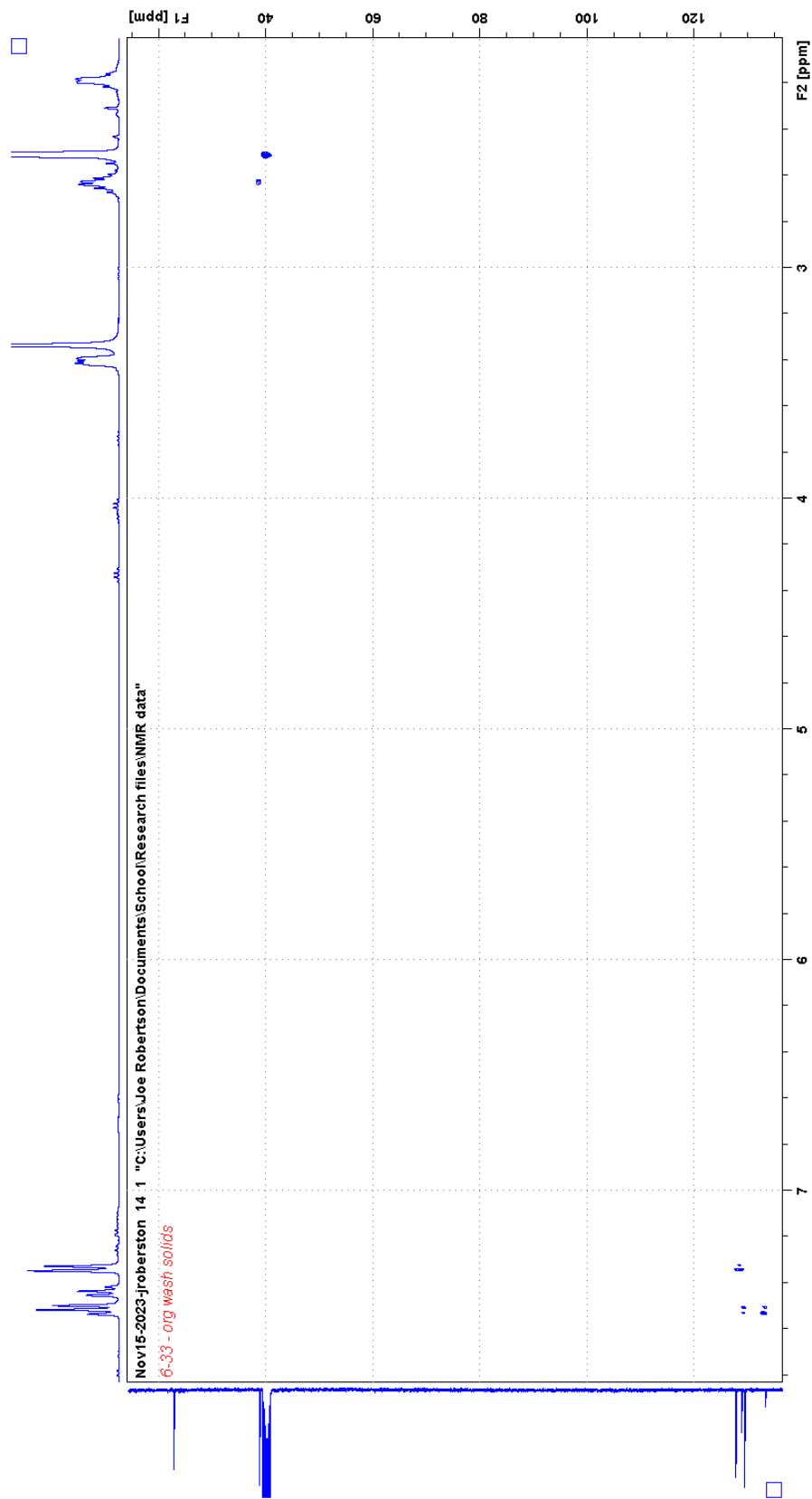


Figure A 66: HMBC of CBI-1

## Appendix B: Crystallographic Data

Crystal parameters	CBDA-7
<b>Formula</b>	C <sub>16</sub> H <sub>18</sub> N <sub>2</sub> O <sub>8</sub>
<b>MW (g/mol)</b>	366.32
<b>Crystal System</b>	Monoclinic
<b>Space Group</b>	P 1 21/n 1
<b>a (Å)</b>	8.9175(3)
<b>b (Å)</b>	7.6475(3)
<b>c (Å)</b>	12.0351(4)
<b>α (°)</b>	90
<b>β (°)</b>	104.277(2)
<b>γ (°)</b>	90
<b>V (Å<sup>3</sup>)</b>	795.40(5)
<b>Z</b>	2
<b>Temp. (K)</b>	273
<b>ρ (g/cm<sup>3</sup>)</b>	1.530
<b>μ (mm<sup>-1</sup>)</b>	1.063
<b>Radiation type</b>	CuKα (λ = 1.54178)
<b>F(000)</b>	384.0
<b># of measured refl.</b>	6041
<b># of independent refl.</b>	1396
<b># of refl. (I ≥ 2σ)</b>	1250

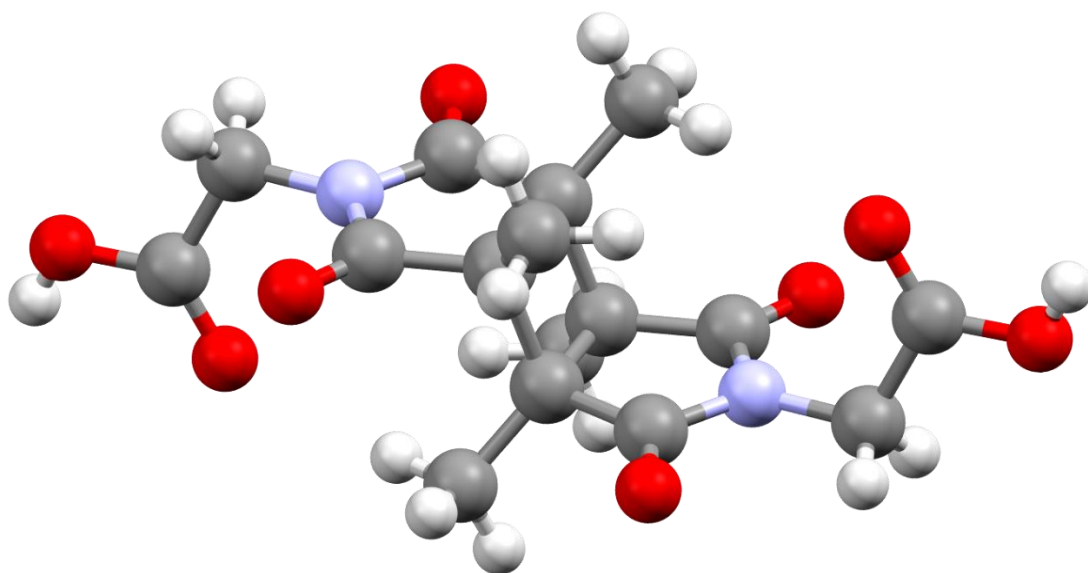


Figure B 1: Crystal data and structure for CBDA-7

Crystal parameters	CBDE-6
<b>Formula</b>	C <sub>20</sub> H <sub>26</sub> N <sub>2</sub> O <sub>8</sub>
<b>MW (g/mol)</b>	422.43
<b>Crystal System</b>	Triclinic
<b>Space Group</b>	P-1
<b>a (Å)</b>	7.3922(10)
<b>b (Å)</b>	7.9131(10)
<b>c (Å)</b>	9.6896(14)
<b>α (°)</b>	108.249(6)
<b>β (°)</b>	95.699(7)
<b>γ (°)</b>	107.905(6)
<b>V (Å<sup>3</sup>)</b>	500.08(12)
<b>Z</b>	1
<b>Temp. (K)</b>	116
<b>ρ (g/cm<sup>3</sup>)</b>	1.403
<b>μ (mm<sup>-1</sup>)</b>	0.918
<b>Radiation type</b>	CuKα (λ = 1.54178)
<b>F(000)</b>	224.0
<b># of measured refl.</b>	5658
<b># of independent refl.</b>	1762
<b># of refl. (I ≥ 2σ)</b>	1696

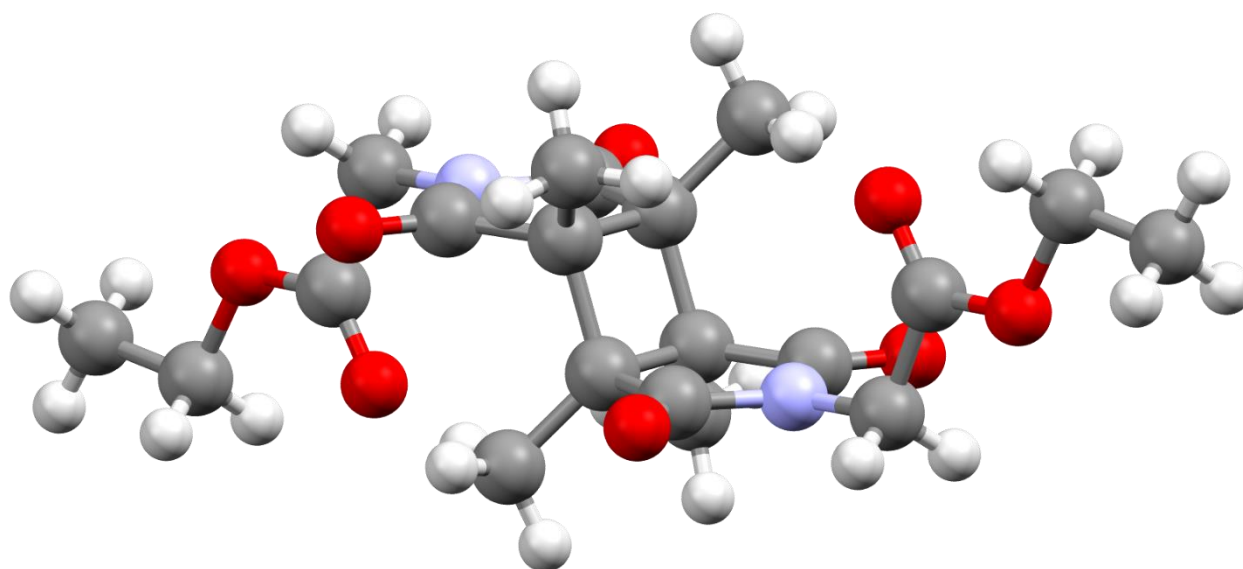


Figure B 2: Crystal data and structure for CBDE-6

Crystal parameters	CBDE-7
<b>Formula</b>	C <sub>20</sub> H <sub>26</sub> N <sub>2</sub> O <sub>8</sub>
<b>MW (g/mol)</b>	422.43
<b>Crystal System</b>	Monoclinic
<b>Space Group</b>	P 1 2 <sub>1</sub> 1
<b>a (Å)</b>	8.8450(5)
<b>b (Å)</b>	2.9486(7)
<b>c (Å)</b>	9.1272(6)
<b>α (°)</b>	90
<b>β (°)</b>	100.881(4)
<b>γ (°)</b>	90
<b>V (Å<sup>3</sup>)</b>	1026.55(11)
<b>Z</b>	2
<b>Temp. (K)</b>	107
<b>ρ (g/cm<sup>3</sup>)</b>	1.367
<b>μ (mm<sup>-1</sup>)</b>	0.895
<b>Radiation type</b>	CuKα (λ = 1.54178)
<b>F(000)</b>	448.0
<b># of measured refl.</b>	8728
<b># of independent refl.</b>	3604
<b># of refl. (I ≥ 2σ)</b>	3069

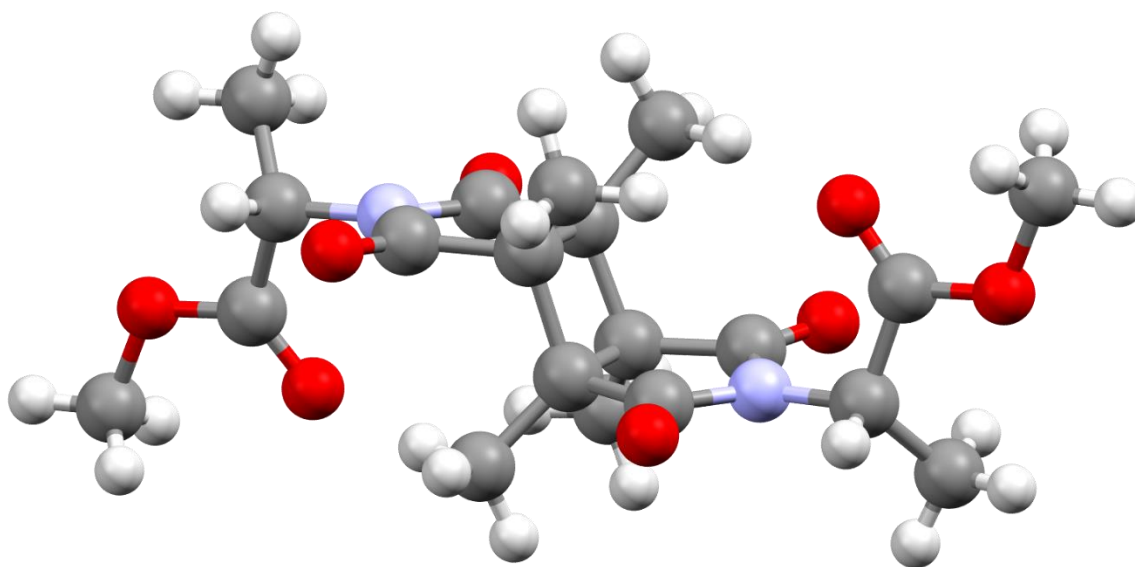


Figure B 3: Crystal data and structure for CBDE-7

Crystal parameters	CBDH-1
<b>Formula</b>	C <sub>12</sub> H <sub>18</sub> N <sub>2</sub> O <sub>8</sub>
<b>MW (g/mol)</b>	318.28
<b>Crystal System</b>	monoclinic
<b>Space Group</b>	P 1 2 <sub>1</sub> /c 1
<b>a (Å)</b>	7.4023(3)
<b>b (Å)</b>	12.4329(5)
<b>c (Å)</b>	7.9684(3)
<b>α (°)</b>	90
<b>β (°)</b>	96.891(2)
<b>γ (°)</b>	90
<b>V (Å<sup>3</sup>)</b>	728.05(5)
<b>Z</b>	2
<b>Temp. (K)</b>	107.01
<b>ρ (g/cm<sup>3</sup>)</b>	1.452
<b>μ (mm<sup>-1</sup>)</b>	1.063
<b>Radiation type</b>	CuKα (λ = 1.54178)
<b>F(000)</b>	336.0
<b># of measured refl.</b>	5786
<b># of independent refl.</b>	1284
<b># of refl. (I ≥ 2σ)</b>	1178

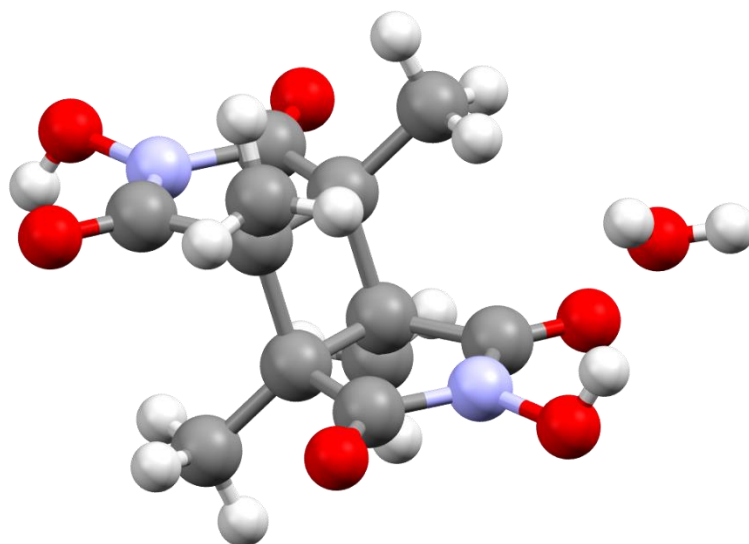


Figure B 4: Crystal data and structure for CBDH-1

Crystal parameters	CBDO-1
<b>Formula</b>	C <sub>16</sub> H <sub>22</sub> N <sub>2</sub> O <sub>6</sub>
<b>MW (g/mol)</b>	338.35
<b>Crystal System</b>	Monoclinic
<b>Space Group</b>	P 1 2 <sub>1</sub> /c 1
<b>a (Å)</b>	9.2397(3)
<b>b (Å)</b>	11.2061(4)
<b>c (Å)</b>	8.0558(3)
<b>α (°)</b>	90
<b>β (°)</b>	112.766(2)
<b>γ (°)</b>	90
<b>V (Å<sup>3</sup>)</b>	769.12(5)
<b>Z</b>	2
<b>Temp. (K)</b>	107
<b>ρ (g/cm<sup>3</sup>)</b>	1.461
<b>μ (mm<sup>-1</sup>)</b>	0.942
<b>Radiation type</b>	CuKα (λ = 1.54178)
<b>F(000)</b>	360.0
<b># of measured refl.</b>	8525
<b># of independent refl.</b>	1370
<b># of refl. (I ≥ 2σ)</b>	1286

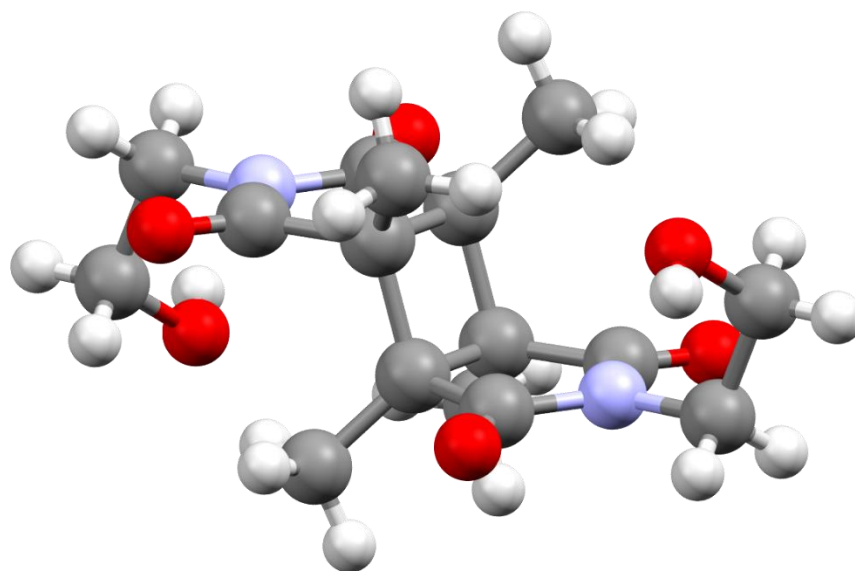


Figure B 5: Crystal data and structure for CBDO-1



Crystal parameters	protoCBDAc-1
<b>Formula</b>	C <sub>8</sub> H <sub>9</sub> NO <sub>4</sub>
<b>MW (g/mol)</b>	183.16
<b>Crystal System</b>	Monoclinic
<b>Space Group</b>	P 1 2 <sub>1</sub> /c 1
<b>a (Å)</b>	10.7607(4)
<b>b (Å)</b>	9.3294(3)
<b>c (Å)</b>	9.0641(3)
<b>α (°)</b>	90
<b>β (°)</b>	110.205(3)
<b>γ (°)</b>	90
<b>V (Å<sup>3</sup>)</b>	853.96(5)
<b>Z</b>	4
<b>Temp. (K)</b>	107
<b>ρ (g/cm<sup>3</sup>)</b>	1.425
<b>μ (mm<sup>-1</sup>)</b>	0.990
<b>Radiation type</b>	CuKα (λ = 1.54178)
<b>F(000)</b>	384.0
<b># of measured refl.</b>	9165
<b># of independent refl.</b>	1499
<b># of refl. (I ≥ 2σ)</b>	1235

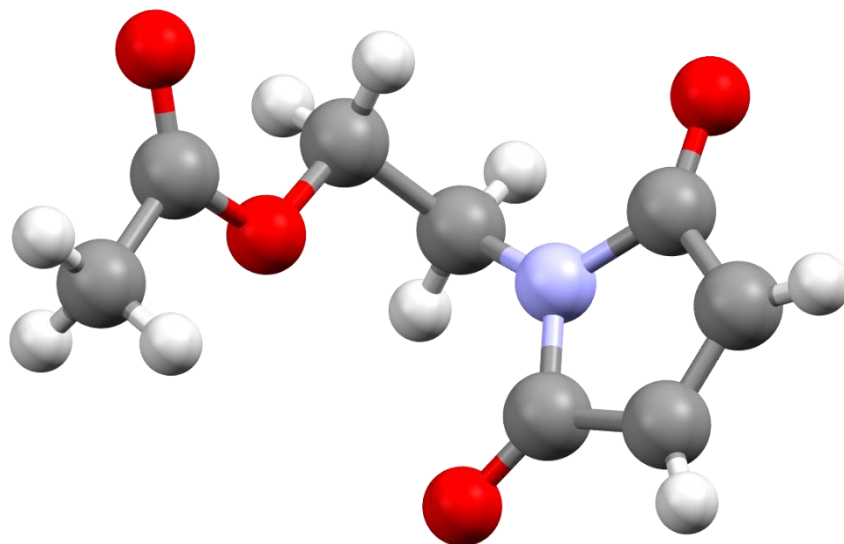


Figure B 6: Crystal data and structure for protoCBDAc-1

Crystal parameters	protoCBDE-6
<b>Formula</b>	C <sub>10</sub> H <sub>13</sub> NO <sub>4</sub>
<b>MW (g/mol)</b>	211.21
<b>Crystal System</b>	Monoclinic
<b>Space Group</b>	P 1 2 <sub>1</sub> /c 1
<b>a (Å)</b>	7.7975(4)
<b>b (Å)</b>	15.6353(6)
<b>c (Å)</b>	8.8250(3)
<b>α (°)</b>	90
<b>β (°)</b>	100.236(3)
<b>γ (°)</b>	90
<b>V (Å<sup>3</sup>)</b>	1058.79(8)
<b>Z</b>	4
<b>Temp. (K)</b>	111.14
<b>ρ (g/cm<sup>3</sup>)</b>	1.325
<b>μ (mm<sup>-1</sup>)</b>	0.868
<b>Radiation type</b>	CuKα (λ = 1.54178)
<b>F(000)</b>	448.0
<b># of measured refl.</b>	9167
<b># of independent refl.</b>	1884
<b># of refl. (I ≥ 2σ)</b>	1650

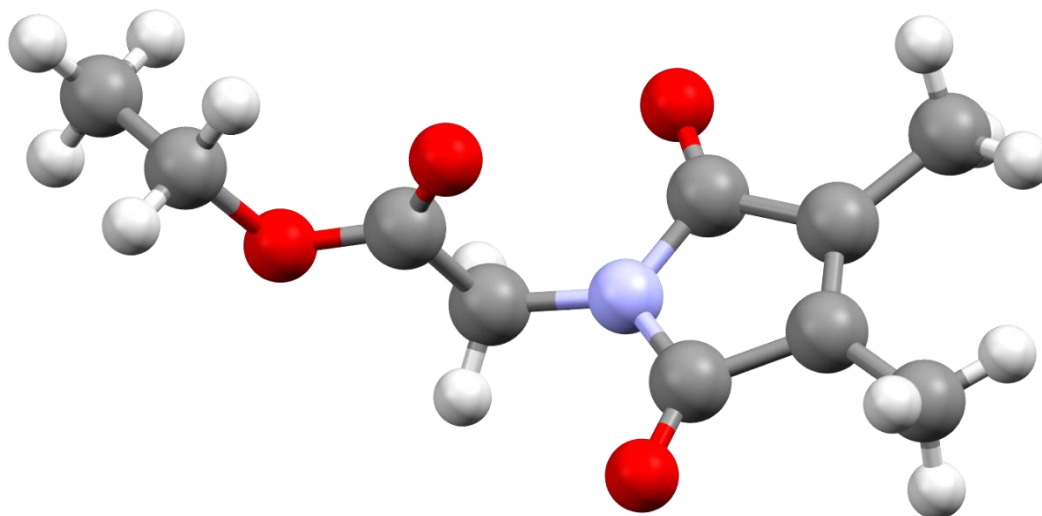


Figure B 7: Crystal data and structure for protoCBDE-6

Crystal parameters	protoCBDH-1
<b>Formula</b>	C <sub>6</sub> H <sub>7</sub> NO <sub>3</sub>
<b>MW (g/mol)</b>	114.13
<b>Crystal System</b>	Orthorhombic
<b>Space Group</b>	P2 <sub>1</sub> 2 <sub>1</sub> 2 <sub>1</sub>
<b>a (Å)</b>	3.8352(2)
<b>b (Å)</b>	11.2144(6)
<b>c (Å)</b>	14.9702(8)
<b>α (°)</b>	90
<b>β (°)</b>	90
<b>γ (°)</b>	90
<b>V (Å<sup>3</sup>)</b>	643.86(6)
<b>Z</b>	4
<b>Temp. (K)</b>	273.15
<b>ρ (g/cm<sup>3</sup>)</b>	1.456
<b>μ (mm<sup>-1</sup>)</b>	1.012
<b>Radiation type</b>	CuKα (λ = 1.54178)
<b>F(000)</b>	296.0
<b># of measured refl.</b>	7514
<b># of independent refl.</b>	1138
<b># of refl. (I ≥ 2σ)</b>	1043

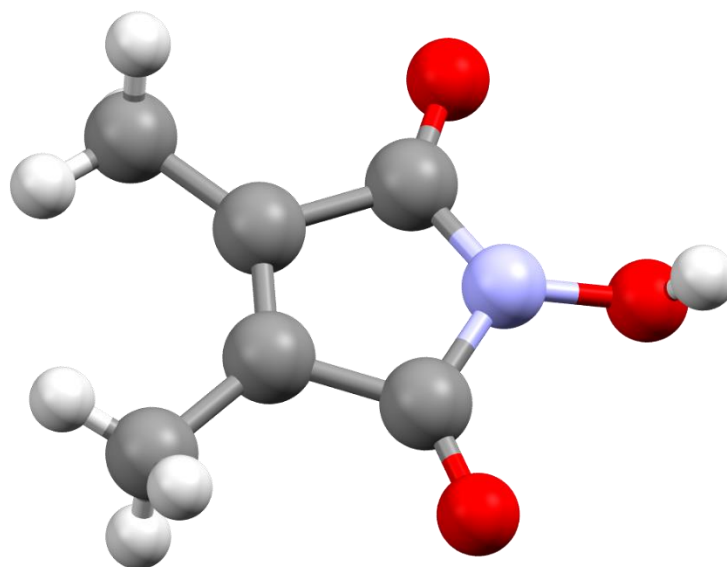


Figure B 8: Crystal data and structure for protoCBDH-1

Crystal parameters	CBeAn-1
<b>Formula</b>	C <sub>6</sub> H <sub>4</sub> O <sub>3</sub>
<b>MW (g/mol)</b>	124.09
<b>Crystal System</b>	Orthorhombic
<b>Space Group</b>	P n m a
<b>a (Å)</b>	5.0155(2)
<b>b (Å)</b>	10.4273(5)
<b>c (Å)</b>	10.0627(5)
<b>α (°)</b>	90
<b>β (°)</b>	90
<b>γ (°)</b>	90
<b>V (Å<sup>3</sup>)</b>	526.26(4)
<b>Z</b>	4
<b>Temp. (K)</b>	296
<b>ρ (g/cm<sup>3</sup>)</b>	1.566
<b>μ (mm<sup>-1</sup>)</b>	1.105
<b>Radiation type</b>	CuKα (λ = 1.54178)
<b>F(000)</b>	256.0
<b># of measured refl.</b>	2152
<b># of independent refl.</b>	486
<b># of refl. (I ≥ 2σ)</b>	452

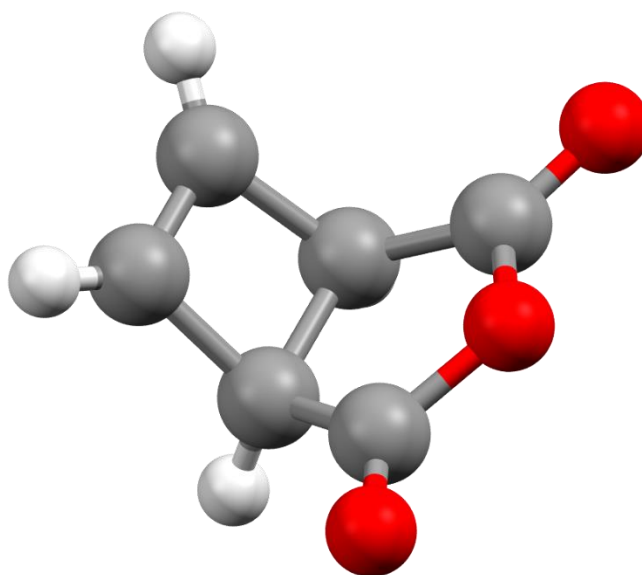


Figure B 9: Crystal data and structure for CBeAn-1

Crystal parameters	CPDAn-1
<b>Empirical Formula</b>	C <sub>5</sub> H <sub>3</sub> O <sub>3</sub>
<b>MW (g/mol)</b>	111.07
<b>Crystal System</b>	Orthorhombic
<b>Space Group</b>	P b c a
<b>a (Å)</b>	9.8332(4)
<b>b (Å)</b>	8.4059(3)
<b>c (Å)</b>	10.5584(4)
<b>α (°)</b>	90
<b>β (°)</b>	90
<b>γ (°)</b>	90
<b>V (Å<sup>3</sup>)</b>	872.72(6)
<b>Z</b>	8
<b>Temp. (K)</b>	107
<b>ρ (g/cm<sup>3</sup>)</b>	1.691
<b>μ (mm<sup>-1</sup>)</b>	1.250
<b>Radiation type</b>	CuKα (λ = 1.54178)
<b>F(000)</b>	456.0
<b># of measured refl.</b>	3985
<b># of independent refl.</b>	772
<b># of refl. (I ≥ 2σ)</b>	748

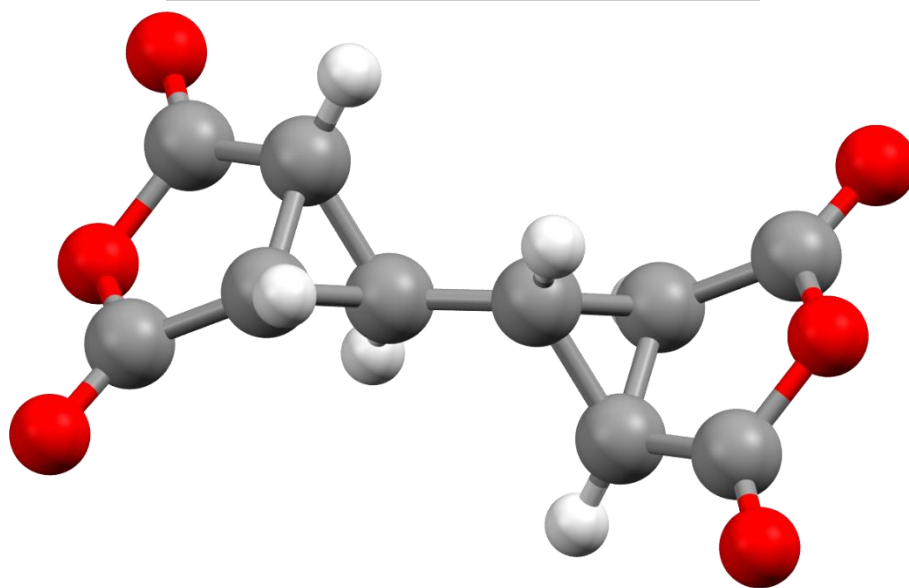


Figure B 10: Crystal data and structure for CPDAn-1

Appendix C: Selected HRMS spectra

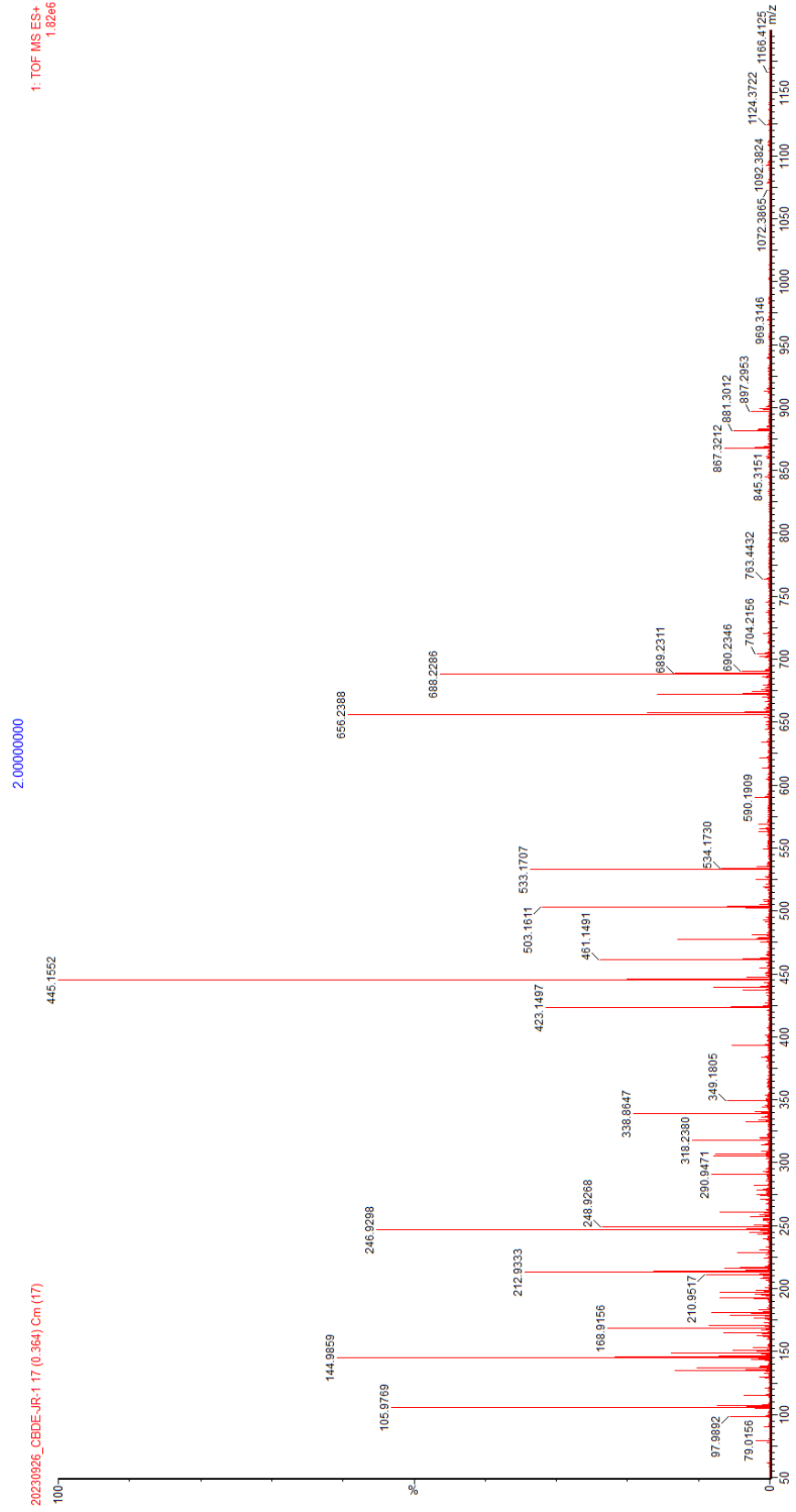


Figure C 1: Full high resolution mass spectrum for CBDE-6

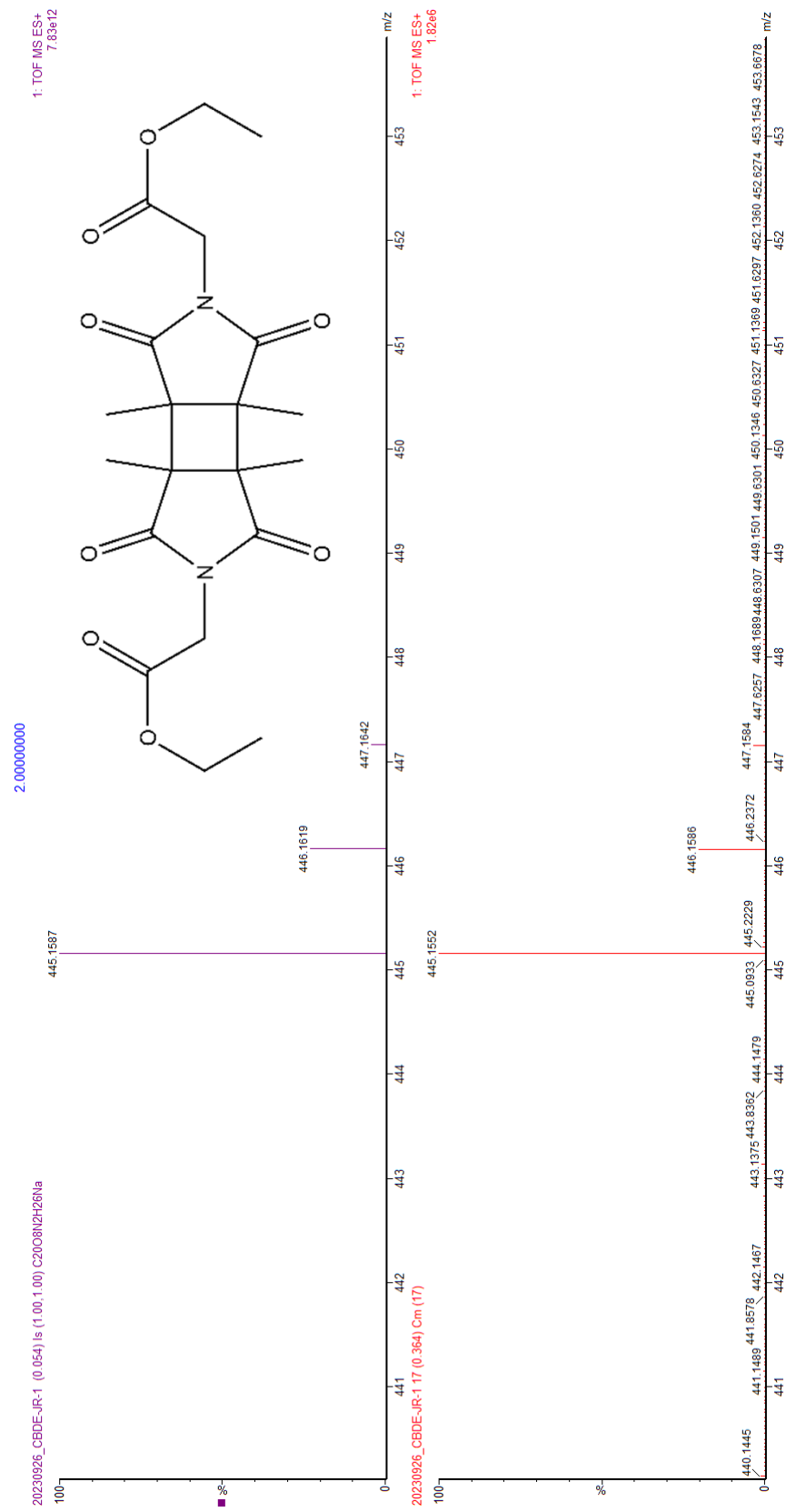


Figure C 2: Predicted [M+Na] peaks for CBDE-6 (top) and measured (bottom)





Figure C 3: Full high resolution mass spectrum for PCBI-1

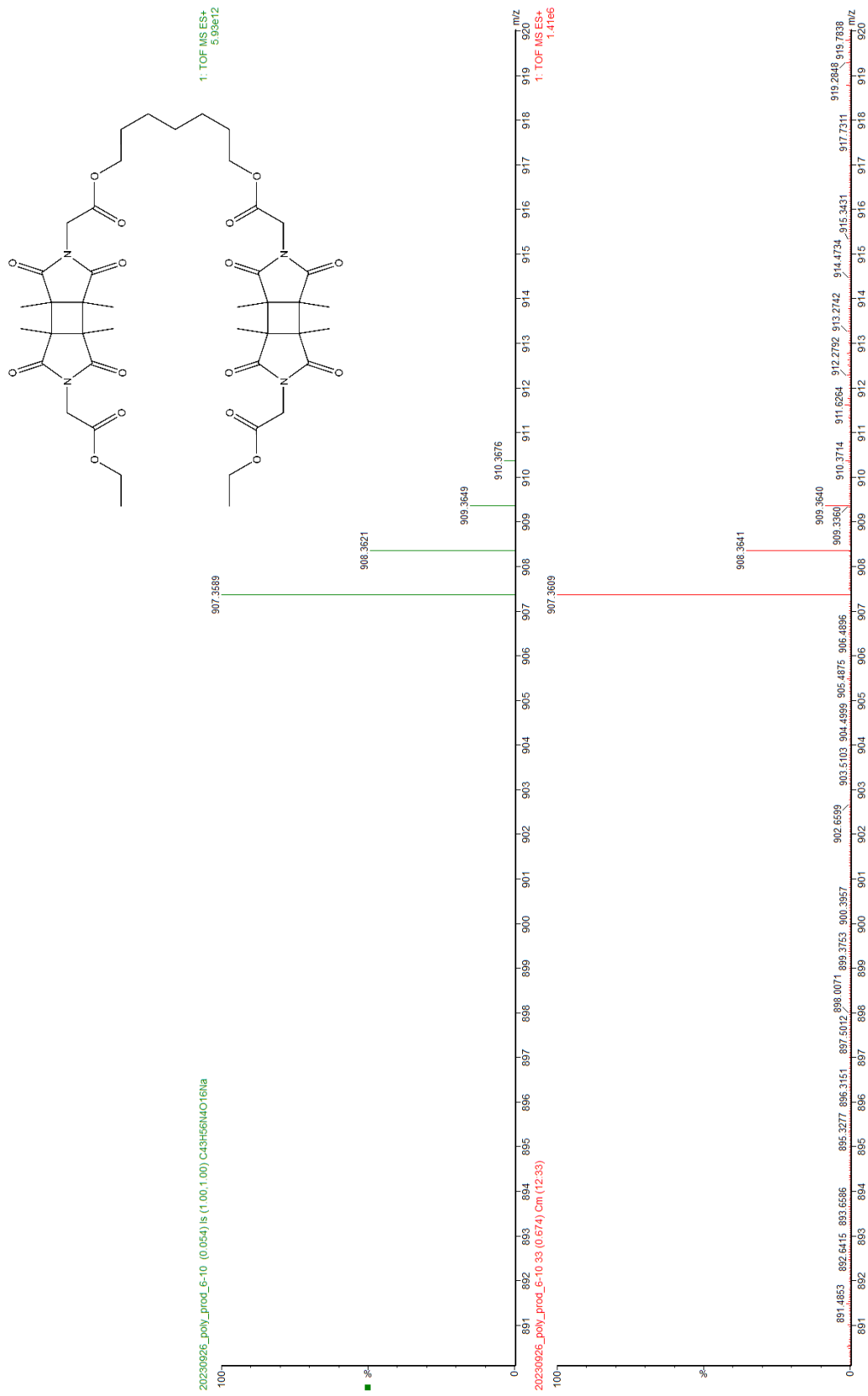
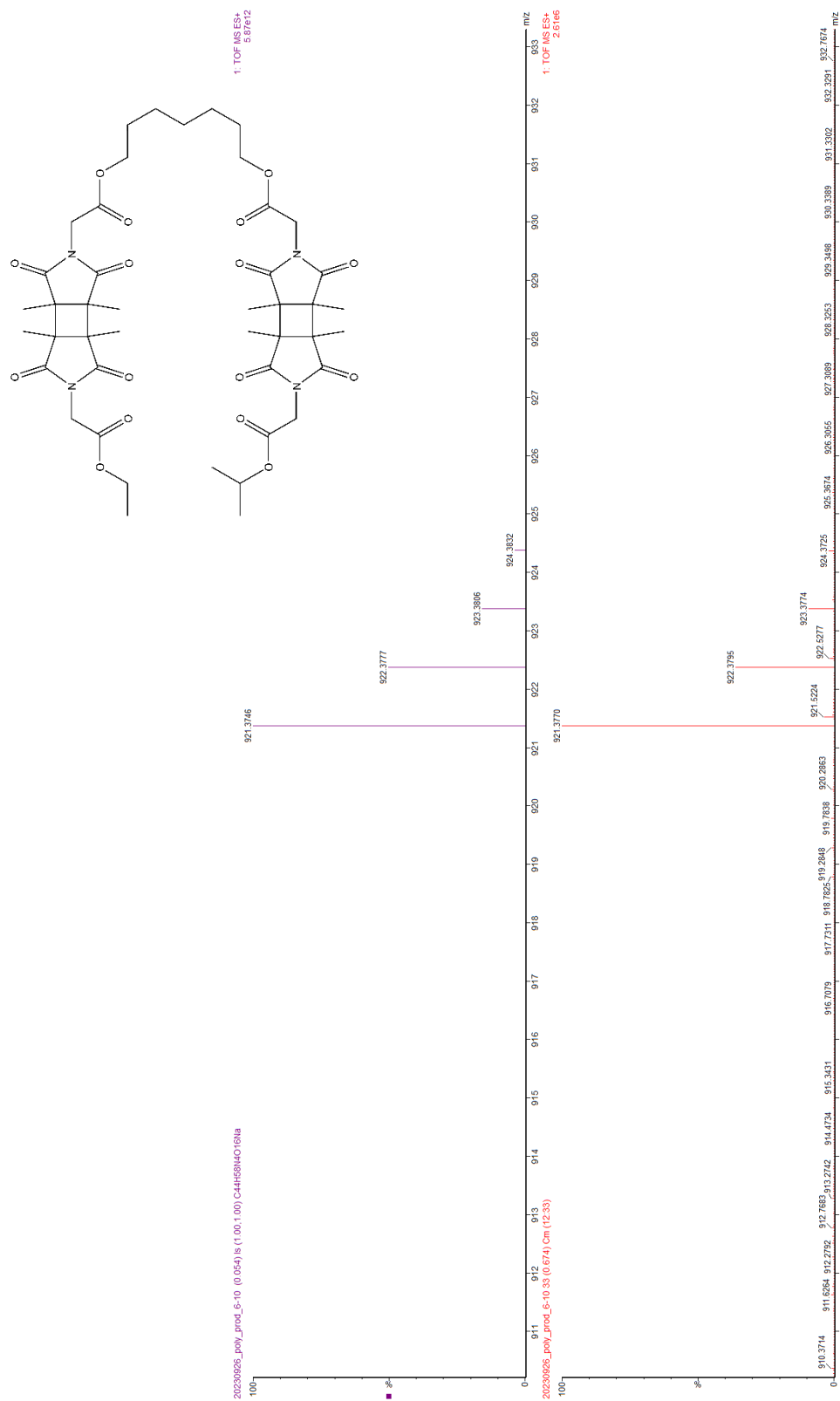


Figure C 4: Predicted  $[M+Na]$  peaks for a-b-a oligomer of PCBBI-1 (top) and measured (bottom)



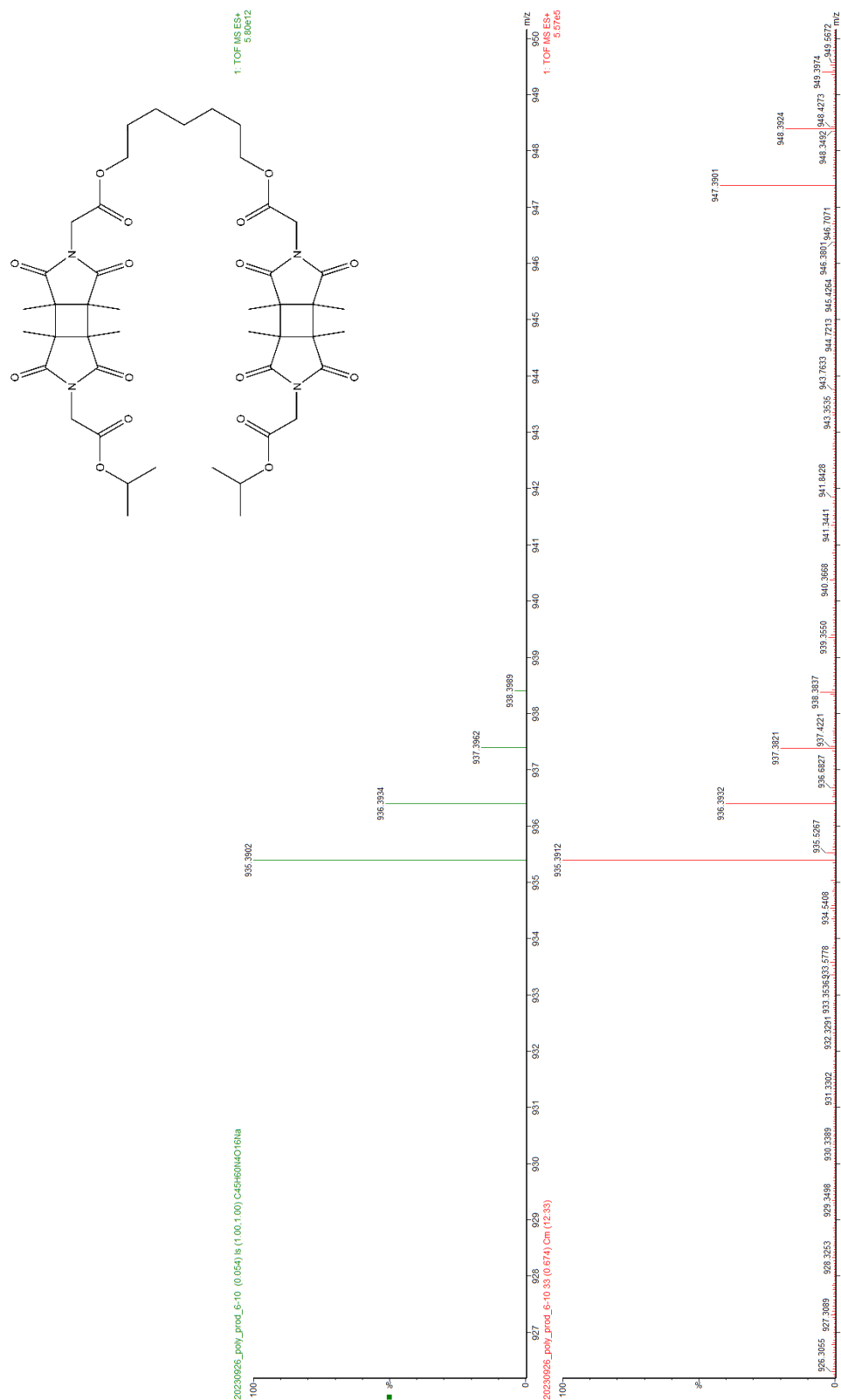


Figure C 6: Predicted  $[M+Na]$  peaks for dipropyl-substituted  $\alpha$ -b-a oligomer of PCBBI-1 (top) and measured (bottom)

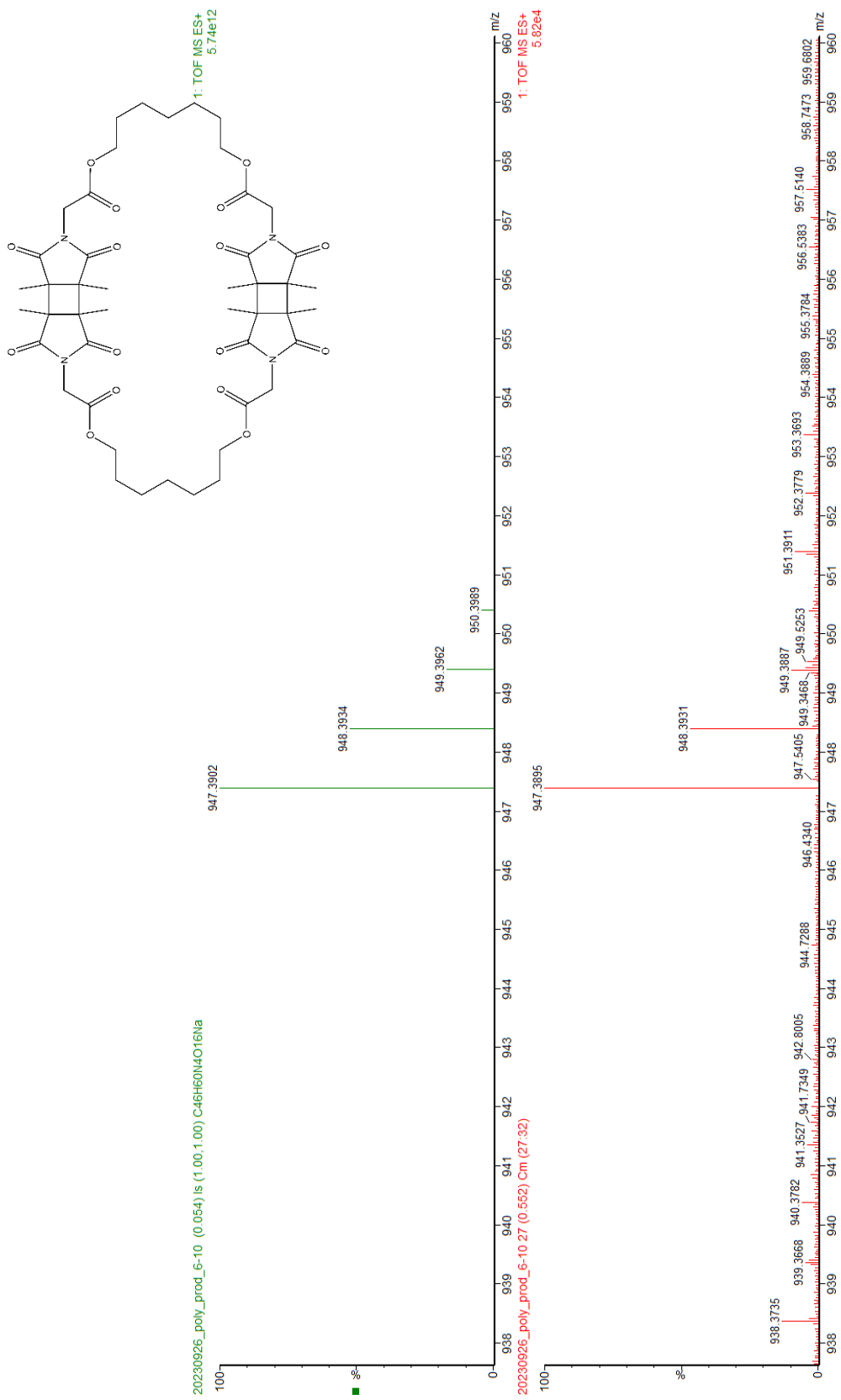


Figure C 7: Predicted [M+Na] peaks for cyclic dimer of PCBBI-1 (top) and measured (bottom)

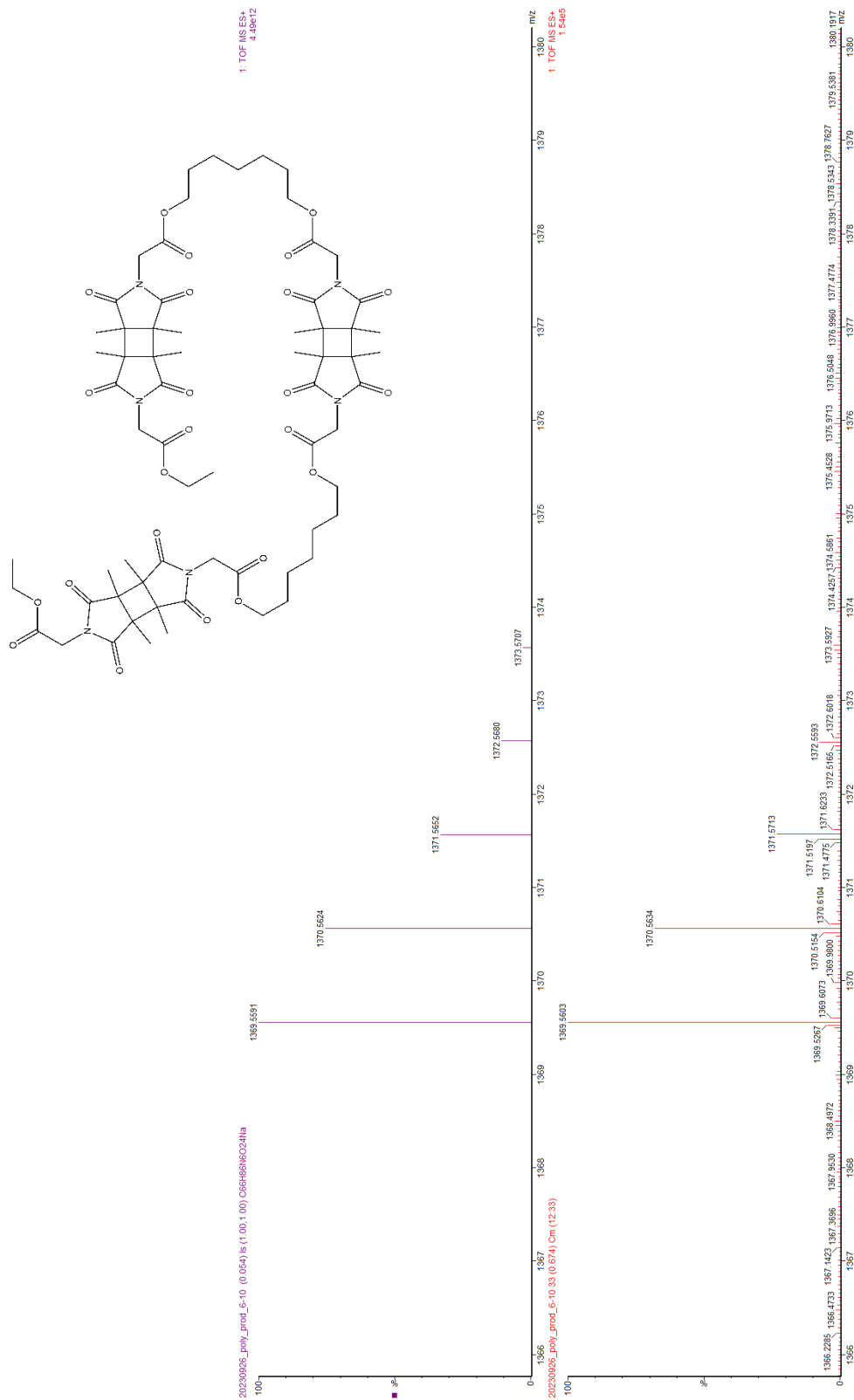


Figure C 8: Predicted  $[M+Na]$  peaks for a-b-a-b-a oligomer of PCBBI-1 (top) and measured (bottom)

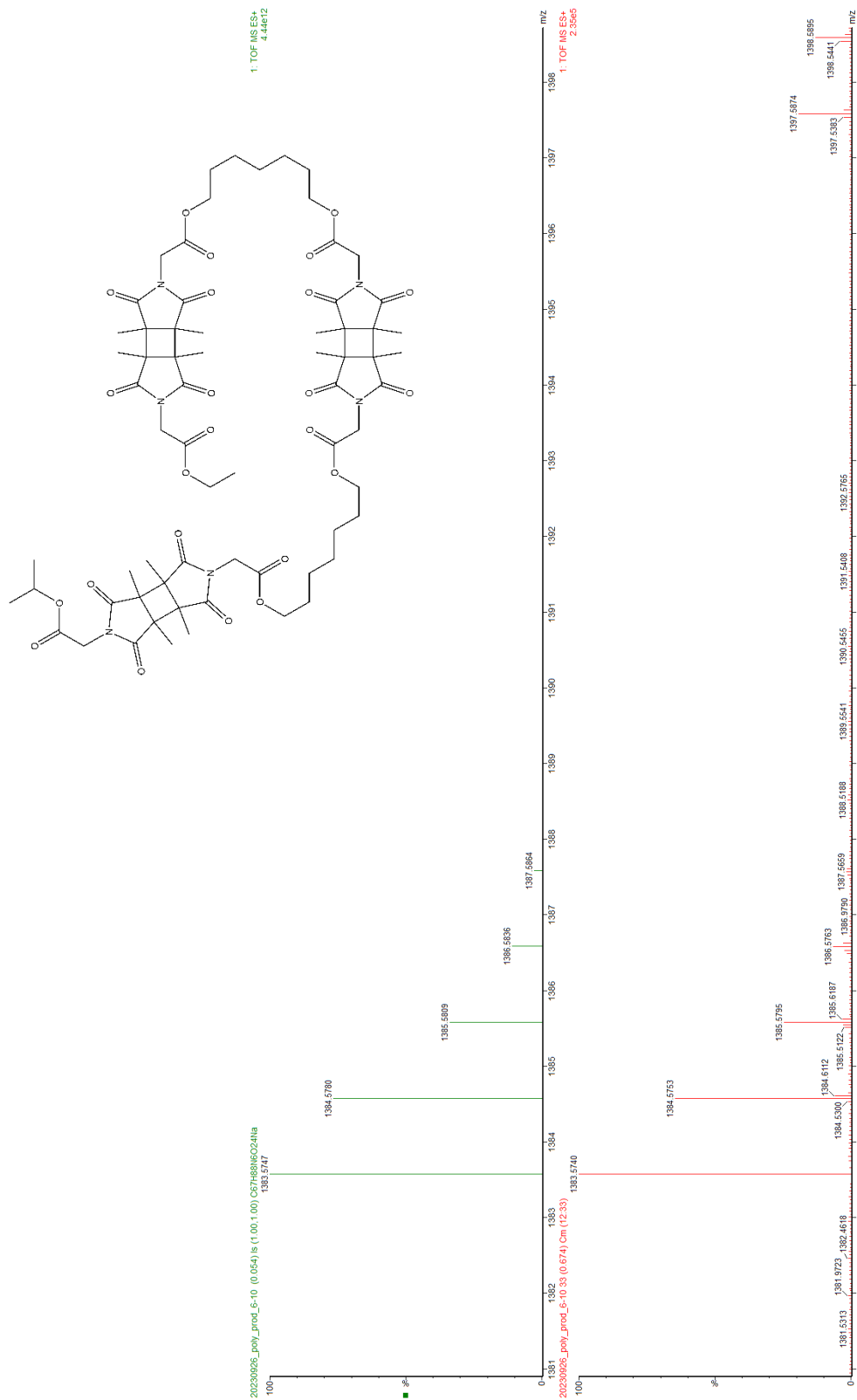


Figure C 9: Predicted  $[M+Na]$  peaks for monopropyl-substituted a-b-a-b-a oligomer of PCBBI-1 (top) and measured (bottom)

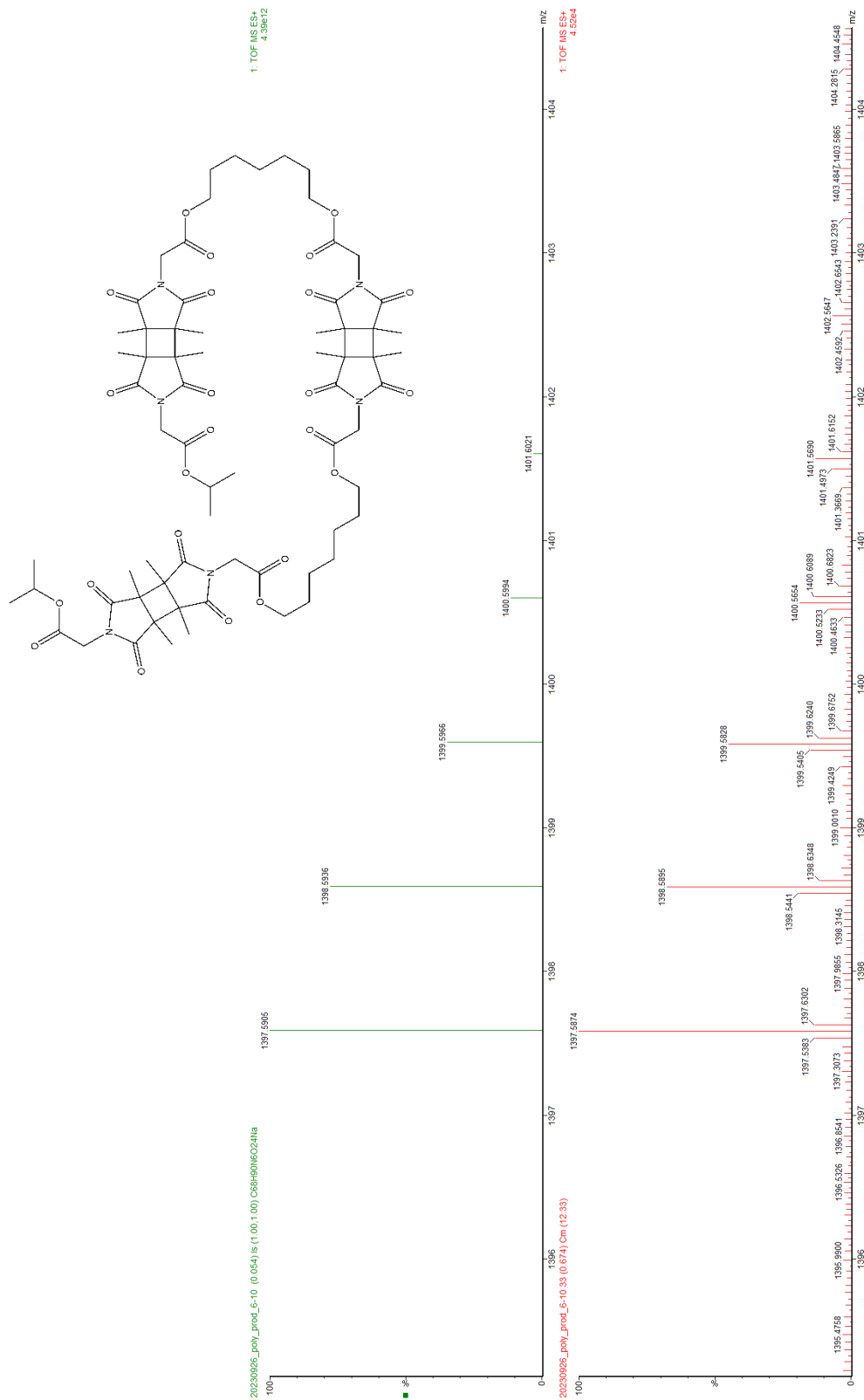


Figure C 10: Predicted  $[M+Na]$  peaks for dipropyl-substituted a-b-a-b-a oligomer of PCBBI-1 (top) and measured (bottom)



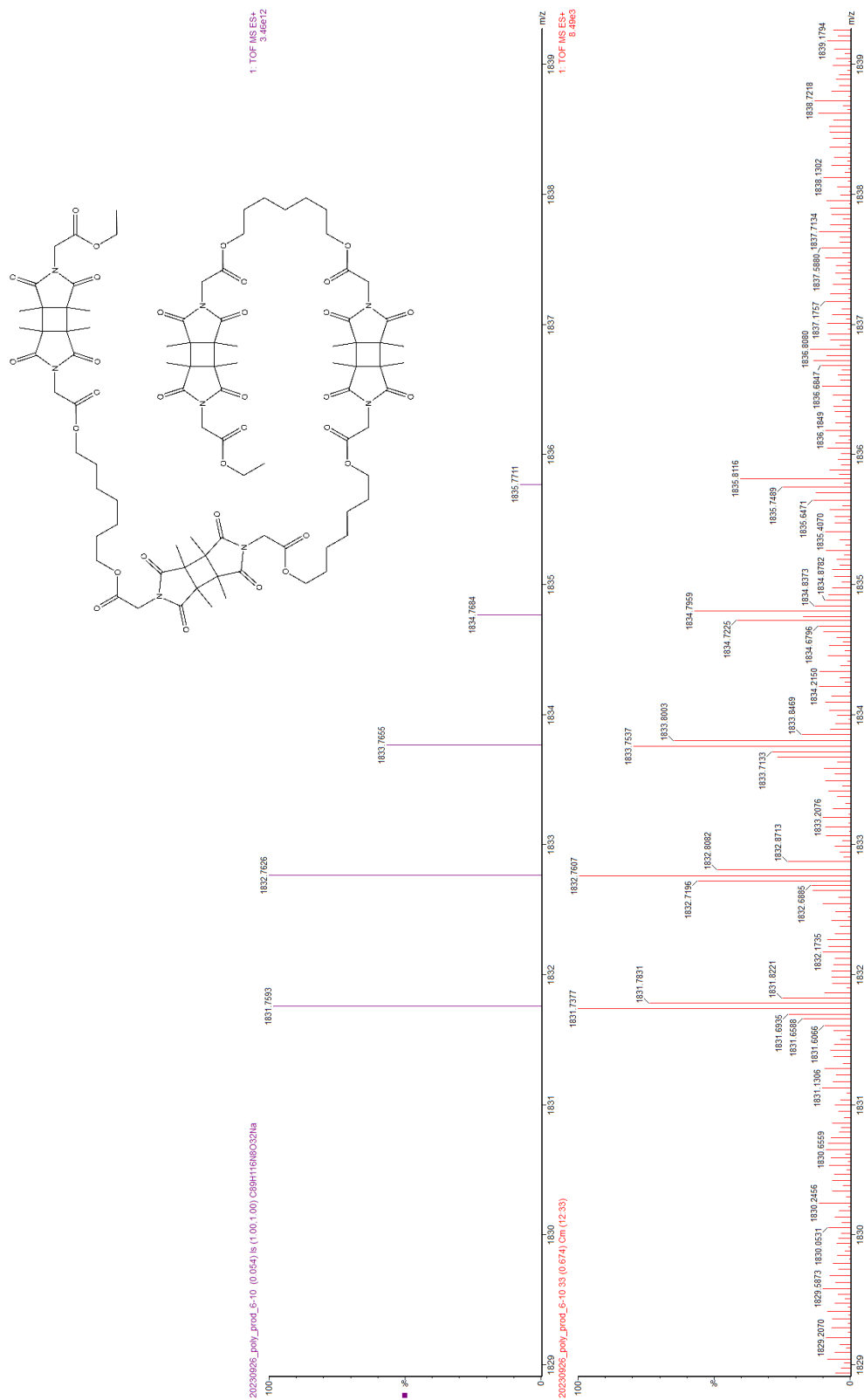
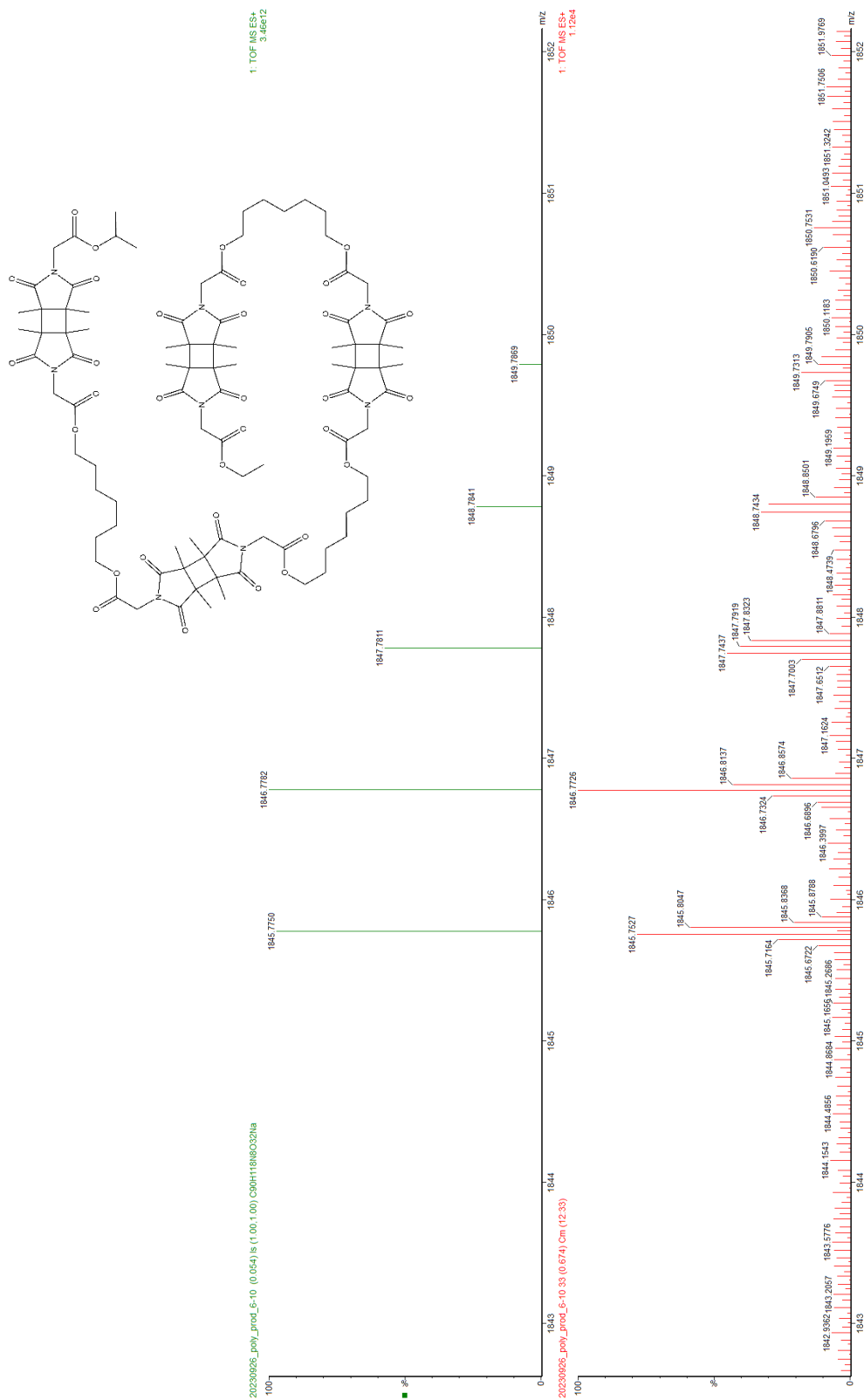


Figure C 11: Predicted  $[M+Na]$  peaks for a-b-a-b-a-b-a oligomer of PCBBI-1 (top) and measured (bottom)



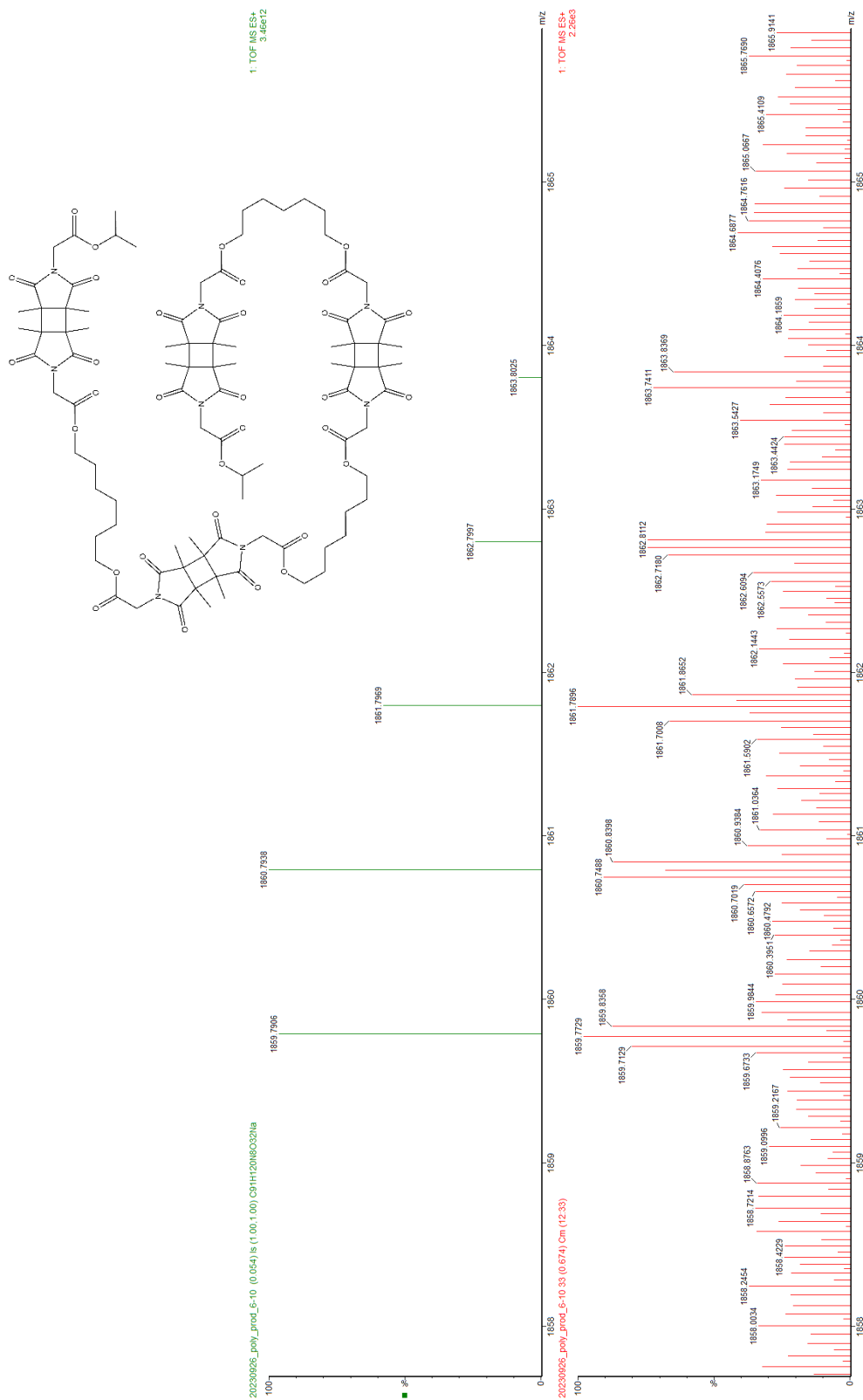


Figure C 13: Predicted  $[M+Na]$  peaks for monopropyl-substituted a-b-a-b-a-b-a oligomer of PCBBI-1 (top) and measured (bottom)

Appendix D: Selected IR spectra

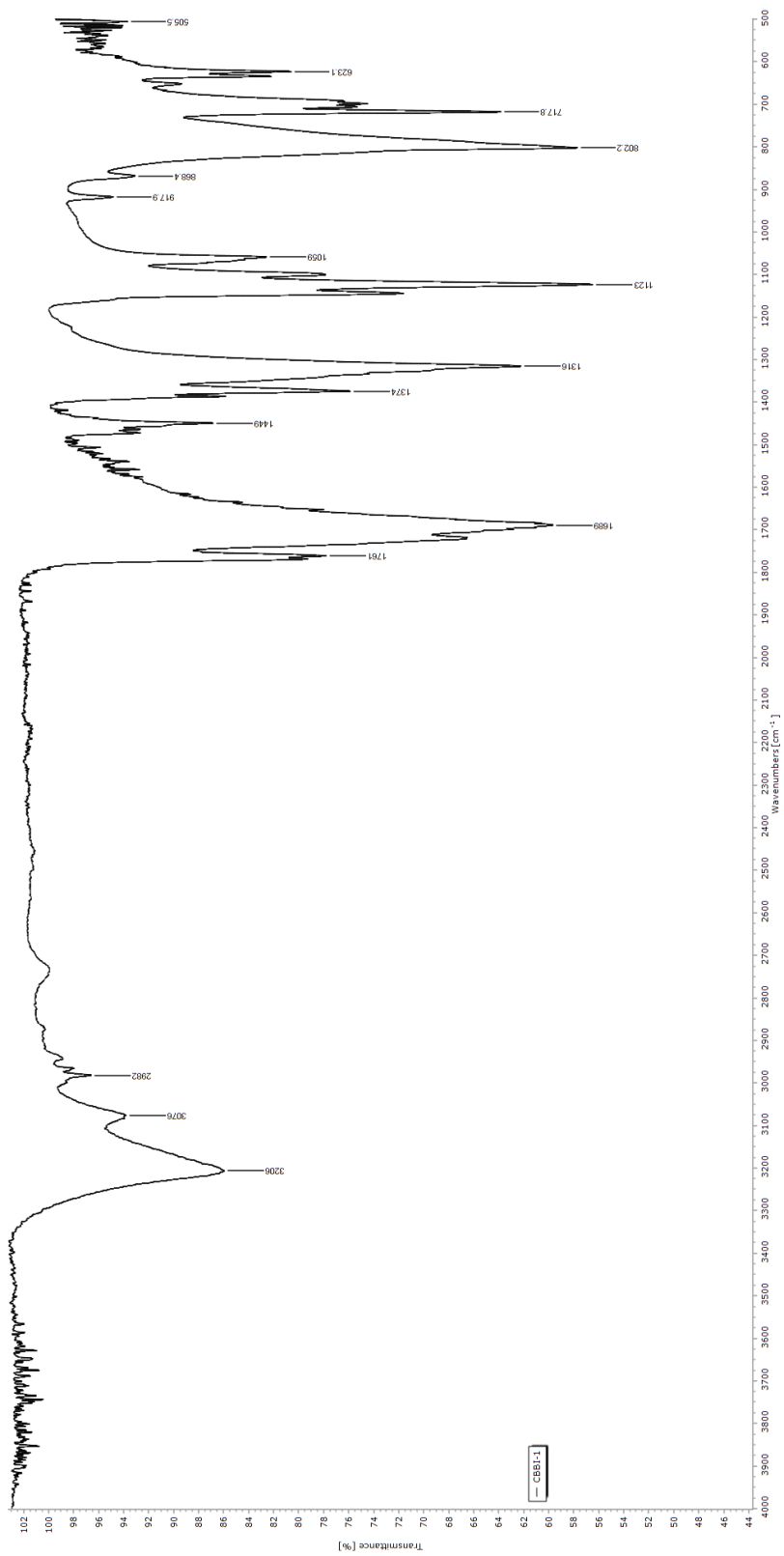


Figure D 1: IR spectra for CBBI-1

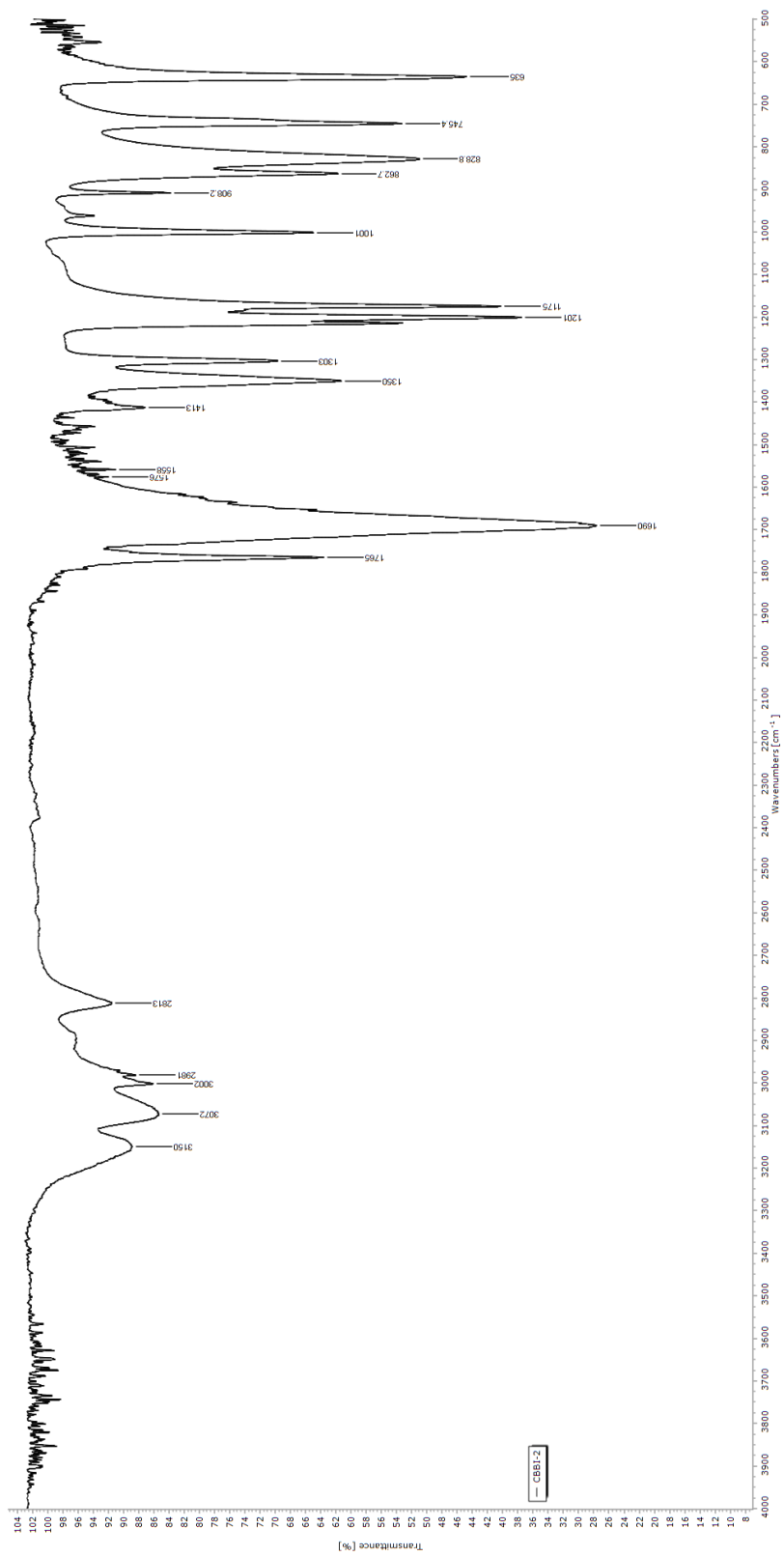


Figure D 2: IR spectra for CBBI-2

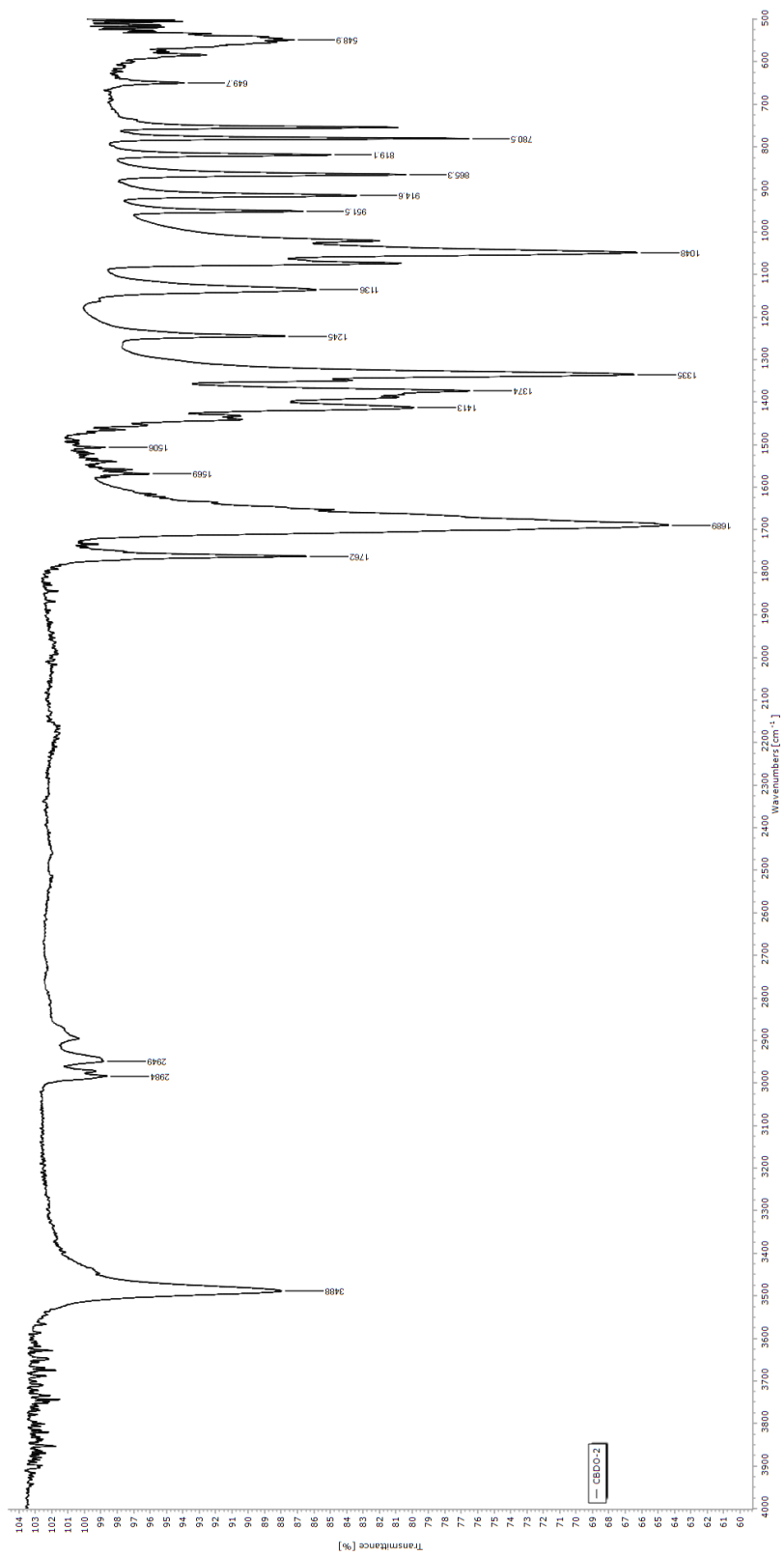


Figure D 3: IR spectra for CBDO-2

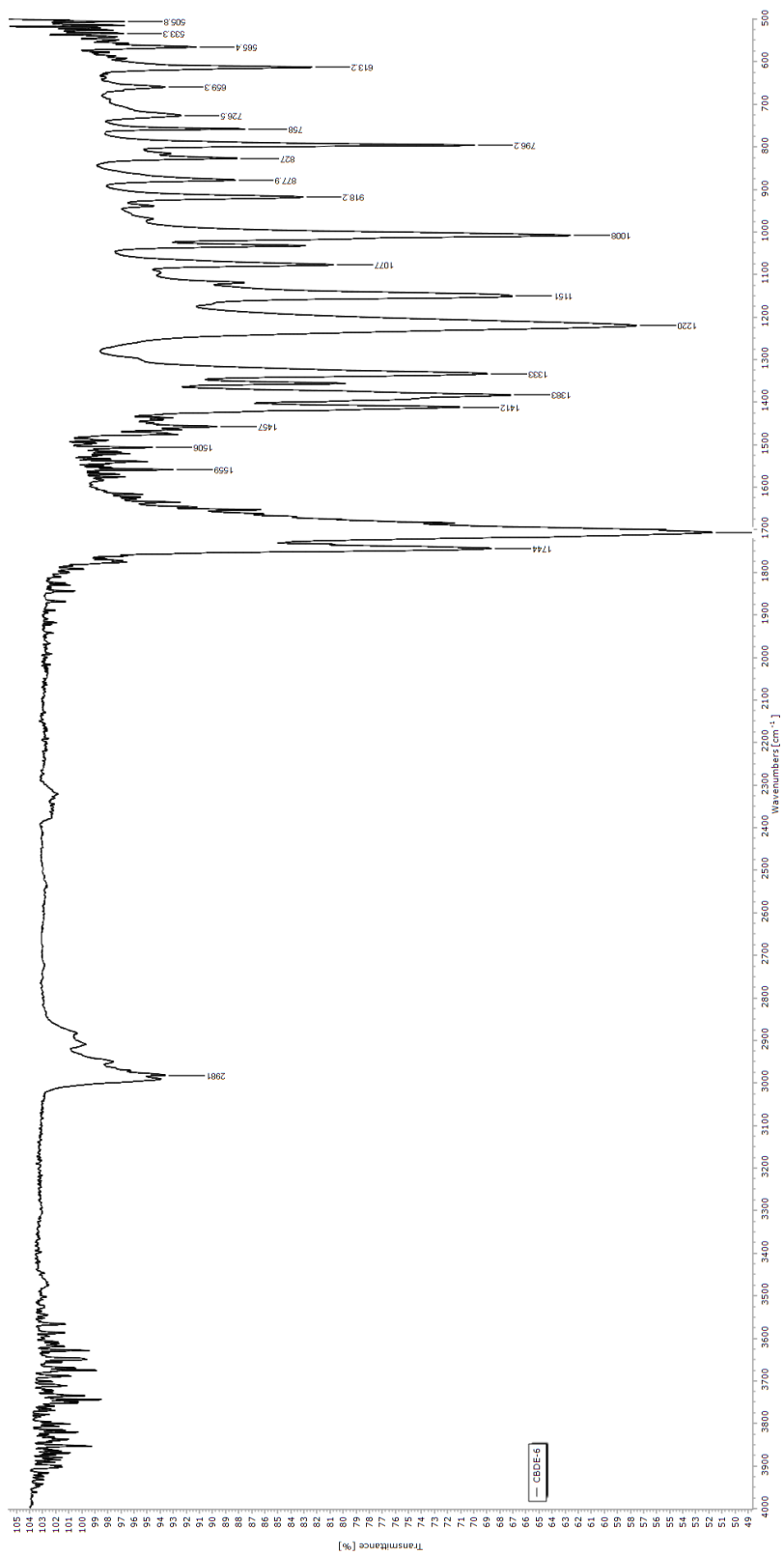


Figure D 4: IR spectra for CBDE-6



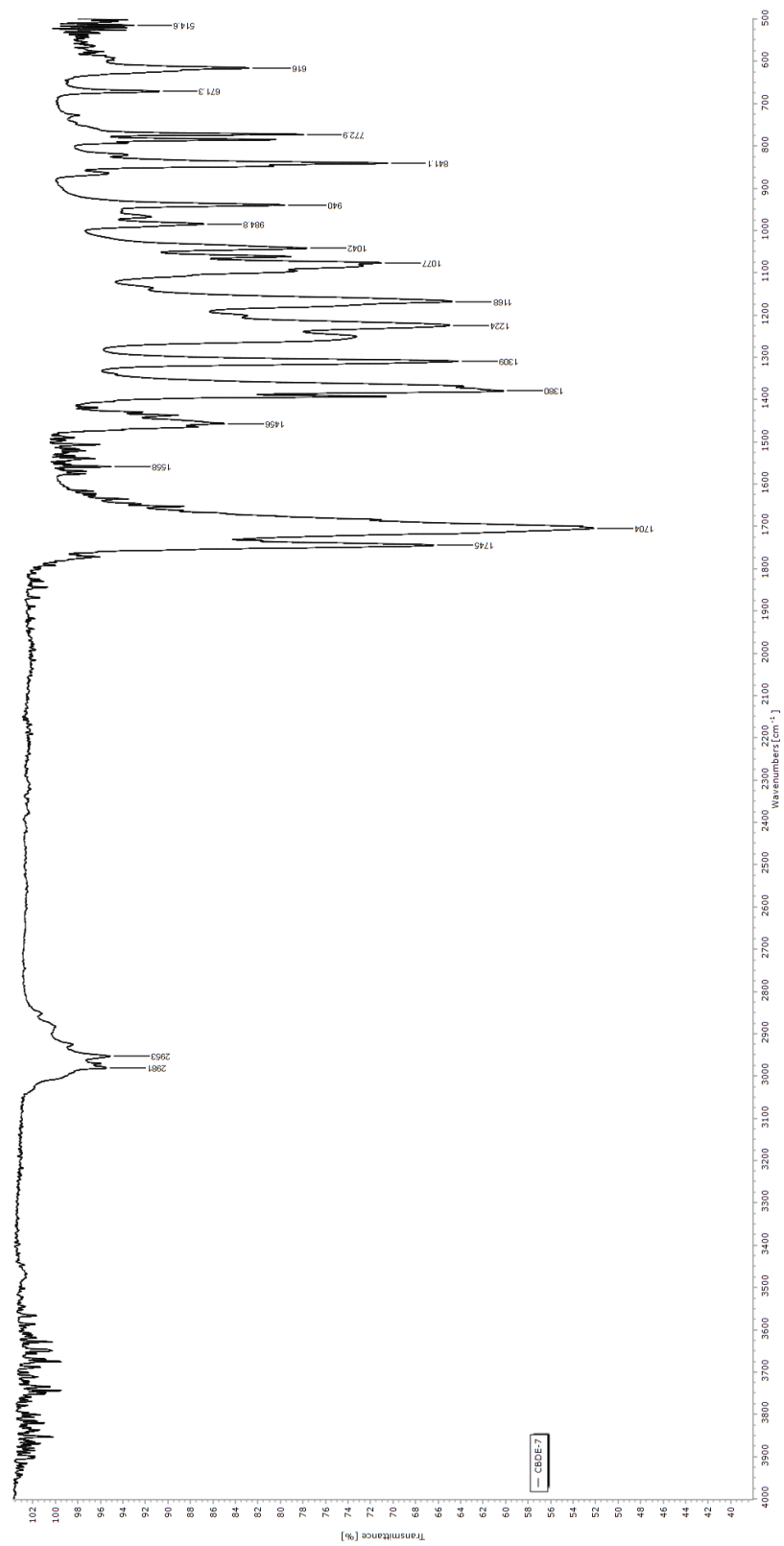


Figure D 5: IR spectra for CBDE-7

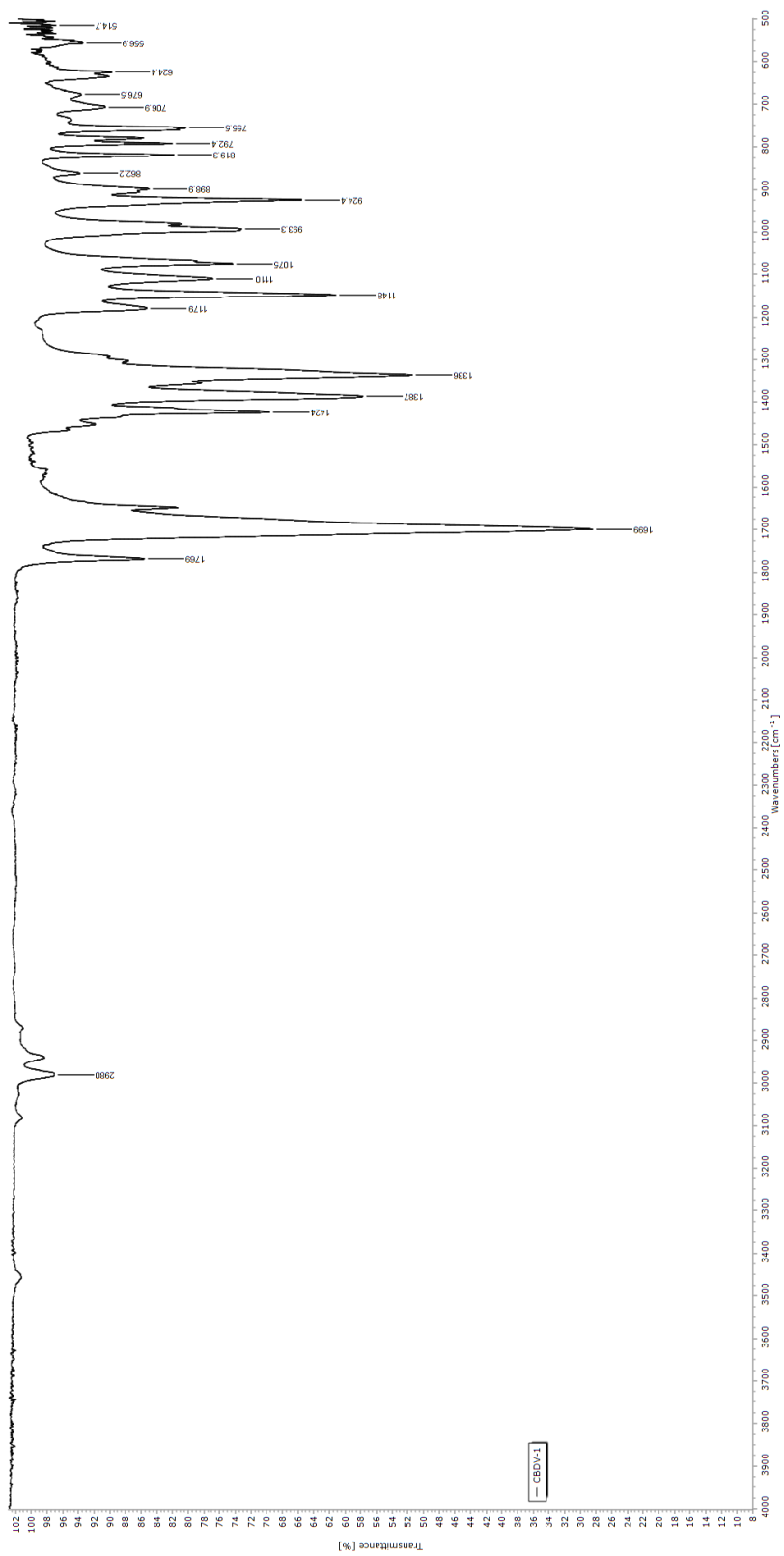


Figure D 6: IR spectra for CBDV-1

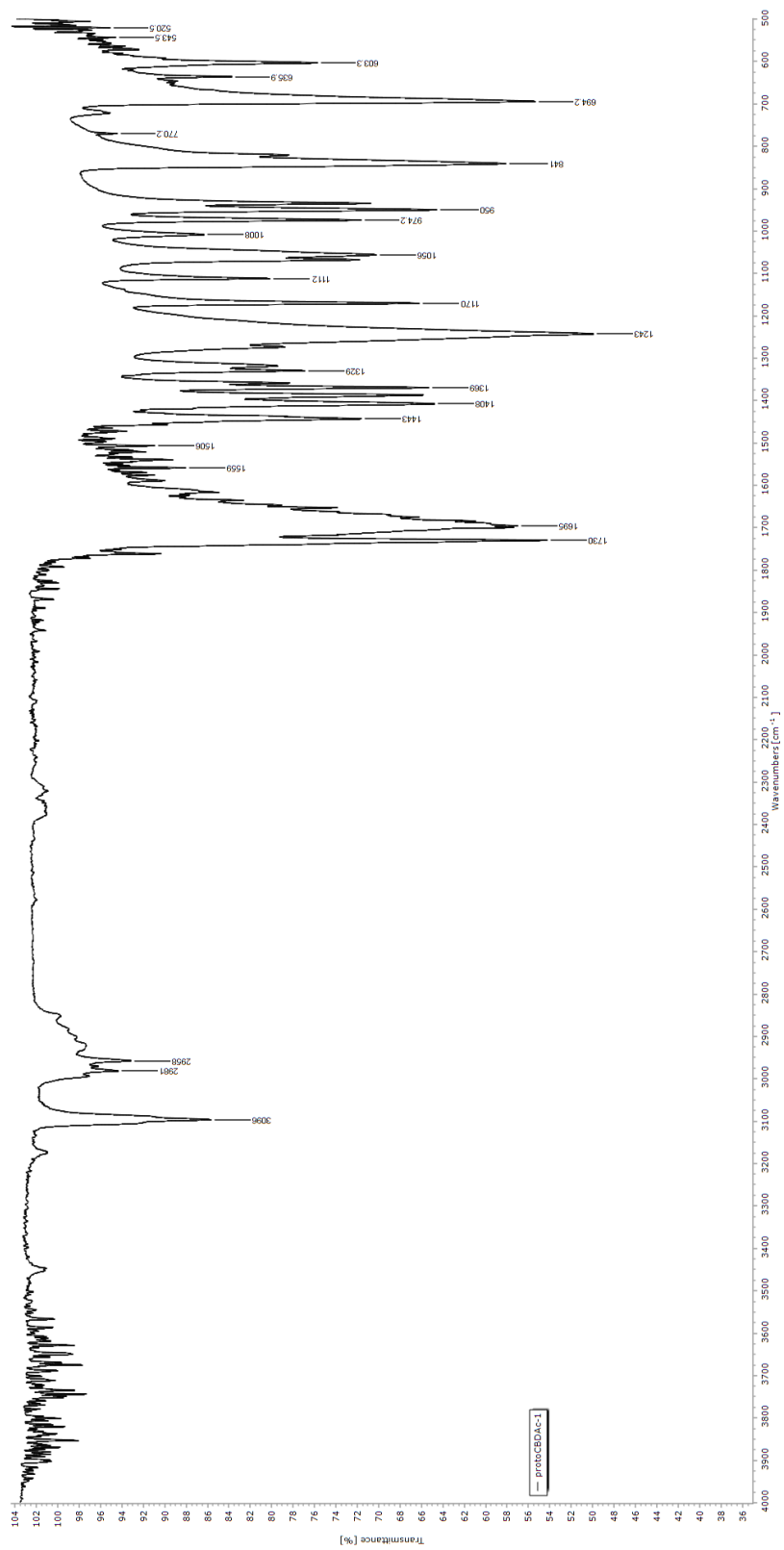


Figure D 7: IR spectra for protoCBDAc-1



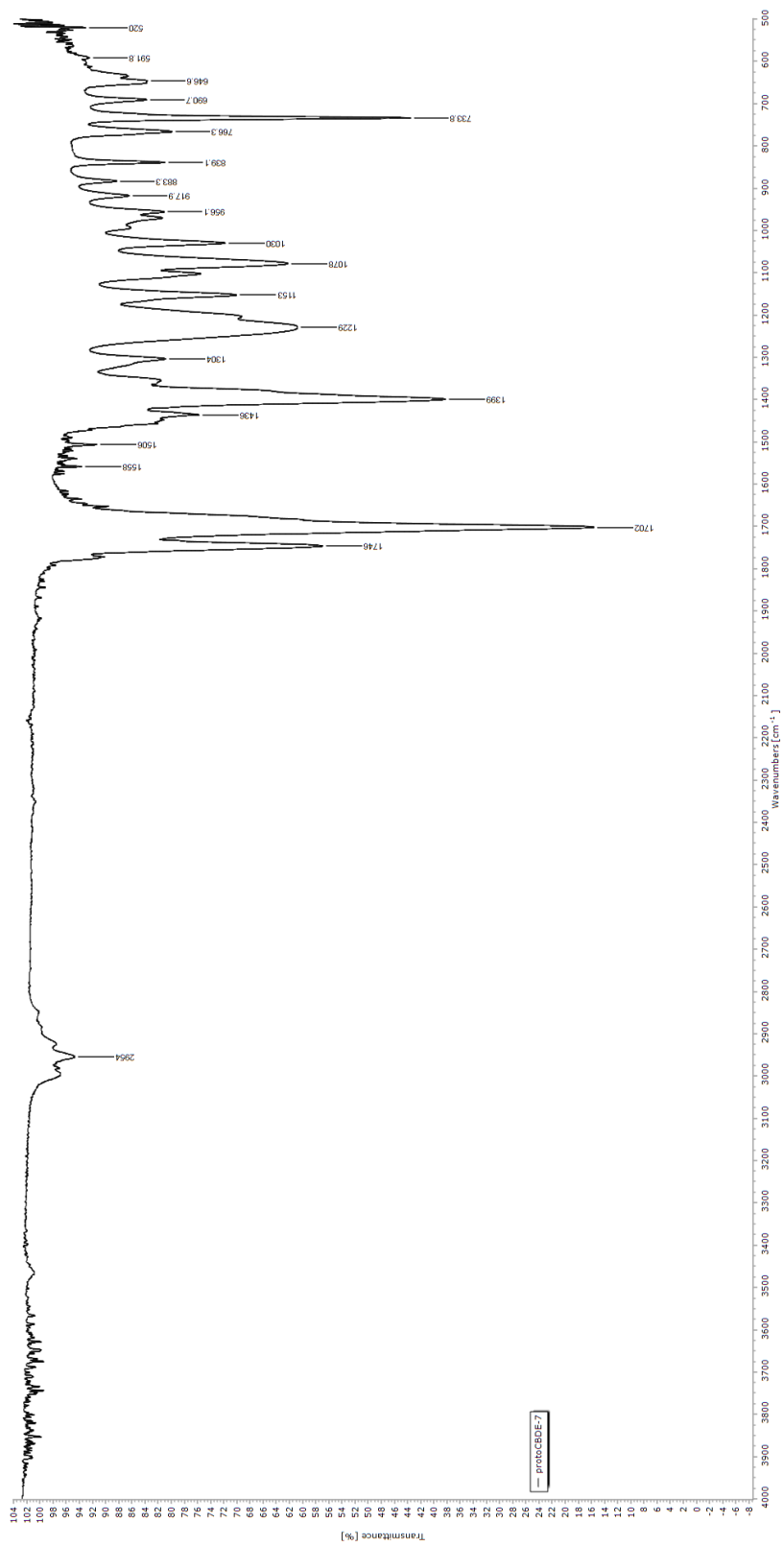


Figure D 9: IR spectra for protoCBDE-7

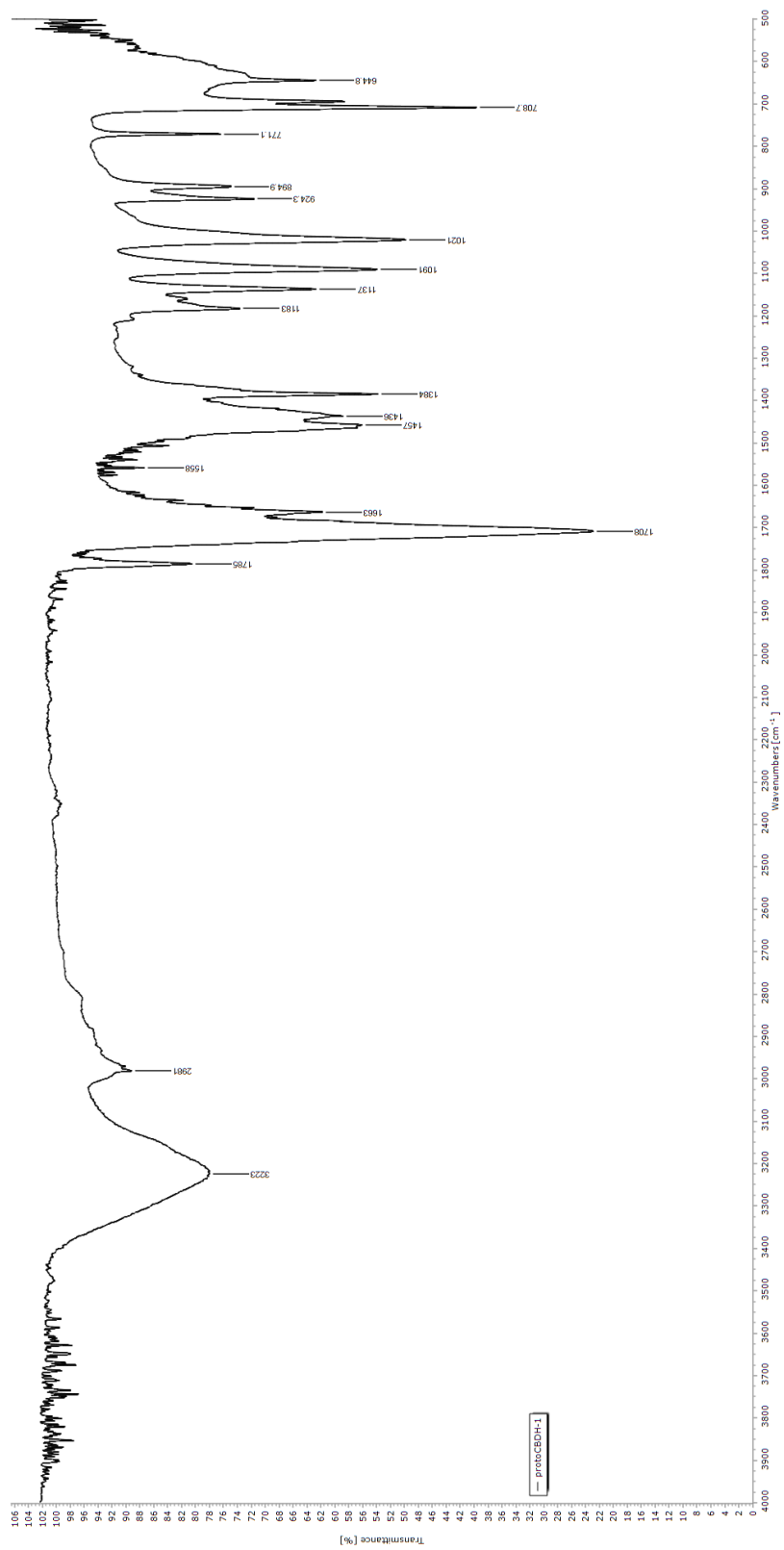


Figure D 10: IR spectra for protoCBDH-1

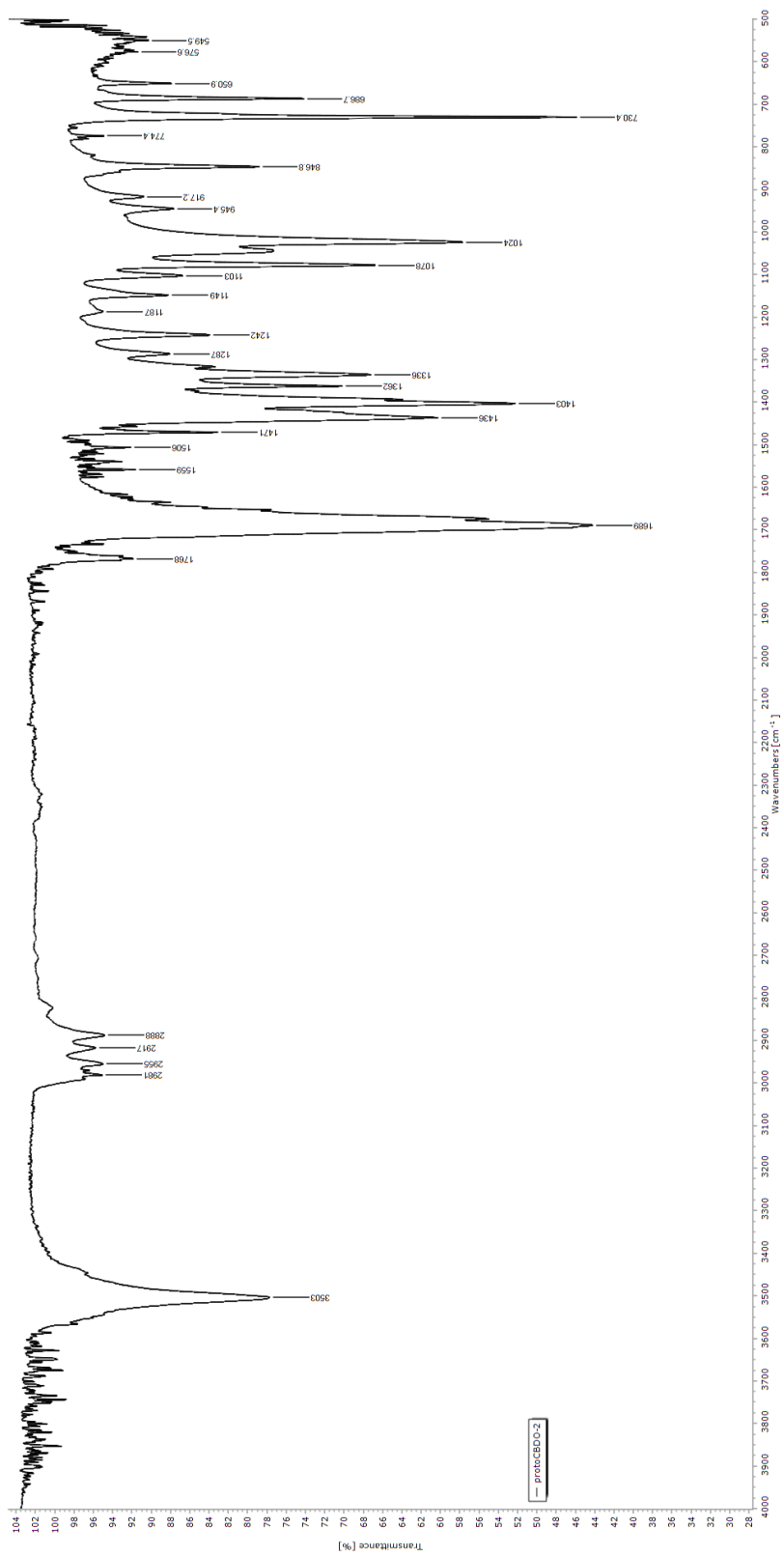


Figure D 11: IR spectra for protoCBDO-2

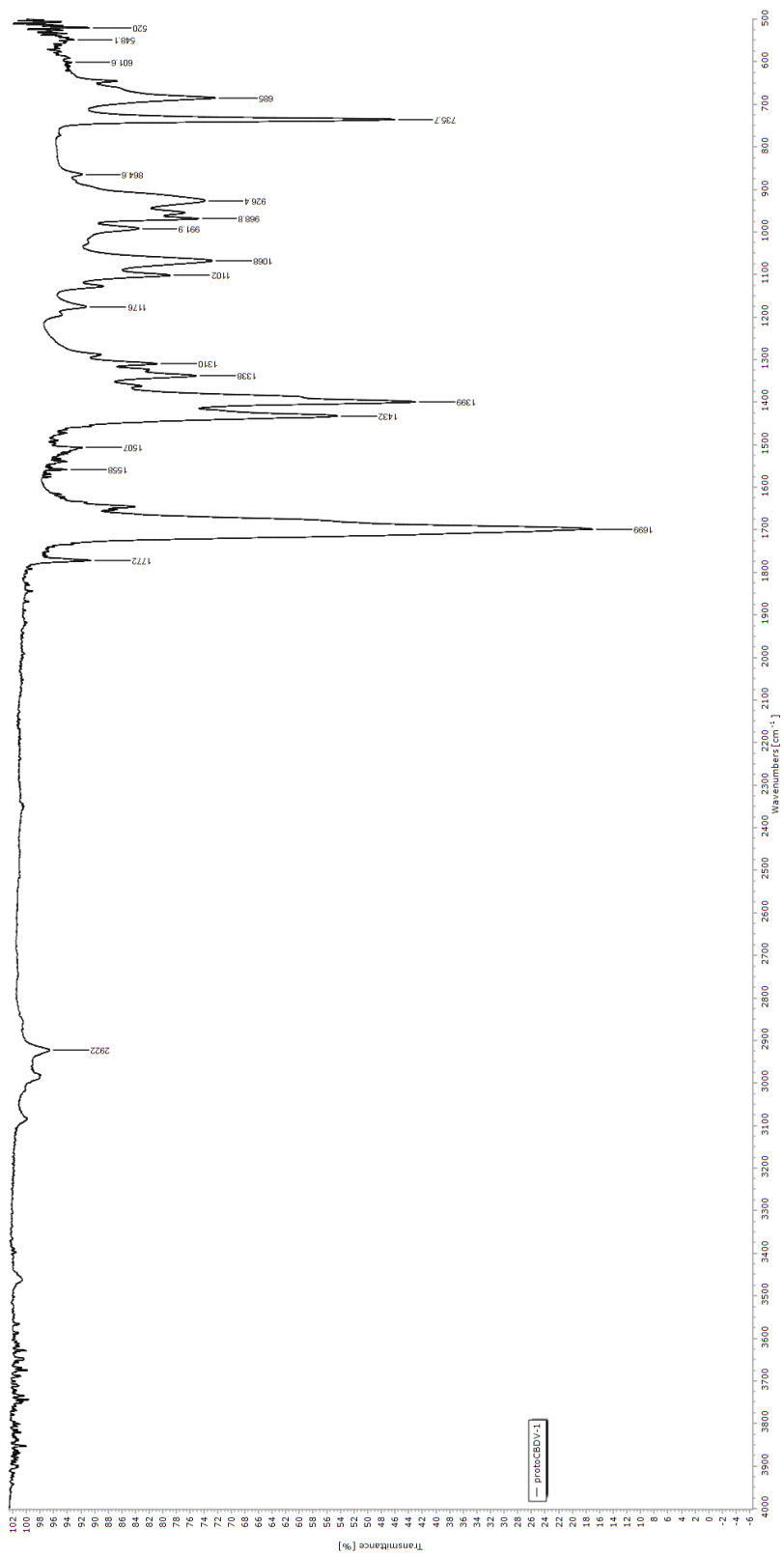


Figure D 12: IR spectra for protoCBDV-1



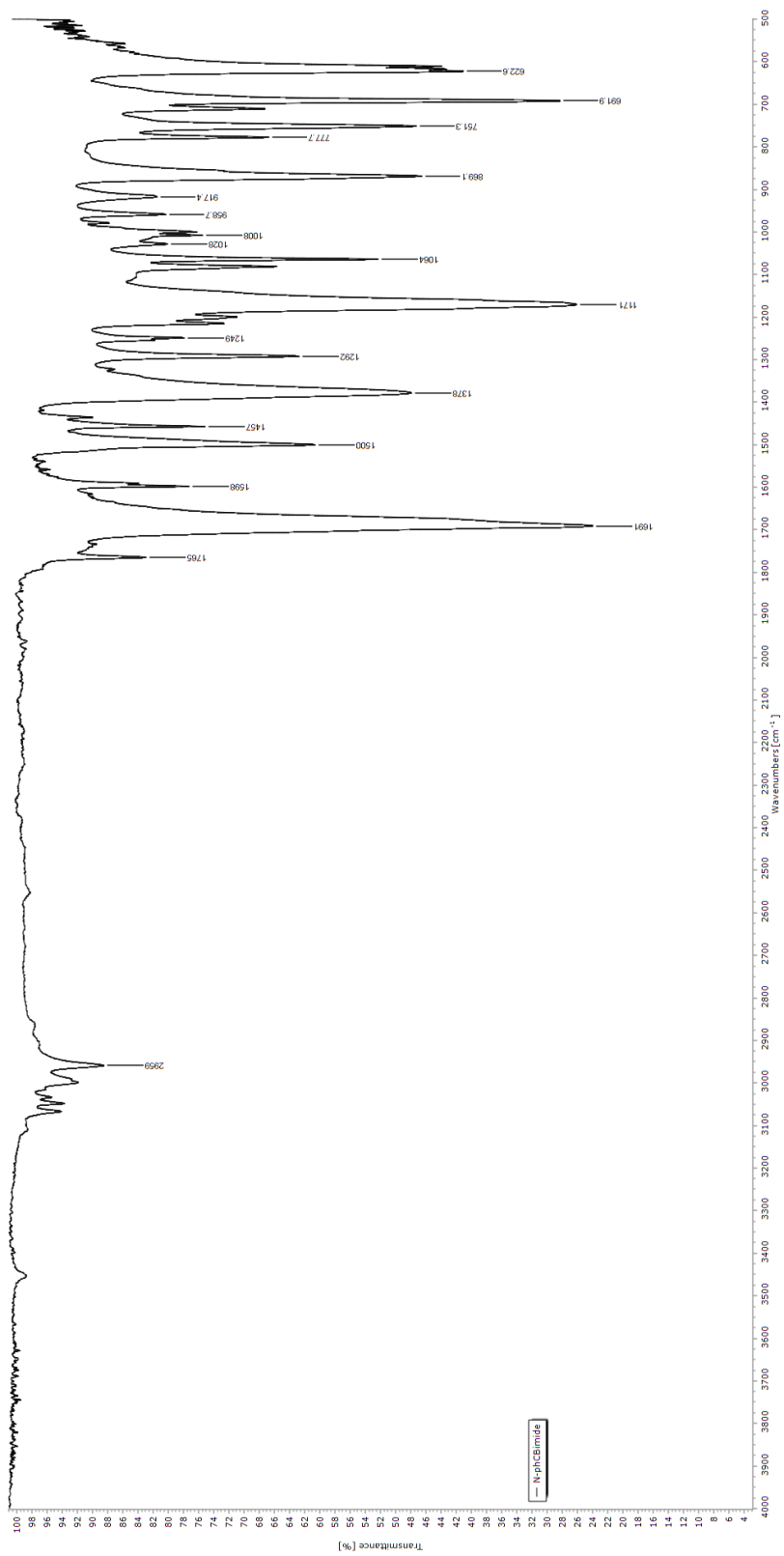


Figure D 13: IR spectra for (N-phenyl)-cis-1,2-cyclobutanecarboximide

Appendix E: Rigidity Data

Figure E 1: Data for Figure 3

E <sub>win</sub>	nC	Chain				Cyclic				
		V <sub>w</sub> mean		V <sub>w</sub>	V <sub>wpot</sub>	V <sub>w</sub> mean		V <sub>w</sub>	V <sub>wpot</sub>	
		V <sub>wpot</sub> mean	R <sub>gr</sub>			V <sub>wpot</sub> mean	R <sub>gr</sub>			Std dev
2.5	4	79.756	± 0.769	78.924	100.945	67.727	± 1.447	67.204	78.836	
		102.524	± 4.990	80.441	108.112	78.556	± 2.370	66.614	80.773	
		0.778	± 0.039	79.902	98.514	0.862	± 0.032	69.363	76.058	
	5	94.414	± 0.877	94.394	159.462	86.439	± 0.837	86.410	109.030	
		157.557	± 1.737	95.301	156.061	109.540	± 0.578	85.616	109.422	
		0.599	± 0.009	93.547	157.149	0.789	± 0.009	87.290	110.168	
	6	111.902	± 2.590	109.209	208.914	100.709	± 2.456	101.669	114.990	
		208.490	± 6.703	114.376	201.586	117.117	± 1.928	97.918	117.611	
		0.537	± 0.021	112.121	214.971	0.860	± 0.025	102.539	118.749	
	7	128.452	± 1.860	130.498	272.920	116.838	± 2.671	117.070	163.851	
		268.665	± 3.687	127.993	266.403	166.276	± 2.481	119.385	166.168	
		0.478	± 0.010	126.864	266.673	0.703	± 0.019	114.058	168.810	
	8	145.083	± 1.329	143.799	354.026	134.694	± 0.871	133.827	203.622	
		352.689	± 3.065	146.453	354.858	205.544	± 1.667	135.569	206.423	
		0.411	± 0.005	144.996	349.182	0.655	± 0.007	134.687	206.588	
	9	159.940	± 3.078	163.402	418.264	151.520	± 2.150	150.817	241.636	
		429.025	± 9.481	157.509	432.662	242.030	± 5.771	149.810	247.988	
		0.373	± 0.011	158.909	436.150	0.626	± 0.017	153.933	236.467	
	10	177.152	± 5.845	182.984	581.641	166.493	± 3.637	164.625	279.273	
		587.965	± 10.006	177.178	599.501	280.183	± 1.156	164.169	281.484	
		0.301	± 0.011	171.293	582.752	0.594	± 0.013	170.684	279.792	
	6.0	4	78.371	± 0.835	77.407	105.544	69.469	± 2.168	69.469	75.912
			105.343	± 1.019	78.842	106.246	77.585	± 1.553	71.636	78.982
			0.744	± 0.011	78.865	104.238	0.895	± 0.033	67.301	77.860
5		95.700	± 2.052	96.200	161.208	85.816	± 1.772	86.870	109.580	
		161.370	± 0.878	97.456	160.584	110.822	± 1.287	83.771	110.737	
		0.593	± 0.013	93.444	162.317	0.774	± 0.018	86.808	112.150	
6		109.112	± 2.338	107.901	224.880	99.129	± 1.930	97.632	141.687	
		225.515	± 0.601	111.807	225.590	139.276	± 2.623	98.447	139.658	
		0.484	± 0.010	107.628	226.075	0.712	± 0.019	101.307	136.483	
7		128.624	± 3.088	129.606	293.829	117.281	± 0.858	118.079	175.232	
		294.630	± 3.361	131.102	298.319	173.390	± 1.756	116.373	171.735	
		0.437	± 0.012	125.164	291.742	0.676	± 0.008	117.390	173.202	
8		144.808	± 3.626	146.970	412.668	136.672	± 0.556	136.341	202.211	
		406.651	± 5.255	146.832	404.320	204.720	± 2.734	136.362	207.633	
		0.356	± 0.010	140.621	402.965	0.668	± 0.009	137.314	204.315	
9		161.443	± 1.996	162.213	474.279	150.558	± 2.176	148.753	249.426	
		489.517	± 18.860	159.176	510.609	245.384	± 5.779	149.946	247.961	
		0.330	± 0.013	162.939	483.661	0.614	± 0.017	152.974	238.764	
10		179.146	± 1.190	178.897	644.237	168.008	± 4.266	166.028	289.883	
		656.036	± 16.943	180.441	648.420	286.350	± 6.190	172.904	279.202	
		0.273	± 0.007	178.101	675.450	0.587	± 0.020	165.092	289.964	

Figure E 2: Data for Figure 4 when  $E_{win} = 2.5$  kcal/mol

Name	Rgf	Rgf error	Sconf mean	Sconf sd	Sconf1	Sconf2	Sconf3	Vw mean	Vw sd	Vw1	Vw2	Vw3	Vwpot mean	Vwpot sd	Vwpot1	Vwpot2	Vwpot3
(1a,2a,3a,4a)-2,4-dimethyl-1,3-diol	0.764	0.039	2.225	0.001	2.224	2.225	2.225	117.599	5.460	112.090	117.698	123.009	153.987	3.375	157.159	154.362	150.441
(1a,2a,3b,4a)-2,4-dimethyl-1,3-diol	0.788	0.010	4.087	0.143	3.922	4.170	4.170	117.199	1.497	116.465	116.211	118.922	148.662	0.287	148.938	148.366	148.681
(1a,2a,3b,4b)-2,4-dimethyl-1,3-diol	0.783	0.017	2.278	0.001	2.277	2.278	2.279	118.731	1.329	119.854	119.075	117.264	151.605	2.714	149.997	154.738	150.078
(1a,2b,3a,4b)-2,4-dimethyl-1,3-diol	0.864	0.026	1.327	0.000	1.327	1.327	1.327	117.263	1.582	116.116	116.605	119.067	135.668	3.707	131.900	139.311	135.792
1-(4-hydroxybutyl) hexanoate	0.666	0.018	4.440	0.485	4.144	5.000	4.176	209.813	1.723	210.298	211.242	207.899	314.936	8.301	319.208	305.369	320.231
1,3-propanediol	0.602	0.020	2.739	0.000	2.739	2.739	2.739	79.193	1.866	79.886	77.079	80.614	131.486	3.196	135.158	129.980	129.321
1,4-butanediol	0.549	0.008	5.310	0.133	5.233	5.233	5.463	95.756	0.949	96.472	94.679	96.115	174.514	1.997	172.213	175.787	175.544
1,6-hexanediol	0.416	0.010	11.039	0.039	11.079	11.001	11.039	126.783	2.236	124.848	129.231	126.269	304.527	4.785	303.560	300.300	309.722
1,8-octanediol	0.350	0.004	12.128	0.071	12.180	12.048	12.158	179.163	1.060	178.259	178.901	180.330	512.088	4.502	514.920	514.447	506.897
2,2,3,3-tetramethylbutane	0.793	0.019	0.356	0.617	0.000	0.000	1.068	144.170	3.080	142.490	147.725	142.296	181.831	1.728	182.806	182.851	179.836
2,2,4-trimethylpentane	0.614	0.021	2.919	0.001	2.918	2.919	2.919	146.794	4.075	143.690	145.282	151.409	239.240	4.945	237.622	244.791	235.307
2,2-dimethylhexane	0.582	0.016	2.945	0.136	2.788	3.023	3.023	140.639	3.693	141.238	143.996	136.683	241.458	1.763	239.687	241.472	243.214
2,3,3-trimethylpentane	0.624	0.023	4.714	0.000	4.714	4.714	4.714	145.971	3.860	143.712	143.774	150.429	233.871	6.033	238.095	236.556	226.962
2,3,4-trimethylpentane	0.573	0.013	3.272	0.108	3.147	3.335	3.334	142.289	1.058	143.326	142.329	141.211	248.461	5.403	243.015	253.821	248.546
2,5-dimethylhexane	0.543	0.010	5.460	0.000	5.460	5.460	5.460	147.003	1.132	145.930	148.186	146.892	270.810	4.429	275.878	268.866	267.685
2,6-naphthoic dicarboxylic acid	0.963	0.025	0.000	0.000	0.000	0.000	0.000	180.582	3.404	183.253	176.750	181.744	187.514	3.327	188.527	190.215	183.798
2-Hydroxyethyl 4-formylbenzoate	0.447	0.011	4.456	0.047	4.429	4.510	4.428	168.383	1.886	169.193	166.228	169.729	377.002	8.329	377.697	384.961	368.347
2-methylheptane	0.481	0.010	7.324	0.052	7.380	7.315	7.277	145.604	2.855	142.316	147.455	147.041	302.586	2.651	305.328	302.394	300.037
3,3-dimethylhexane	0.603	0.009	4.703	0.030	4.686	4.686	4.738	146.339	1.289	145.720	147.821	145.478	242.731	2.987	239.454	243.436	245.302
3-ethyl-2-methylpentane	0.566	0.014	4.428	0.155	4.256	4.556	4.471	144.095	1.730	144.874	145.298	142.112	254.476	5.340	248.602	255.789	259.037
3-ethyl-3-methylpentane	0.553	0.017	3.150	0.061	3.087	3.210	3.152	144.070	3.336	145.451	146.495	140.266	260.643	5.374	266.821	258.059	257.049
3-ethylhexane	0.507	0.011	6.626	0.201	6.562	6.851	6.466	142.601	1.526	144.206	142.428	141.169	281.098	4.981	285.980	276.024	281.289
4-methoxy-1-butanol	0.532	0.017	4.971	0.000	4.971	4.971	4.971	111.718	2.667	110.219	114.797	110.139	209.815	4.723	206.096	208.219	215.129
4-methylheptane	0.509	0.011	8.333	0.067	8.410	8.303	8.286	144.277	3.157	141.900	143.072	147.859	283.296	1.471	282.106	284.941	282.842
adipic acid	0.393	0.011	8.134	0.057	8.091	8.113	8.198	131.871	1.963	132.927	129.606	133.080	335.238	8.421	336.023	326.452	343.239
adipic acid mono(ethylene glycol) ester	0.675	0.017	3.154	0.670	3.757	3.273	2.433	170.918	2.432	173.635	170.175	168.944	253.225	5.251	249.076	251.471	259.128
aspartic acid mono(ethylene glycol) ester	0.505	0.010	7.220	0.045	7.253	7.238	7.169	153.607	2.858	152.222	156.893	151.705	303.938	1.606	302.142	304.436	305.235
BPA	0.624	0.004	2.830	0.046	2.803	2.883	2.803	220.607	1.336	221.029	219.111	221.680	353.585	1.242	354.485	354.102	352.168
butane	0.778	0.039	1.938	0.000	1.938	1.938	1.938	79.756	0.769	78.924	80.441	79.902	102.523	4.990	100.945	108.112	98.514
CBBI-1	1.006	0.019	0.000	0.000	0.000	0.000	0.000	148.773	1.778	150.617	147.069	148.634	147.922	2.128	150.234	147.487	146.046
CBBI-2	0.975	0.027	0.000	0.000	0.000	0.000	0.000	209.839	4.685	211.327	213.599	204.591	215.287	3.648	211.159	216.623	218.079
CBDA-1	0.616	0.020	2.511	0.257	2.363	2.807	2.363	268.315	7.338	266.291	276.452	262.201	435.346	7.160	440.933	427.275	437.830
CBDA-4	0.556	0.019	4.919	0.467	4.439	5.373	4.945	265.023	7.532	259.745	261.674	273.649	476.447	9.014	472.890	486.697	469.753
CBDA-6	0.552	0.018	2.480	0.000	2.480	2.480	2.480	333.623	3.426	332.473	330.920	337.477	604.646	18.599	625.599	590.087	598.252
CBDA-7	0.711	0.017	0.365	0.000	0.365	0.365	0.365	300.934	6.927	296.470	297.419	308.914	423.279	3.411	424.810	425.657	419.371
CBDac-1	0.622	0.015	2.323	0.247	2.180	2.608	2.180	307.518	5.777	314.175	304.561	303.818	494.304	7.331	492.437	502.388	488.088
CBDA-1	1.035	0.027	0.000	0.000	0.000	0.000	0.000	143.440	2.530	145.000	144.799	140.521	138.588	2.732	141.721	137.349	136.695
CBDA-5	0.989	0.018	0.000	0.000	0.000	0.000	0.000	205.662	2.902	204.264	203.724	208.999	207.915	2.235	208.229	205.539	209.975
CBDE-6	0.507	0.008	6.432	0.007	6.431	6.439	6.426	370.711	1.810	370.278	369.157	372.699	730.986	10.571	722.417	727.742	742.799
CBDE-7	0.620	0.012	1.611	0.476	1.986	1.075	1.771	372.471	5.769	372.989	377.963	366.461	600.319	6.836	607.746	594.290	598.923

<i>CBDH-1</i>	0.936	0.037	0.000	0.000	0.000	0.000	0.000	228.467	1.087	229.688	227.602	228.112	244.216	9.521	253.947	243.779	234.920
<i>CBDO-2</i>	0.615	0.008	2.712	0.183	2.697	2.902	2.538	300.342	3.050	302.496	296.852	301.677	488.324	4.558	484.098	487.722	493.154
<i>CBDO-3</i>	0.529	0.013	4.790	0.000	4.790	4.790	4.790	227.659	1.934	226.321	226.780	229.877	430.584	9.786	434.609	437.715	419.428
<i>CBDV-1</i>	0.568	0.013	3.802	0.152	3.744	3.974	3.688	303.488	4.424	305.604	298.403	306.457	534.646	9.940	523.618	542.915	537.405
<i>cis-1,4-cyclohexane dicarboxylic acid</i>	0.575	0.018	3.242	0.172	3.137	3.148	3.440	155.359	3.411	151.922	158.744	155.411	270.037	6.244	262.832	273.890	273.388
<i>cis-1,4-cyclohexanedimethanol</i>	0.598	0.015	5.364	0.002	5.363	5.365	5.363	151.542	3.333	147.850	152.445	154.331	253.495	2.856	250.502	256.191	253.792
<i>cis-1,4-cyclohexanediol</i>	0.679	0.023	2.411	0.000	2.411	2.411	2.411	115.775	2.854	119.070	114.147	114.108	170.495	3.967	165.918	172.630	172.937
<i>cis-2,2,4,4-tetramethyl-1,3-diol</i>	0.899	0.019	1.087	0.000	1.087	1.087	1.087	152.175	1.558	153.964	151.120	151.441	169.246	3.059	172.151	169.533	166.053
<i>cyclobutane</i>	0.862	0.032	1.377	0.000	1.377	1.377	1.377	67.727	1.447	67.204	66.614	69.363	78.556	2.370	78.836	80.773	76.058
<i>cyclodecane</i>	0.594	0.013	3.085	0.000	3.085	3.085	3.085	166.493	3.637	164.625	164.169	170.684	280.183	1.156	279.273	281.484	279.792
<i>cycloheptane</i>	0.703	0.019	0.283	0.490	0.849	0.000	0.000	116.838	2.671	117.070	119.385	114.058	166.276	2.481	163.851	166.168	168.810
<i>cyclohexane</i>	0.860	0.025	0.000	0.000	0.000	0.000	0.000	100.709	2.456	101.669	97.918	102.539	117.117	1.927	114.990	117.611	118.749
<i>cyclononane</i>	0.626	0.017	1.995	0.000	1.996	1.995	1.995	151.520	2.150	150.817	149.810	153.933	242.030	5.771	241.636	247.988	236.467
<i>cyclooctane</i>	0.655	0.007	2.575	0.681	2.969	1.789	2.969	134.694	0.871	133.827	135.569	134.687	205.544	1.667	203.622	206.423	206.588
<i>cyclopentane</i>	0.789	0.009	0.000	0.000	0.000	0.000	0.000	86.439	0.837	86.410	85.616	87.290	109.540	0.578	109.030	109.422	110.168
<i>cyclopropane</i>	0.968	0.030	0.000	0.000	0.000	0.000	0.000	54.337	0.699	54.464	53.583	54.964	56.105	1.572	55.705	54.771	57.838
<i>decane</i>	0.301	0.011	11.486	0.081	11.445	11.580	11.434	177.152	5.845	182.984	177.178	171.293	587.965	10.006	581.641	599.501	582.752
<i>difluorobenzophenone</i>	0.599	0.023	1.438	0.105	1.377	1.377	1.558	180.675	4.342	177.208	179.273	185.545	301.553	9.294	293.119	300.025	311.516
<i>dimethylmaleic anhydride</i>	0.993	0.020	0.000	0.000	0.000	0.000	0.000	209.756	3.846	207.879	214.180	207.210	211.132	1.873	211.209	209.222	212.965
<i>ethylene glycol fumaric acid mono(ethylene glycol) ester</i>	0.612	0.023	4.347	0.000	4.347	4.347	4.347	61.563	1.782	61.845	59.657	63.187	100.587	2.449	102.442	101.507	97.811
<i>glutaric acid glutaric acid mono(ethylene glycol) ester</i>	0.491	0.010	4.238	0.129	4.189	4.140	4.383	114.692	1.465	113.043	115.844	115.188	233.792	3.725	231.791	231.496	238.090
<i>heptane</i>	0.557	0.015	6.398	0.058	6.431	6.431	6.331	153.647	3.104	150.980	152.907	157.054	275.982	4.939	272.500	273.812	281.634
<i>hexane</i>	0.478	0.010	5.824	0.000	5.824	5.824	5.824	128.452	1.860	130.498	127.993	126.864	268.665	3.687	272.920	266.403	266.673
<i>hydroquinone</i>	0.953	0.028	1.358	0.000	1.358	1.358	1.358	99.083	2.715	96.247	101.659	99.343	103.977	1.056	102.933	103.955	105.044
<i>isophthalic acid isophthalic acid mono(ethylene glycol) ester</i>	0.955	0.033	1.995	0.000	1.995	1.995	1.995	134.823	4.452	131.135	133.566	139.769	141.204	1.637	141.333	142.773	139.507
<i>maleic acid mono(ethylene glycol) ester</i>	0.578	0.023	5.509	0.033	5.471	5.528	5.529	176.779	6.227	183.964	172.939	173.433	305.897	5.320	299.758	309.145	308.788
<i>malic acid mono(ethylene glycol) ester</i>	0.516	0.013	5.028	0.193	5.000	4.850	5.233	135.284	2.407	135.321	132.858	137.673	261.938	4.485	262.259	257.301	266.254
<i>malonic acid malonic acid mono(ethylene glycol) ester</i>	0.526	0.011	5.579	0.031	5.574	5.612	5.551	147.215	1.541	146.460	148.989	146.197	279.979	5.000	285.425	278.918	275.596
<i>meso-3,4-dimethylhexane</i>	0.520	0.015	5.007	0.145	5.150	5.010	4.860	82.555	1.440	82.037	84.183	81.446	158.799	3.515	160.842	154.741	160.815
<i>monomethyl succinate</i>	0.523	0.013	6.560	0.272	6.500	6.324	6.857	126.822	3.009	125.936	124.356	130.175	242.536	1.994	244.191	243.094	240.322
<i>nonane</i>	0.508	0.008	3.595	0.073	3.511	3.637	3.637	145.178	1.453	144.256	146.852	144.425	285.645	3.346	289.433	284.413	283.090
<i>octane</i>	0.442	0.013	7.673	0.267	7.953	7.645	7.422	118.092	2.595	118.235	115.427	120.612	267.298	5.076	264.540	273.156	264.197
<i>oxalic acid</i>	0.373	0.011	9.573	0.118	9.594	9.680	9.446	159.940	3.078	163.402	157.509	158.909	429.025	9.481	418.264	432.662	436.150
<i>para-phenylenediacetic acid</i>	0.411	0.005	7.647	0.078	7.737	7.605	7.600	145.083	1.329	143.799	146.453	144.996	352.689	3.065	354.026	354.858	349.182
<i>para-xylene glycol</i>	0.652	0.015	3.016	0.000	3.016	3.016	3.016	66.725	0.372	66.790	66.325	67.061	102.353	2.256	104.796	100.347	101.917
<i>phosgene</i>	0.554	0.012	3.744	0.206	3.543	3.954	3.736	169.516	0.537	170.031	169.559	168.960	305.824	6.773	302.552	301.309	313.612
<i>phthalic acid</i>	0.603	0.022	5.486	0.029	5.461	5.519	5.478	132.870	2.968	136.141	130.350	132.119	220.362	6.234	225.788	213.553	221.747
<i>pentane</i>	0.599	0.009	2.866	0.074	2.823	2.823	2.952	94.414	0.877	94.394	95.301	93.547	157.557	1.737	159.462	156.061	157.149
<i>phthalic acid</i>	1.017	0.021	0.000	0.000	0.000	0.000	0.000	59.640	1.059	58.822	59.261	60.836	58.632	0.606	57.932	58.999	58.964
<i>phthalic acid</i>	0.694	0.013	3.124	0.389	3.349	3.348	2.674	135.689	1.005	135.562	136.752	134.754	195.569	3.277	193.344	199.333	194.031

<i>phthalic acid mono(ethylene glycol) ester</i>	0.549	0.017	5.296	0.167	5.198	5.489	5.201	176.369	5.159	173.671	173.118	182.318	321.358	3.174	320.671	324.820	318.584
<i>pimelic acid</i>	0.401	0.012	6.303	0.050	6.339	6.246	6.323	147.181	3.383	147.592	150.341	143.612	367.344	7.197	374.929	366.493	360.610
<i>poly(cis-1,6-dimethoxycyclohexane)terephthalate model</i>	0.323	0.008	8.878	0.204	8.967	9.022	8.644	267.632	6.278	268.540	273.407	260.949	829.216	6.461	834.904	822.191	830.552
<i>polyBPA terephthalate model</i>	0.386	0.007	7.197	0.111	7.072	7.283	7.238	337.863	6.065	334.161	344.862	334.567	875.954	4.717	881.261	874.361	872.239
<i>polybutylenesuccinate model</i>	0.674	0.016	5.074	0.032	5.037	5.085	5.098	172.914	2.322	171.995	175.555	171.193	256.569	5.213	262.334	255.188	252.187
<i>polybutylenesuccinate model, methylated</i>	0.285	0.005	12.738	0.391	12.528	12.497	13.190	205.008	2.188	205.670	202.565	206.789	718.822	9.914	729.794	710.506	716.167
<i>polybutyleneterephthalate model</i>	0.384	0.010	5.651	0.071	5.732	5.607	5.613	212.105	4.888	212.903	206.867	216.545	551.652	7.033	548.312	559.733	546.912
<i>polycarbonate model</i>	0.505	0.022	7.276	0.050	7.221	7.290	7.318	244.291	10.362	254.644	244.309	233.919	483.709	2.630	483.278	481.321	486.527
<i>polyether ether ketone model</i>	0.354	0.010	6.424	0.532	6.956	6.426	5.891	269.918	6.341	272.381	262.716	274.658	763.030	13.607	747.352	771.772	769.965
<i>polyethylene naphthalate model</i>	0.543	0.018	4.119	0.000	4.119	4.118	4.119	225.200	5.977	228.508	218.300	228.792	414.693	7.757	408.292	423.319	412.468
<i>polyethyleneterephthalate model</i>	0.458	0.018	2.995	0.001	2.994	2.995	2.995	180.861	5.880	183.893	174.084	184.606	395.162	8.710	399.487	385.137	400.863
<i>polypropyleneterephthalate model</i>	0.431	0.008	4.155	0.025	4.183	4.136	4.146	195.463	3.058	195.882	198.289	192.217	453.501	4.243	449.776	458.119	452.606
<i>propane</i>	0.993	0.032	0.000	0.000	0.000	0.000	0.000	60.865	0.388	61.267	60.834	60.494	61.293	1.936	63.524	60.043	60.314
<i>R,R-3,4-dimethylhexane</i>	0.492	0.011	5.132	0.034	5.119	5.107	5.171	144.319	2.331	146.329	144.866	141.764	293.312	4.285	298.192	290.170	291.573
<i>R-2,2,3-trimethylpentane</i>	0.595	0.020	2.278	0.000	2.278	2.278	2.278	143.341	2.583	141.967	141.735	146.320	241.020	6.816	248.748	235.865	238.446
<i>R-2,3-dimethylhexane</i>	0.545	0.013	6.779	0.079	6.716	6.868	6.753	144.810	2.657	141.993	145.167	147.270	265.881	4.285	265.694	261.692	270.256
<i>R-2,4-dimethylhexane</i>	0.526	0.009	6.719	0.119	6.765	6.583	6.808	144.742	1.614	142.954	145.182	146.091	274.931	3.276	278.423	274.445	271.926
<i>R-3-methylheptane</i>	0.499	0.015	8.591	0.037	8.549	8.610	8.615	146.337	1.714	144.750	146.106	148.154	293.104	8.365	302.304	291.053	285.956
<i>S,S-3,4-dimethylhexane</i>	0.506	0.014	5.146	0.128	4.998	5.213	5.226	147.270	3.266	146.267	144.623	150.919	290.772	4.311	295.125	290.686	286.504
<i>S-2,2,3-trimethylpentane</i>	0.606	0.021	2.278	0.000	2.278	2.278	2.278	145.992	4.190	150.757	144.334	142.885	240.953	4.786	243.929	243.497	235.432
<i>S-2,3-dimethylhexane</i>	0.544	0.007	6.844	0.091	6.935	6.842	6.754	144.224	1.587	145.788	144.270	142.615	264.882	1.856	266.333	265.523	262.791
<i>S-2,4-dimethylhexane</i>	0.531	0.010	6.669	0.092	6.598	6.773	6.635	146.982	2.441	146.811	149.504	144.631	276.588	2.678	279.651	274.686	275.429
<i>S-3-methylheptane</i>	0.490	0.015	8.619	0.008	8.611	8.626	8.621	142.495	3.992	138.043	143.686	145.756	290.842	3.496	290.239	287.687	294.600
<i>sebacic acid</i>	0.574	0.015	6.135	0.180	5.966	6.114	6.325	192.961	4.296	197.914	190.235	190.735	339.460	4.505	330.025	338.823	336.103
<i>suberic acid</i>	0.592	0.014	3.523	0.090	3.575	3.575	3.418	164.188	2.324	166.585	161.945	164.034	277.344	5.079	271.549	281.024	279.458
<i>succinic acid</i>	0.464	0.009	5.762	0.300	6.011	5.429	5.846	98.147	1.494	98.170	99.629	96.642	211.494	2.460	213.125	212.692	208.665
<i>succinic acid mono(ethylene glycol) ester</i>	0.451	0.010	6.951	0.161	7.077	7.008	6.770	140.692	2.501	142.706	141.477	137.892	311.772	3.584	310.864	315.723	308.729
<i>terephthalic acid</i>	0.953	0.012	0.000	0.000	0.000	0.000	0.000	136.481	0.990	137.126	136.976	135.341	143.281	1.412	144.889	142.710	142.243
<i>trans-1,4-cyclohexane dicarboxylic acid</i>	0.616	0.023	4.040	0.370	3.652	4.079	4.389	153.761	4.797	150.036	159.174	152.072	249.452	5.295	244.991	248.061	255.304
<i>trans-1,4-cyclohexanedimethanol</i>	0.634	0.017	4.970	0.016	4.951	4.979	4.979	151.279	3.080	149.404	149.600	154.834	238.794	4.194	235.460	243.503	237.420
<i>trans-1,4-cyclohexanediol</i>	0.801	0.021	1.055	0.000	1.055	1.055	1.055	118.013	0.215	118.199	118.062	117.777	147.329	3.811	143.072	148.491	150.423
<i>trans-2,2,4,4-tetramethyl-1,3-diol</i>	0.869	0.003	0.686	0.000	0.686	0.686	0.686	152.448	0.302	152.365	152.784	152.197	175.368	0.614	176.067	174.916	175.122

Figure E 3: Data for Figure 4 when  $E_{win} = 6.0$  kcal/mol

Name	Rgf	Rgf error	Sconf mean	Sconf sd	Sconf1	Sconf2	Sconf3	Vw mean	Vw sd	Vw1	Vw2	Vw3	Vwpot mean	Vwpot sd	Vwpot1	Vwpot2	Vwpot3
<i>(1a,2a,3a,4b)-2,4-dimethyl-1,3-diol</i>	0.755	0.013	2.296	0.006	2.293	2.293	2.303	118.203	1.397	116.605	119.191	118.812	156.638	1.889	157.557	154.465	157.892
<i>(1a,2a,3b,4a)-2,4-dimethyl-1,3-diol</i>	0.809	0.014	4.006	0.155	4.185	3.914	3.920	119.821	1.267	120.642	120.459	118.362	148.063	2.080	150.443	146.597	147.148
<i>(1a,2a,3b,4b)-2,4-dimethyl-1,3-diol</i>	0.778	0.019	2.517	0.162	2.432	2.703	2.415	120.108	1.685	118.306	120.374	121.645	154.373	3.047	156.827	150.963	155.329
<i>(1a,2b,3a,4b)-2,4-dimethyl-1,3-diol</i>	0.909	0.032	1.419	0.000	1.419	1.419	1.419	121.206	1.003	120.325	120.995	122.297	133.270	4.487	134.102	128.426	137.283
<i>1-(4-hydroxybutyl) hexanedioate</i>	0.447	0.013	6.753	0.076	6.669	6.772	6.818	202.743	2.314	204.836	200.258	203.134	453.115	11.641	464.479	453.650	441.215
<i>1,3-propanediol</i>	0.544	0.007	3.362	0.003	3.364	3.364	3.358	77.251	0.944	76.330	77.207	78.216	141.957	0.711	141.151	142.220	142.499
<i>1,4-butanediol</i>	0.491	0.017	6.019	0.004	6.021	6.020	6.014	94.682	0.898	95.602	94.636	93.808	192.764	6.401	185.375	196.596	196.322
<i>1,6-hexanediol</i>	0.391	0.010	11.693	0.009	11.685	11.692	11.703	125.151	2.946	127.263	121.785	126.405	319.686	2.541	319.733	322.203	317.122
<i>2,2,3,3-tetramethylbutane</i>	0.780	0.032	0.000	0.000	0.000	0.000	0.000	142.747	2.251	141.560	145.343	141.338	183.070	7.034	178.090	180.002	191.117
<i>2,2,4-trimethylpentane</i>	0.599	0.022	2.939	0.003	2.936	2.940	2.941	144.035	3.952	139.472	146.316	146.316	240.348	6.025	247.148	235.673	238.223
<i>2,2-dimethylhexane</i>	0.573	0.014	2.932	0.083	2.884	3.027	2.884	144.914	0.550	145.354	145.089	144.297	252.717	6.178	252.458	259.021	246.674
<i>2,3,3-trimethylpentane</i>	0.614	0.021	4.758	0.023	4.734	4.779	4.760	144.000	2.929	147.044	143.754	141.202	234.427	6.304	241.158	233.463	228.660
<i>2,3,4-trimethylpentane</i>	0.562	0.009	3.354	0.015	3.370	3.350	3.341	147.559	0.780	147.936	148.079	146.662	262.657	3.890	266.253	258.527	263.191
<i>2,5-dimethylhexane</i>	0.525	0.017	5.519	0.086	5.422	5.548	5.587	145.448	3.802	142.682	143.877	149.784	277.230	5.001	271.569	279.080	281.043
<i>2,6-naphthoic dicarboxylic acid</i>	0.954	0.033	0.000	0.000	0.000	0.000	0.000	179.148	3.619	177.030	183.327	177.086	187.778	5.388	183.659	185.801	193.875
<i>2-Hydroxyethyl 4-formylbenzoate</i>	0.420	0.014	4.743	0.042	4.719	4.718	4.792	172.935	4.173	168.198	174.538	176.068	411.894	9.824	422.538	403.177	409.967
<i>2-methylheptane</i>	0.452	0.021	7.816	0.032	7.809	7.788	7.851	145.817	6.648	150.250	149.028	138.172	322.501	1.616	321.375	321.776	324.353
<i>3,3-dimethylhexane</i>	0.567	0.014	5.136	0.120	5.050	5.085	5.273	145.140	3.475	144.726	148.803	141.890	256.159	1.981	257.294	257.311	253.872
<i>3-ethyl-2-methylpentane</i>	0.553	0.020	4.606	0.101	4.644	4.684	4.491	146.639	4.499	151.763	143.335	144.820	264.969	4.997	264.367	260.300	270.240
<i>3-ethyl-3-methylpentane</i>	0.555	0.015	3.172	0.035	3.212	3.154	3.148	143.487	3.377	141.205	141.889	147.367	258.375	3.184	260.683	259.698	254.743
<i>3-ethylhexane</i>	0.510	0.011	6.972	0.045	7.017	6.927	6.973	147.687	2.503	146.911	150.486	145.665	289.426	3.527	285.538	290.320	292.420
<i>4-methoxy-1-butanol</i>	0.446	0.007	6.329	0.029	6.361	6.307	6.318	109.870	1.187	108.719	111.090	109.801	246.504	2.677	243.495	247.397	248.621
<i>4-methylheptane</i>	0.482	0.012	8.458	0.152	8.313	8.615	8.446	144.774	2.587	145.024	147.227	142.071	300.378	5.065	304.610	301.758	294.766
<i>adipic acid</i>	0.389	0.004	8.328	0.115	8.241	8.286	8.458	131.616	0.878	132.630	131.130	131.088	338.579	3.039	340.262	335.070	340.403
<i>adipic acid mono(ethylene glycol) ester</i>	0.469	0.015	4.297	0.001	4.297	4.296	4.298	172.642	4.543	173.648	176.598	167.681	368.425	7.144	365.465	363.236	376.573
<i>aspartic acid mono(ethylene glycol) ester</i>	0.362	0.008	8.115	0.190	8.330	7.969	8.045	152.011	2.574	149.183	154.216	152.635	419.730	6.524	427.208	415.201	416.780
<i>BPA</i>	0.652	0.019	2.811	0.074	2.735	2.883	2.816	219.843	6.402	213.959	226.660	218.908	337.256	0.320	336.913	337.545	337.309
<i>butane</i>	0.744	0.011	2.037	0.086	2.087	1.938	2.087	78.371	0.835	77.407	78.842	78.865	105.343	1.019	105.544	106.246	104.238
<i>CBBI-1</i>	0.982	0.022	0.000	0.000	0.000	0.000	0.000	146.805	1.779	147.270	148.306	144.840	149.513	2.846	147.581	148.178	152.781
<i>CBBI-2</i>	0.959	0.016	0.000	0.000	0.000	0.000	0.000	210.355	2.946	213.513	209.871	207.682	219.317	2.155	221.665	218.858	217.429
<i>CBDA-6</i>	0.411	0.012	2.764	0.007	2.767	2.769	2.756	330.193	6.289	337.036	324.664	328.880	802.637	17.322	805.283	784.143	818.484
<i>CBDA-7</i>	0.621	0.013	0.438	0.001	0.439	0.437	0.439	302.581	2.040	303.524	300.240	303.978	487.187	9.919	496.034	476.465	489.063
<i>CBDAc-1</i>	0.333	0.015	2.606	0.059	2.652	2.540	2.628	301.238	12.197	299.762	289.845	314.106	903.887	15.807	906.459	918.250	886.951
<i>CBDAAn-1</i>	0.997	0.019	0.000	0.000	0.000	0.000	0.000	141.793	1.102	140.766	141.658	142.957	142.243	2.547	144.879	139.794	142.057
<i>CBDAAn-5</i>	0.995	0.031	0.000	0.000	0.000	0.000	0.000	209.908	1.724	210.048	208.118	211.557	210.892	6.251	209.285	205.601	217.789
<i>CBDE-7</i>	0.475	0.020	2.062	0.395	1.717	1.976	2.493	368.873	9.052	362.450	379.225	364.943	776.142	26.741	806.925	758.655	762.846

<i>CBDH-1</i>	0.942	0.006	0.000	0.000	0.000	0.000	0.000	232.966	0.967	232.771	234.015	232.112	247.411	1.023	246.274	247.704	248.256
<i>CBDO-2</i>	0.534	0.017	3.550	0.615	3.194	4.260	3.194	299.535	9.139	304.032	289.019	305.554	561.077	5.029	556.702	559.959	566.571
<i>CBDO-3</i>	0.472	0.018	4.968	0.002	4.966	4.970	4.968	230.774	8.575	223.934	227.994	240.394	489.388	4.825	493.783	484.225	490.155
<i>CBDV-1</i>	0.583	0.009	3.828	0.127	3.974	3.766	3.744	309.205	4.031	309.572	305.003	313.039	530.358	4.242	533.745	531.730	525.600
<i>cis-1,4-cyclohexane dicarboxylic acid</i>	0.500	0.009	3.344	0.453	2.889	3.349	3.795	153.527	1.959	151.351	155.151	154.079	307.098	3.889	310.832	307.393	303.070
<i>cis-1,4-cyclohexanedimethanol</i>	0.515	0.013	5.563	0.007	5.557	5.570	5.563	152.543	2.517	151.371	150.826	155.433	296.477	5.882	302.677	295.781	290.974
<i>cis-1,4-cyclohexanediol</i>	0.627	0.019	2.482	0.002	2.482	2.484	2.481	118.644	2.748	117.099	121.817	117.016	189.086	3.520	193.119	186.632	187.507
<i>cis-2,2,4,4-tetramethyl-1,3-diol</i>	0.861	0.022	1.197	0.000	1.197	1.197	1.197	152.430	3.683	148.639	152.656	155.994	177.043	1.351	176.651	175.932	178.547
<i>cyclobutane</i>	0.895	0.033	1.377	0.000	1.377	1.377	1.377	69.469	2.168	69.469	71.636	67.301	77.585	1.553	75.912	78.982	77.860
<i>cyclodecane</i>	0.587	0.020	3.273	0.065	3.210	3.269	3.341	168.008	4.266	166.028	172.904	165.092	286.350	6.190	289.883	279.202	289.964
<i>cycloheptane</i>	0.676	0.008	0.040	0.000	0.040	0.040	0.040	117.281	0.858	118.079	116.373	117.390	173.390	1.756	175.232	171.735	173.202
<i>cyclohexane</i>	0.712	0.019	0.002	0.000	0.002	0.002	0.002	99.128	1.930	97.632	98.447	101.307	139.276	2.623	141.687	139.658	136.483
<i>cyclononane</i>	0.614	0.017	2.016	0.000	2.016	2.016	2.016	150.558	2.176	148.753	149.946	152.974	245.384	5.779	249.426	247.961	238.764
<i>cyclooctane</i>	0.668	0.009	1.738	0.050	1.710	1.796	1.708	136.672	0.556	136.341	136.362	137.314	204.720	2.734	202.211	207.633	204.315
<i>cyclopentane</i>	0.774	0.018	0.000	0.000	0.000	0.000	0.000	85.817	1.771	86.870	83.771	86.808	110.823	1.287	109.580	110.737	112.150
<i>cyclopropane</i>	1.024	0.014	0.000	0.000	0.000	0.000	0.000	54.108	0.665	54.745	53.418	54.163	52.863	0.369	52.922	53.198	52.468
<i>decane</i>	0.273	0.007	71.504	145.629	12.419	239.661	12.731	179.146	1.190	178.897	180.441	178.101	656.036	16.943	644.237	648.420	675.450
<i>difluorobenzophenone</i>	0.621	0.019	1.438	0.104	1.377	1.377	1.558	182.265	3.455	183.056	185.256	178.483	293.464	6.820	299.077	295.441	285.875
<i>dimethylmaleic anhydride</i>	0.765	0.010	0.053	0.092	0.159	0.000	0.000	204.309	0.988	203.657	205.446	203.824	266.897	3.062	264.592	270.371	265.729
<i>ethylene glycol fumaric acid mono(ethylene glycol) ester</i>	0.617	0.019	4.470	0.156	4.380	4.380	4.651	62.601	1.554	62.673	64.117	61.011	101.416	1.879	101.933	102.982	99.333
<i>glutaric acid glutaric acid mono(ethylene glycol) ester</i>	0.392	0.008	5.495	0.046	5.536	5.503	5.445	134.229	2.620	131.511	134.435	136.740	342.484	1.899	344.391	340.594	342.469
<i>glutaric acid glutaric acid mono(ethylene glycol) ester</i>	0.464	0.023	4.918	0.273	5.065	5.086	4.604	116.873	4.169	115.880	121.448	113.290	252.007	9.039	242.982	261.060	251.980
<i>heptane</i>	0.437	0.012	6.314	0.021	6.311	6.296	6.337	128.624	3.089	129.606	131.102	125.164	294.630	3.361	293.829	298.319	291.742
<i>hexane</i>	0.484	0.010	4.872	0.030	4.855	4.907	4.854	109.112	2.338	107.901	111.807	107.628	225.515	0.601	224.880	225.590	226.075
<i>hydroquinone</i>	0.917	0.018	1.358	0.000	1.358	1.358	1.358	96.800	0.967	95.937	97.845	96.616	105.527	1.827	105.859	107.165	103.556
<i>isophthalic acid isophthalic acid mono(ethylene glycol) ester</i>	0.961	0.022	1.995	0.000	1.995	1.995	1.995	138.679	3.078	138.424	135.737	141.878	144.377	0.711	145.147	144.239	143.745
<i>maleic acid mono(ethylene glycol) ester</i>	0.521	0.015	5.890	0.066	5.859	5.845	5.965	180.769	3.710	183.985	176.710	181.612	346.837	6.606	339.210	350.800	350.500
<i>maleic acid mono(ethylene glycol) ester</i>	0.398	0.011	6.233	0.042	6.233	6.274	6.190	133.550	2.636	135.962	133.951	130.736	335.949	6.237	329.153	337.286	341.409
<i>malic acid mono(ethylene glycol) ester</i>	0.372	0.017	6.676	0.054	6.733	6.668	6.627	148.967	6.428	149.599	142.247	155.055	400.187	6.938	392.232	403.344	404.984
<i>malonic acid malonic acid mono(ethylene glycol) ester</i>	0.525	0.009	5.205	0.205	5.425	5.171	5.019	83.176	0.794	82.370	83.958	83.199	158.550	2.214	160.695	156.272	158.682
<i>meso-3,4-dimethylhexane</i>	0.491	0.006	3.933	0.126	3.954	3.798	4.047	146.505	1.565	144.908	148.035	146.571	298.286	1.180	299.615	297.883	297.361
<i>monomethyl succinate</i>	0.430	0.011	7.769	0.079	7.851	7.693	7.762	114.706	1.955	115.445	116.183	112.488	267.056	4.764	271.915	262.393	266.859
<i>nonane</i>	0.330	0.013	10.479	0.037	10.510	10.488	10.439	161.443	1.996	162.213	159.176	162.939	489.517	18.860	474.279	510.609	483.661
<i>octane</i>	0.356	0.010	8.108	0.260	7.814	8.198	8.310	144.808	3.626	146.970	146.832	140.621	406.651	5.255	412.668	404.320	402.965
<i>oxalic acid</i>	0.599	0.018	3.279	0.000	3.279	3.279	3.279	66.485	1.694	68.431	65.334	65.690	110.932	1.582	110.225	112.745	109.826
<i>para-phenylenediacetic acid</i>	0.472	0.015	4.304	0.401	4.378	3.870	4.662	168.814	1.992	170.313	169.575	166.554	357.693	10.160	368.016	357.359	347.704
<i>para-xylene glycol</i>	0.611	0.006	5.509	0.234	5.510	5.273	5.742	134.208	1.142	134.807	132.890	134.925	219.544	1.208	219.517	218.348	220.765
<i>pentane</i>	0.593	0.013	2.968	0.027	2.998	2.949	2.956	95.700	2.052	96.200	97.456	93.444	161.369	0.878	161.208	160.584	162.317



<i>phosgene</i>	1.006	0.041	0.000	0.000	0.000	0.000	0.000	58.701	1.179	60.062	58.030	58.010	58.342	2.093	59.383	55.933	59.711
<i>phthalic acid</i>	0.690	0.018	2.964	0.380	2.749	2.740	3.403	138.157	2.370	139.094	135.462	139.916	200.261	3.778	203.800	200.701	196.282
<i>phthalic acid mono(ethylene glycol) ester</i>	0.433	0.015	5.971	0.060	6.000	5.902	6.012	182.059	2.556	184.436	179.356	182.386	420.842	13.488	405.295	429.428	427.801
<i>pimelic acid poly(cis-1,6-dimethoxycyclohexane)terephthalate model</i>	0.353	0.010	8.140	0.060	8.209	8.102	8.109	148.325	4.004	150.619	143.701	150.655	420.048	3.939	415.521	422.699	421.924
<i>polyBPA terephthalate model</i>	0.283	0.004	7.290	0.192	7.074	7.441	7.356	338.603	4.180	335.770	343.404	336.634	1196.754	6.081	1201.262	1199.160	1189.838
<i>polybutylenesuccinate model</i>	0.412	0.007	5.528	0.078	5.439	5.584	5.561	175.367	2.112	177.392	173.177	175.532	426.060	5.259	430.218	427.815	420.149
<i>polybutyleneterephthalate model</i>	0.283	0.006	9.063	0.069	9.079	8.987	9.123	209.635	4.072	213.832	209.371	205.701	740.697	8.872	743.508	747.824	730.760
<i>polycarbonate model</i>	0.507	0.010	7.282	0.076	7.251	7.226	7.369	247.586	2.669	247.681	250.206	244.871	488.651	7.654	480.658	495.915	489.379
<i>polyether ether ketone model</i>	0.356	0.016	6.575	0.206	6.370	6.783	6.573	269.441	6.649	269.116	276.247	262.961	755.824	27.700	723.926	773.813	769.732
<i>polyethylene naphthalate model</i>	0.492	0.015	4.443	0.031	4.447	4.472	4.410	220.842	4.228	216.852	220.400	225.274	449.123	10.190	439.372	448.297	459.701
<i>polyethyleneterephthalate model</i>	0.419	0.010	3.527	0.018	3.516	3.518	3.548	182.633	2.063	184.060	180.268	183.571	436.278	9.411	442.232	441.173	425.428
<i>polypropyleneterephthalate model</i>	0.361	0.009	5.198	0.060	5.175	5.266	5.152	196.310	3.857	192.207	196.864	199.860	544.186	8.687	550.710	547.523	534.325
<i>propane</i>	0.954	0.015	0.000	0.000	0.000	0.000	0.000	59.673	0.162	59.782	59.750	59.487	62.548	0.980	63.581	61.631	62.433
<i>R,R-3,4-dimethylhexane</i>	0.453	0.019	5.291	0.098	5.267	5.399	5.208	143.538	5.307	138.077	148.678	143.860	317.066	6.659	322.887	309.805	318.507
<i>R-2,2,3-trimethylpentane</i>	0.567	0.022	2.368	0.025	2.384	2.381	2.339	142.791	3.054	140.260	141.929	146.184	251.879	8.112	253.569	259.013	243.055
<i>R-2,3-dimethylhexane</i>	0.525	0.007	7.111	0.263	6.904	7.023	7.407	145.010	1.132	143.770	145.987	145.273	275.988	3.267	277.680	272.222	278.061
<i>R-2,4-dimethylhexane</i>	0.506	0.006	6.861	0.050	6.808	6.869	6.907	144.205	0.891	145.097	144.202	143.315	284.823	2.943	287.640	281.768	285.061
<i>R-3-methylheptane</i>	0.483	0.008	8.776	0.084	8.792	8.685	8.850	149.166	2.513	150.401	146.275	150.823	308.947	1.250	307.69	308.97	310.19
<i>S,S-3,4-dimethylhexane</i>	0.457	0.013	5.294	0.094	5.358	5.339	5.186	145.790	3.579	144.189	149.891	143.291	319.071	5.186	324.887	317.394	314.930
<i>S-2,2,3-trimethylpentane</i>	0.588	0.014	2.368	0.049	2.339	2.341	2.425	144.471	3.363	145.474	147.219	140.720	245.555	1.118	244.916	246.845	244.902
<i>S-2,3-dimethylhexane</i>	0.535	0.017	6.994	0.065	7.069	6.948	6.966	146.544	1.569	148.217	145.106	146.310	273.741	8.161	275.366	280.967	264.890
<i>S-2,4-dimethylhexane</i>	0.500	0.013	6.861	0.061	6.854	6.804	6.924	142.095	1.407	143.641	141.757	140.888	284.444	6.747	282.254	279.064	292.015
<i>S-3-methylheptane</i>	0.462	0.012	8.722	0.032	8.717	8.755	8.692	145.033	3.081	141.863	145.219	148.016	314.202	4.122	309.797	314.845	317.965
<i>sebacic acid</i>	0.444	0.005	6.511	0.031	6.546	6.489	6.497	196.734	1.908	195.972	198.906	195.324	443.579	3.221	446.735	440.297	443.706
<i>suberic acid</i>	0.341	0.005	4.043	0.174	3.866	4.050	4.213	165.032	1.099	164.524	166.293	164.278	483.724	6.716	475.979	487.947	487.244
<i>succinic acid</i>	0.457	0.014	5.882	0.158	5.701	5.991	5.954	95.468	2.667	97.976	92.665	95.763	208.747	2.716	211.868	206.922	207.451
<i>succinic acid mono(ethylene glycol) ester</i>	0.380	0.006	8.219	0.119	8.348	8.112	8.198	139.342	0.610	140.027	138.858	139.140	366.311	5.958	368.084	359.668	371.181
<i>terephthalic acid</i>	0.955	0.033	0.000	0.000	0.000	0.000	0.000	135.578	1.193	134.461	136.834	135.440	142.008	4.749	137.037	142.486	146.500
<i>trans-1,4-cyclohexane dicarboxylic acid</i>	0.484	0.008	4.179	0.196	4.185	4.372	3.980	154.730	1.434	153.208	154.924	156.057	319.943	4.030	315.642	323.631	320.557
<i>trans-1,4-cyclohexanedimethanol</i>	0.532	0.014	5.092	0.000	5.092	5.092	5.092	151.824	3.955	149.170	156.369	149.932	285.121	1.804	286.531	283.089	285.744
<i>trans-1,4-cyclohexanediol</i>	0.668	0.010	1.349	0.037	1.327	1.327	1.391	117.696	1.559	116.052	119.153	117.882	176.296	1.080	177.540	175.600	175.747
<i>trans-2,2,4,4-tetramethyl-1,3-diol</i>	0.840	0.026	0.898	0.000	0.898	0.898	0.898	152.856	1.543	152.369	154.584	151.616	181.982	5.326	177.843	180.114	187.991

## References

- (1) Rabinovich, A. L.; Dashevskii(dec.), V. G. The Study of Structural Non-Rigidity of Molecules with Double Bonds in the Main Chain. *Polym. Sci. USSR* **1984**, *26* (9), 2133–2147. [https://doi.org/10.1016/0032-3950\(84\)90457-X](https://doi.org/10.1016/0032-3950(84)90457-X).
- (2) Huyskens, P.; Vandevijvere, P.; Siegel, G. The Influence of Molecular Rigidity on Enthalpy and Entropy. *J. Mol. Struct. THEOCHEM* **1989**, *200*, 555–563. [https://doi.org/10.1016/0166-1280\(89\)85078-X](https://doi.org/10.1016/0166-1280(89)85078-X).
- (3) Karshikoff, A.; Nilsson, L.; Ladenstein, R. Rigidity versus Flexibility: The Dilemma of Understanding Protein Thermal Stability. *FEBS J.* **2015**, *282* (20), 3899–3917. <https://doi.org/10.1111/febs.13343>.
- (4) Ni, Y.; Gordillo-Gómez, F.; Peña Alvarez, M.; Nan, Z.; Li, Z.; Wu, S.; Han, Y.; Casado, J.; Wu, J. A Chichibabin's Hydrocarbon-Based Molecular Cage: The Impact of Structural Rigidity on Dynamics, Stability, and Electronic Properties. *J. Am. Chem. Soc.* **2020**, *142* (29), 12730–12742. <https://doi.org/10.1021/jacs.0c04876>.
- (5) Lawson, A. D. G.; MacCoss, M.; Heer, J. P. Importance of Rigidity in Designing Small Molecule Drugs To Tackle Protein–Protein Interactions (PPIs) through Stabilization of Desired Conformers: Miniperspective. *J. Med. Chem.* **2018**, *61* (10), 4283–4289. <https://doi.org/10.1021/acs.jmedchem.7b01120>.
- (6) Meng, X.-Y.; Zhang, H.-X.; Mezei, M.; Cui, M. Molecular Docking: A Powerful Approach for Structure-Based Drug Discovery. *Curr. Comput. Aided-Drug Des.* **2011**, *7* (2), 146–157. <https://doi.org/10.2174/157340911795677602>.
- (7) Wolfe, J. F.; Arnold, F. E. Rigid-Rod Polymers. 1. Synthesis and Thermal Properties of Para-Aromatic Polymers with 2,6-Benzobisoxazole Units in the Main Chain. *Macromolecules* **1981**, *14* (4), 909–915. <https://doi.org/10.1021/ma50005a004>.
- (8) Roberts, M. F.; Jenekhe, S. A. Molecular Composites of Rigid-Rod Polymers in the Matrix of Flexible-Coil Polymers. Preparation of Thin-Film Nonlinear Optical Materials via Soluble Complexes. *Chem. Mater.* **1990**, *2* (6), 629–631. <https://doi.org/10.1021/cm00012a003>.
- (9) Casanova, R. D. J. P.; González, W. E. S.; Loria, J. D. C. Z.; García, A. N.; Cervantes, M. A. Y.; Vega, M. D. J. A.; López, L. A. D. Structure and Kinetic Rigidity of Polymers as Related to Chain Relaxations. *J. Thermoplast. Compos. Mater.* **2021**, *34* (5), 596–613. <https://doi.org/10.1177/0892705719847517>.
- (10) Luisi, P. L. Molecular Conformational Rigidity: An Approach to Quantification. *Naturwissenschaften* **1977**, *64* (11), 569–574. <https://doi.org/10.1007/BF00450635>.
- (11) Jacobs, D. J.; Hendrickson, B. An Algorithm for Two-Dimensional Rigidity Percolation: The Pebble Game. *J. Comput. Phys.* **1997**, *137* (2), 346–365. <https://doi.org/10.1006/jcph.1997.5809>.
- (12) Budday, D.; Leyendecker, S.; van den Bedem, H. Geometric Analysis Characterizes Molecular Rigidity in Generic and Non-Generic Protein Configurations. *J. Mech. Phys. Solids* **2015**, *83*, 36–47. <https://doi.org/10.1016/j.jmps.2015.06.006>.
- (13) Bondi, A. Van Der Waals Volumes and Radii. *J. Phys. Chem.* **1964**, *68* (3), 441–451. <https://doi.org/10.1021/j100785a001>.
- (14) Full Text PDF. <https://pubs.rsc.org/en/content/articlepdf/2020/cp/c9cp06869d> (accessed 2023-12-03).

- (15) Bannwarth, C.; Ehlert, S.; Grimme, S. GFN2-xTB - An Accurate and Broadly Parametrized Self-Consistent Tight-Binding Quantum Chemical Method with Multipole Electrostatics and Density-Dependent Dispersion Contributions. *J. Chem. Theory Comput.* **2019**, *15* (3), 1652–1671. <https://doi.org/10.1021/acs.jctc.8b01176>.
- (16) Zhao, Y. H.; Abraham, M. H.; Zissimos, A. M. Fast Calculation of van Der Waals Volume as a Sum of Atomic and Bond Contributions and Its Application to Drug Compounds. *J. Org. Chem.* **2003**, *68* (19), 7368–7373. <https://doi.org/10.1021/jo034808o>.
- (17) Chan, L.; Morris, G. M.; Hutchison, G. R. Understanding Conformational Entropy in Small Molecules. *J. Chem. Theory Comput.* **2021**, *17* (4), 2099–2106. <https://doi.org/10.1021/acs.jctc.0c01213>.
- (18) Pracht, P.; Grimme, S. Calculation of Absolute Molecular Entropies and Heat Capacities Made Simple. *Chem. Sci.* **2021**, *12* (19), 6551–6568. <https://doi.org/10.1039/D1SC00621E>.
- (19) Suárez, D.; Díaz, N. Direct Methods for Computing Single-molecule Entropies from Molecular Simulations. *WIREs Comput. Mol. Sci.* **2015**, *5* (1), 1–26. <https://doi.org/10.1002/wcms.1195>.
- (20) Wang, Z.; Miller, B.; Mabin, M.; Shahni, R.; Wang, Z. D.; Ugrinov, A.; Chu, Q. R. Cyclobutane-1,3-Diacid (CBDA): A Semi-Rigid Building Block Prepared by [2+2] Photocyclization for Polymeric Materials. *Sci. Rep.* **2017**, *7* (1), 13704. <https://doi.org/10.1038/s41598-017-13983-z>.
- (21) Hasegawa, M.; Horiuchi, M.; Kumakura, K.; Koyama, J. Colorless Polyimides with Low Coefficient of Thermal Expansion Derived from Alkyl-Substituted Cyclobutanetetracarboxylic Dianhydrides: Low-CTE Colorless Polyimides. *Polym. Int.* **2014**, *63* (3), 486–500. <https://doi.org/10.1002/pi.4532>.
- (22) *Kapton® Film Sheets (No adhesive) | 12" x12" | CS Hyde Company | USA*. CS Hyde Company. <https://catalog.cshyde.com/viewitems/plastic-film-tape-sheets/kapton-film-sheets-12x12> (accessed 2023-10-18).
- (23) Shahni, R. K.; Mabin, M.; Wang, Z.; Shaik, M.; Ugrinov, A.; Chu, Q. R. Synthesis and Characterization of BPA-Free Polyesters by Incorporating a Semi-Rigid Cyclobutanediol Monomer. *Polym. Chem.* **2020**, *11* (37), 6081–6090. <https://doi.org/10.1039/D0PY01098G>.
- (24) Nkemngong, D. N. Exploring [2+2] Photoreaction To Synthesize Cyclobutane Di- And Tetracarboxylic Acid Building Blocks From Biomass-Derived Precursors. Dissertation, University of North Dakota, Grand Forks, North Dakota, 2022. <https://commons.und.edu/theses/4364>.
- (25) Song, M.; Ma, H.; Ren, M.; Ai, Z.; Li, M. Diacetylene-Based C<sub>2h</sub>-Symmetric Monomers for Two-Dimensional-Polymer Synthesis. *Synlett* **2016**, *28* (04), 445–450. <https://doi.org/10.1055/s-0036-1588664>.
- (26) Tedaldi, L. M.; Aliev, A. E.; Baker, J. R. [2 + 2] Photocycloadditions of Thiomaleimides. *Chem. Commun.* **2012**, *48* (39), 4725. <https://doi.org/10.1039/c2cc31673k>.
- (27) Parcheta, P.; Datta, J. Influence of Chemical Structure on Physicochemical Properties and Thermal Decomposition of the Fully Bio-Based Poly(Propylene Succinate-Co-Butylene Succinate)s. *Polym. Test.* **2020**, *83*, 106337. <https://doi.org/10.1016/j.polymertesting.2020.106337>.
- (28) Wang, Z.; Scheuring, M.; Mabin, M.; Shahni, R.; Wang, Z. D.; Ugrinov, A.; Butz, J.; Chu, Q. R. Renewable Cyclobutane-1,3-Dicarboxylic Acid (CBDA) Building Block Synthesized from

- Furfural via Photocyclization. *ACS Sustain. Chem. Eng.* **2020**, *8* (24), 8909–8917. <https://doi.org/10.1021/acssuschemeng.0c00708>.
- (29) Abdelaty, M. S. A. The Influence of Vanillin Acrylate Derivative on the Phase Separation Temperature of Environmental Photo-Cross-Linked N-Isopropylacrylamide Copolymer and Hydrogel Thin Films. *J. Polym. Environ.* **2020**, *28* (10), 2599–2615. <https://doi.org/10.1007/s10924-020-01793-w>.
- (30) Sati, G. C.; Crich, D. Facile Synthesis of 3- *N*-Alkyl Pyrimidin-2,4-Diones from *N*-Sulfonyloxy Maleimides and Amines. *Org. Lett.* **2015**, *17* (16), 4122–4124. <https://doi.org/10.1021/acs.orglett.5b02079>.
- (31) Schmidt, G. M. J. 385. Topochemistry. Part III. The Crystal Chemistry of Some Trans-Cinnamic Acids. *J. Chem. Soc. Resumed* **1964**, 2014. <https://doi.org/10.1039/jr9640002014>.
- (32) Patil, S. V.; Mahale, K. A.; Gosavi, K. S.; Deshmukh, G. B.; Patil, N. S. Solvent-Mediated One-Pot Synthesis of Cyclic *N*-Substituted Imides. *Org. Prep. Proced. Int.* **2013**, *45* (4), 314–320. <https://doi.org/10.1080/00304948.2013.798569>.
- (33) Von Sonntag, J.; Knolle, W.; Naumov, S.; Mehnert, R. Deprotonation and Dimerization of Maleimide in the Triplet State: A Laser Flash Photolysis Study with Optical and Conductometric Detection. *Chem. - Eur. J.* **2002**, *8* (18), 4199–4209. [https://doi.org/10.1002/1521-3765\(20020916\)8:18<4199::AID-CHEM4199>3.0.CO;2-H](https://doi.org/10.1002/1521-3765(20020916)8:18<4199::AID-CHEM4199>3.0.CO;2-H).
- (34) Bloomfield, J. J.; Owsley, D. C. Photochemical [2 + 2] Cycloaddition Reactions at Low Temperatures. Synthesis of Bridgehead Substituted Bicyclo [n.2.0]Dicarboxylates from Maleic Acid Derivatives and Ethylene. *J. Org. Chem.* **1971**, *36* (24), 3768–3773. <https://doi.org/10.1021/jo00823a023>.
- (35) Roth, H. D. The Beginnings of Organic Photochemistry. *Angew. Chem. Int. Ed. Engl.* **1989**, *28* (9), 1193–1207. <https://doi.org/10.1002/anie.198911931>.
- (36) Mercer, J. A. M.; Cohen, C. M.; Shuken, S. R.; Wagner, A. M.; Smith, M. W.; Moss, F. R.; Smith, M. D.; Vahala, R.; Gonzalez-Martinez, A.; Boxer, S. G.; Burns, N. Z. Chemical Synthesis and Self-Assembly of a Ladderane Phospholipid. *J. Am. Chem. Soc.* **2016**, *138* (49), 15845–15848. <https://doi.org/10.1021/jacs.6b10706>.
- (37) Lukes, P.; Clupek, M.; Babicky, V.; Sunka, P. Ultraviolet Radiation from the Pulsed Corona Discharge in Water. *Plasma Sources Sci. Technol.* **2008**, *17* (2), 024012. <https://doi.org/10.1088/0963-0252/17/2/024012>.
- (38) Wang, Z. Polycyclobutanes Constructed From Biomass-Based Building Blocks. Dissertation, University of North Dakota, Grand Forks, North Dakota, 2017. <https://commons.und.edu/theses/2153>.
- (39) Wang, Z. D. Synthesis And Applications Of Symmetric Building Blocks In Supramolecular, Single-Stranded, And Double-Stranded Polymers. Dissertation, University of North Dakota, Grand Forks, North Dakota, 2016. <https://commons.und.edu/theses/2085>.
- (40) Shahni, R. K. Synthesis Of A Gemini Monomer And Cyclobutane-Containing Bifunctional Building Blocks For Novel Materials. Dissertation, University of North Dakota, Grand Forks, North Dakota, 2021. <https://commons.und.edu/theses/4102>.
- (41) Faure, S.; Jensen, A. A.; Maurat, V.; Gu, X.; Sagot, E.; Aitken, D. J.; Bolte, J.; Gefflaut, T.; Bunch, L. Stereoselective Chemoenzymatic Synthesis of the Four Stereoisomers of L -2-(2-Carboxycyclobutyl)Glycine and Pharmacological Characterization at Human Excitatory

- Amino Acid Transporter Subtypes 1, 2, and 3. *J. Med. Chem.* **2006**, *49* (22), 6532–6538. <https://doi.org/10.1021/jm060822s>.
- (42) Beaver, M. G.; Zhang, E.; Liu, Z.; Zheng, S.; Wang, B.; Lu, J.; Tao, J.; Gonzalez, M.; Jones, S.; Tedrow, J. S. Development and Execution of a Production-Scale Continuous [2 + 2] Photocycloaddition. *Org. Process Res. Dev.* **2020**, *24* (10), 2139–2146. <https://doi.org/10.1021/acs.oprd.0c00185>.
- (43) Williams, J. D.; Nakano, M.; Gérardy, R.; Rincón, J. A.; de Frutos; Mateos, C.; Monbaliu, J.-C. M.; Kappe, C. O. Finding the Perfect Match: A Combined Computational and Experimental Study Towards Efficient and Scalable Photosensitized [2+2] Cycloadditions in Flow. *Org Process Res Dev* **2019**, *23*, 78–87. <https://doi.org/10.1021/acs.oprd.8b00375>.
- (44) Corcoran, E. B.; Lévesque, F.; McMullen, J. P.; Naber, J. R. Studies Toward the Scaling of Gas-Liquid Photocycloadditions. *ChemPhotoChem* **2018**, *2* (10), 931–937. <https://doi.org/10.1002/cptc.201800098>.
- (45) Hartmann, W. Photosensibilisierte Addition von Maleinsäureanhydrid an terminale Alkine. *Chem. Ber.* **1969**, *102* (12), 3974–3984. <https://doi.org/10.1002/cber.19691021204>.
- (46) Koltzenburg, G.; Fuss, P. G.; Leitich, J. Die photosensibilisierte cycloaddition von maleinsäureanhydrid und einigen seiner derivaten an acetylen und an 3-cyclobuten-1,2-dicarbonensäureanhydrid. Darstellung von derivaten des bicyclopropyls und des Bicyclo [2.2.0] hexans. *Tetrahedron Lett.* **1966**, *7* (29), 3409–3414. [https://doi.org/10.1016/S0040-4039\(01\)82802-1](https://doi.org/10.1016/S0040-4039(01)82802-1).
- (47) Bloomfield, J. J.; Owsley, D. C.; Srinivasan, R. Cis-3,4-Cyclobutenedicarboxylic Acid Anhydride. *Org. Photochem. Synth.* **1976**, *2*, 36–40.
- (48) Gauvry, N.; Comoy, C.; Lescop, C.; Huet, F. A New Synthesis of Cis-Cyclobut-3-Ene-1,2-Dicarboxylic Anhydride. *Synthesis* **1999**, *1999* (04), 574–576. <https://doi.org/10.1055/s-1999-3441>.
- (49) Schenck, G. O.; Hartmann, W.; Mannsfeld, S.; Metzner, W.; Krauch, C. H. Vierringsynthesen durch photosensibilisierte symmetrische und gemischte Cyclo-Additionen. *Chem. Ber.* **1962**, *95* (7), 1642–1647. <https://doi.org/10.1002/cber.19620950711>.
- (50) Suzuki, H.; Tamura, T.; Ohmori, K. POLYAMIC ACID AND POLYIMIDE. 7,906,611 B2, March 15, 2011.